U.S.NRC
United States Nuclear Regulatory Commission
Protecting People and the Environment

NUREG/CR-7181
BNL-NUREG-105328-2014

BWR Anticipated Transients Without Scram in the MELLLA+ Expanded Operating Domain

Part 3:
Events Leading to Emergency Depressurization

Office of Nuclear Regulatory Research

AVAILABILITY OF REFERENCE MATERIALS IN NRC PUBLICATIONS

NRC Reference Material

As of November 1999, you may electronically access NUREG-series publications and other NRC records at NRC's Library at www.nrc.gov/reading-rm.html. Publicly released records include, to name a few, NUREG-series publications; *Federal Register* notices; applicant, licensee, and vendor documents and correspondence; NRC correspondence and internal memoranda; bulletins and information notices; inspection and investigative reports; licensee event reports; and Commission papers and their attachments.

NRC publications in the NUREG series, NRC regulations, and Title 10, "Energy," in the *Code of Federal Regulations* may also be purchased from one of these two sources.

1. **The Superintendent of Documents**
   U.S. Government Publishing Office
   Mail Stop IDCC
   Washington, DC 20402-0001
   Internet: bookstore.gpo.gov
   Telephone: (202) 512-1800
   Fax: (202) 512-2104

2. **The National Technical Information Service**
   5301 Shawnee Rd., Alexandria, VA 22312-0002
   www.ntis.gov
   1-800-553-6847 or, locally, (703) 605-6000

A single copy of each NRC draft report for comment is available free, to the extent of supply, upon written request as follows:

Address: **U.S. Nuclear Regulatory Commission**
Office of Administration
Publications Branch
Washington, DC 20555-0001
E-mail: distribution.resource@nrc.gov
Facsimile: (301) 415-2289

Some publications in the NUREG series that are posted at NRC's Web site address www.nrc.gov/reading-rm/doc-collections/nuregs are updated periodically and may differ from the last printed version. Although references to material found on a Web site bear the date the material was accessed, the material available on the date cited may subsequently be removed from the site.

Non-NRC Reference Material

Documents available from public and special technical libraries include all open literature items, such as books, journal articles, transactions, *Federal Register* notices, Federal and State legislation, and congressional reports. Such documents as theses, dissertations, foreign reports and translations, and non-NRC conference proceedings may be purchased from their sponsoring organization.

Copies of industry codes and standards used in a substantive manner in the NRC regulatory process are maintained at—

The NRC Technical Library
Two White Flint North
11545 Rockville Pike
Rockville, MD 20852-2738

These standards are available in the library for reference use by the public. Codes and standards are usually copyrighted and may be purchased from the originating organization or, if they are American National Standards, from—

American National Standards Institute
11 West 42nd Street
New York, NY 10036-8002
www.ansi.org
(212) 642-4900

Legally binding regulatory requirements are stated only in laws; NRC regulations; licenses, including technical specifications; or orders, not in NUREG-series publications. The views expressed in contractorprepared publications in this series are not necessarily those of the NRC.

The NUREG series comprises (1) technical and administrative reports and books prepared by the staff (NUREG–XXXX) or agency contractors (NUREG/CR–XXXX), (2) proceedings of conferences (NUREG/CP–XXXX), (3) reports resulting from international agreements (NUREG/IA–XXXX), (4) brochures (NUREG/BR–XXXX), and (5) compilations of legal decisions and orders of the Commission and Atomic and Safety Licensing Boards and of Directors' decisions under Section 2.206 of NRC's regulations (NUREG–0750).

U.S.NRC
United States Nuclear Regulatory Commission
Protecting People and the Environment

NUREG/CR-7181
BNL-NUREG-105328-2014

BWR Anticipated Transients Without Scram in the MELLLA+ Expanded Operating Domain

Part 3:
Events Leading to Emergency Depressurization

Manuscript Completed: April 2014
Date Published: June 2015

Prepared by:
Lap-Yan Cheng, Joo Seok Baek, Arantxa Cuadra, Arnold Aronson,
David Diamond, and Peter Yarsky*

Nuclear Science and Technology Department
Brookhaven National Laboratory

*U.S. Nuclear Regulatory Commission

Tarek Zaki, NRC Project Manager

NRC Job Codes V6150 and F6018

Office of Nuclear Regulatory Research

ABSTRACT

This is the third in a series of reports on the response of a BWR/5 boiling water reactor to anticipated transients without reactor scram (ATWS) when operating in the expanded operating domain “MELLLA+.” In this report ATWS events initiated by the closure of main steam isolation valves are analyzed. The objectives were to improve the ability to model such events with the TRACE/PARCS code package, and to simulate them for a sufficiently long time (2500 s) to understand the response of key components and also the potential for fuel damage or damage to the wetwell (suppression pool). These events automatically trip the recirculation pumps. The operator’s responses are to activate the emergency depressurization system when the wetwell has reached the heat capacity temperature limit, and to control power through controlling water level and injecting soluble boron.

Models were developed for three different statepoints in the fuel cycle: beginning-of-cycle, peak-hot-excess-reactivity, and end-of-full-power-life. Eleven cases were assessed to determine the effect of three different strategies for controlling water level, two initial flowrates, two different locations for injecting boron, and two different numerical schemes. In all cases, the event is mitigated successfully in terms of minimizing the degree of damage to the fuel, and assuring the ability of the containment to fulfill its function.

TABLE OF CONTENTS

LIST OF FIGURES

LIST OF TABLES

ACKNOWLEDGMENTS

This project was a joint effort of Brookhaven National Laboratory (BNL) and U.S. Nuclear Regulatory Commission staff. The authors wish to thank the Project Manager, Tarek Zaki, and his predecessor, Istvan Frankl, for their support and technical feedback. We greatly appreciated the efforts of the staff in the Office of Nuclear Regulatory Research, Reactor Systems Code Development Branch, to quickly assess and implement improvements, as they were identified, in the computer codes used in the project. We also appreciate the work done by Lynda Fitz in finalizing this document and providing administrative support.

ACRONYMS

3D	Three Dimensional
ADF	Assembly Discontinuity Factor
ADI	Alternating Direction Implicit
ADS	Automatic Depressurization System
ATWS	Anticipated Transient Without SCRAM
ATWS-ED	Anticipated Transient Without SCRAM with Emergency Depressurization
ATWS-I	Anticipated Transient Without SCRAM with Instability
BLP	Bottom of Lower Plenum
BNL	Brookhaven National Laboratory
BOC	Beginning-of-Cycle
BWR	Boiling Water Reactor
CB	Control Block in TRACE/PARCSInput
CHAN	Channel Componenet in TRACE Input
CONTAN	Containment Component in TRACE/PARCSInput
CMFD	Course-Mesh Finite-Difference
DC	Downcomer
DW	Drywell
DWO	Density-Wave Oscillation
ED	Emergency Depressurization
EOFPL	End-of-Full-Power-Life
EPU	Extended Power Uprate
FCT	Fuel Centerline Temperature
FOW	Figure-of-Merit
FW	Feedwater
FWC	Feedwater Controller
GE	General Electric
GEH	GE Hitachi
HCTL	Heat Capacity Temperature Limit
HWL	High Water Level
ISL	InformationSystems Laboratories
LOCA	Loss-of-Coolant Accident
LP	Lower Plenum
LPV	Lower Plenum Value
LTR	Licensing Topical Report
LWL	Low Water Level
MELLLA+	Maximum Extended Load Line Limit Analysis Plus
MSFBT	Minimum Stable Film Boiling Temperature
MSIV	Main Steam Isolation Valve
NEM	Nodal Expansion Method
NMP2	Nine Mile Point Unit 2
NRC	U.S. Nuclear Regulatory Commission
OOS	Out of Service
PARCS	Purdue Advanced Reactor Core Simulator
PCT	Peak Clad Temperature
PHE	Peak-Hot-Excess-Reactivity
RAI	Request for Additional Information
RCIC	Reactor Core Isolation Cooling
RHR	Residual Heat Removal
RPS	Reactor Protection System

RPT	Recirculation Pump Trip
RPV	Reactor Pressure Vessel
RWLC	Reactor Water Level Control
SC	Suppression Chamber
SEPD	Steam Separator/Dryer Componenet in TRACE Input
SETS	Stability Enhancing Two-Step method
S-I	Semi-Implicit Numerics
SLCS	Standby Liquid Control System
SP	Suppression Pool
SRV	Safety Relief Valve
SRVOOS	Safety Relief Valve Out of Service
SV	Signal Variable in TRACE Input
TAF	Top-of-Active Fuel
TRACE	TRAC-RELAP Advanced Computational Engine
TRACG	Transient Reactor Analysis Code, GE Version
TSV	Turbine Stop Valve
UFSAR	Updated Final Safety Analysis Report
UH	Void History
UHSPH	Void History Spectrally Corrected
WW	Wetwell
Zr	Zirconium
γ	Mixing Coefficient
Θ	Remixing Coefficient

1 INTRODUCTION

1.1 Background

In recent years the operating power of boiling water reactors (BWRs) has been increased, sometimes to 120% of their original licensed thermal power. This places them in an expanded operating domain, and changes how they maneuver in the power-flow operating map. One option being pursued, "maximum extended load line limit analysis plus" (MELLLA+) operation [1], raises questions about how the plant will respond to anticipated transients without scram (ATWS). This report is one of several wherein staff at Brookhaven National Laboratory (BNL) describe how these events were simulated with the state-of-the-art code package TRACE/PARCS, and detail the results of that analysis.

In previous reports [2, 3] there were discussions of how MELLLA+ operation affects the power-flow operating map, and of the impact of this in an ATWS event initiated by a turbine trip in a BWR/5 design. In these scenarios, after the recirculation pumps automatically tripped, the reactor evolved to a relatively high power-to-flow condition, and specifically, to a region of the power-flow map wherein unstable power oscillations are likely to occur. These power oscillations, if left unmitigated, may result in fuel damage. Additionally, the violence of the power oscillations may hamper the effectiveness of mitigation strategies. For example, these events (labelled ATWS-I) are typically mitigated by injecting a dissolved neutron absorber (boron) via the standby liquid control system; the occurrence of oscillation-induced reversal of the core inlet flow may reduce the rate at which this soluble absorber is delivered to the the reactor core.

In addition to the ATWS-I scenarios initiated by turbine trip, there are events due to closure of main steamline isolation valves. In these cases, the concern is the amount of energy being placed into the containment during the mitigation period. This thermal load may exhaust the available capacity for pressure suppression of the containment wetwell, which would prompt an emergency depressurization, according to standard emergency operating procedures. Emergency depressurization raises several concerns: 1) the reactor has undergone a beyond-design-basis event, and fuel may have been damaged; 2) the pressure-suppression capacity of the containment has been exhausted; and, 3) the reactor coolant pressure boundary has been bypassed by manually opening the valves of the automatic depressurization system. These events are discussed in the present report.

1.2 Objectives

The objective of this work was to first develop TRACE/PARCS models supporting ATWS confirmatory analyses at MELLLA+ operating conditions for an event that requires emergency depressurization (ATWS-ED). To accommodate updated guidance from staff of the U.S. Nuclear Regulatory Commmission (NRC) and different plant conditions for an ATWS-ED transient, the TRACE/PARCS model used for the ATWS-I studies required several modifications. An ancillary objective was to assess the capabilities of this model and the TRACE/PARCS code to calculate the thermal-hydraulic and neutronic phenomena associated with BWR ATWS and an emergency depressurization .

The second major objective was to analyze ATWS-ED events with different assumptions about plant conditions and/or modeling. This encompasses different strategies for water level control and different initial flowrates at three different times during a typical fuel cycle: beginning-of-

cycle (BOC), peak-hot-excess-reactivity (PHE, near the middle of the cycle), and end-of-full-power-life (EOFPL). It also includes looking at a different location for injecting soluble boron. The calculations are analyzed by detailing the dynamic response in many of the reactor components. In particular, the following parameters serve as figures-of-merit for indicating the severity of the consequences of an ATWS-ED event.

1) Peak clad temperature (PCT) – This parameter is a surrogate for fuel damage. Models have been updated to enhance the fidelity of predicting the PCT; they include metal-water reactions and axial heat conduction in the TRACE/PARCS calculations.

2) Recriticality – In an ATWS event the reactor power is controlled by auxiliary shutdown systems, such as the standby liquid control system, and other operator actions, such as water level control and emergency depressurization. However, some phenomena might lead to recriticality during the later phase of the transient such as:
    a. choking in the safety/relief valves (SRVs) that leads to a pressure/power excursion later in the transient, and,
    b. a decrease in boron concentration with an approximately constant boron mass while the water density increases.

    Several updates were made to the base BWR/5 plant model to capture the thermal-hydraulic phenomena that might be conducive to recriticality. These include a modified level tracking scheme near the feedwater sparger, a refinement of SRV grouping, and a new model for the mixing and transport of boron in the lower plenum.

3) Wetwell temperature – In an ATWS transient initiated by MSIV closure, the entire heat-load of the reactor is transferred to the suppression pool via the SRVs. If the ATWS heat-load was large enough to cause bulk boiling in the suppression pool, the containment's subsequent pressurization might be a concern. The base BWR/5 model was updated to more accurately represent the active and passive heat sinks in the wetwell. They include using the equivalent of two residual heat removal loops in the suppression pool's cooling mode and adding heat structures in the suppression pool and the airspace in the wetwell.

4) Containment pressure – This parameter indicates the impact of the ATWS heat-load relative to the containment pressure limits. It also gives an indication of the margin to net positive suction head limits for coolant pumps taking suction from the suppression pool.

1.3 Organization of Report

Chapter 2 discusses the methodology used for the simulations, focusing on the changes made to the model relative to what was used for the ATWS-I study. It also explains the sequence of calculations in running TRACE/PARCS. Appendix A has a more detailed explanation of the model. Chapter 3 provides steady-state results for all cases. For all three exposure points (BOC, PHE, and EOFPL), comparisons of power distributions are made with results generated with the model used for the ATWS-I analysis, the latter having a more detailed thermal-hydraulic channel representation. Chapter 4 analyzes the results obtained for 11 different cases looking at different assumptions on modeling and the initial conditions. Chapter 5 gives a summary and our conclusions; the references are provided in Chapter 6.

2 METHODOLOGY

2.1 Code Execution

The simulation with TRACE/PARCS of an ATWS event requires three successive steps (Figure 2.1). In these steps below, substitute 'xxx' for the appropriate case identifier (e.g. 'boc27ch-atwsED13'):

- Perform a TRACE stand-alone calculation for the initialization of flow (with a constant power specified through a table; that is no PARCS calculations). A restart file ('xxx.tpr') is generated at the end of this calculation.
- Using the above restart file (renamed to 'xxx-rc.rst'), run the coupled steady-state calculation, by setting the itdmr flag to 1 in the TRACE input deck ('xxx-rc.inp'), and including the PARCS input deck ('xxx-rc.parcs_inp') in the same directory. Restart files are generated for both PARCS ('xxx-rc.parcs_rst') and TRACE ('xxx-rc.tpr').
- Using these restart files ('xxx-rc.parcs_rst' and 'xxx-rc.tpr' renamed as 'xxx-tr.rst'), run the coupled-transient calculation. The itdmr flag in the TRACE input deck ('xxx-tr.inp') is 1, and the PARCS input deck ('xxx-tr.parcs_inp') is in the same directory.

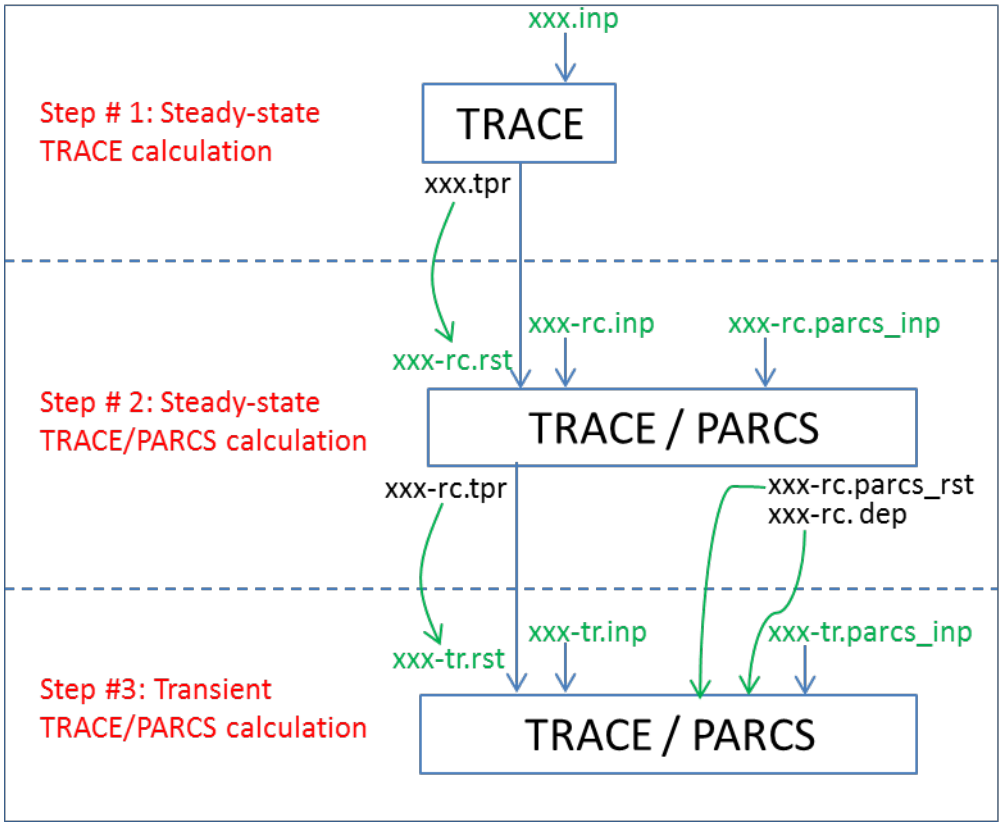

Figure 2.1 Procedure for Executing the TRACE/PARCS Code

2.2 Modifications to Base Model

In its review of the results of preliminary calculations of ATWS-ED events, BNL and NRC staff noted several areas where the results were not consistent with expectations [4]. In particular, they found that the predicted reponse of the core-inlet subcooling to changes in water level were not consistent with TRACG calculations from GE Hitachi (GEH). BNL and NRC staff identified several modifications to the plant model to garner better agreement in the performance of several components. Additionally, they identified a change in the modeling guidance for level tracking, and subsequently updated the guidance for ATWS-ED simulations in a series of documents [4, 5]. Implementing the updated guidance engendered several modifications to the TRACE base BWR/5 model [2]: upates to the characteristics of the safety/relief valves (SRVs), the transient feedwater controller, level tracking in the vessel downcomer, separator carryover/ carryunder, water-rod flow characteristics, the heat capacity temperature limit (HCTL), the suppression pool, the boron transport methodology, and the fuel models.

2.3 Model Updates

The anticipated modifications in the TRACE base BWR/5 model for simulating ATWS-ED transients were cited in footnotes in Appendix A of the documentation for the base model [2]. These modifications are given in Table 2.1 and provide the context of the updates to the TRACE model described in Sections 2.3.1 through 2.3.9. Appendix A has details of these modeling changes.

Table 2.1 Summary of Required Changes to the Base BWR/5 Model

Item	Comment
1	The following models for the VESSEL component will be modified for the ATWS-ED analysis: • addition of a new boron-mixing model and the removal of the flow control valve in the lower plenum • modification of the three dimensional (3D) level tracking for the vessel.
2	For the ATWS-ED analysis, the 3D level tracking will be turned off in ring 3 between axial levels 9 (top-of-active-fuel, TAF) and 12 (feedwater sparger).
3	For the ATWS-ED analysis, a different dynamic gas-gap option will be used (NFCI=3 initially, however NFCI=-13 was the eventual guidance) to support modeling of clad rupture. In addition, the metal-water reaction and axial conduction (NMWRX=1 and IAXCND=1) will be activated for the TRACE calculations.
4	A higher reverse loss coefficient of K=97.3E9 will be used in the ATWS-ED model to mitigate negative flow in the water rods.
5	For the ATWS-ED analysis, a small amount of carryover (XCO=0.001) and carryunder (XCU=0.0025) will be specified to better emulate the performance of real steam separators.
6	A new signal variable for the mass flow in the steamline will be defined for the ATWS-ED analysis. The flow sensor will be located downstream of the MSIVs, reflecting the instrumentation in the model BWR/5 plant.
7	The modeling of SRV/ADS valves will be modified for the ATWS-ED analysis. The valve loss coefficient, its delay and its rate of opening will be revised. In addition, individual valves with modified control logic are to be used to represent the different banks of SRVs.
8	The HCTL limit will be changed to 344.26 K (160°F) for the ATWS-ED analysis.
9	For the ATWS-ED analysis, the “Relief Mode Analytical Limit” will be used as the setpoints for the opening pressures.
10	Several settings of the FW controller will be modified for the ATWS-ED analysis, among which are the maximum FW flowrate, the location of the steam-flow sensor, and the proportional gain of the water level differential.
11	For modeling boron mixing in the lower plenum, its flow valve will be replaced in the ATWS-ED analysis by a control logic that releases the appropriate amount of boron into the core flow to emulate the effect of boron mixing/remixing.
12	Heat structures in the wetwell of the containment will be incorporated in the ATWS-ED analysis.
13	The ATWS-I analysis assumed one train of the residual heat removal system (RHR) was operational. In the ATWS-ED analysis, two trains of RHR will be assumed to be operational, and thus, two suppression pool coolers will be modeled.

2.3.1 VESSEL Component

Two changes were made in the VESSEL component. One was removing the lower plenum flow valve (LPV), and the other was modifying the 3-D level tracking option for ring 3 (R3) of the vessel.

In the base BWR/5 model, the opening and closing of the LPV was used to model the mixing and remixing of entrained boron in the coolant. However,after implementing a new boron transport model (see Section 2.3.7), the LPV is no longer needed. Figure 2.2 is a node diagram showing the component view of the revised model. Other new features of models, such as the location of the boron-injection point, and the layout of the SRVs are described in later sections.

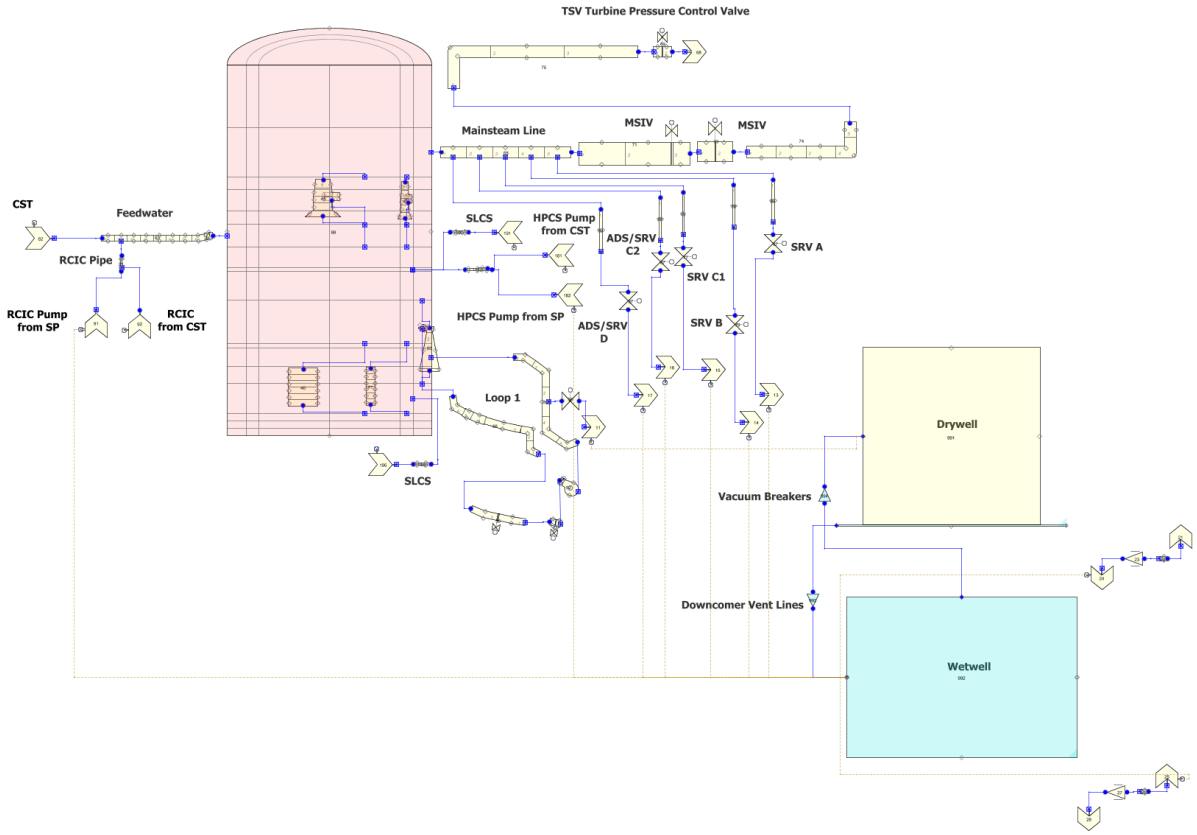

Figure 2.2 Component View of the BWR/5 Plant

The NRC staff recommended disabling level tracking in the vessel's ring 3 for all nodes, starting at the FW injection sparger and below until reaching a node near the level tracking strategy area (e.g., top-of-active-fuel, TAF). This change is intended to overcome the underestimation of interfacial heat-transfer area when level tracking is on. In addition, they suggested disabling level tracking in axial levels 1 through 4 (the base model assumed no level in that region of the vessel). Table 2.2 details the updated level tracking scheme, highlighting the new changes (a '1' indicates level tracking is on and a '-1' indicates it is off).

Table 2.2 3D Level Tracking Option for the VESSEL

Axial Level	Ring 1	Ring2	Ring3
17	-1	-1	-1
16	-1	-1	-1
15	1	1	1
14	1	1	1
13	1	1	1
12	1	1	-1
11	-1	-1	-1
10	-1	-1	-1
9	-1	-1	-1
8	-1	-1	1
7	-1	-1	1
6	-1	-1	1
5	-1	-1	1
4	-1	-1	-1
3	-1	-1	-1
2	-1	-1	-1
1	-1	-1	-1

2.3.2 CHAN Component

The staff provided the following guidance [4] on updating the input for the CHAN (thermal-hydraulic channel) component:

1. retard reverse flow in the water rod by increasing the reverse flow loss coefficient
2. activate the TRACE cladding-rupture model
3. activate the option for the metal-water reaction in TRACE
4. specify some nominal initial oxide thickness
5. enable axial conduction for the CHAN component and solve with implicit numerics

These five updates are explained below.

1. Staff experience indicated flow reversal in the water rods seemingly challenged the execution of the code. Since such reversal is beneficial in providing cooling to the active channel, this flow reversal was retarded artificially by increasing the reverse-flow loss coefficient by a factor of 1.0E9 at the water rod's inlet (at the bottom of the water rod). This was accomplished by setting **wrrlossi**=9.73E10. The rest of the changes in the input of the CHAN component were to activate several fuel models to capture the onset of certain phenomena at high temperatures.
2. The first change was to activate the TRACE cladding-rupture model. The particular fuel-clad interaction (FCI) option that the staff recommended was **NFCI**=-13, a dynamic gas-gap model with elastic-cladding deformation, plastic-cladding deformation, clad rupture and the FRAPCON relocation model turned on. The initial recommendation of **NFCI**=3 [4] later was found to not be working properly.

3. The staff also directed BNL to activate the option for the metal-water reaction. At high temperatures (around 1000 K), the cladding oxidation reaction is exothermic, and adds additional heat as the zirconium in the cladding reacts with the water coolant. TRACE has two options for treating this, viz., the Baker-Just model, and the Cathcart-Pawel model. The former is consistent with Title 10 Code of Federal Regulations Part 50's Appendix K, and is considered conservative. The Cathcart-Pawel model is the best-estimate one, and should be used for ATWS calculations. The latter was selected by setting **nmwrx**=1.

4. When using either of the metal-water reaction options, the TRACE User Manual [6] recommends specifying some initial thickness of the oxide layer. If none is specified, then TRACE will conservatively overpredict the rate of the metal-water reaction, even at temperatures below the threshold temperature (around 1000 K). Therefore, the staff directed BNL to specify a nominal thickness.

The initial oxide thickness may be specified in one of two ways by setting the **FOXLAYER** NAMELIST flag to either 1 or -1:

> 1: Initial oxide layer thickness is defined for each heat structure and channel in the model.
> -1: The value of the **DOXLAYER** namelist variable defines the initial thickness of the oxide layer for all components in the model.

The -1 option was specified for the ATWS-ED model. The constant initial oxide- layer thickness was derived from a set of FRAPCON outputs [7] from the NRC staff. Based on the FRAPCON results, the average thickness of the oxide layer for a full-length fuel rod is shown in Figure 2.3 as a function of burnup. The initial oxide layer thickness for BOC, PHE, and EOFPL can be inferred from Figure 2.3 based on the burnup corresponding to the respective cycle's condition.

Table 2.3 gives the average core burnup at the three exposure points of interest. The data are derived from the PARCS steady-state .dep file for the model BWR/5 core with GE14 fuel assemblies and MELLLA+ operating conditions. Based on the average burnup from Table 2.3, and the corresponding average oxide layer thickness from Figure 2.3, the following initial oxide layer thicknesses are suggested for each cycle condition of interest.

- BOC: 3 microns
- PHE: 6 microns
- EOFPL: 10 microns

The above values were suggested with consideration of the existence of lower-than-average burnup in some fuel rods at any given cycle condition. In summary, the following NAMELIST specified variables define the initial-oxide thicknesses:

FOXLAYER=-1
DOXLAYER=3.0E-6 (for BOC)
=6.0E-6 (for PHE)
=10.0E-6 (for EOFPL)

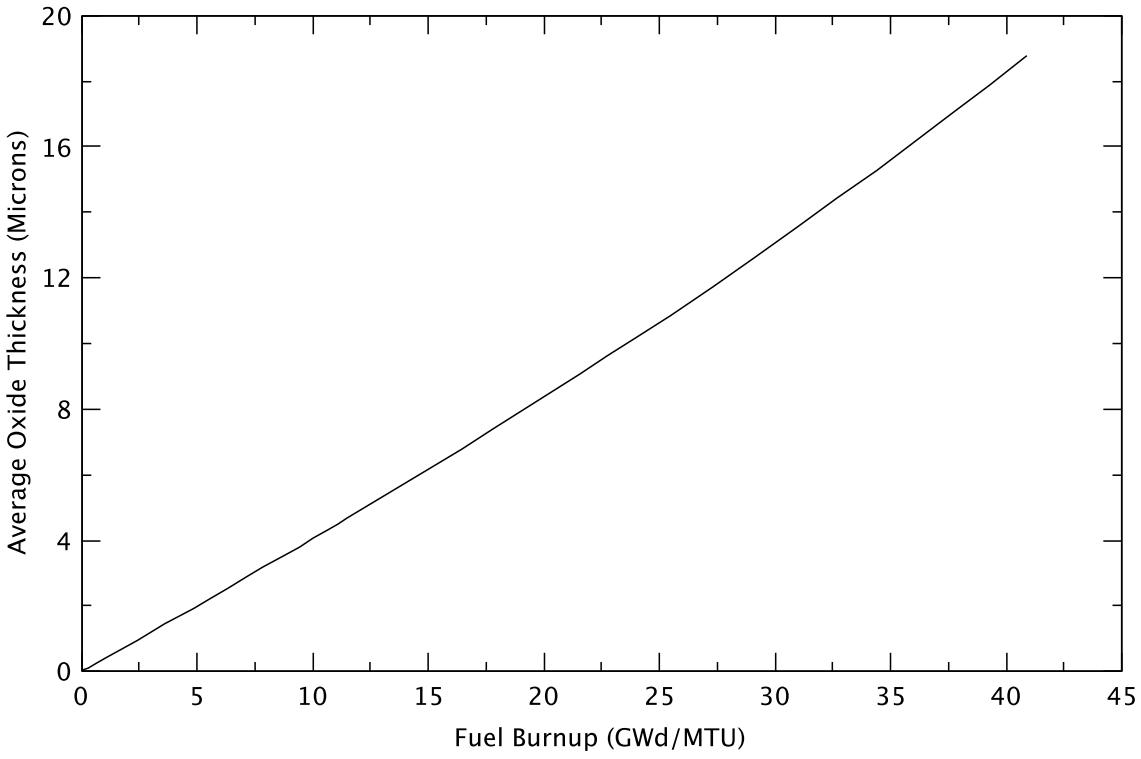

Figure 2.3 Average Oxide Layer Thickness as a Function of Burnup

Table 2.3 Core Average Burnup

Average Burnup (GWd/t)		
BOC	PHE	EOFPL
13.8	23.9	32.2

5. The staff recommended enabling the axial-conduction option for the fuel channels because it more realistically treats heat transfer in the fuel clad when the cladding surface has exceeded the minimum stable film-boiling temperature (MSFBT). This option was activated by setting the NAMELIST variable **iaxcnd**=1. When axial conduction (**iaxcnd**=1) is enabled, the NAMELIST variable **NRSLV** controls the scheme for numerical solution of axial conduction. The default is to treat the axial conduction with explicit numerics. However, **NRSLV**=1 allows the problem to be treated with alternating direction implicit (ADI) numerics (i.e., implicit ones). The latter method is preferred, and this value was specified in the new model.

2.3.3 SEPD Component

The base BWR/5 steam separator/dryer model (SEPD) currently is an ideal-ideal separator without carryover or carryunder. Since the transient response is highly sensitive to the inlet enthalpy response, the staff recommended our specifying a realistic carryunder [4]. Specifying a fixed carryover and carryunder in the staff's ATWS-I sensitivity study [4] seemingly improved

the prediction of the reponse of the dynamic vessel level. Therefore, the staff directed BNL to specify a carryover of 0.1% and a carryunder of 0.25% for the ATWS-ED calculations. For SEPD components 45 and 46 (Figure 2.2) the following two input parameters were specified:

xco=0.001
xcu=0.0025

2.3.4 Feedwater Control System

In the TRACE base BWR/5 model, the signal for steam flow for the feedwater controller (FWC) was taken at the main steamline flow restrictor. The staff recommended that to better match the reference analysis, the BWR/5 model's FWC-sensed steam-flow signal should be derived from a point in the steamline downstream of the MSIVs.

Compared to the TRACG analyses for the reference plant, the staff noted that the base BWR/5 FWC did not provide as rapid a dynamic response to reduce FW flow during the transient [4]. This likely reflects the relatively strong contribution to the FW controller's response from 1) the nominal FW flowrate, and 2) the integrated level-difference signal. The staff recommended setting an upper bound of 130% rated for the feedwater flow, and increasing the integral gain of the level-difference signal.

Based on the staff's three recommendations, the following changes were made to the BWR/5 model:

- defined **SV**-161 to provide steam flow downstream of the MSIVs and to use this SV as input to **CB**-72 and **CB**-51
- in **CB**-71, the proportional gain of level difference was increased to 10
- in **CB**-76, the maximum feedwater flowrate was increased to 2954.95 kg/s (1.3 x rated).

2.3.5 Safety/Relief Valve Model

Substantial changes were made in modeling the SRVs, in particular replacing the single-valve model with a multi-valve model. In the revised model, each bank of the operable SRVs is modeled by a separate valve. Their opening and closing are controlled by logic that reflects the two functional modes of the SRVS; the relief mode and the auto-depressurization mode.

Table 2.4 defines the operational characteristics of the SRVs by group, A, B, C1, C2, and D, respectively. The two valves in Bank 1 are assumed to be out of service (OOS) and are ignored in the model. It is noted that valve group C is sub-divided into C1 and C2 because only three out of the four valves in group C are assumed to be part of the automatic depressurization system (ADS). The staff directed BNL to use the relief mode analytical limit values for the valves' opening pressures. The new values are higher than the ones that correspond to the nominal value of the relief mode. Figure 2.4 shows the TRACE layout of the new groupings of the valves. The main steamline (**PIPE** 65) was re-nodalized from four to five nodes. Each valve group branches off from a different node of the main steamline.

Table 2.4 SRV Grouping

Bank	Number of Valves	Opening Pressure (MPa)	Closing Pressure (MPa)	Valve Group	Number of Valves in Group	ADS
1	2	7.830	7.327	OOS	2	No
2	4	7.899	7.396	A	4	No
3	4	7.968	7.465	B	4	No
4	4	8.037	7.534	C1	1	No
				C2	3	Yes
5	4	8.106	7.603	D	4	Yes

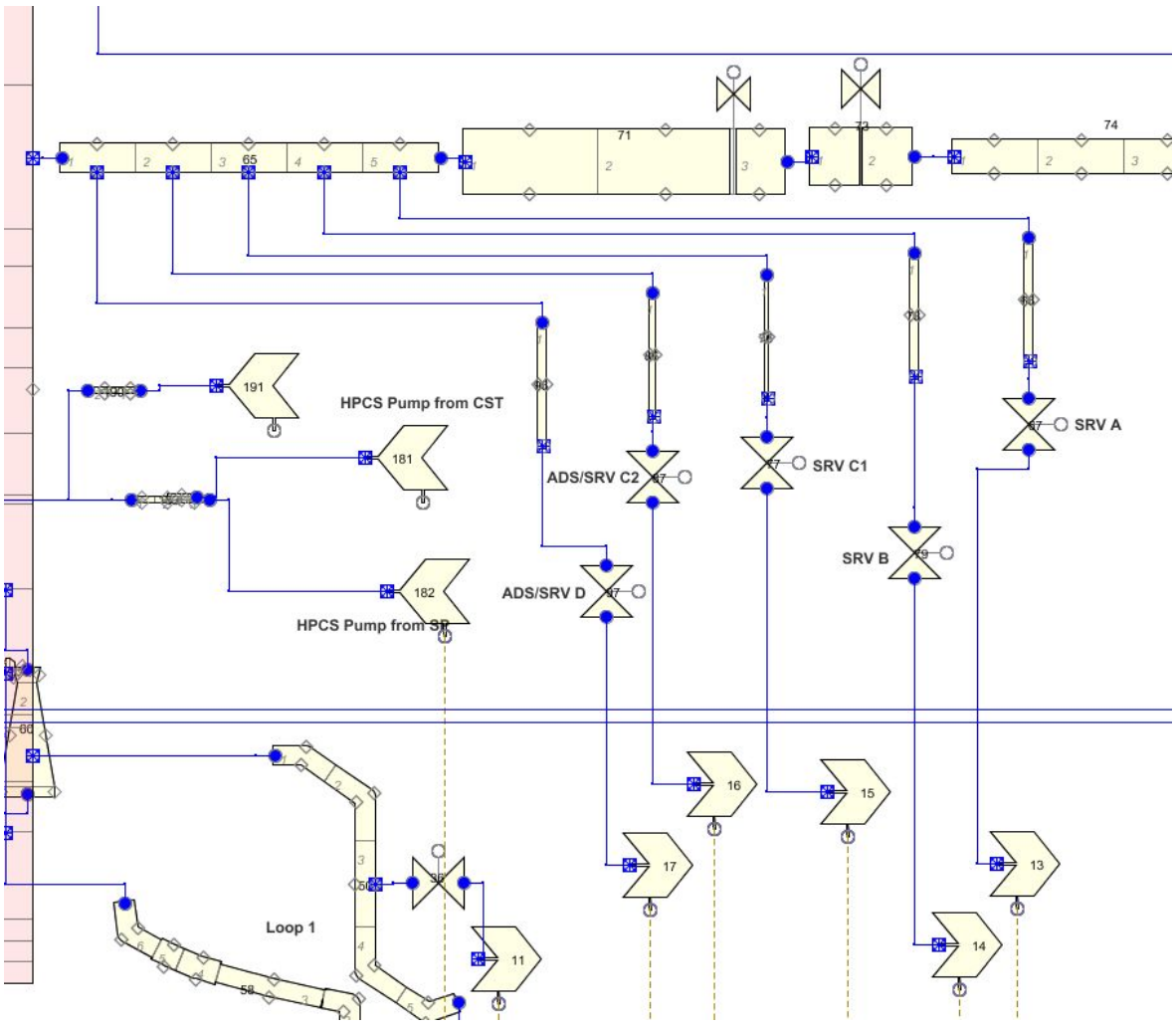

Figure 2.4 Layout of SRV Banks

The staff recommended [4] replacing the loss coefficient of 4.5 for the SRV with 0.786 from the Nine Mile Point Unit 2 Updated Final Safety Analysis Report (UFSAR). The higher loss coefficient (4.5) in the base BWR/5 model was derived by lumping losses in the SRV discharge

line into a local loss at the valve's throat. The resultant lumped-loss coefficient is too large so that TRACE no longer properly predicts SRV choking.
When the SRV is partially open, local losses are increased. To account for this effect, the staff recommended [4] using loss parameters taken from the reference TRACG input deck [8]. The KOPEN data necessary for the TRACE input is specified as a function of the open fraction.

In summary, the following are the additional changes made to the TRACE input for the single junction valves (**VALVE** 97, 87, 77, 79 and 67) that represent the SRVs:

Kfac = **Kfacr** = 0.786 [4]
Intlossoff = 1 (TRACE internal additive valve-flow-loss model is not included and the flow loss is based on the KOPEN table)
NKOPEN = 11 (number of pairs of data in the KOPEN table)
KOPEN table
rvmx = 2.0 (maximum rate of VALVE flow-area fraction or relative valve-stem position adjustment (1/s)) [4]

Figure 2.5 illustrates the control logic for the SRV/ADS. Appendix A defines the various trips, signal variables and control blocks. An adjustment table is given for each valve group to control its opening and closing according to the output of one of the two control blocks, CB-31 and CB-32. The two valve groups that perform the ADS function, C2 and D, receive their control input from CB-31, while the other valve groups receive their control signal from CB-32.

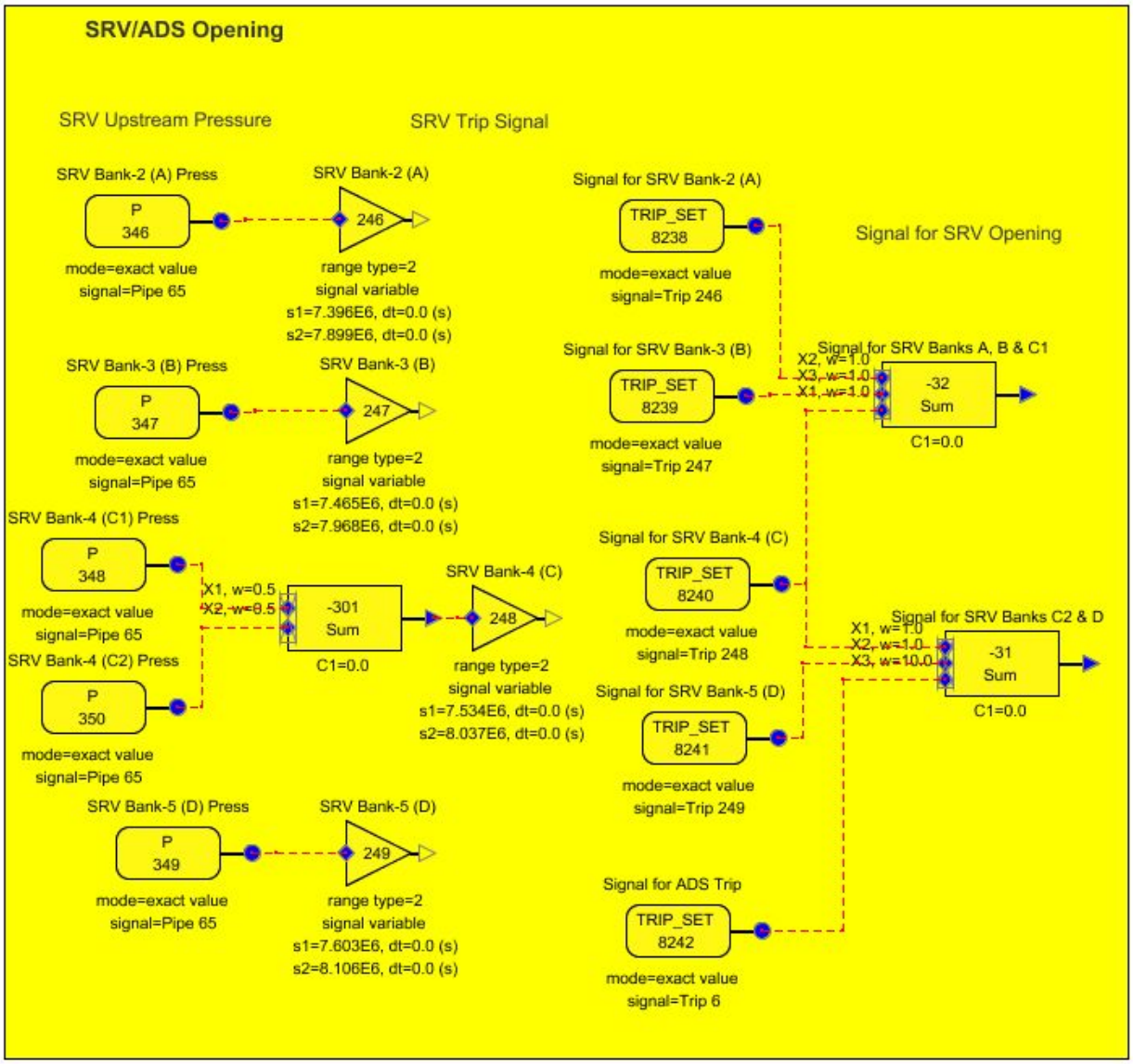

Figure 2.5 Control logic for SRV/ADS

2.3.6 Heat Capacity Temperature Limit (HCTL)

The staff directed BNL to revise the HCTL from 175°F to 160°F. **TRIP** 6 that actuates the ADS for the ED cases on the temperature of the suppression pool was revised to have a setpoint of 344.26 K (160°F).

2.3.7 Boron Transport Model

During executable testing, the staff found that the transient reactor power response was sensitive to the selected size of the time-step, due to the action of the boron-mixing valve in the lower plenum. This finding was not considered acceptable and, therefore, the staff sought to develop revised guidance for treating lower-plenum boron injection to achieve a more robust calculation scheme. The new methodology is described in the boron transport methodology document, which was provided to BNL [5].

The new approach is based on an external control system that evaluates flow conditions in the lower plenum to judge whether entraining conditions exist. If they do, then the controller allows the injection of boron into the TRACE vessel. TRACE then internally tracks the entrained boron. If the boron becomes stratified, the controller will externally track the amount of it by solving the equation for stratified boron continuity. Herein, it is useful to think of stratified boron and entrained boron as two different masses. Remixing is the phenomenon that occurs when the core flowrate is sufficiently high to entrain the borated solution that previously stratified in the bottom of the lower plenum. In this equation, the source term for the stratified boron mass is injected boron that is not entrained at the time of injection. The boron transport model is designed to keep track of the delivery of entrained boron into the core due to mixing and remixing. In the BWR/5 TRACE/PARCS model, an effective injection concentration is calculated via a control system. Appendix A details the boron transport model and its implementation in TRACE. A control system (Figure 2.6), was established in the TRACE/PARCS BWR/5 model to implement the new boron transport methodology. Definitions of trips, signal variables, and control blocks for the control system are discussed in Appendix A.

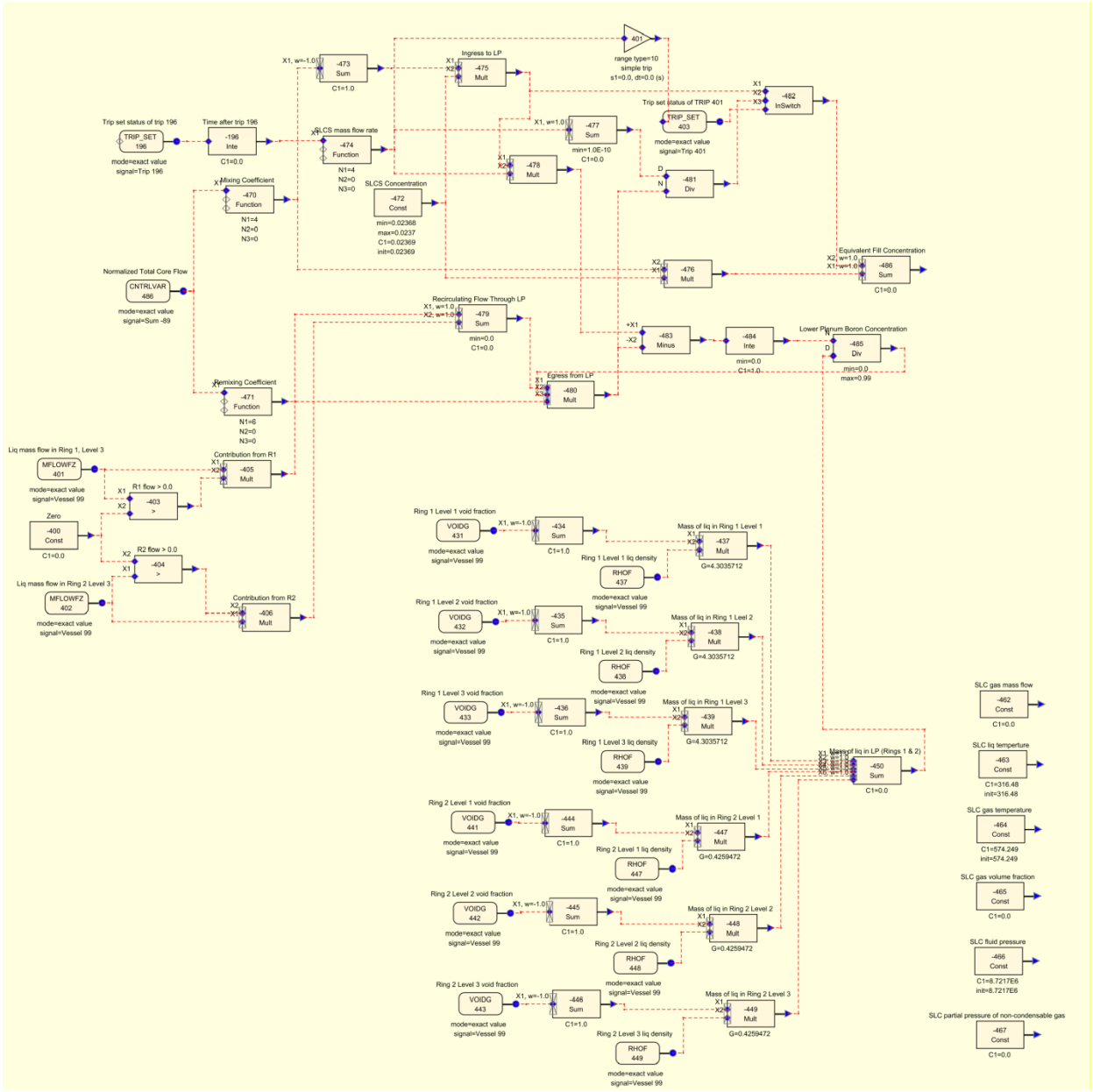

Figure 2.6 Boron Transport Control System

2.3.8 Suppression Pool Heat Structures

A recent fix of the TRACE code in V5.509 corrects an error in previous calculations of heat transfer between the containment fluid and the heat structures. For calculations where the heat capacity of the containment is important, as in the case of ATWS-ED, the staff recommended modeling the containment's heat structures in the TRACE CONTAN component [4]; their addition offers heat sinks and increases the suppression pool's overall heat capacity.

The modified CONTAN component retains the basic two-compartment setup of the original CONTAN model [8], a drywell and a wetwell. There is no change to the junction connections between the two compartments. The following are the notable changes to the original model:

- updated geometrical inputs to align with the parameters of the containment's design used in analyzing the uprated power of the reference BWR/5 plant [9], and,
- added containment-specific heat structures

Appendix A discusses the modeling for the two CONTAN compartments. These two compartments represent the drywell and the wetwell of a typical Mark II containment for a BWR plant. All geometric data are derived with the assumption that the suppression pool is at the minimum LWL (low water level) of 7.154 m (23.47 ft) [9]. The updated CONTAN model incorporated the following four containment-heat structures in the wetwell:

IHSTB 1 = suppression pool (SP) wall
IHSTB 2 = suppression chamber (SC) wall (wetwell airspace)
IHSTB 3 = reactor pedestal (RP) in SP
IHSTB 4 = reactor pedestal in SC

Table 2.5 lists some basic parameters of these four heat structures:

Table 2.5 CONTAN Heat Structures for a BWR/5

IHSTB	Description	Exposed Surface Area [9] (ft^2)	Inner Radius [8] (ft)	Thickness[1] [9] (ft)	Material [9]
1	SP Wall	6706 (623.0 m^2)	45.5 (13.87 m)	5.22 (1.59 m)	Concrete
2	SC Wall	10363 (962.8 m^2)	45.5 (13.87 m)	5.22 (1.59 m)	Concrete
3	RP in SP	1430 (132.9 m^2)	10.125 (3.086 m)	4. (1.219 m)	Concrete
4	RP in SC	2134 (198.3 m^2)	10.125 (3.086 m)	4. (1.219 m)	Concrete

[1]Wall thickness does not include stainless-steel liner.

For all heat structures in the SP (**IHSTB** = 1 and 3) both the inner and outer surfaces are located in the liquid region. For all heat structures in the SC (**IHSTB** = 2 and 4) both the inner and outer surfaces are located in the vapor region. For the walls of the SP and the SC, the outer heat-transfer area is set to zero to simulate an insulated boundary condition. A uniform initial temperature is assumed for all heat structures that is equal to the wetwell temperature.

2.3.9 Suppression Pool Heat Exchanger

The base BWR/5 model assumed that one train of the RHR was operational. In the ATWS-ED analysis, the assumption was that two trains were and thus, two suppression pool coolers are modeled. This modification is realized by doubling the flow of the suppression pool cooler to 236 kg/s in control block **CB**-34.

2.4 Core Input Model for PARCS

2.4.1 Cross Sections

Reference [10] describes cross-section set revision 4 (Rev. 4), provided by Oak Ridge National Laboratory to the NRC in January 2012. An inconsistency in the SCALE/TRITON branch structure used to generate the nodal data for this set led to a branch structure that is not orthogonal. In particular, the cross-section set has three boron branches at 1400 ppm, and one at 1500 ppm. While PARCS can use any branch structure ([11], Section 2.4), the recommended one is an orthogonal branch structure to prevent problems with convergence [4]. To avoid possible numerical difficulties, it was decided to "orthogonalize" the cross section set by relabeling the 1400 ppm branches as 1500 ppm. This alteration introduces a conservative bias because it underpredicts boron reactivity that is calculated using the relabeled branches.

2.4.2 TRACE/PARCS Mapping

The channel grouping scheme for ATWS-ED is based on geometrical and fuel-cycle considerations. This is possible because in a core with an Extended Power Uprate (EPU), the radial power shape is flattened, and reload fractions are high [1], so position- based grouping is similar to power grouping.

Figure 2.7 describes the mapping strategy for the 27-channel model. Each box with a zero is a fresh fuel bundle at BOC. The fuel assemblies mapped into ring 2 of the VESSEL component are marked in different shades of pink. The outermost assemblies in this peripheral region (with different effective loss coefficients for the lumped leakage flow path), are lumped together into channel 752, while the remaining assemblies are assigned to channels 751 (fresh assemblies) and 753 (burned assemblies). In ring 1 of the VESSEL, the different colors correspond to approximately equally sized rings, which are segmented into groups based primarily on BOC exposures, as indicated by different shades of the same color. The stars in the figure indicate the positions of the control rods where the blades are significantly inserted during cycle depletion. The controlled locations require additional detailed radial mapping; thus, these channels are further subdivided into smaller channel groups.

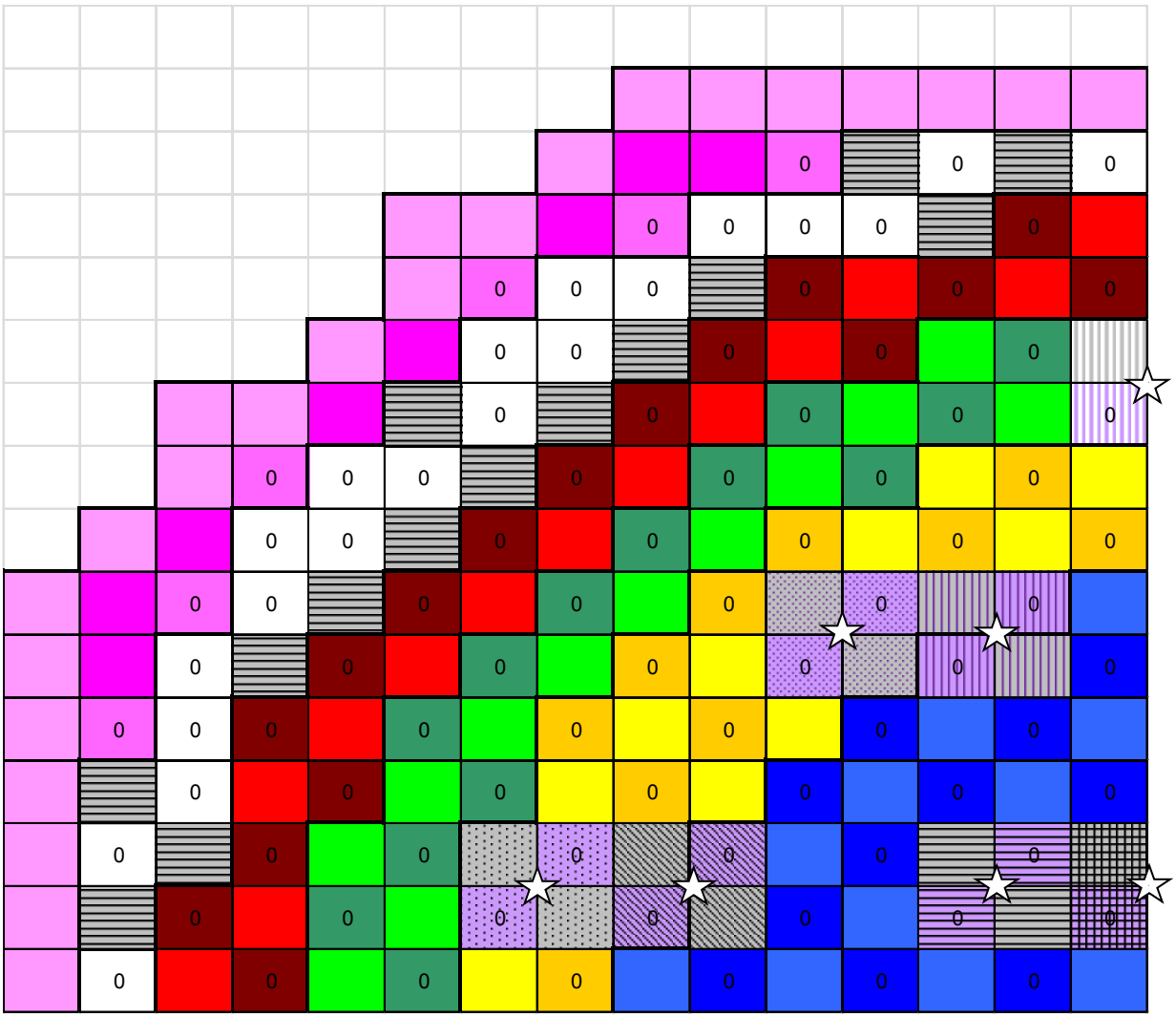

Figure 2.7 Mapping Strategy - 27-Channel Model

Figure 2.7 shows the “interior” region of the core, mapped into ring 1 of the VESSEL, that is divided in five annular regions with approximately the same number of assemblies. In each annular region, fresh and burned assemblies are separated and assigned to two different channels (251/252 for annular region 1; 351/352 for annular region 2; 451/452 for annular region 3; 551/552 for annular region 4; and, 651/652 for annular region 5). Since the bundles that experience significant control would have a different exposure history relative to bundles of similar instantaneous power levels, further detail is introduced around the control rods which are “significantly” inserted (by more than 10 steps) either for BOC or PHE; for each of the seven control rods in a quadrant, two new channels are added (for fresh and burned bundles). The result is the mapping shown in Figure 2.8. The PARCS model using this mapping is referred to as the 27-channel model. The 27-channel grouping scheme ultimately is justified by comparing the power distributions for the 27- and 382-channel models (Section 3.4).

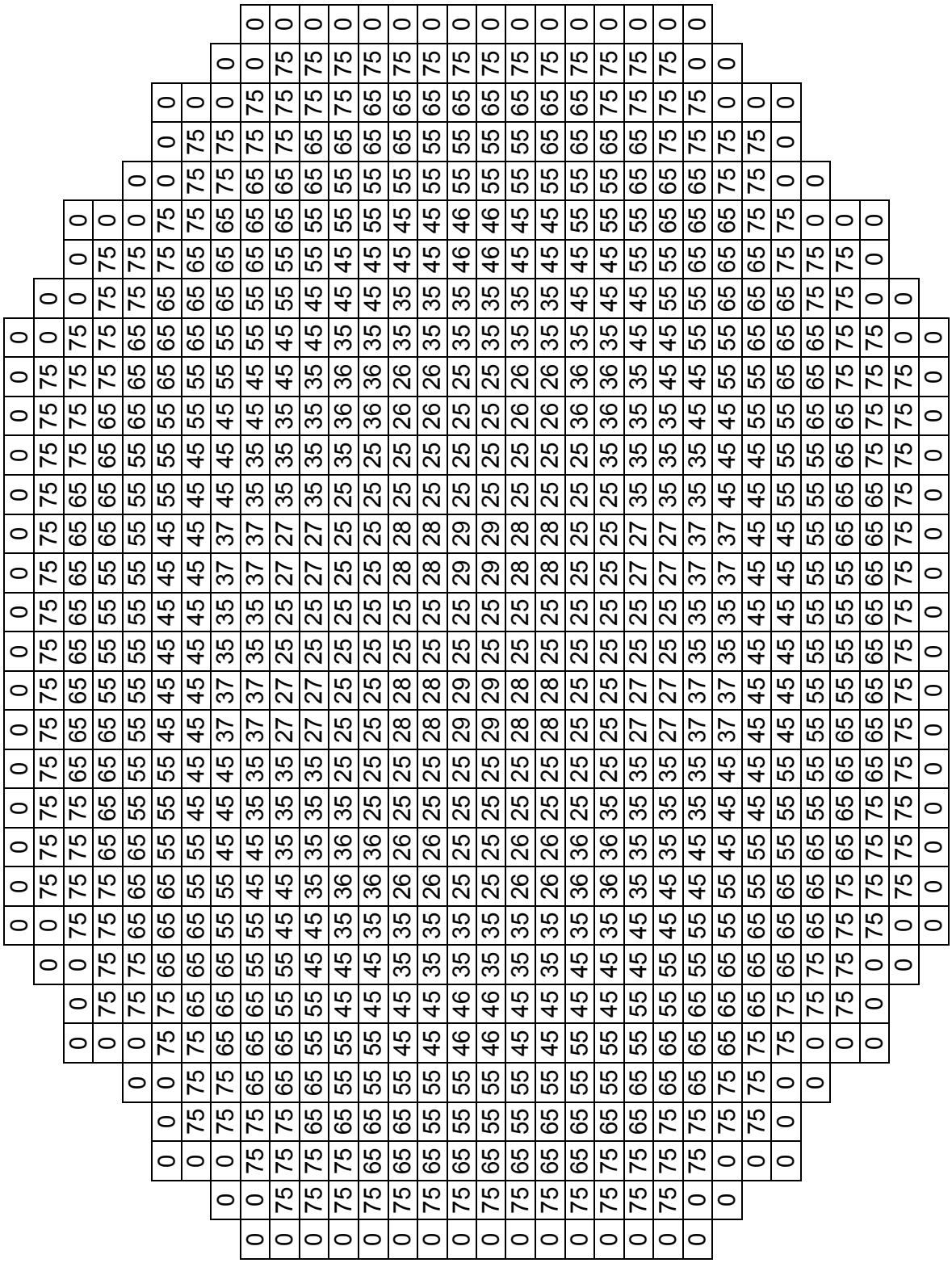

Figure 2.8 Mapping for ATWS-ED - 27 Channels

2.4.3 Numerics

Table 2.6 shows some options used in PARCS to improve convergence and avoid code crashes. The current choices were selected after extensive experimentation both by BNL and NRC staff. Previous attempts with different options led to the code calculating negative fluxes, which, in turn, led to code failure. The current model takes advantage of a more robust coarse-mesh finite-difference (CMFD) acceleration method recently implemented in PARCS (CMFD 2) [12]. Using this CMFD option automatically updates the nodal solver to NEMMG. A more robust linear solver (GMRES) was used. The temporal differencing scheme in PARCS is the theta method, and a value of theta of 0.6 was used to make the problem more implicit in time (default theta is 0.5). Finally, to run the calculation to completion, the extrapolation guess of the power at the end of the time step in PARCS was turned off (expo_opt F F).

Table 2.6 Numerical Options in PARCS

Numerical Option	ATWS-ED v.13
PARCS coarse-mesh finite-difference method	CMFD 2
PARCS nodal kernel	NEMMG
PARCS linear solver	GMRES (option 1)
PARCS exponential extrapolation option	Expo_opt=F F
PARCS implicitness (THETA)	(0.6 1.0 1.0)

2.5 MATLAB Script

Several modifications were made to the MATLAB script described in [2] to address the modeling changes in the CHAN components described in Section 2.3.2; all of them were made to the CHAN template. The MATLAB script developed for ATWS-ED was labeled Revision 12.

2.6 Summary of Modifications

The analysis of ATWS-ED transients utilizes not only a modified TRACE BWR/5 model but also a modified set of PARCS input options and cross-section set. Table 2.7 summarizes the differences between the TRACE/PARCS inputs for the ATWS-I and ATWS-ED analyses.

Table 2.7 Input Differences: ATWS-I versus ATWS-ED

	ATWS-I	ATWS-ED v.13
TRACE executable	V5.450-Fix-7M (Linux and PC 64-bit)	V5.540_fxValveChoke (Linux and PC 64-bit)
Number of channels	382	27
Lower plenum	Boron transport is treated with a finite-volume valve between levels 2 and 3, ring 2. The flow area between ring 1 and ring 2 in level 3 is blocked. The volume of the lower plenum is increased artificially by the presence of the finite- volume valve.	No valve is present in the lower plenum. Boron transport is treated using the revised methodology and additional control system.
Numerical integration	Semi-Implicit	SETS
Axial conduction scheme	Implicit	Implicit
Pressure boundary condition	Steamline BREAK pressure set to the long-term pressure inferred from TRACG runs to simulate turbine bypass	Steamline BREAK pressure set to turbine firststage inlet pressure
Representative channel signal variables	Since the number of channels and the numbering schemes differ, these vary between the models.	
Transient simulation time	400 s	2500 s
Heat capacity temperature limit	175ºF. Note, this does not affect transient calculation since turbine bypass is assumed.	160ºF
SRV characteristics	Operable SRVs are modeled as a single valve. Relief function is modeled, with setpoints based on NMP2 UFSAR nominal trip setpoints; internal losses are evaluated by TRACE. No safety function delays, 1.0 s opening time. Loss coefficient includes discharge-line losses (coefficient is 4.5)	Operable SRVs are grouped into five separate valves. Relief function is modeled, based on NMP2 EPU relief-mode analytical limit setpoints; internal losses are evaluated according to coefficients supplied in the TRACG input deck. A relief delay of 0.4 s incorporated, opening time of 0.5 s is assumed. K-loss factor is set to 0.786 based on NMP2 UFSAR
Feedwater controller	Level mismatch proportional gain is set to 5. Maximum feedwater flow = 2500 kg/s	Level mismatch proportional gain set to 10. Maximum feedwater flow = 2954.95 kg/s

	ATWS-I	ATWS-ED v.13
Vessel level tracking options	Level tracked in the DC and the separator region	Level tracked in the separator region, top of downcomer, and the jet pump region. No level tracking between feedwater sparger and top of active fuel (corresponds to levels 9 through 12 in ring 3)
Separators	Ideal with no carryover/carryunder	Ideal with 0.1% carryover, and 0.25% carryunder
Water rods	Forward- and reverse- loss coefficients are input	Reverse flow prevented at the water-rod inlet by applying a factor of 1E9 to the inlet reverse-flow loss coefficient
Suppression pool heat structures	None	Concrete surrounding the suppression pool is modeled with an adiabatic outer-wall boundary condition. The stainless-steel liner is neglected. The initial condition is isothermal at the analysis temperature for the suppression pool.
Suppression pool heat exchanger	One train of RHR in SP cooling mode	Two trains of RHR in SP cooling mode
Metal-water reaction	Off	Cathcart-Pawel (NMWRX=1)
Oxide layer	Not modeled (FOXLAYER=0)	Modeled to capture the best estimate of the dynamics of the metal-water reaction, FOXLAYER=1. Default oxide layer option applied (DOXLAYER) based on average oxide thickness at each cycle exposure point.
Axial conduction in fuel	Off	On (IAXCND=1)
Cladding rupture model	Off (NFCI=2)	On (NFCI=-13)
SLCS injection location	Core spray sparger in the upper plenum (level 10, into ring 2)	Below jet pump outlet nozzle (level 4, into ring 3)
Cross-section set	Rev. 3.2	Rev. 4.1

	ATWS-I	ATWS-ED v.13
PARCS noise options	Core-wide noise simulated. This necessitates calculating and supplying the file of harmonic shape in the transient calculation	No noise
PARCS coarse-mesh finite-difference method	CMFD 1 (default)	CMFD 2
PARCS nodal kernel	HYBRID	NEMMG
PARCS linear solver	biCGSTAB (option 2)	GMRES (option 1)
PARCS exponential extrapolation option	Expo_opt=F T (default)	Expo_opt=F F
PARCS implicitness (THETA)	Default (0.5 1.0 0.5)	(0.6 1.0 1.0)

3 STEADY-STATE RESULTS

The MELLLA+ domain expands the operating domain of a BWR up to 120% of the originally licensed thermal power (the result of an extended power uprate, or EPU) for core flows as low as 80% of the rated value. In the work reported here, three "reference" models were set up at three different exposures: beginning-of-cycle (BOC), peak-hot-excess-reactivity (PHE), and end-of-full-power-life (EOFPL). The thermal power for these three models is 3988 MW, or 120% of the original licensed thermal power. The design of the reactor core is based on an equilibrium cycle of GE14 fuel. The BOC and PHE reference models have 85% of rated core flow, while the EOFPL reference model had one of 105%. Two additional EOFPL models were developed: a "low flow" EOFPL model with 85% of rated flow, and one using spectrally corrected moderator density information.

Two "low-low" flow models also were developed; one for BOC and one for EOFPL. The core flow for these was 75% of the rated flow, i.e., lower than the minimum MELLLA+ flowrate. This lower rate should result in a higher power after the dual recirculation pump trip (2RPT), and be bounding.

This section summarizes the results of the coupled TRACE/PARCS steady-state calculations and offers comparisons with nodal power information received from GEH [13] for the reference models at BOC, PHE, and EOFPL. Additionally, it presents results for the models with decreased core flow for BOC and EOFPL, and a model using spectrally corrected moderator density history information for EOFPL. TRACE/PARCS Version 5.540 (with an additional fix for single junction (SJC) valve choking) was used. The results are summarized in Sections 3.1, 3.2, and 3.3, respectively, for BOC, PHE, and EOFPL. Axially and radially averaged power distributions are cited in these sections.

The steady-state calculations were carried out in two steps, as described in Section 2.1. The convergence of the coupled steady-state solution was confirmed by running a null- transient for ten seconds.

3.1 ATWS-ED 27-Channel BOC Model

At BOC, approximately half of the fuel bundles are fresh and half are once-burned, with exceptions in the periphery of the core where some fuel bundles are twice-burned. The power shape is bottom-peaked, and the control rods are partially inserted to shape the power and to control the excess reactivity. The multiplication constant, k_{eff}, (henceforth referred to as the eigenvalue) calculated for the coupled steady-state is 1.01745.

3.1.1 Initial and Boundary Conditions

Table 3.1 compares the initial values of reactor power and some key thermal-hydraulic parameters that result from the TRACE/PARCS null transient calculation for ten seconds, to the reference values described in [2]. As shown in the table, the calculated steady-state values agree well with the reference ones.

Table 3.1 Comparison of Steady-State Thermal-Hydraulic Parameters at BOC

Parameter	Units	TRACE/PARCS Value	Reference Value [14]	Diff. (%)
Core Power	MWt	3,988	3,988	0.0
Steam Dome Pressure	kPa	7,141	7,136	0.1
Main Steamline Flow	kg/s	2,219	2,222	-0.1
Total Core Flow	kg/s	11,625	11,620	-0.1
Feedwater Flow	kg/s	2,219	2,222	-0.1
Feedwater Temperature	K	500	500	0.0
Downcomer Level	m	14.3	14.5	-1.0
Inlet Temperature	K	550	not available	-

3.1.2 Radial Power Distribution

One characteristic of an EPU core is the flattening of the radial power distribution [1]. It is apparent in the normalized axially averaged radial power calculated by PARCS, and shown in each box for a quarter-core (Figure 3.1). The shaded boxes in the figure correspond to partially rodded locations. The darker color is for rods that are inserted more than 70%, and the lighter shade corresponds to rods inserted less than 25%; the effect of the former is to decrease the power in those locations.

The peak relative bundle power is 1.30 (in bold in Figure 3.1) and occurs in a location included in a channel group represented by CHAN 371. The channel group with maximum average bundle power is CHAN 461.

							0.33	0.37	0.41	0.52	0.49	0.59	0.60
						0.41	0.61	0.71	0.74	0.79	0.81	0.85	0.85
				0.31	0.49	0.65	0.80	0.85	0.92	1.01	1.07	1.04	1.01
				0.45	0.68	0.79	0.92	0.98	1.06	1.11	1.18	1.20	1.19
			0.50	0.79	0.85	0.96	1.02	1.04	1.17	1.24	1.25	1.26	1.21
		0.31	0.45	0.79	0.91	1.04	1.08	1.08	1.13	1.22	1.26	1.29	1.28	1.28
		0.49	0.68	0.85	1.04	1.14	1.18	1.21	1.22	1.24	1.28	1.28	**1.30**	1.29
	0.41	0.65	0.79	0.96	1.08	1.18	1.22	1.22	1.22	1.28	1.24	1.22	1.19	1.23
0.33	0.61	0.80	0.92	1.02	1.07	1.21	1.22	1.15	1.19	1.23	1.20	0.98	0.96	1.16
0.37	0.71	0.85	0.98	1.04	1.13	1.22	1.21	1.19	1.16	1.23	1.16	0.95	0.93	1.13
0.41	0.74	0.92	1.06	1.17	1.22	1.24	1.27	1.21	1.22	1.20	1.21	1.13	1.11	1.13
0.52	0.78	1.01	1.11	1.24	1.25	1.27	1.23	1.19	1.14	1.21	1.22	1.12	1.09	1.12
0.48	0.81	1.07	1.18	1.25	1.29	1.26	1.20	0.97	0.94	1.13	1.12	0.93	0.91	1.08
0.59	0.85	1.04	1.20	1.26	1.28	1.28	1.18	0.96	0.93	1.11	1.08	0.90	0.90	1.07
0.60	0.85	1.01	1.20	1.23	1.30	1.29	1.23	1.16	1.13	1.12	1.11	1.05	1.04	1.06

Figure 3.1 Axially Averaged Radial Power Distribution at BOC

The calculated root mean square (RMS) of the difference in relative bundle power between PARCS and GEH results is 0.03 for the whole core; the agreement between PARCS and GEH is good. To quantify “how good” the agreement, it is necessary to know the uncertainty in the corresponding methods used to generate each result. GEH methods for MELLLA+ were

evaluated by the NRC staff [15]. For high power-to-flow ratios, the GEH uncertainty in the shape of the radial power is based on using data collected while calibrating the local power range monitors (LPRMs) using the traveling incore probe (TIP) system. The corresponding number for TRACE/PARCS has not been derived. However, PARCS/PATHS [16] has an uncertainty of approximately 8%; and this uncertainty is expected to be essentially the same as for TRACE/PARCS.

3.1.3 Axial Power Distribution

The normalized, radially averaged axial power calculated by PARCS is shown in Figure 3.2. As described in [2], there are 25, 15.24-cm axial nodes for a total core height of 381 cm. As expected, the power is bottom-peaked, consistent with the axial void distribution, or the corresponding moderator density (Figure 3.3). The shape of the axial power also is influenced by the design of the fuel bundle. The discontinuity observed at 267 cm reflects the insertion to 259 cm of twelve control rods into the core. The RMS of the difference between PARCS and GEH results is 0.1 for all axial nodes. As with the radial shape, there have been no comparisons of data to assess the expected uncertainty in TRACE/PARCS. However, results for PARCS/PATHS [16] give an expected uncertainty of 4%.

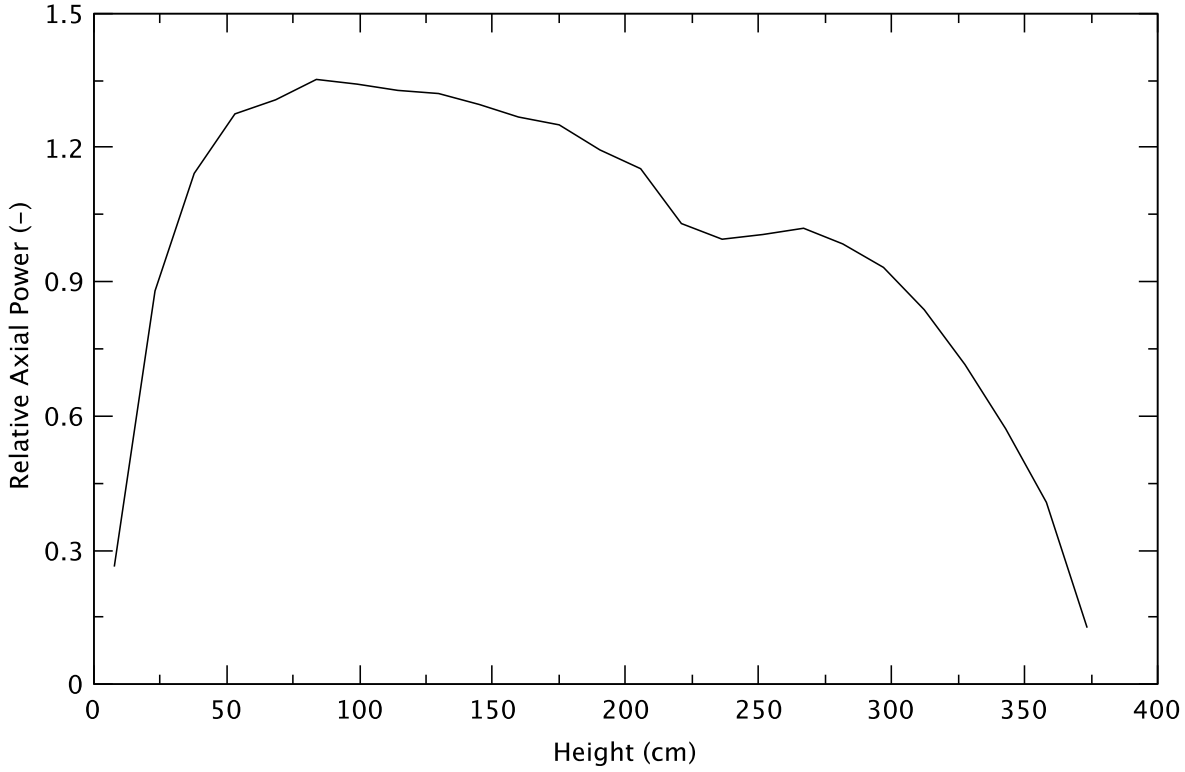

Figure 3.2 Radially Averaged Axial Power Distribution at BOC

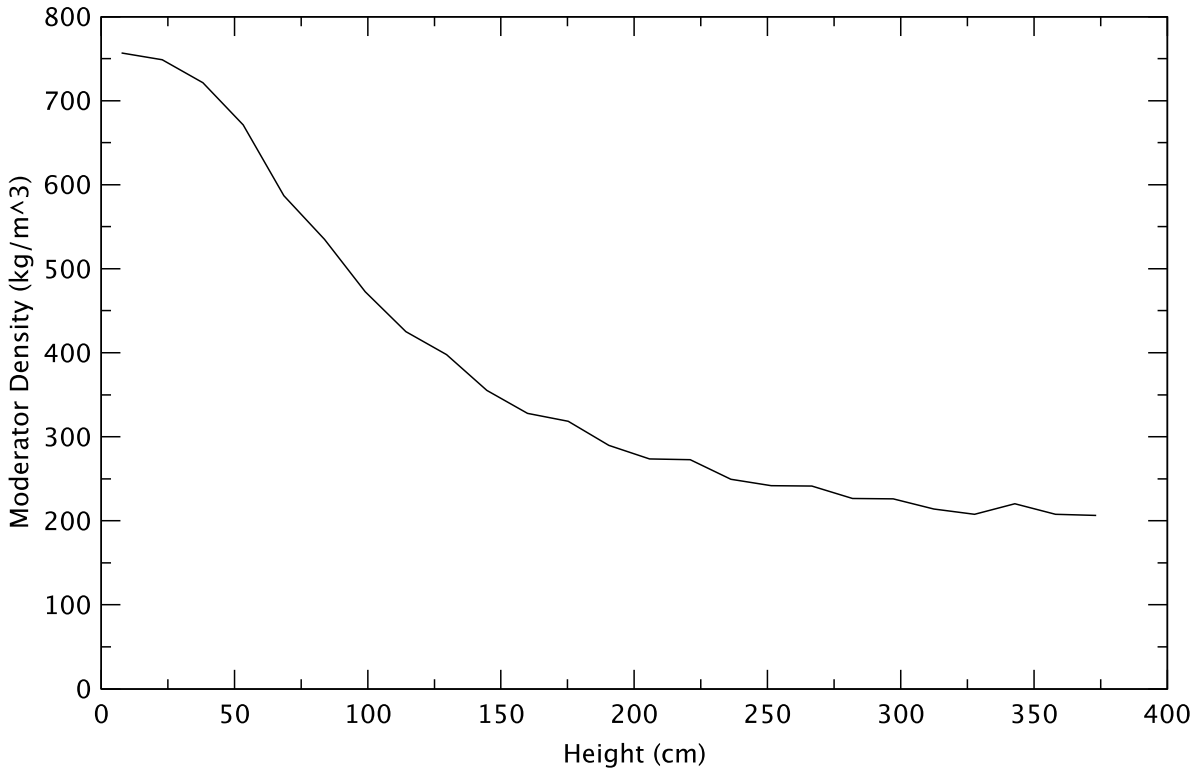

Figure 3.3 Radially Averaged Axial Moderator Density at BOC

3.1.4 Effect of Reduced Core Flow (75% Flow)

As stated, MELLLA+ operation expands the operating domain of a BWR up to 120% of the originally licensed thermal power for core flows as low as 80% of the rated value. A model with 75% of rated flow is outside the MELLLA+ domain, but can be considered to be bounding as it weakens the impact of a trip of the recirculation pumps by reducing the induced negative reactivity insertion. The reduced core flow will be used in a sensitivity analysis and included in a subsequent report in this series of ATWS analyses.

Table 3.2 compares several key thermal-hydraulic and neutronic parameters. Except for total core flow, they are comparable (recalling the reference model is for an 85% core flow case).

Figure 3.4 compares the axially averaged radial power distribution for the base BOC model (85% of rated flow), and a BOC model with reduced core flow (75% of rated flow). The impact of reducing the flow on the radial power is minimal: the peak power stays in the same location, a bundle located in the channel group represented by CHAN 371 (outlined in bold in Figure 3.4), the channel group with maximum average bundle power still is CHAN 461, and the maximum difference for the whole core is less than 1% for interior bundles, or less than 2% for peripheral bundles. The RMS difference for the whole core is less than 0.01.

Table 3.2 Comparison of Steady-State Parameters at BOC - Effect of Reduced Core Flow

Parameter	Units	Reference Model Value	75% Flow Model Value
K_{eff}	-	1.01745	1.01412
Core Power	MWt	3,988	3,988
Steam Dome Pressure	kPa	7,141	7,141
Main Steamline Flow	kg/s	2,219	2,220
Total Core Flow	kg/s	11,625	10,252
Feedwater Flow	kg/s	2,219	2,220
Feedwater Temperature	K	500	500
Downcomer Level	m	14.3	14.3
Inlet Temperature	K	550	549

Figure 3.5 shows the radially averaged axial power distribution for both the base and the reduced core flow cases. The axial power distributions are very similar, both peaking at axial node 6. The power difference for the node with highest power is less than 0.1%, and the RMS is 0.02. As is evident, the power is slightly more bottom-peaked when the core flow is reduced, consistent with the axial moderator density distributions (Figure 3.6). Reducing the flow shifts the boiling boundary downward, which causes the power to also shift downward.

							0.33 *0.33* -1.65	0.37 *0.38* -1.37	0.41 *0.42* -1.35	0.52 *0.53* -1.29	0.49 *0.49* -1.30	0.59 *0.59* -1.21	0.60 *0.61* -1.19
		Base *75%FI* Diff(%)				0.41 *0.42* -1.42	0.61 *0.61* -0.51	0.71 *0.72* -0.42	0.74 *0.74* -0.45	0.79 *0.79* -0.17	0.81 *0.82* -0.22	0.85 *0.85* -0.11	0.85 *0.85* -0.24
				0.31 *0.31* -1.85	0.49 *0.50* -1.15	0.65 *0.66* -0.35	0.80 *0.80* -0.23	0.85 *0.86* -0.15	0.92 *0.93* -0.14	1.01 *1.02* -0.04	1.07 *1.07* 0.14	1.04 *1.04* 0.00	1.01 *1.01* 0.08
				0.45 *0.46* -1.19	0.68 *0.68* -0.37	0.79 *0.79* -0.10	0.92 *0.92* 0.09	0.98 *0.98* 0.24	1.06 *1.06* 0.10	1.11 *1.11* 0.21	1.18 *1.18* 0.08	1.20 *1.20* 0.20	1.19 *1.19* 0.03
			0.50 *0.51* -1.24	0.79 *0.79* -0.19	0.85 *0.85* -0.01	0.96 *0.96* 0.18	1.02 *1.01* 0.65	1.04 *1.04* 0.49	1.17 *1.17* 0.37	1.24 *1.24* 0.15	1.25 *1.25* 0.18	1.26 *1.26* 0.00	1.21 *1.21* 0.19
		0.31 *0.31* -1.85	0.45 *0.46* -1.19	0.79 *0.79* -0.19	0.91 *0.91* 0.22	1.04 *1.03* 0.23	1.08 *1.07* 0.46	1.08 *1.07* 0.56	1.13 *1.12* 0.66	1.22 *1.22* 0.18	1.26 *1.25* 0.23	1.29 *1.29* 0.01	1.28 *1.28* 0.12	1.28 *1.28* -0.01
		0.49 *0.50* -1.15	0.68 *0.68* -0.38	0.85 *0.85* 0.00	1.04 *1.03* 0.23	1.14 *1.14* 0.46	1.18 *1.17* 0.36	1.21 *1.20* 0.51	1.22 *1.22* 0.25	1.24 *1.24* 0.29	1.28 *1.28* 0.03	1.28 *1.28* 0.14	**1.30** ***1.30*** -0.08	1.29 *1.29* 0.08
	0.41 *0.42* -1.42	0.65 *0.66* -0.35	0.79 *0.79* -0.10	0.96 *0.96* 0.19	1.08 *1.07* 0.46	1.18 *1.17* 0.35	1.22 *1.22* 0.50	1.22 *1.22* 0.27	1.22 *1.21* 0.35	1.28 *1.27* 0.11	1.24 *1.24* 0.15	1.22 *1.22* -0.14	1.19 *1.19* -0.02	1.23 *1.24* -0.19
0.33 *0.33* -1.65	0.61 *0.61* -0.51	0.80 *0.80* -0.23	0.92 *0.92* 0.09	1.02 *1.01* 0.65	1.07 *1.07* 0.56	1.21 *1.20* 0.51	1.22 *1.22* 0.27	1.15 *1.15* 0.53	1.19 *1.19* 0.34	1.23 *1.22* 0.26	1.20 *1.20* -0.08	0.98 *0.98* 0.07	0.96 *0.96* -0.19	1.16 *1.16* 0.06
0.37 *0.38* -1.37	0.71 *0.72* -0.42	0.85 *0.86* -0.15	0.98 *0.98* 0.23	1.04 *1.03* 0.48	1.13 *1.12* 0.66	1.22 *1.22* 0.24	1.21 *1.21* 0.35	1.19 *1.18* 0.34	1.16 *1.15* 0.47	1.23 *1.23* 0.05	1.16 *1.16* 0.03	0.95 *0.95* -0.15	0.93 *0.93* -0.02	1.13 *1.13* -0.16
0.41 *0.42* -1.35	0.74 *0.74* -0.46	0.92 *0.92* -0.14	1.06 *1.06* 0.09	1.17 *1.17* 0.37	1.22 *1.21* 0.18	1.24 *1.23* 0.28	1.27 *1.27* 0.11	1.21 *1.20* 0.24	1.22 *1.22* 0.02	1.20 *1.19* 0.13	1.21 *1.21* 0.04	1.13 *1.13* 0.07	1.11 *1.12* -0.16	1.13 *1.13* 0.04
0.52 *0.53* -1.29	0.78 *0.79* -0.18	1.01 *1.01* -0.05	1.11 *1.11* 0.21	1.24 *1.24* 0.14	1.25 *1.25* 0.23	1.27 *1.27* 0.03	1.23 *1.23* 0.15	1.19 *1.19* -0.11	1.14 *1.14* 0.02	1.21 *1.21* 0.03	1.22 *1.21* 0.17	1.12 *1.12* -0.12	1.09 *1.09* 0.00	1.12 *1.12* -0.15
0.48 *0.49* -1.30	0.81 *0.82* -0.23	1.07 *1.07* 0.12	1.18 *1.18* 0.08	1.25 *1.25* 0.18	1.29 *1.29* 0.01	1.26 *1.26* 0.19	1.20 *1.20* -0.08	0.97 *0.97* 0.07	0.94 *0.94* -0.16	1.13 *1.13* 0.07	1.12 *1.12* -0.12	0.93 *0.93* -0.04	0.91 *0.91* -0.25	1.08 *1.08* -0.04
0.59 *0.59* -1.23	0.85 *0.85* -0.12	1.04 *1.04* -0.01	1.20 *1.20* 0.19	1.26 *1.26* -0.02	1.28 *1.28* 0.11	1.28 *1.28* -0.02	1.18 *1.18* 0.03	0.96 *0.96* -0.19	0.93 *0.93* -0.02	1.11 *1.11* -0.17	1.08 *1.08* -0.02	0.90 *0.91* -0.27	0.90 *0.90* -0.07	1.07 *1.07* -0.21
0.60 *0.61* -1.21	0.85 *0.85* -0.25	1.01 *1.01* 0.07	1.20 *1.20* 0.01	1.23 *1.23* 0.09	1.30 *1.30* -0.08	1.29 *1.28* 0.07	1.23 *1.23* -0.19	1.16 *1.16* 0.06	1.13 *1.13* -0.16	1.12 *1.12* 0.03	1.11 *1.11* -0.15	1.05 *1.05* -0.08	1.04 *1.04* -0.25	1.06 *1.06* -0.03

Figure 3.4 Radial Power Distribution at BOC - Effect of Reduced Core Flow

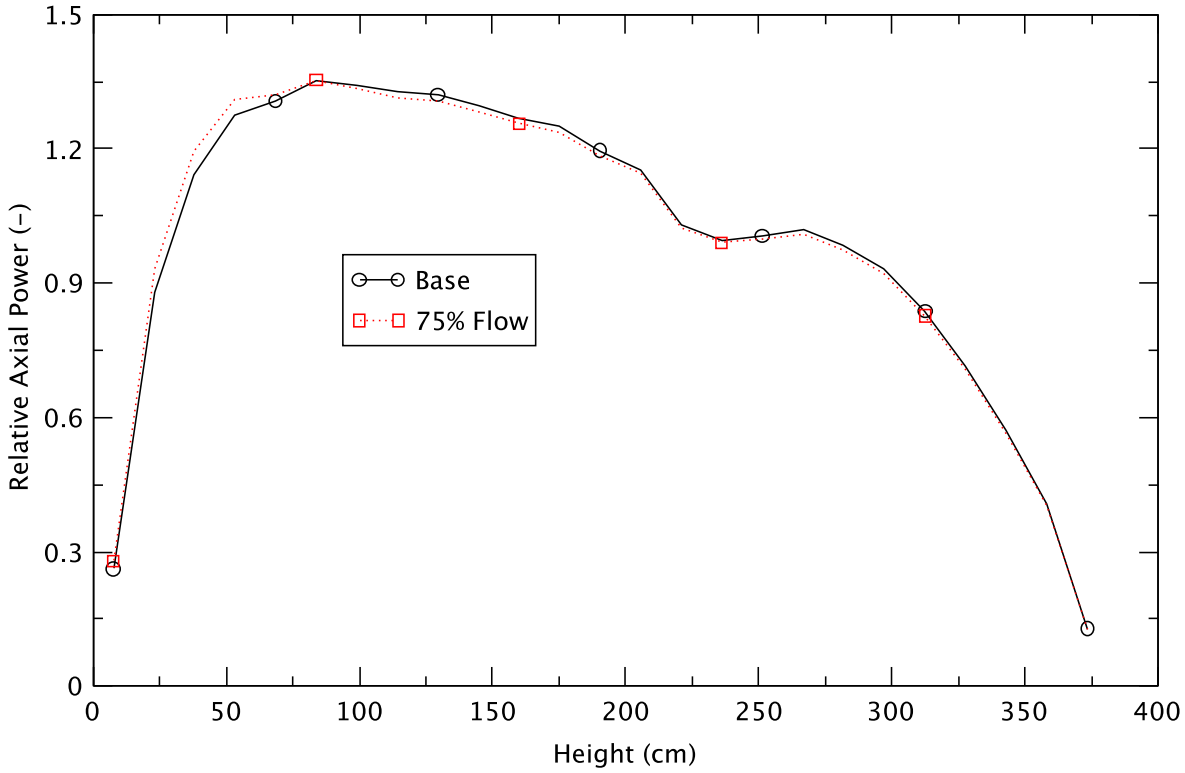

Figure 3.5 Axial Power Distribution at BOC - Effect of Reduced Core Flow

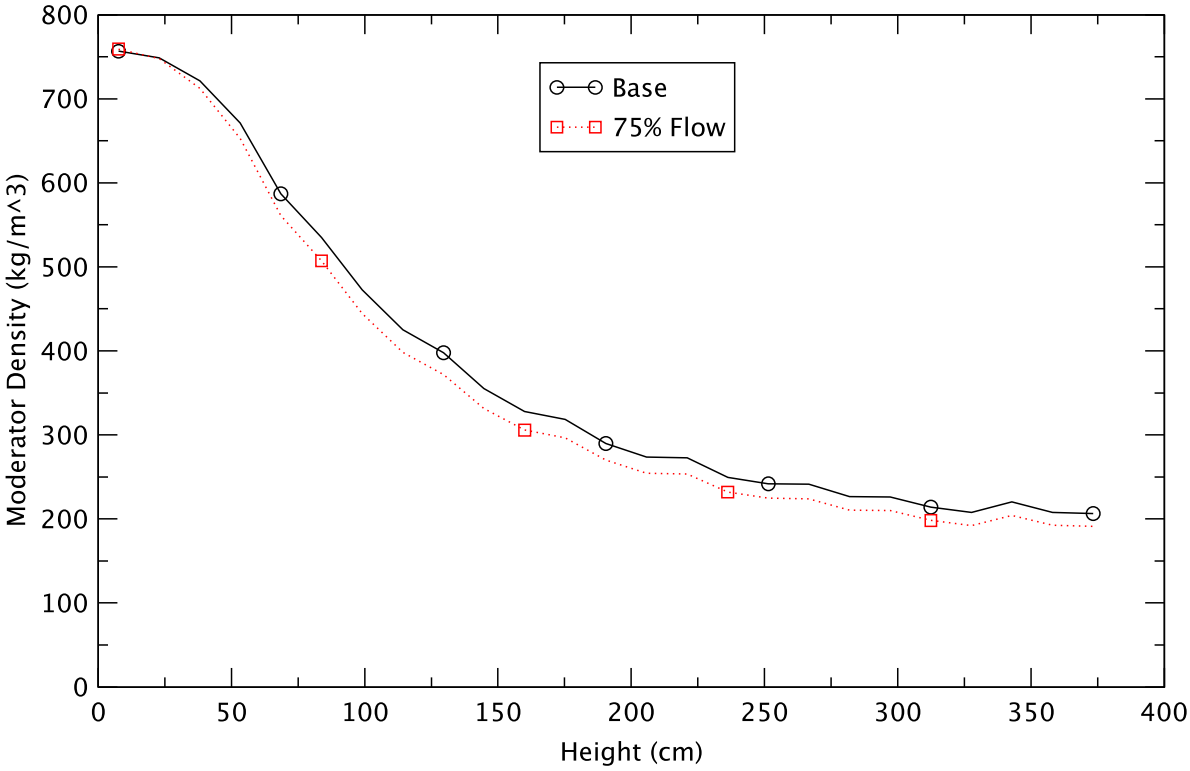

Figure 3.6 Axial Moderator Density at BOC - Effect of Reduced Core Flow

3.2 ATWS-ED 27-Channel PHE Model

PHE corresponds to the point in the cycle with peak excess reactivity. It takes place close to the middle of the cycle, after some of the gadolinia in the fresh fuel has been depleted. The power still is bottom-peaked, and control rods are partially or fully inserted to counter the excess reactivity. The eigenvalue is 1.010378.

3.2.1 Initial and Boundary Conditions

Table 3.3 compares TRACE/PARCS to reference values for the initial values of reactor power and key thermal-hydraulic parameters at PHE. The results for TRACE/PARCS come from a null transient calculation for ten seconds. As shown in the table, the calculated steady-state values agree well with the reference ones.

Table 3.3 Comparison of Steady-State Thermal-Hydraulic Parameters at PHE

Parameter	Units	TRACE/PARCS Value	Reference Value [14]	Diff. (%)
Core Power	MWt	3,988	3,988	0.0
Steam Dome Pressure	kPa	7,141	7,136	0.1
Main Steamline Flow	kg/s	2,219	2,222	-0.1
Total Core Flow	kg/s	11,612	11,620	-0.1
Feedwater Flow	kg/s	2,219	2,222	-0.1
Feedwater Temperature	K	500	500	0.0
Downcomer Level	M	14.3	14.5	-1.0
Inlet Temperature	K	550	not available	-

3.2.2 Radial Power Distribution

Figure 3.7 shows the normalized, axially averaged radial power distribution for PHE, calculated by PARCS. In the central part of the core there is an apparent checkerboard pattern, with alternating ‘high’- (around 1.3) and ‘low’- (around 1.1) powered assemblies, except for those locations where the control rods are inserted. The low-powered assemblies are ones that previously were burned for a full cycle, while the high-powered assemblies were fresh at the beginning of the cycle, and have had their gadolinia depleted. The core is EPU, and overall the shape of the radial power is relatively flat except at the periphery. The shaded boxes correspond to fully or partially rodded locations. The darker shade represents rods that are inserted more than 70%, and the lighter shade corresponds to rods inserted less than 25%. The effect of the control rods that are significantly inserted is to considerably decrease the power. The peak relative bundle power is 1.43, occurring in a location in Channel 451 (outlined in bold in Figure 3.7), and the channel with maximum average bundle power is Channel 281. Overall, the agreement between PARCS and GEH is reasonable, the RMS for the difference of powers being 0.06.

3.2.3 Axial Power Distribution

Figure 3.8 shows the normalized, radially averaged axial power calculated by PARCS. The power is bottom-peaked, more so than at BOC because of the depletion of some of the gadolinia, especially in the bottom part of the fresh fuel bundles. The presence of the gadolinia absorber contributes to a local suppression of power. The shape of axial power is reasonably

consistent with the axial profile of the moderator density in Figure 3.9. The effect of the design of the fuel bundle also is evident. The RMS of the difference in the axial powers calculated by PARCS and those obtained from GEH is 0.07, i.e. the agreement between PARCS and GEH is reasonable.

							0.33	0.37	0.39	0.45	0.39	0.44	0.44
						0.44	0.64	0.72	0.77	0.70	0.71	0.64	0.66
					0.34	0.55	0.71	0.93	0.98	1.00	0.99	0.85	0.86	0.71
					0.50	0.82	0.98	1.12	1.01	1.16	0.97	1.07	0.88	0.91
				0.52	0.83	1.03	1.19	1.14	1.28	1.11	1.24	1.02	1.05	0.72
		0.34	0.51	0.83	0.96	1.22	1.12	1.35	1.18	1.33	1.11	1.22	0.97	0.88
		0.56	0.83	1.04	1.23	1.17	1.38	1.21	1.37	1.13	1.28	1.09	1.20	1.00
	0.44	0.72	1.00	1.20	1.13	1.39	1.23	1.40	1.13	1.25	1.05	1.24	1.08	1.22
0.34	0.65	0.94	1.13	1.15	1.37	1.23	**1.43**	1.18	1.28	0.79	0.90	1.04	1.27	1.04
0.38	0.74	1.00	1.02	1.30	1.20	1.41	1.20	1.38	1.09	0.92	0.79	1.24	1.11	1.24
0.41	0.79	1.03	1.18	1.13	1.33	1.16	1.37	1.16	1.31	1.09	1.26	1.12	1.33	1.13
0.48	0.73	1.03	1.00	1.25	1.08	1.24	1.09	1.30	1.15	1.34	1.22	1.36	1.13	1.27
0.42	0.75	0.91	1.13	1.05	1.16	0.83	0.96	1.08	1.33	1.11	1.30	1.16	1.28	0.87
0.48	0.70	0.95	0.97	1.14	0.97	0.90	0.82	1.23	1.14	1.30	1.12	1.35	1.09	0.99
0.48	0.73	0.80	1.07	0.97	1.11	0.96	1.13	1.08	1.35	1.19	1.39	1.18	1.27	1.04

Figure 3.7 Axially Averaged Radial Power Distribution at PHE

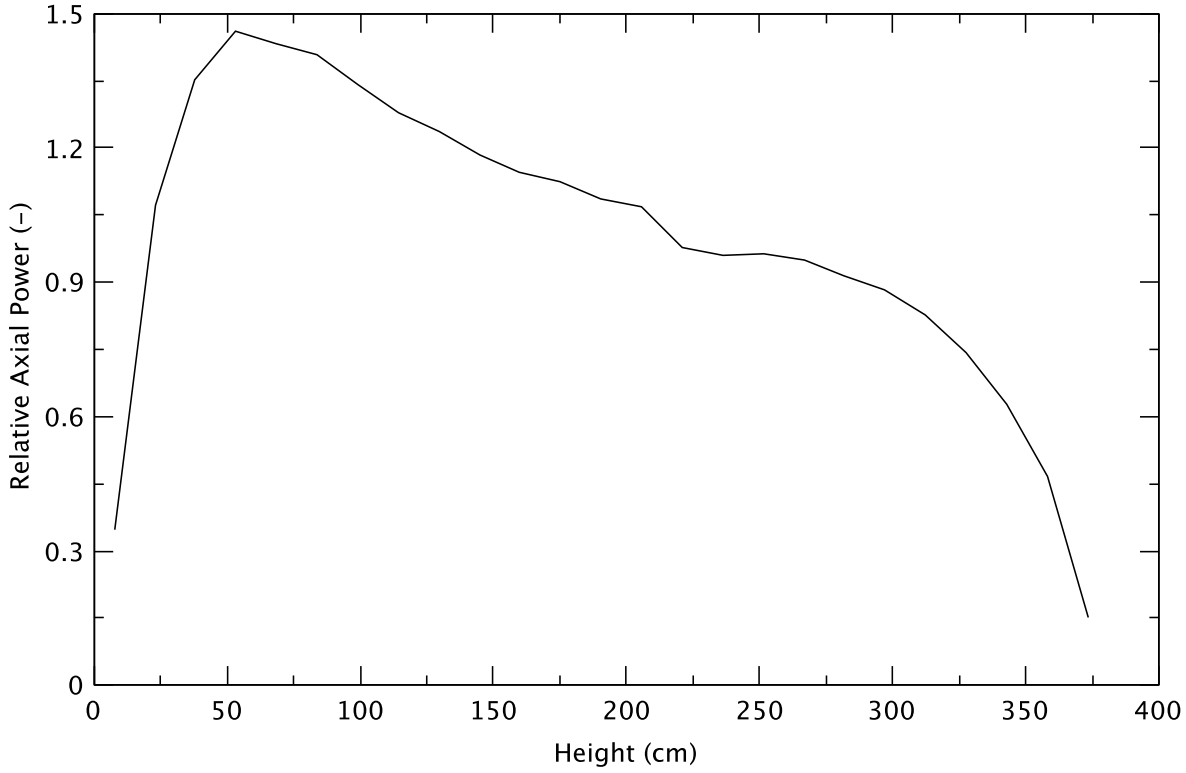

Figure 3.8 Radially Averaged Axial Power Distribution at PHE

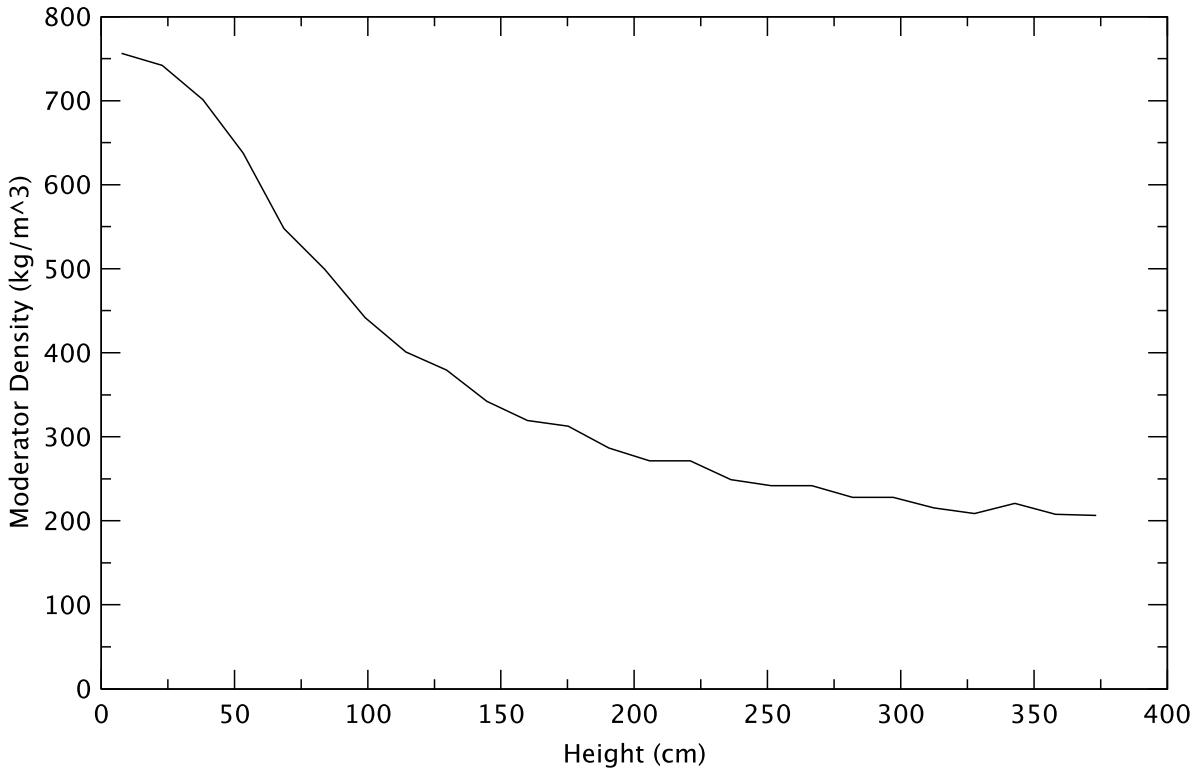

Figure 3.9 Radially Averaged Axial Moderator Density at PHE

3.3 ATWS-ED 27-Channel EOFPL Model

EOFPL represents end-of-full-power-life near the end of the reactor's fuel cycle. It is the last exposure point in the cycle where power is maintained at 120% of the original power, which is realized by operating at the highest core flowrate. This condition is characterized by a top-peaked axial power shape, all control rods out (ARO) configuration, and increased core flow to 105% of rated. The eigenvalue for the coupled steady-state calculation is 1.009419.

3.3.1 Initial and Boundary Conditions

Table 3.4 shows the initial values of reactor power and some key thermal-hydraulic parameters, which are the results of comparing the TRACE/PARCS coupled null transient calculation for ten seconds to reference values. The calculated steady-state values agree well with the reference ones.

Table 3.4 Comparison of Steady-State Thermal-Hydraulic Parameters at EOFPL

Parameter	Units	TRACE/PARCS Value	Reference Value [14]	Diff. (%)
Core Power	MWt	3,988	3,988	0.0
Steam Dome Pressure	kPa	7,141	7,136	0.1
Main Steamline Flow	kg/s	2,219	2,222	-0.1
Total Core Flow	kg/s	14,338	14,350	-0.1
Feedwater Flow	kg/s	2,219	2,222	-0.1
Feedwater Temperature	K	500	500	0.0
Downcomer Level	m	14.3	14.5	-1.0
Inlet Temperature	K	552	not available	-

3.3.2 Radial Power Distribution

Figure 3.10 shows the normalized, axially averaged radial power distribution calculated by PARCS for EOFPL. As for PHE, in the central part of the core, a checkerboard pattern is distinguishable, with alternating 'high'- (around 1.2) and 'low'- (around 1.0) powered assemblies. Overall, the radial power shape is flat, characteristic of an EPU core. The peak relative bundle power is 1.28, found in a bundle located in the channel group represented by CHAN 451 (printed in bold in Figure 3.10). The channel group with maximum average bundle power is CHAN 371. The RMS value for the difference in powers between PARCS and GEH is 0.04 for all 764 assemblies, which implies the agreement is good.

							0.35	0.39	0.43	0.48	0.42	0.47	0.48
						0.45	0.67	0.78	0.89	0.76	0.83	0.72	0.81
					0.35	0.56	0.73	1.03	1.09	1.11	1.10	0.92	1.02	0.82
					0.49	0.90	1.08	1.18	0.99	1.21	0.98	1.17	0.98	1.14
				0.49	0.79	1.08	1.21	1.08	1.26	1.06	1.24	1.03	1.21	0.99
		0.35	0.49	0.79	0.91	1.18	1.02	1.26	1.07	1.26	1.04	1.25	1.04	1.25
		0.56	0.90	1.08	1.18	1.04	1.25	1.06	1.26	1.05	**1.28**	1.04	1.26	1.04
	0.45	0.73	1.08	1.21	1.02	1.25	1.05	1.25	1.03	1.26	1.03	1.27	1.04	1.26
0.35	0.67	1.03	1.18	1.08	1.26	1.06	1.24	1.02	1.24	1.02	1.26	1.02	1.25	1.01
0.39	0.77	1.09	0.99	1.25	1.07	1.25	1.02	1.24	1.02	1.25	1.02	1.24	1.01	1.22
0.42	0.88	1.11	1.21	1.06	1.25	1.05	1.26	1.02	1.26	1.03	1.25	1.00	1.22	1.00
0.48	0.76	1.10	0.97	1.23	1.04	1.27	1.03	1.26	1.02	1.25	1.07	1.22	0.99	1.22
0.42	0.82	0.91	1.16	1.03	1.24	1.03	1.26	1.02	1.24	1.00	1.22	0.99	1.21	0.99
0.47	0.72	1.02	0.98	1.20	1.03	1.26	1.04	1.24	1.00	1.22	0.99	1.21	0.99	1.21
0.48	0.80	0.82	1.13	0.98	1.25	1.03	1.26	1.01	1.21	0.99	1.22	0.99	1.21	0.98

Figure 3.10 Axially Averaged Radial Power Distribution at EOFPL

3.3.3 Axial Power Distribution

The normalized, radially averaged axial power calculated by PARCS is shown in Figure 3.11. As expected, the power is top-peaked; the fuel in the bottom of the core has been depleted more than the fuel in the top. The moderator density (Figure 3.12) is slightly higher at the outlet

than at BOC or PHE because the core flow has been increased from 85% to 105% to maintain the power level. The axial power has an unexplained shoulder at around 40 cm. The shape of the axial power also shows a depression at around 220 cm that reflects the fuel geometry. The RMS of the difference of axial powers calculated by PARCS and GEH for all nodes is 0.07, indicating reasonable agreement in view of the relatively high uncertainties associated with predicting the shape of axial power.

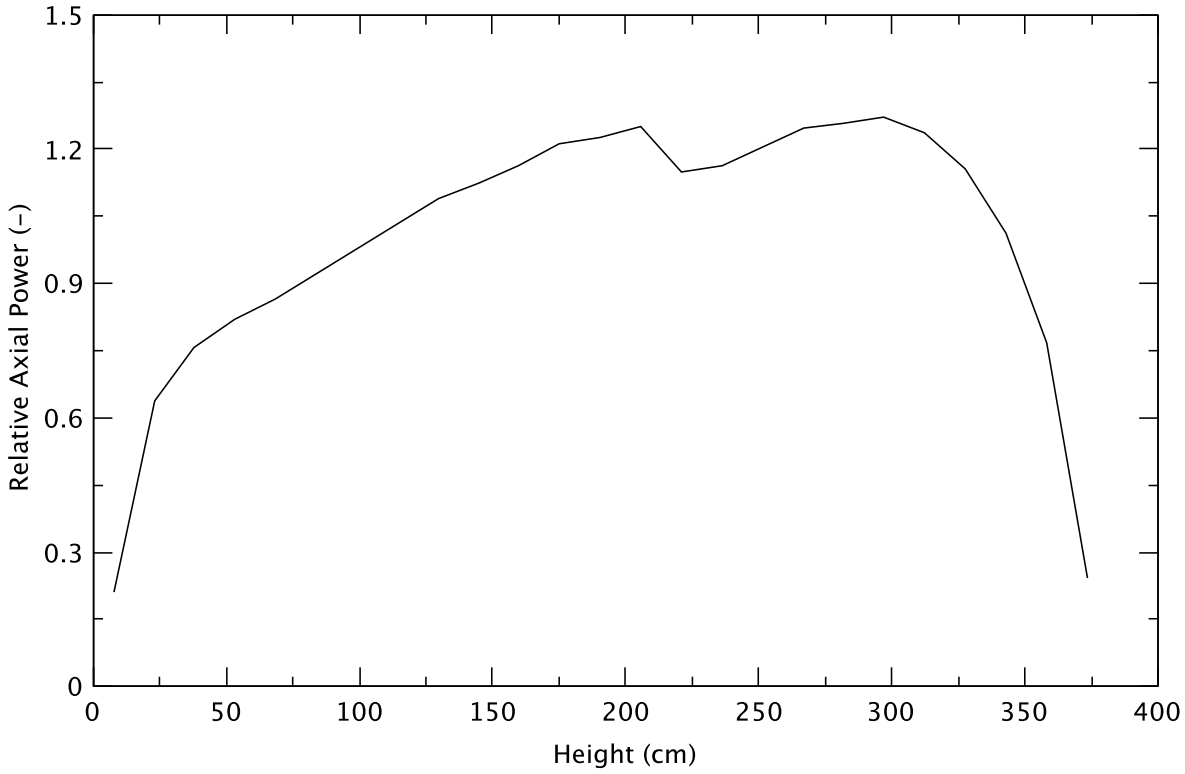

Figure 3.11 Radially Averaged Axial Power Distribution at EOFPL

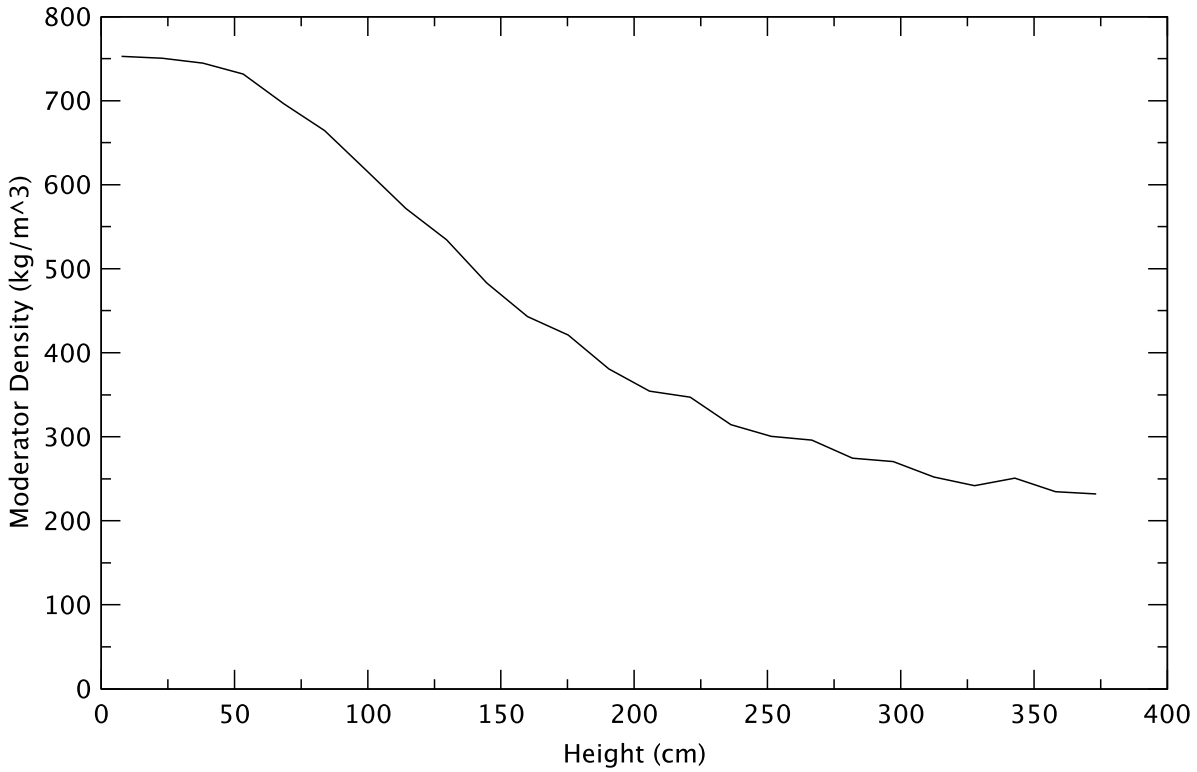

Figure 3.12 Radially Averaged Axial Moderator Density at EOFPL

3.3.4 Effect of Spectrally Corrected Void History

The cross sections used by PARCS depend on the instantaneous variables moderator density, fuel temperature, and boron concentration. They also depend on exposure to take into account burnup, and one or more other "history " parameters to help correct for the effect of the change in energy spectrum during burnup. The history parameter used to generate the cross sections for PARCS is moderator density history (equivalent to void history, UH). However, another parameter that might be used is control-rod-position history.

GEH has an approach whereby they account for the control rod history (and perhaps reflector effects) by changing the void history to provide the same effect. Hence, to test the effect of this additional history, the UH distribution used with the cross section set in PARCS was replaced with a "void history spectrally corrected" (UHSPH) distribution from GEH. This UHSPH will be used in a sensitivity analysis that will be reported subsequently in this series.

Table 3.5 shows that the main thermal-hydraulic and neutronic parameters from the reference EOFPL model (with the UH moderator density history) is almost indistinguishable from the model that uses the spectrally corrected moderator density history (UHSPH). Figure 3.13 and Figure 3.14, respectively, compare the radial and axial power for the PARCS calculations, using the UH moderator density history and the UHSPH moderator density history. They are virtually identical.

Table 3.5 Comparison of Steady-State Thermal-Hydraulic Parameters at EOFPL - Effect of Void History

Parameter	Units	Reference UH Model Value	UHSPH Model Value
Core Power	MWt	3,988	3,988
Steam Dome Pressure	kPa	7,141	7,141
Main Steamline Flow	kg/s	2,219	2,219
Total Core Flow	kg/s	14,338	14,339
Feedwater Flow	kg/s	2,219	2,219
Feedwater Temperature	K	500	500
Downcomer Level	m	14.3	14.3
Inlet Temperature	K	552	552

							0.35 *0.35* 0.86	0.39 *0.39* 0.35	0.43 *0.42* 0.28	0.48 *0.48* 0.94	0.42 *0.41* 1.93	0.47 *0.47* 1.01	0.48 *0.48* 1.04
		UH *UHSPH* Diff (%)				0.45 *0.44* 1.49	0.67 *0.67* -0.09	0.78 *0.78* -0.14	0.89 *0.89* -0.05	0.76 *0.76* -0.08	0.83 *0.83* 0.05	0.72 *0.72* -0.07	0.81 *0.80* 0.10
			0.35 *0.34* 1.62	0.56 *0.55* 1.29	0.73 *0.73* 0.16	1.03 *1.03* 0.01	1.09 *1.09* -0.08	1.11 *1.12* -0.19	1.10 *1.10* -0.10	0.92 *0.92* -0.38	1.02 *1.02* -0.04	0.82 *0.82* -0.01
			0.49 *0.48* 2.57	0.90 *0.90* 0.36	1.08 *1.08* 0.14	1.18 *1.19* -0.03	0.99 *1.00* -0.15	1.21 *1.21* -0.11	0.98 *0.98* -0.19	1.17 *1.17* -0.13	0.98 *0.99* -0.51	1.14 *1.14* -0.13
			0.49 *0.47* 3.68	0.79 *0.79* 0.42	1.08 *1.07* 0.24	1.21 *1.21* 0.07	1.08 *1.09* -0.29	1.26 *1.26* -0.06	1.06 *1.06* -0.34	1.24 *1.24* -0.12	1.03 *1.04* -0.44	1.21 *1.21* -0.13	0.99 *1.00* -0.18
		0.35 *0.34* 1.59	0.49 *0.48* 2.57	0.79 *0.79* 0.42	0.91 *0.91* 0.19	1.18 *1.18* 0.14	1.02 *1.02* -0.10	1.26 *1.26* -0.02	1.07 *1.08* -0.26	1.26 *1.26* -0.10	1.04 *1.05* -0.36	1.25 *1.25* -0.12	1.04 *1.04* -0.33	1.25 *1.25* -0.11
		0.56 *0.55* 1.29	0.90 *0.89* 0.37	1.08 *1.07* 0.25	1.18 *1.18* 0.14	1.04 *1.04* -0.16	1.25 *1.25* 0.01	1.06 *1.07* -0.35	1.26 *1.26* -0.06	1.05 *1.05* -0.23	**1.28** ***1.28*** -0.06	1.04 *1.04* -0.28	1.26 *1.26* -0.07	1.04 *1.04* -0.13
	0.45 *0.44* 1.51	0.73 *0.73* 0.16	1.08 *1.08* 0.14	1.21 *1.21* 0.07	1.02 *1.02* -0.10	1.25 *1.25* 0.02	1.05 *1.06* -0.28	1.25 *1.25* -0.03	1.03 *1.03* -0.23	1.26 *1.26* -0.06	1.03 *1.04* -0.24	1.27 *1.27* -0.03	1.04 *1.04* -0.19	1.26 *1.26* -0.06
0.35 *0.34* 0.86	0.67 *0.67* -0.07	1.03 *1.03* 0.02	1.18 *1.18* -0.01	1.08 *1.08* -0.28	1.26 *1.26* -0.02	1.06 *1.07* -0.34	1.24 *1.24* -0.03	1.02 *1.02* -0.16	1.24 *1.24* -0.04	1.02 *1.02* -0.18	1.26 *1.26* -0.02	1.02 *1.02* -0.15	1.25 *1.25* 0.00	1.01 *1.01* -0.15
0.39 *0.39* 0.38	0.77 *0.77* -0.13	1.09 *1.09* -0.07	0.99 *0.99* -0.14	1.25 *1.25* -0.06	1.07 *1.07* -0.26	1.25 *1.26* -0.06	1.02 *1.03* -0.23	1.24 *1.24* -0.04	1.02 *1.02* -0.17	1.25 *1.25* -0.01	1.02 *1.03* -0.16	1.24 *1.24* 0.02	1.01 *1.01* -0.08	1.22 *1.22* -0.03
0.42 *0.42* 0.31	0.88 *0.88* -0.03	1.11 *1.11* -0.17	1.21 *1.21* -0.09	1.06 *1.06* -0.33	1.25 *1.26* -0.09	1.05 *1.05* -0.22	1.26 *1.26* -0.04	1.02 *1.02* -0.18	1.26 *1.26* 0.02	1.03 *1.03* -0.07	1.25 *1.25* -0.01	1.00 *1.00* -0.15	1.22 *1.22* 0.03	1.00 *1.00* 0.04
0.48 *0.47* 0.96	0.76 *0.76* -0.07	1.10 *1.10* -0.08	0.97 *0.97* -0.19	1.23 *1.24* -0.11	1.04 *1.04* -0.36	1.27 *1.27* -0.05	1.03 *1.03* -0.22	1.26 *1.26* 0.00	1.02 *1.02* -0.16	1.25 *1.25* 0.01	1.07 *1.07* -0.36	1.22 *1.22* 0.02	0.99 *0.99* -0.07	1.22 *1.22* 0.05
0.42 *0.41* 1.94	0.82 *0.82* 0.06	0.91 *0.92* -0.37	1.16 *1.17* -0.11	1.03 *1.03* -0.43	1.24 *1.24* -0.10	1.03 *1.04* -0.25	1.26 *1.26* -0.02	1.02 *1.02* -0.14	1.24 *1.24* 0.02	1.00 *1.00* -0.14	1.22 *1.22* 0.02	0.99 *0.99* -0.06	1.21 *1.21* 0.07	0.99 *0.99* 0.04
0.47 *0.47* 1.04	0.72 *0.72* -0.06	1.02 *1.02* -0.02	0.98 *0.98* -0.49	1.20 *1.20* -0.12	1.03 *1.04* -0.32	1.26 *1.26* -0.06	1.04 *1.04* -0.17	1.24 *1.24* 0.00	1.00 *1.00* -0.08	1.22 *1.22* 0.04	0.99 *0.99* -0.07	1.21 *1.21* 0.08	0.99 *0.99* -0.06	1.21 *1.21* 0.07
0.48 *0.47* 1.06	0.80 *0.80* 0.11	0.82 *0.82* 0.00	1.13 *1.13* -0.12	0.98 *0.98* -0.13	1.25 *1.25* -0.09	1.03 *1.03* -0.12	1.26 *1.26* -0.05	1.01 *1.01* -0.14	1.21 *1.21* -0.02	0.99 *0.99* 0.05	1.22 *1.22* 0.07	0.99 *0.99* 0.10	1.21 *1.21* 0.11	0.98 *0.98* 0.15

Figure 3.13 Radial Power Distribution at EOFPL - Effect of Spectrally Corrected Void History

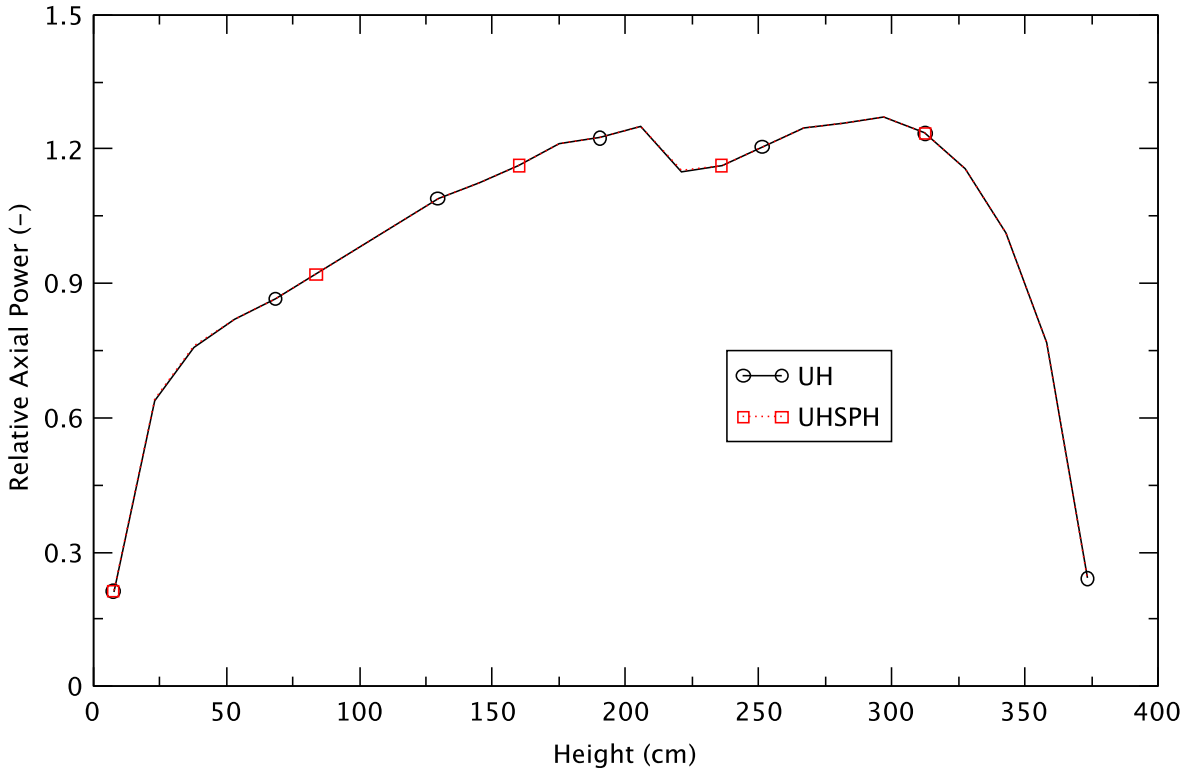

Figure 3.14 Axial Power Distribution at EOFPL - Effect of Spectrally Corrected Void History

3.3.5 Effect of Reduced Core Flow (85% and 75% Flow)

Figure 3.15 and Figure 3.16 compare the axially averaged radial power distribution for the reference model (105% of rated flow) and the models with 85% and 75% of rated flow, respectively, at EOFPL. These reduced core flows will be used in a sensitivity study that will be described in a subsequent report in this series of ATWS analyses. The impact of reducing core flow on the radial power is minimal: The power peaks in the same location (a bundle in the channel group represented by CHAN 451), and, in both cases, the RMS of the power difference is around 0.01. The channel group with maximum average bundle power for the reduced flow cases is CHAN 361, and is CHAN 371for the reference EOFPL case.

							0.35	0.39	0.43	0.48	0.42	0.47	0.48
							0.35	*0.40*	*0.43*	*0.49*	*0.43*	*0.48*	*0.49*
							-1.87	-1.39	-1.29	-1.56	-1.76	-1.90	-1.88
		Ref.				0.45	0.67	0.78	0.89	0.76	0.83	0.72	0.81
		85%Fl				*0.46*	*0.67*	*0.77*	*0.88*	*0.76*	*0.83*	*0.72*	*0.81*
		Diff(%)				-1.55	0.00	0.39	0.60	0.46	0.23	0.12	0.00
				0.35	0.56	0.73	1.03	1.09	1.11	1.10	0.92	1.02	0.82
				0.35	*0.57*	*0.73*	*1.02*	*1.08*	*1.10*	*1.09*	*0.91*	*1.02*	*0.82*
				-2.37	-1.16	0.18	0.87	1.03	1.11	0.88	0.67	0.60	0.33
				0.49	0.90	1.08	1.18	0.99	1.21	0.98	1.17	0.98	1.14
				0.50	*0.90*	*1.07*	*1.17*	*0.99*	*1.20*	*0.97*	*1.16*	*0.97*	*1.13*
				-1.46	0.41	0.96	1.03	0.84	1.05	0.75	0.74	0.63	0.51
			0.49	0.79	1.08	1.21	1.08	1.26	1.06	1.24	1.03	1.21	0.99
			0.50	*0.79*	*1.07*	*1.20*	*1.07*	*1.25*	*1.05*	*1.23*	*1.03*	*1.20*	*0.99*
			-1.92	-0.13	0.80	0.96	0.84	0.81	0.75	0.64	0.66	0.55	0.27
		0.35	0.49	0.79	0.91	1.18	1.02	1.26	1.07	1.26	1.04	1.25	1.04	1.25
		0.35	*0.50*	*0.79*	*0.91*	*1.17*	*1.02*	*1.26*	*1.07*	*1.25*	*1.04*	*1.24*	*1.04*	*1.25*
		-2.41	-1.46	-0.13	0.53	0.73	0.62	0.64	0.50	0.53	0.38	0.37	0.28	0.24
		0.56	0.90	1.08	1.18	1.04	1.25	1.06	1.26	1.05	**1.28**	1.04	1.26	1.04
		0.56	*0.89*	*1.07*	*1.17*	*1.03*	*1.24*	*1.06*	*1.25*	*1.05*	***1.27***	*1.03*	*1.26*	*1.04*
		-1.18	0.39	0.79	0.73	0.59	0.53	0.37	0.32	0.12	0.07	0.11	0.13	-0.03
	0.45	0.73	1.08	1.21	1.02	1.25	1.05	1.25	1.03	1.26	1.03	1.27	1.04	1.26
	0.46	*0.73*	*1.07*	*1.20*	*1.01*	*1.24*	*1.05*	*1.24*	*1.03*	*1.26*	*1.04*	*1.27*	*1.04*	*1.27*
	-1.53	0.15	0.94	0.94	0.60	0.52	0.30	0.19	-0.05	-0.01	-0.24	-0.13	-0.20	-0.15
0.35	0.67	1.03	1.18	1.08	1.26	1.06	1.24	1.02	1.24	1.02	1.26	1.02	1.25	1.01
0.35	*0.67*	*1.02*	*1.17*	*1.07*	*1.25*	*1.06*	*1.24*	*1.02*	*1.24*	*1.02*	*1.26*	*1.03*	*1.25*	*1.02*
-1.93	-0.01	0.85	1.01	0.81	0.61	0.35	0.18	-0.21	-0.14	-0.23	-0.29	-0.44	-0.39	-0.40
0.39	0.77	1.09	0.99	1.25	1.07	1.25	1.02	1.24	1.02	1.25	1.02	1.24	1.01	1.22
0.40	*0.77*	*1.08*	*0.98*	*1.24*	*1.06*	*1.25*	*1.03*	*1.24*	*1.02*	*1.26*	*1.03*	*1.25*	*1.01*	*1.23*
-1.40	0.35	1.00	0.80	0.77	0.47	0.29	-0.09	-0.16	-0.42	-0.41	-0.66	-0.57	-0.79	-0.60
0.42	0.88	1.11	1.21	1.06	1.25	1.05	1.26	1.02	1.26	1.03	1.25	1.00	1.22	1.00
0.43	*0.88*	*1.10*	*1.20*	*1.05*	*1.25*	*1.05*	*1.26*	*1.02*	*1.26*	*1.04*	*1.26*	*1.01*	*1.23*	*1.01*
-1.30	0.57	1.08	1.02	0.70	0.49	0.08	-0.06	-0.35	-0.49	-0.72	-0.54	-0.80	-0.80	-1.02
0.48	0.76	1.10	0.97	1.23	1.04	1.27	1.03	1.26	1.02	1.25	1.07	1.22	0.99	1.22
0.49	*0.76*	*1.09*	*0.96*	*1.23*	*1.04*	*1.27*	*1.03*	*1.26*	*1.03*	*1.26*	*1.08*	*1.23*	*1.00*	*1.23*
-1.59	0.43	0.86	0.71	0.60	0.33	0.01	-0.30	-0.41	-0.80	-0.57	-0.65	-0.79	-1.05	-0.93
0.42	0.82	0.91	1.16	1.03	1.24	1.03	1.26	1.02	1.24	1.00	1.22	0.99	1.21	0.99
0.43	*0.82*	*0.91*	*1.16*	*1.02*	*1.24*	*1.03*	*1.26*	*1.02*	*1.25*	*1.01*	*1.23*	*1.00*	*1.22*	*1.00*
-1.79	0.19	0.62	0.70	0.61	0.31	-0.02	-0.24	-0.51	-0.62	-0.85	-0.82	-1.04	-0.96	-1.17
0.47	0.72	1.02	0.98	1.20	1.03	1.26	1.04	1.24	1.00	1.22	0.99	1.21	0.99	1.21
0.48	*0.72*	*1.01*	*0.97*	*1.20*	*1.03*	*1.26*	*1.04*	*1.25*	*1.01*	*1.23*	*1.00*	*1.23*	*1.00*	*1.22*
-1.91	0.08	0.56	0.59	0.52	0.21	0.03	-0.34	-0.44	-0.84	-0.86	-1.10	-0.99	-1.11	-1.03
0.48	0.80	0.82	1.13	0.98	1.25	1.03	1.26	1.01	1.21	0.99	1.22	0.99	1.21	0.98
0.49	*0.80*	*0.81*	*1.12*	*0.98*	*1.24*	*1.03*	*1.26*	*1.01*	*1.22*	*1.01*	*1.23*	*1.00*	*1.22*	*0.99*
-1.94	-0.05	0.28	0.48	0.31	0.22	-0.09	-0.21	-0.46	-0.65	-1.08	-0.99	-1.27	-1.07	-1.38

Figure 3.15 Radial Power Distribution at EOFPL - Effect of Reduced (85%) Core Flow

							0.35 *0.36* -3.04	0.39 *0.40* -2.23	0.43 *0.43* -2.07	0.48 *0.49* -2.52	0.42 *0.43* -2.88	0.47 *0.49* -3.05	0.48 *0.50* -3.07
		Ref. *75%Fl* Diff(%)				0.45 *0.46* -2.44	0.67 *0.67* 0.10	0.78 *0.77* 0.72	0.89 *0.88* 1.03	0.76 *0.76* 0.80	0.83 *0.82* 0.40	0.72 *0.72* 0.24	0.81 *0.81* 0.02
				0.35 *0.36* -3.79	0.56 *0.57* -1.82	0.73 *0.73* 0.40	1.03 *1.02* 1.49	1.09 *1.07* 1.70	1.11 *1.09* 1.80	1.10 *1.08* 1.44	0.92 *0.91* 1.09	1.02 *1.01* 0.93	0.82 *0.82* 0.55
				0.49 *0.51* -2.29	0.90 *0.89* 0.76	1.08 *1.06* 1.60	1.18 *1.16* 1.70	0.99 *0.98* 1.39	1.21 *1.19* 1.67	0.98 *0.96* 1.22	1.17 *1.16* 1.16	0.98 *0.97* 1.01	1.14 *1.13* 0.78
			0.49 *0.50* -3.05	0.79 *0.79* -0.09	1.08 *1.06* 1.35	1.21 *1.19* 1.58	1.08 *1.07* 1.38	1.26 *1.24* 1.28	1.06 *1.05* 1.20	1.24 *1.23* 0.99	1.03 *1.02* 1.05	1.21 *1.20* 0.82	0.99 *0.99* 0.43
		0.35 *0.36* -3.82	0.49 *0.50* -2.31	0.79 *0.79* -0.10	0.91 *0.90* 0.92	1.18 *1.17* 1.22	1.02 *1.01* 1.03	1.26 *1.25* 1.01	1.07 *1.06* 0.82	1.26 *1.25* 0.79	1.04 *1.04* 0.61	1.25 *1.24* 0.53	1.04 *1.03* 0.44	1.25 *1.24* 0.31
		0.56 *0.57* -1.84	0.90 *0.89* 0.72	1.08 *1.06* 1.33	1.18 *1.17* 1.21	1.04 *1.03* 0.98	1.25 *1.24* 0.83	1.06 *1.06* 0.61	1.26 *1.25* 0.46	1.05 *1.05* 0.22	**1.28** ***1.27*** 0.06	1.04 *1.03* 0.17	1.26 *1.26* 0.14	1.04 *1.04* -0.04
	0.45 *0.46* -2.44	0.73 *0.73* 0.36	1.08 *1.06* 1.57	1.21 *1.19* 1.55	1.02 *1.01* 1.00	1.25 *1.24* 0.83	1.05 *1.05* 0.49	1.25 *1.24* 0.26	1.03 *1.03* -0.07	1.26 *1.26* -0.07	1.03 *1.04* -0.36	1.27 *1.27* -0.27	1.04 *1.04* -0.32	1.26 *1.27* -0.32
0.35 *0.36* -3.11	0.67 *0.67* 0.07	1.03 *1.01* 1.45	1.18 *1.16* 1.67	1.08 *1.07* 1.35	1.26 *1.25* 0.98	1.06 *1.06* 0.57	1.24 *1.24* 0.23	1.02 *1.02* -0.30	1.24 *1.24* -0.28	1.02 *1.03* -0.36	1.26 *1.27* -0.52	1.02 *1.03* -0.68	1.25 *1.25* -0.69	1.01 *1.02* -0.62
0.39 *0.40* -2.26	0.77 *0.77* 0.67	1.09 *1.07* 1.67	0.99 *0.98* 1.33	1.25 *1.24* 1.24	1.07 *1.06* 0.77	1.25 *1.25* 0.41	1.02 *1.03* -0.12	1.24 *1.24* -0.32	1.02 *1.02* -0.65	1.25 *1.26* -0.71	1.02 *1.03* -1.04	1.24 *1.25* -0.98	1.01 *1.02* -1.22	1.22 *1.23* -1.03
0.42 *0.43* -2.10	0.88 *0.87* 0.97	1.11 *1.09* 1.77	1.21 *1.19* 1.62	1.06 *1.04* 1.14	1.25 *1.25* 0.73	1.05 *1.05* 0.14	1.26 *1.26* -0.15	1.02 *1.02* -0.55	1.26 *1.27* -0.84	1.03 *1.04* -1.12	1.25 *1.26* -0.93	1.00 *1.02* -1.25	1.22 *1.23* -1.33	1.00 *1.01* -1.59
0.48 *0.49* -2.59	0.76 *0.75* 0.74	1.10 *1.08* 1.40	0.97 *0.96* 1.16	1.23 *1.22* 0.93	1.04 *1.03* 0.54	1.27 *1.27* -0.02	1.03 *1.03* -0.47	1.26 *1.27* -0.72	1.02 *1.03* -1.24	1.25 *1.26* -0.98	1.07 *1.08* -1.04	1.22 *1.24* -1.33	0.99 *1.01* -1.65	1.22 *1.24* -1.55
0.42 *0.43* -2.92	0.82 *0.82* 0.34	0.91 *0.90* 1.03	1.16 *1.15* 1.10	1.03 *1.02* 0.99	1.24 *1.24* 0.44	1.03 *1.03* -0.02	1.26 *1.27* -0.44	1.02 *1.03* -0.79	1.24 *1.25* -1.06	1.00 *1.01* -1.32	1.22 *1.24* -1.37	0.99 *1.01* -1.62	1.21 *1.23* -1.60	0.99 *1.00* -1.84
0.47 *0.49* -3.11	0.72 *0.72* 0.17	1.02 *1.01* 0.87	0.98 *0.97* 0.94	1.20 *1.19* 0.77	1.03 *1.03* 0.35	1.26 *1.26* -0.02	1.04 *1.04* -0.52	1.24 *1.25* -0.77	1.00 *1.01* -1.30	1.22 *1.23* -1.41	0.99 *1.01* -1.72	1.21 *1.23* -1.64	0.99 *1.01* -1.75	1.21 *1.23* -1.72
0.48 *0.50* -3.13	0.80 *0.80* -0.05	0.82 *0.81* 0.48	1.13 *1.12* 0.74	0.98 *0.98* 0.51	1.25 *1.24* 0.27	1.03 *1.03* -0.13	1.26 *1.26* -0.42	1.01 *1.01* -0.72	1.21 *1.23* -1.10	0.99 *1.01* -1.68	1.22 *1.24* -1.63	0.99 *1.01* -1.98	1.21 *1.23* -1.78	0.98 *1.00* -2.14

Figure 3.16 Radial Power Distribution at EOFPL - Effect of Reduced (75%) Core Flow

Table 3.6 lists the main thermal-hydraulic and neutronic parameters from the reference EOFPL model and with the reduced flow models. Obviously, the most significant difference is the total core flow; however, it is notable that the eigenvalue decreases with flow, and the system is subcritical for 75% flow (k_{eff} automatically is set to unity at the beginning of the transient).

Table 3.6 Comparison of Steady-State Thermal-Hydraulic Parameters at EOFPL - Effect of Reduced Core Flow

Parameter	Units	Reference Model Value	85% Flow Model Value	75% Flow Model Value
K_{eff}	-	1.00942	1.00232	0.99817
Core Power	MWt	3988	3988	3988
Steam Dome Pressure	kPa	7.14	7.14	7.14
Main Steamline Flow	kg/s	2219	2220	2220
Total Core Flow	kg/s	14,340	11,630	10,260
Feedwater Flow	kg/s	2219	2220	2220
Feedwater Temperature	K	500	500	500
Downcomer Level	m	14.3	14.3	14.3
Inlet Temperature	K	552	550	549

Figure 3.17 compares the radially averaged axial power distribution for the reference EOFPL model, and the models with 85% and 75% of rated flow. Figure 3.18, as in previous sections, shows the comparisons of the axial profiles of the moderator density. The most significant outcome of reducing the flow is that as it occurs, the shoulder that is apparent in the reference case around 50 cm is exacerbated, becoming a local peak for the case of 75% of rated flow. For low flow, the boiling boundary will shift downward (as seen in the moderator density in Figure 3.18). The downward shift in the boiling boundary in steady-state calculations also will pull the shape of the axial power downward. Above 50 cm, the power flattens or decreases, respectively, for the cases of 85% and 75% of rated flow. That finding is consistent with the expected high burnup for heights between 50 and 100 cm where the moderator density is relatively high.

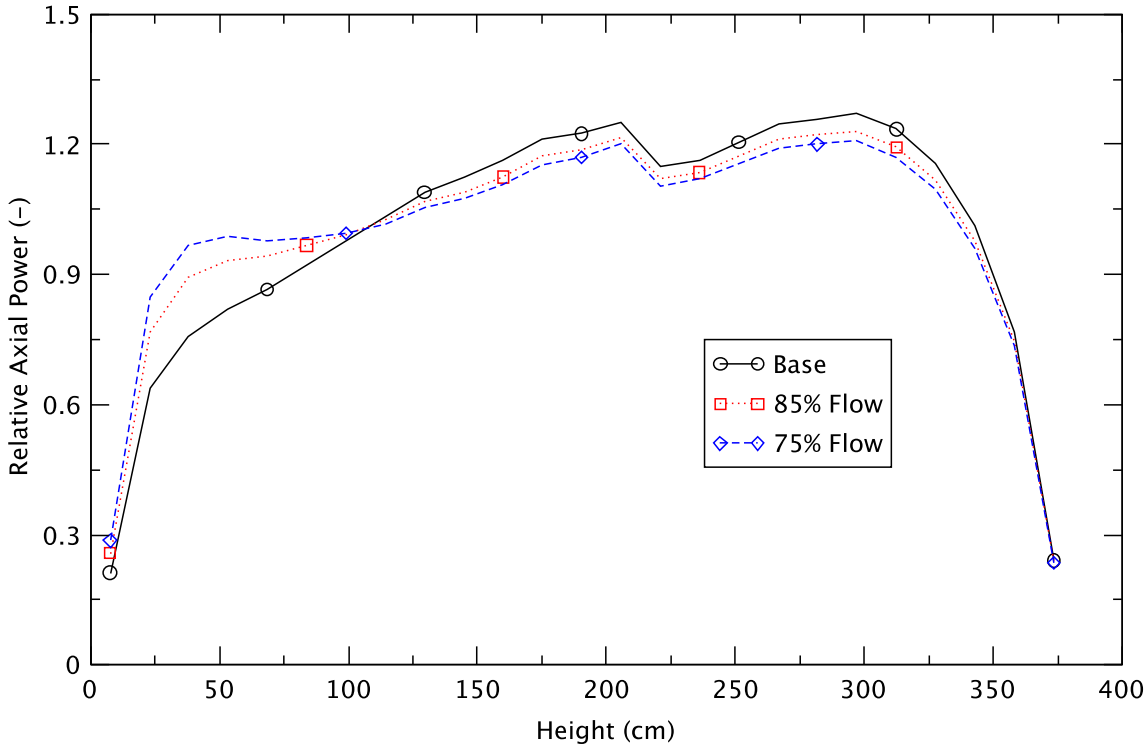

Figure 3.17 Axial Power Distribution at EOFPL - Effect of Reduced Core Flow

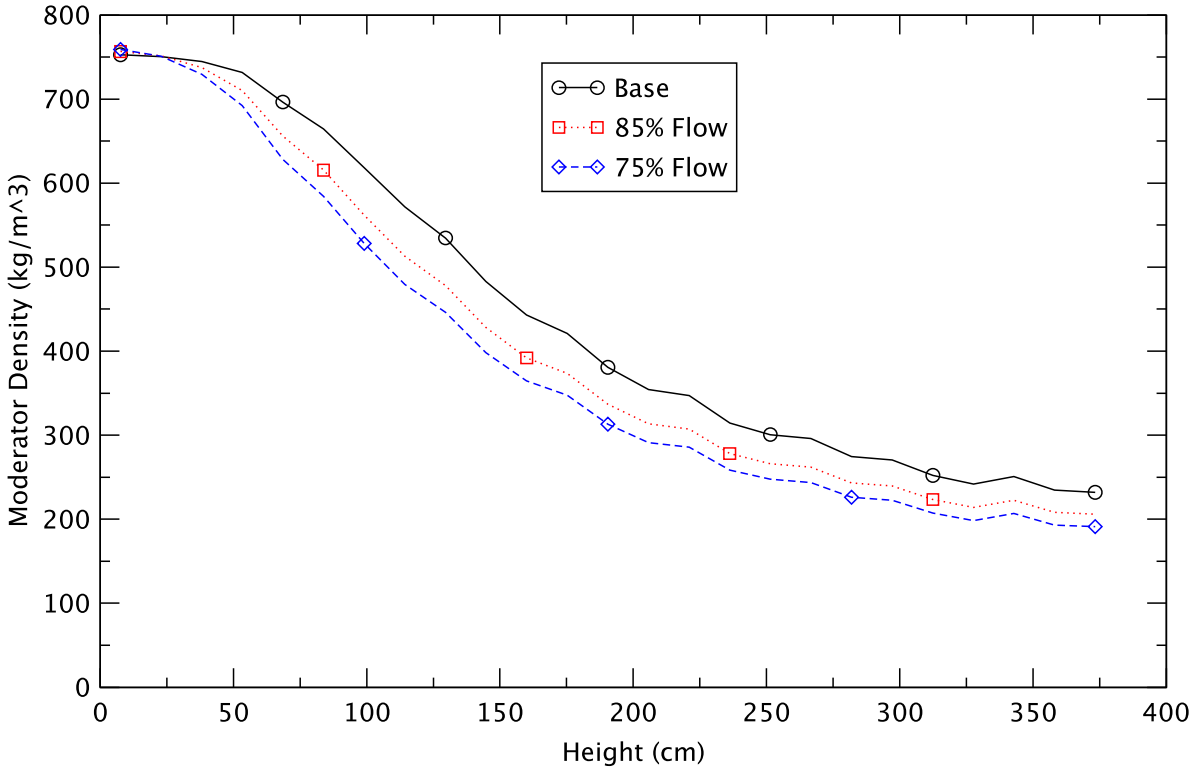

Figure 3.18 Axial Moderator Density Distribution at EOFPL - Effect of Reduced Core Flow

3.4 Comparison of Power Distribution from the 27- and 382-Channel Models

Figure 3.19, Figure 3.20 and Figure 3.21, respectively, compare the axially averaged radial power distributions, calculated by TRACE/PARCS, for the 27- and 382-channel models for BOC, PHE, and EOFPL. The agreement is very good for BOC and EOFPL; for those points in the cycle, the RMS of the power difference is 0.02 and 0.03, respectively. For PHE the agreement is reasonable, with an RMS of 0.05.

Figure 3.22, Figure 3.23, and Figure 3.24 compare the radially averaged axial power distributions for the 27- and 382-channel models; they are almost identical.

The comparison of power distributions from the 27- and the 382-channel models imply that the 27-channel grouping strategy is acceptable for core-wide transients over the full range of exposures considered herein.

							0.33 *0.36* 10.07	0.37 *0.40* -7.67	0.41 *0.43* -4.67	0.52 *0.52* 0.42	0.49 *0.48* 0.62	0.59 *0.56* 4.38	0.60 *0.57* 5.42
		27Ch *382Ch* Diff(%)				0.41 *0.43* -5.37	0.61 *0.64* -5.65	0.71 *0.72* -1.43	0.74 *0.75* -1.18	0.79 *0.81* -3.72	0.81 *0.82* -0.98	0.85 *0.86* -0.73	0.85 *0.84* 0.84
				0.31 *0.34* -9.33	0.49 *0.50* -2.21	0.65 *0.68* -3.82	0.80 *0.80* -0.58	0.85 *0.87* -1.77	0.92 *0.92* 0.57	1.01 *0.98* 3.30	1.07 *1.03* 4.00	1.04 *1.03* 0.65	1.01 *1.01* -0.08
				0.45 *0.46* -2.54	0.68 *0.71* -4.10	0.79 *0.83* -4.76	0.92 *0.93* -1.27	0.98 *0.99* -0.46	1.06 *1.07* -0.72	1.11 *1.09* 1.44	1.18 *1.14* 3.26	1.20 *1.16* 3.42	1.19 *1.15* 3.48
			0.50 *0.50* -0.06	0.79 *0.77* 1.48	0.85 *0.87* -2.20	0.96 *0.97* -0.32	1.02 *1.03* -1.70	1.04 *1.08* -3.75	1.17 *1.17* 0.47	1.24 *1.20* 3.08	1.25 *1.22* 2.54	1.26 *1.23* 2.59	1.21 *1.20* 1.29
		0.31 *0.34* -9.36	0.45 *0.46* -2.54	0.79 *0.77* 1.46	0.91 *0.92* -1.33	1.04 *1.01* 2.26	1.08 *1.06* 1.41	1.08 *1.11* -3.22	1.13 *1.16* -2.84	1.22 *1.23* -0.62	1.26 *1.24* 1.49	1.29 *1.26* 2.43	1.28 *1.25* 2.76	1.28 *1.26* 1.37
		0.49 *0.50* -2.25	0.68 *0.71* -4.13	0.85 *0.87* -2.22	1.04 *1.01* 2.24	1.14 *1.11* 3.35	1.18 *1.17* 0.48	1.21 *1.21* -0.33	1.22 *1.24* -1.56	1.24 *1.24* -0.21	1.28 *1.26* 1.08	1.28 *1.24* 2.86	1.30 *1.26* 3.62	1.29 *1.24* 3.65
	0.41 *0.43* -5.42	0.65 *0.68* -3.87	0.79 *0.83* -4.82	0.96 *0.97* -0.37	1.08 *1.06* 1.38	1.18 *1.17* 0.45	1.22 *1.22* 0.33	1.22 *1.25* -1.85	1.22 *1.24* -1.64	1.28 *1.26* 1.11	1.24 *1.22* 1.18	1.22 *1.21* 0.99	1.19 *1.18* 0.45	1.23 *1.21* 1.82
0.33 *0.36* 10.11	0.61 *0.64* -5.70	0.80 *0.80* -0.63	0.92 *0.93* -1.34	1.02 *1.03* -1.78	1.07 *1.11* -3.32	1.21 *1.21* -0.43	1.22 *1.25* -1.93	1.15 *1.20* -4.40	1.19 *1.22* -2.55	1.23 *1.22* 0.68	1.20 *1.20* 0.19	0.98 *0.97* 1.12	0.96 *0.95* 0.71	1.16 *1.14* 1.93
0.37 *0.40* -7.73	0.71 *0.72* -1.49	0.85 *0.87* -1.83	0.98 *0.99* -0.50	1.04 *1.08* -3.86	1.13 *1.16* -3.00	1.22 *1.24* -1.75	1.21 *1.24* -1.87	1.19 *1.22* -2.81	1.16 *1.20* -3.42	1.23 *1.23* -0.06	1.16 *1.17* -0.35	0.95 *0.95* -0.30	0.93 *0.94* -0.88	1.13 *1.13* 0.45
0.41 *0.43* -4.72	0.74 *0.75* -1.23	0.92 *0.92* 0.51	1.06 *1.07* -0.80	1.17 *1.17* 0.32	1.22 *1.23* -0.82	1.24 *1.24* -0.49	1.27 *1.26* 0.69	1.21 *1.22* -1.16	1.22 *1.23* -1.08	1.20 *1.21* -0.83	1.21 *1.19* 2.00	1.13 *1.13* 0.39	1.11 *1.12* -0.48	1.13 *1.12* 0.38
0.52 *0.52* 0.40	0.78 *0.81* -3.76	1.01 *0.98* 3.25	1.11 *1.09* 1.35	1.24 *1.20* 2.93	1.25 *1.24* 1.24	1.27 *1.26* 0.68	1.23 *1.22* 0.62	1.19 *1.20* -1.02	1.14 *1.17* -2.17	1.21 *1.19* 1.75	1.22 *1.19* 2.15	1.12 *1.12* -0.27	1.09 *1.10* -1.10	1.12 *1.12* -0.56
0.48 *0.48* 0.56	0.81 *0.82* -1.02	1.07 *1.03* 3.98	1.18 *1.14* 3.20	1.25 *1.22* 2.43	1.29 *1.26* 2.15	1.26 *1.24* 1.81	1.20 *1.21* -0.72	0.97 *0.97* 0.77	0.94 *0.95* -0.56	1.13 *1.13* 0.15	1.12 *1.12* -0.41	0.93 *0.93* 0.39	0.91 *0.91* -0.48	1.08 *1.08* -0.49
0.59 *0.56* 4.32	0.85 *0.86* -0.74	1.04 *1.03* 0.67	1.20 *1.16* 3.47	1.26 *1.23* 2.68	1.28 *1.25* 2.65	1.28 *1.26* 2.02	1.18 *1.18* -0.60	0.96 *0.95* 0.43	0.93 *0.94* -1.07	1.11 *1.12* -0.79	1.08 *1.10* -1.44	0.90 *0.91* -0.85	0.90 *0.92* -1.67	1.07 *1.08* -1.11
0.60 *0.57* 5.42	0.85 *0.84* 0.87	1.01 *1.01* -0.01	1.20 *1.15* 3.70	1.23 *1.20* 2.76	1.30 *1.26* 3.00	1.29 *1.24* 3.45	1.23 *1.21* 1.42	1.16 *1.14* 1.58	1.13 *1.13* 0.10	1.12 *1.12* 0.02	1.11 *1.12* -1.15	1.05 *1.08* -3.05	1.04 *1.08* -4.06	1.06 *1.10* -3.62

Figure 3.19 Radial Power at BOC - 382-Channel Model versus 27-Channel Model

							0.33	0.37	0.39	0.45	0.39	0.44	0.44
							0.36	*0.40*	*0.42*	*0.48*	*0.44*	*0.49*	*0.49*
							-8.06	-7.56	-7.58	-6.62	-10.76	-10.56	-11.36
		27Ch				0.44	0.64	0.72	0.77	0.70	0.71	0.64	0.66
		382Ch				*0.44*	*0.67*	*0.75*	*0.82*	*0.78*	*0.82*	*0.76*	*0.80*
		Diff(%)				-1.06	-4.98	-3.11	-6.44	-12.45	-16.62	-19.84	-21.93
				0.34	0.55	0.71	0.93	0.98	1.00	0.99	0.85	0.86	0.71
				0.35	*0.52*	*0.70*	*0.91*	*0.99*	*1.02*	*1.04*	*0.93*	*1.00*	*0.85*
				-2.53	4.72	0.03	1.67	-0.77	-1.95	-4.52	-9.34	-16.44	-19.88
				0.50	0.82	0.98	1.12	1.01	1.16	0.97	1.07	0.88	0.91
				0.48	*0.81*	*0.97*	*1.07*	*0.98*	*1.16*	*1.00*	*1.14*	*0.98*	*1.04*
				4.69	1.45	1.99	4.28	2.73	-0.41	-3.41	-6.84	-11.59	-14.91
			0.52	0.83	1.03	1.19	1.14	1.28	1.11	1.24	1.02	1.05	0.72
			0.49	*0.78*	*0.99*	*1.11*	*1.06*	*1.23*	*1.09*	*1.24*	*1.06*	*1.14*	*0.76*
			5.54	5.50	4.18	6.95	6.93	4.02	1.92	-0.36	-4.27	-8.96	-5.09
		0.34	0.51	0.83	0.96	1.22	1.12	1.35	1.18	1.33	1.11	1.22	0.97	0.88
		0.35	*0.48*	*0.78*	*0.91*	*1.12*	*1.03*	*1.26*	*1.12*	*1.29*	*1.10*	*1.25*	*1.03*	*0.90*
		-1.95	5.11	5.73	4.65	8.17	7.99	6.57	5.23	2.65	0.51	-2.72	-6.07	-3.26
		0.56	0.83	1.04	1.23	1.17	1.38	1.21	1.37	1.13	1.28	1.09	1.20	1.00
		0.52	*0.81*	*0.99*	*1.13*	*1.06*	*1.27*	*1.13*	*1.30*	*1.10*	*1.28*	*1.09*	*1.23*	*1.04*
		5.46	2.09	4.64	8.41	9.02	7.81	6.67	4.67	2.74	0.42	-0.41	-3.25	-4.27
	0.44	0.72	1.00	1.20	1.13	1.39	1.23	1.40	1.13	1.25	1.05	1.24	1.08	1.22
	0.44	*0.71*	*0.97*	*1.11*	*1.04*	*1.28*	*1.14*	*1.31*	*1.09*	*1.23*	*1.05*	*1.25*	*1.10*	*1.26*
	0.05	1.02	2.83	7.61	8.48	8.13	7.57	6.00	3.78	1.78	0.29	-1.07	-1.64	-3.61
0.34	0.65	0.94	1.13	1.15	1.37	1.23	1.43	1.18	1.28	0.79	0.90	1.04	1.27	1.04
0.36	*0.67*	*0.92*	*1.07*	*1.06*	*1.27*	*1.14*	*1.33*	*1.11*	*1.24*	*0.78*	*0.90*	*1.05*	*1.28*	*1.08*
-6.54	-3.54	2.88	5.30	7.76	7.31	7.41	6.65	5.63	3.21	1.25	-0.09	-0.62	-0.70	-3.78
0.38	0.74	1.00	1.02	1.30	1.20	1.41	1.20	1.38	1.09	0.92	0.79	1.24	1.11	1.24
0.40	*0.75*	*0.99*	*0.98*	*1.24*	*1.13*	*1.33*	*1.13*	*1.31*	*1.06*	*0.91*	*0.79*	*1.24*	*1.11*	*1.27*
-5.73	-1.39	0.75	3.97	4.99	6.11	5.81	5.65	5.08	2.73	1.30	0.10	-0.04	0.10	-2.83
0.41	0.79	1.03	1.18	1.13	1.33	1.16	1.37	1.16	1.31	1.09	1.26	1.12	1.33	1.13
0.43	*0.83*	*1.03*	*1.17*	*1.09*	*1.29*	*1.12*	*1.31*	*1.11*	*1.28*	*1.07*	*1.25*	*1.10*	*1.32*	*1.12*
-5.34	-4.22	-0.07	1.06	2.87	3.31	3.76	4.33	4.05	2.30	1.14	1.19	1.54	1.17	0.37
0.48	0.73	1.03	1.00	1.25	1.08	1.24	1.09	1.30	1.15	1.34	1.22	1.36	1.13	1.27
0.49	*0.80*	*1.05*	*1.01*	*1.24*	*1.08*	*1.24*	*1.07*	*1.28*	*1.12*	*1.31*	*1.19*	*1.33*	*1.12*	*1.28*
-3.75	-9.38	-1.96	-1.47	0.60	0.27	0.02	1.67	1.76	2.60	2.29	2.92	1.98	1.03	-0.42
0.42	0.75	0.91	1.13	1.05	1.16	0.83	0.96	1.08	1.33	1.11	1.30	1.16	1.28	0.87
0.45	*0.84*	*0.96*	*1.17*	*1.07*	*1.20*	*0.83*	*0.96*	*1.08*	*1.31*	*1.11*	*1.31*	*1.14*	*1.28*	*0.88*
-7.05	-12.42	-5.59	-3.83	-2.74	-3.56	-0.30	0.70	0.22	1.40	-0.35	-0.61	1.35	-0.28	-0.29
0.48	0.70	0.95	0.97	1.14	0.97	0.90	0.82	1.23	1.14	1.30	1.12	1.35	1.09	0.99
0.51	*0.79*	*1.05*	*1.03*	*1.21*	*1.03*	*0.93*	*0.83*	*1.24*	*1.13*	*1.31*	*1.12*	*1.34*	*1.10*	*1.00*
-6.01	-14.28	-10.93	-6.45	-5.71	-6.05	-2.89	-1.63	-0.96	0.68	-0.75	-0.64	0.76	-0.94	-0.53
0.48	0.73	0.80	1.07	0.97	1.11	0.96	1.13	1.08	1.35	1.19	1.39	1.18	1.27	1.04
0.51	*0.84*	*0.91*	*1.15*	*1.04*	*1.19*	*1.02*	*1.19*	*1.09*	*1.33*	*1.16*	*1.37*	*1.15*	*1.28*	*1.07*
-6.19	-15.47	-12.83	-7.89	-6.59	-7.19	-5.84	-5.14	-1.01	1.35	2.15	1.72	1.75	-1.03	-2.98

Figure 3.20 Radial Power at PHE - 382-Channel Model versus 27-Channel Model

							0.35	0.39	0.43	0.48	0.42	0.47	0.48
							0.37	*0.42*	*0.44*	*0.50*	*0.45*	*0.50*	*0.51*
							-6.40	-5.19	-4.40	-3.15	-6.14	-5.05	-5.01
		27Ch				0.45	0.67	0.78	0.89	0.76	0.83	0.72	0.81
		382Ch				*0.45*	*0.69*	*0.78*	*0.91*	*0.81*	*0.91*	*0.79*	*0.90*
		Diff(%)				-0.71	-3.14	-0.71	-3.32	-6.09	-9.42	-9.94	-11.53
					0.35	0.56	0.73	1.03	1.09	1.11	1.10	0.92	1.02	0.82
					0.36	*0.54*	*0.73*	*1.01*	*1.08*	*1.11*	*1.11*	*0.94*	*1.09*	*0.89*
					-3.67	3.68	0.37	1.81	1.14	0.57	-1.15	-3.01	-6.57	-7.86
					0.49	0.90	1.08	1.18	0.99	1.21	0.98	1.17	0.98	1.14
					0.48	*0.90*	*1.06*	*1.14*	*0.96*	*1.20*	*0.98*	*1.19*	*1.01*	*1.18*
					2.07	0.11	2.04	3.73	3.00	1.29	-0.27	-1.64	-2.51	-3.52
				0.49	0.79	1.08	1.21	1.08	1.26	1.06	1.24	1.03	1.21	0.99
				0.48	*0.78*	*1.06*	*1.16*	*1.03*	*1.22*	*1.04*	*1.23*	*1.04*	*1.23*	*1.01*
				1.74	1.87	1.86	4.32	4.96	2.78	2.02	0.80	-0.49	-1.52	-1.15
		0.35	0.49	0.79	0.91	1.18	1.02	1.26	1.07	1.26	1.04	1.25	1.04	1.25
		0.36	*0.48*	*0.78*	*0.90*	*1.14*	*0.98*	*1.22*	*1.04*	*1.24*	*1.04*	*1.25*	*1.04*	*1.25*
		-3.77	2.03	1.83	1.36	3.38	3.86	3.07	2.72	1.19	0.76	0.10	-0.13	-0.38
		0.56	0.90	1.08	1.18	1.04	1.25	1.06	1.26	1.05	1.28	1.04	1.26	1.04
		0.54	*0.90*	*1.06*	*1.14*	*1.00*	*1.22*	*1.04*	*1.24*	*1.04*	*1.26*	*1.03*	*1.26*	*1.03*
		3.56	0.03	1.80	3.35	3.86	2.59	2.44	1.37	1.32	1.25	0.17	0.08	0.07
	0.45	0.73	1.08	1.21	1.02	1.25	1.05	1.25	1.03	1.26	1.03	1.27	1.04	1.26
	0.45	*0.73*	*1.06*	*1.16*	*0.98*	*1.22*	*1.03*	*1.23*	*1.02*	*1.25*	*1.03*	*1.26*	*1.04*	*1.26*
	-0.84	0.23	1.93	4.25	3.78	2.56	2.19	1.05	0.83	0.60	0.74	0.68	0.33	0.55
0.35	0.67	1.03	1.18	1.08	1.26	1.06	1.24	1.02	1.24	1.02	1.26	1.02	1.25	1.01
0.37	*0.69*	*1.01*	*1.14*	*1.03*	*1.22*	*1.04*	*1.23*	*1.01*	*1.24*	*1.02*	*1.25*	*1.02*	*1.24*	*1.01*
-6.62	-3.31	1.66	3.60	4.84	2.97	2.36	1.01	0.72	0.13	0.25	0.59	0.45	0.24	-0.26
0.39	0.77	1.09	0.99	1.25	1.07	1.25	1.02	1.24	1.02	1.25	1.02	1.24	1.01	1.22
0.41	*0.78*	*1.08*	*0.96*	*1.22*	*1.04*	*1.24*	*1.02*	*1.24*	*1.01*	*1.25*	*1.01*	*1.24*	*1.00*	*1.22*
-5.39	-0.91	0.98	2.85	2.63	2.58	1.26	0.75	0.11	0.17	0.55	0.86	0.52	0.28	-0.13
0.42	0.88	1.11	1.21	1.06	1.25	1.05	1.26	1.02	1.26	1.03	1.25	1.00	1.22	1.00
0.44	*0.91*	*1.11*	*1.20*	*1.04*	*1.24*	*1.04*	*1.25*	*1.02*	*1.24*	*1.02*	*1.24*	*1.00*	*1.22*	*0.99*
-4.60	-3.54	0.37	1.09	1.83	1.04	1.18	0.52	0.20	0.85	0.96	0.70	0.30	0.13	0.30
0.48	0.76	1.10	0.97	1.23	1.04	1.27	1.03	1.26	1.02	1.25	1.07	1.22	0.99	1.22
0.49	*0.81*	*1.11*	*0.98*	*1.23*	*1.03*	*1.26*	*1.02*	*1.25*	*1.01*	*1.24*	*1.05*	*1.22*	*0.99*	*1.21*
-3.39	-6.33	-1.37	-0.50	0.58	0.56	1.12	0.65	0.83	0.85	0.70	1.40	0.40	0.26	0.51
0.42	0.82	0.91	1.16	1.03	1.24	1.03	1.26	1.02	1.24	1.00	1.22	0.99	1.21	0.99
0.44	*0.90*	*0.94*	*1.19*	*1.04*	*1.24*	*1.03*	*1.26*	*1.01*	*1.23*	*1.00*	*1.22*	*0.99*	*1.21*	*0.98*
-6.46	-9.70	-3.30	-1.92	-0.76	-0.12	0.10	0.48	0.37	0.48	0.32	0.44	0.33	0.26	0.25
0.47	0.72	1.02	0.98	1.20	1.03	1.26	1.04	1.24	1.00	1.22	0.99	1.21	0.99	1.21
0.50	*0.79*	*1.09*	*1.00*	*1.22*	*1.04*	*1.26*	*1.03*	*1.24*	*1.00*	*1.21*	*0.99*	*1.21*	*0.99*	*1.20*
-5.38	-10.28	-6.88	-2.84	-1.89	-0.40	-0.21	0.25	0.10	0.20	0.15	0.30	0.31	0.25	0.21
0.48	0.80	0.82	1.13	0.98	1.25	1.03	1.26	1.01	1.21	0.99	1.22	0.99	1.21	0.98
0.51	*0.90*	*0.88*	*1.17*	*1.00*	*1.25*	*1.03*	*1.25*	*1.01*	*1.22*	*0.99*	*1.21*	*0.98*	*1.20*	*0.98*
-5.35	-11.89	-8.22	-3.93	-2.31	-0.42	-0.16	0.34	-0.45	-0.25	0.28	0.58	0.69	0.57	0.03

Figure 3.21 Radial Power at EOFPL - 382-Channel Model versus 27-Channel Model

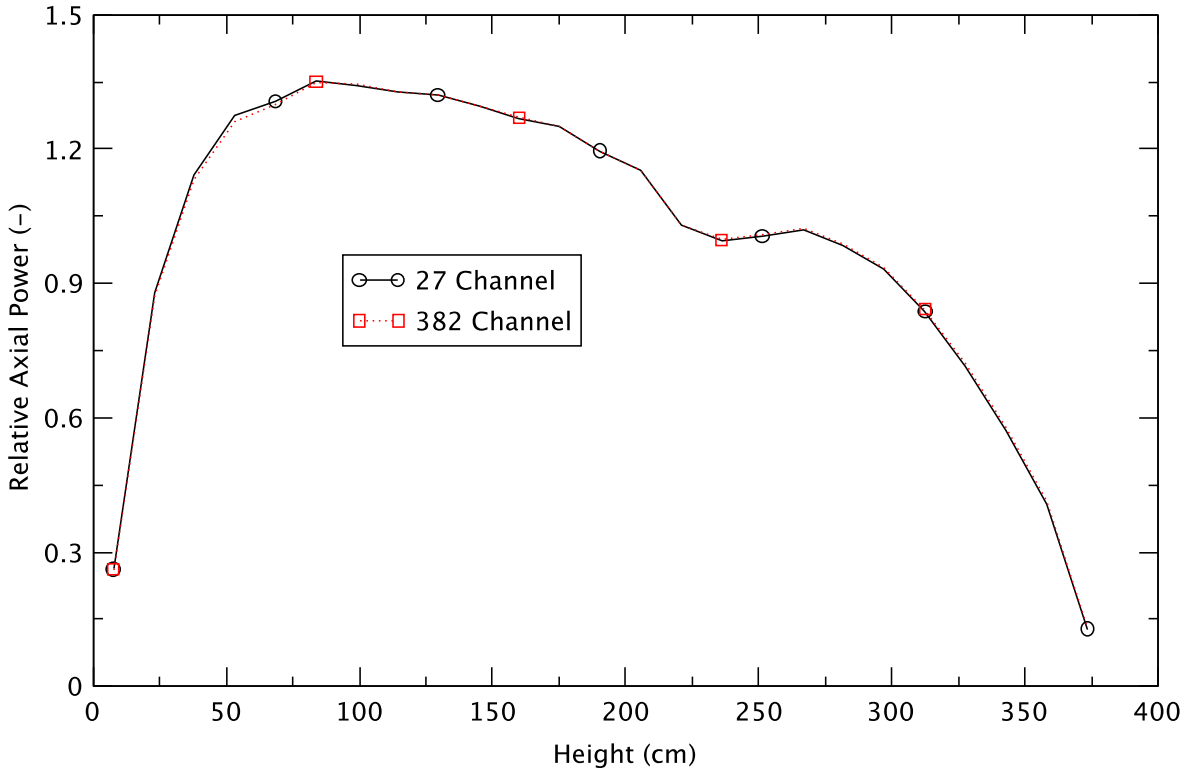

Figure 3.22 Axial Power at BOC - 382-Channel Model versus 27-Channel Model

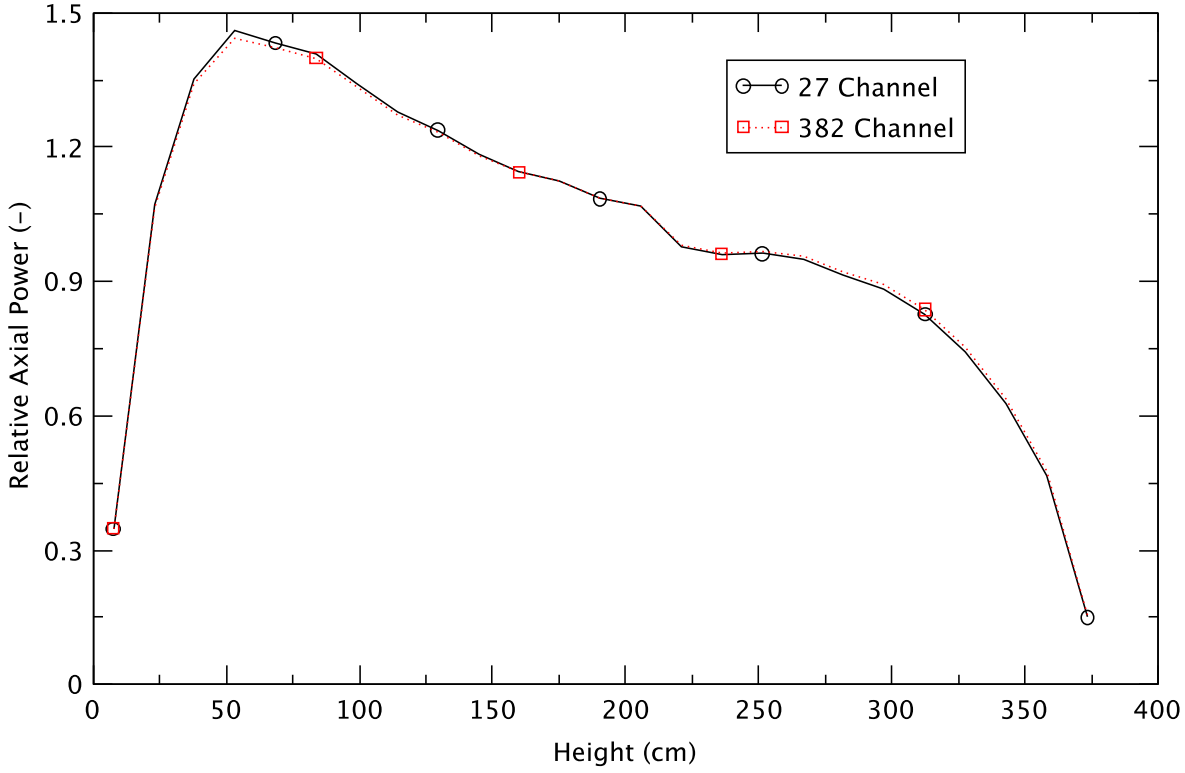

Figure 3.23 Axial Power at PHE - 382-Channel Model versus 27-Channel Model

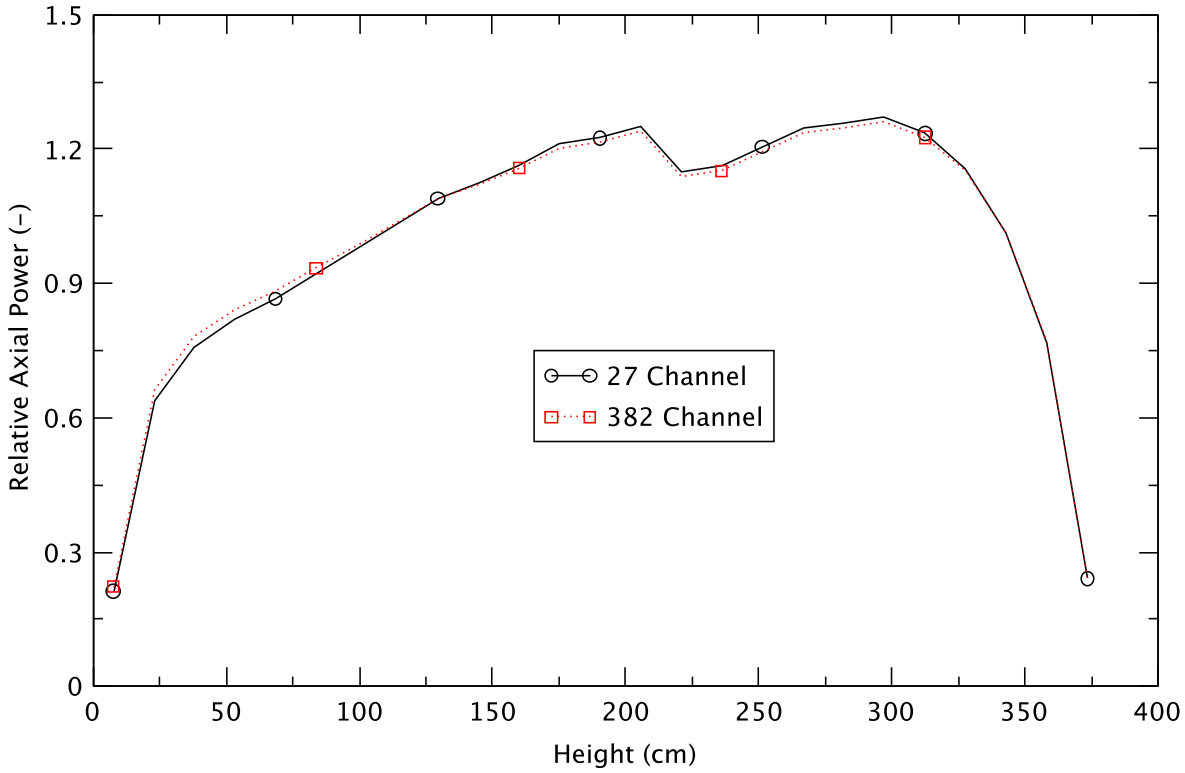

Figure 3.24 Axial Power at EOFPL - 382-Channel Model versus 27-Channel Model

4 MSIV CLOSURE EVENTS WITH EMERGENCY DEPRESSURIZATION

The ATWS with emergency depressurization (ATWS-ED) is initiated by a spurious closure of the main steam isolation valves (MSIVs), with the subsequent failure of the reactor protection system (RPS) to trip the reactor. Table 4.1 identifies the events defining the ATWS-ED scenario.

Table 4.1 ATWS-ED Scenario

Event	Timing/Setpoint
Begin transient simulation	0.0 s
MSIV closure	10.0 s (0.5 s delay + 4 s closure time)
Recirculationpump trip	Reactor pressure vessel pressure exceeds 7.651 MPa
SRVs cycling	See Table 2.4
Reactor water level reduction	130 s
Begin boron injection	211 s
Emergency depressurization	Suppression pool temperature exceeds 344.26 K
Reactor water level recovery	2180 s
End of simulation	2500 s

This event scenario includes four actions by the operator:

1. Water level control to top-of-active-fuel (TAF), and to TAF plus five feet (TAF+5), or TAF-2. This is accomplished at 130 s by artificially raising the calculated water level by a fixed amount (over a 0.1 s interval) and feeding it to the water level control system.
2. Boron injection. This is initiated at 211 s and linearly ramped up to full flow in 60 s.
3. Emergency depressurization (ED). The operator actuates the automatic depressurization system (ADS), triggered by the heat capacity temperature limit (HCTL) of the suppression pool with a setpoint at 344.26 K.
4. Recovery of water level to normal level. This is accomplished at 2180 s by reducing the adjustment of the artificial water level to zero over 100 seconds.

These manual operator actions are simulated to gauge their effectiveness in reducing reactor power. The last action, the recovery of the water level, refers to that period in the transient when the operators restore the vessel level after injecting sufficient boron to shut down the reactor. This amount commonly is referred to as the hot shutdown boron weight (HSBW). Once the SLCS has delivered the HSBW, the reactor operators will cease controlling the level to very low values, and will increase feedwater flow. This has the effect of increasing the core flow. This strategy is reflected in the emergency operating procedures to ensure that the core flow is sufficient to fully entrain any boron that may have stratified in the lower vessel head.

The timing of most operator actions indicated in Table 4.1 is based on GEH analysis of a similar event [17]; a departure from that timing is the initiation of ED. The reference GEH TRACG calculations were based on the same depressurization timing for all water level control strategies. For any given level strategy, the steam released to the suppression pool is the same before initiating manual control of the level. After the lowering of water level, the rate at which vapor is generated in the core is driven by criticality and core flowrate. The reactor power and the void fraction equilibrate to maintain a just-critical reactor. Then, the rate of steam generation is a function of the core flowrate. In essence, the reactor becomes a constant void generator, such that any inflow of liquid is converted to steam to maintain a constant void fraction.

Since the rate of vapor generation is a function of the core flowrate, and the latter under natural circulation is a function of density head difference, while the core void fraction is relatively fixed, then presumably, the rate of steam generation in the core scales with the square root of the downcomer level that drives the core inlet flowrate. The timing of the emergency depressurization is determined by the integral of the rate of vapor generation over time. Therefore, to first order, the timing of the emergency depressurization should scale inversely to the square root of the level. This relationship was not considered in GEH's reference calculations. Since the timing of ED is sensitive to the level strategy, it was decided to base actuation of the ADS on the HCTL of the suppression pool.

The NRC staff recommended that the simulation time should be sufficiently long to capture the water level recovery phase up to the point where recriticality becomes highly unlikely: they identified the point of full-level recovery following depressurization as this point. Reactivity is expected to continue to decrease as additional boron is injected into the vessel thereafter. This effect partially is due to the water level being high, and the subsequent core flowrate will suffice to fully entrain any additional injected boron. The TRACE/PARCS calculation should confirm that at the point of level recovery, the reactor power is continuing to decrease.

Seventeen cases were analyzed; Table 4.2 gives the simulation conditions distinguishing them. Only the first 11 cases in Table 4.2 are discussed herein; a subsequent report will detail the remaining six cases as part of this series of ATWS analyses.

Table 4.2 Simulation Conditions for ATWS-ED Cases

Case ID	Exposure	Core Flowrate, %	Reactor Water level Strategy	SLCS Injection
6	BOC	85	TAF-2	Lower Plenum
7	PHE	85	TAF+5	Lower Plenum
4	BOC	85	TAF+5	Lower Plenum
7C	PHE	85	TAF+5	Upper Plenum
5	BOC	85	TAF	Lower Plenum
10	EOFPL	105	TAF+5	Lower Plenum
12	EOFPL	105	TAF-2	Lower Plenum
EDSI[1]	BOC	85	TAF	Lower Plenum
9	PHE	85	TAF-2	Lower Plenum
8	PHE	85	TAF	Lower Plenum
11	EOFPL	105	TAF	Lower Plenum
4B	BOC	75[3]	TAF+5	Lower Plenum
10D	EOFPL	75[3]	TAF-2	Lower Plenum
10A	EOFPL	85[4]	TAF+5	Lower Plenum
11A	EOFPL	85[4]	TAF	Lower Plenum
12A	EOFPL	85[4]	TAF-2	Lower Plenum
10C	EOFPL UHSPH[2]	105	TAF+5	Lower Plenum

[1]Simulation of ED case with semi-implicit (SI) numeric
[2]Void history spectrally corrected (UHSPH)
[3]Eigenvalue offset for criticality based on low-low core flow analysis requested by NRC
[4]These cases achieve an upper-peaked power shape in the allowable operating domain

4.1 Introduction

For all cases, a null transient is run for 10 s to confirm the establishment of an adequate steady-state condition. The progression of all cases is similar. The ATWS is initiated by an MSIV closure at 10 s into the simulation with subsequent failure of the reactor protection system (RPS) to trip the reactor. There is an assumed 0.5 s delay before the initiation of the valve's closure and the valve's stroke time is assumed to be 4 s.

In response to the pressurization of the RPV following the MSIV closure, reactor power increases due to the collapse of steam voids in the core. The pressurization also engenders a drop in water level in the downcomer and a trip of both recirculation pumps (2RPT). Thereafter, the reactor power declines in response to the coastdown of primary flow. In the meantime, steam pressure is relieved as steam flows to the suppression pool through the safety relief valves (SRVs). As the core flow shifts to natural circulation, the water level begins to recover due to the increased flow of feedwater (FW) combined with a steady decrease in FW temperature, due to the stoppage of the extraction-steam feed to the feedwater heater cascade. This then increases the core inlet subcooling, which is accompanied by a corresponding increase in the reactor power.

The reactor power remains relatively high (roughly 50% of initial power) at the reduced core flowrate. A water level control strategy successfully brings the reactor power on a downward trend. After the initiation of boron injection, there is some delay while its concentration builds up in the core sufficiently to control the power. Once the HCTL is reached in the suppression pool, an emergency depressurization is initiated by actuating the ADS, so causing a momentary swell of the water level in the downcomer. In response to depressurization, the reactor power declines to near decay heat level. At the same time, there is voiding in the lower plenum of the reactor vessel. Its subsequent refilling with coolant drawn from the downcomer causes the water level to drop. In response, the level control system increases the feedwater flow, raising the water level and increasing the core flow, to which the reactor power responds positively.

The operation of the turbine-driven reactor core isolation cooling system (RCIC) is hampered significantly by the RPV depressurization. The periodic voiding and refilling of the lower plenum, and the corresponding responses of the feedwater flow, perturb the water level and core flow. However, the negative reactivity introduced by the boron entrained in the core flow maintains the reactor at low power. Towards the end of the simulation, the water level is restored by operator action to its normal level. The accompanying increases in core flow and core inlet subcooling are overshadowed by the enhanced delivery of boron to the core, so that the core power remains at the decay heat level. In all the cases analyzed, there was no overheating of the clad, the peak clad-temperature (PCT) stayed below 1478 K (2200°F)[1], no recriticality was predicted, and no overheating of the wetwell was observed.

The following key parameters are considered in analyzing the ATWS-ED cases.

- reactor power
- dome pressure
- feedwater flowrate
- reactor water level
- bypass void fraction

[1]This temperature limit is formally applicable only to new plants [21] but is used herein as a reasonable informal limit.

- core average void fraction
- safety relief valve flowrate
- peak cladding temperature
- axial distribution of fuel centerline temperature (limiting rod)
- axial distribution of cladding temperature (limiting rod)
- boron flux or flowrate into the core
- lower plenum void fraction and temperature
- boron concentration in the lower plenum and core average
- recirculation flowrate
- core average boron concentration
- core flowrate
- choking of SRV flow
- feedwater temperature
- suppression pool temperature
- drywell pressure

4.2 Beginning-of-Cycle (BOC) Cases

There are five ATWS-ED cases at BOC. Three of them evaluate different strategies for reactor water level control (RWLC); controlling water level to TAF, TAF+5, and TAF-2 sometime after the initiation of the transient. The TAF case was chosen as the representative case; Section 4.2.1 summarizes the timing of events from the TRACE/PARCS simulation of this case; Section 4.2.2 is a detailed discussion of it. Section4.2.3 discusses the effect of controlling the reactor water level to TAF-2, TAF and TAF+5. The effect of using the semi-implicit numerical scheme in the TRACE/PARCS calculation is explored in Section 4.2.4. The remaining BOC case is a sensitivity case with initial core flow at 75% nominal and level control to TAF+5. This sensitivity case will be included in a subsequent report as part of this series of ATWS analyses.

4.2.1 Sequence of Events for the BOC Representative Case

The progression of this transient, ATWS-ED at BOC with RWLC to TAF, generally follows the generic description in Section 4.1. Table 4.3 shows the time sequence for this event, and there are detailed discussions of the system behavior in the next section.

Table 4.3 Sequence of Events at BOC with RWLC to TAF

Time (s)	Event
0.0	• Null transient simulation starts.
10.0	• Null transient simulation ends. • Trip initiates an MSIV closure.
13.4	• High RPV pressure trips recirculation pumps.
13.8	• First lift of SRV.
14.5	• MSIV completely closed.
130	• Initiation of reactor water level control.
137	• Maximum PCT of 646 K.
211	• Initiation of boron injection.
~248	• Boron starts accumulating in the core (CB 359 > 0.01 kg).
349	• Initiation of emergency depressurization.
538	• Drywell reaches a maximum pressure of 0.162 MPa.
2180	• Initiation of restoring reactor water level over 100 s .
2208	• Suppression pool reached maximum temperature of 359 K.
2500	• Simulation ends.

4.2.2 Transient Response of the BOC Representative Case

In the BOC representative case, TRACE/PARCS predicts an initial increase in power (Figure 4.1) caused by the collapse of the void in the core following MSIV closure. The peak power is limited by fuel temperature feedback but void feedback also plays a role after sufficient time has elapsed for heat transfer to the coolant. The reactor power then drops rapidly in response to the 2RPT to about 50% of the initial level. Several factors influence the post-2RPT reactor power:

- system pressure fluctuation due to SRV cycling
- core flow transitioning to natural circulation
- feedwater flow being modulated to maintain water level
- feedwater temperature decreasing due to loss of feedwater heater
- discharge of saturated water from the steam separator

The oscillation of dome pressure is depicted in Figure 4.2 and the SRV cycling in Figure 4.3 which shows the responses of the main steamline flow to the opening and closing of the SRVs.

As steam is being relieved through the SRVs, feedwater flow (Figure 4.4) at reduced temperatures (Figure 4.5) is injected into the RPV to maintain its water level. With a decreasing temperature in the lower plenum (Figure 4.6), there is a temporary increase in reactor power before the operator acts to reduce water level (at 130 s), while the core flow (Figure 4.7) and downcomer water level (Figure 4.8) remain relatively unchanged.

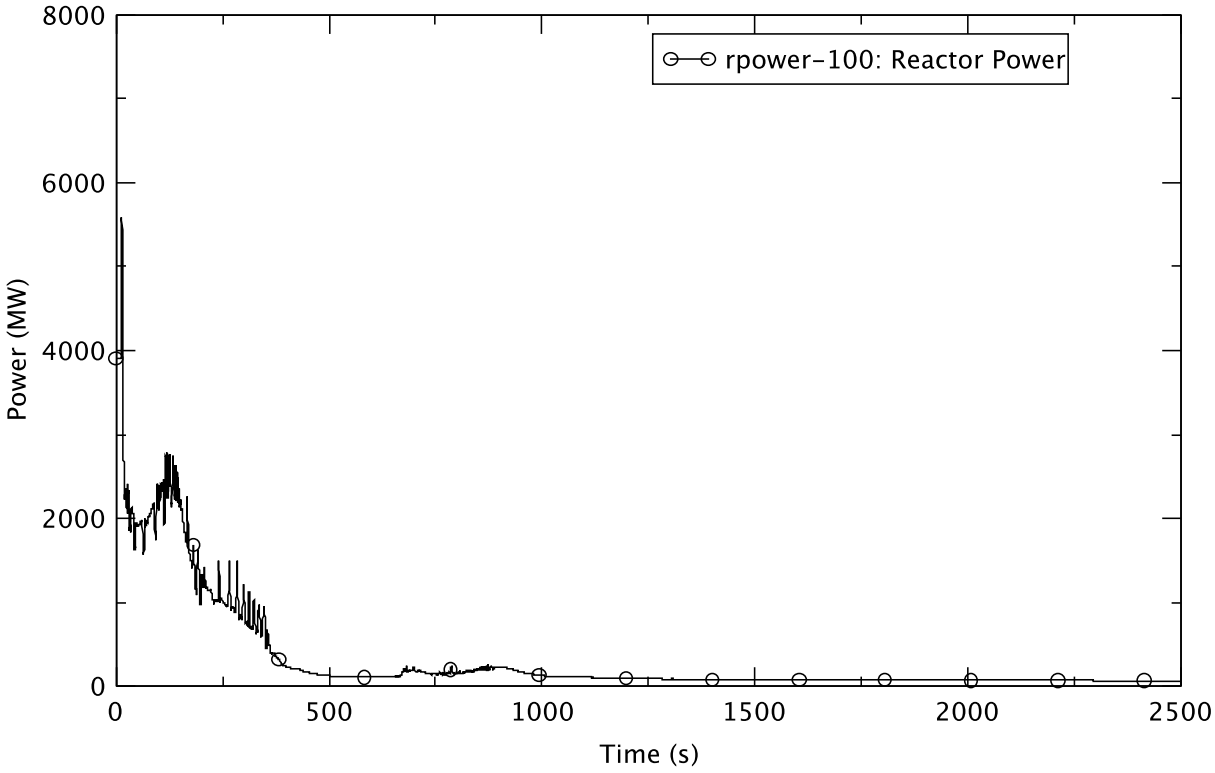

Figure 4.1 Reactor Power - BOC, TAF

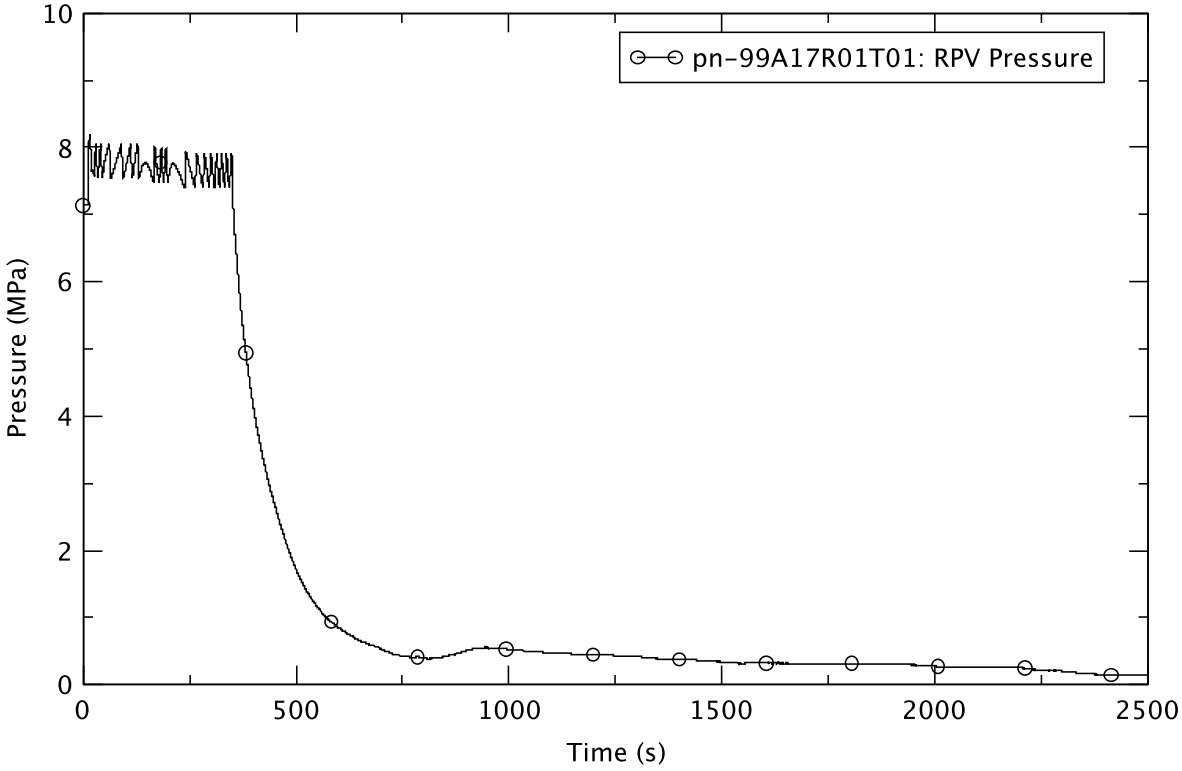

Figure 4.2 Reactor Pressure - BOC, TAF

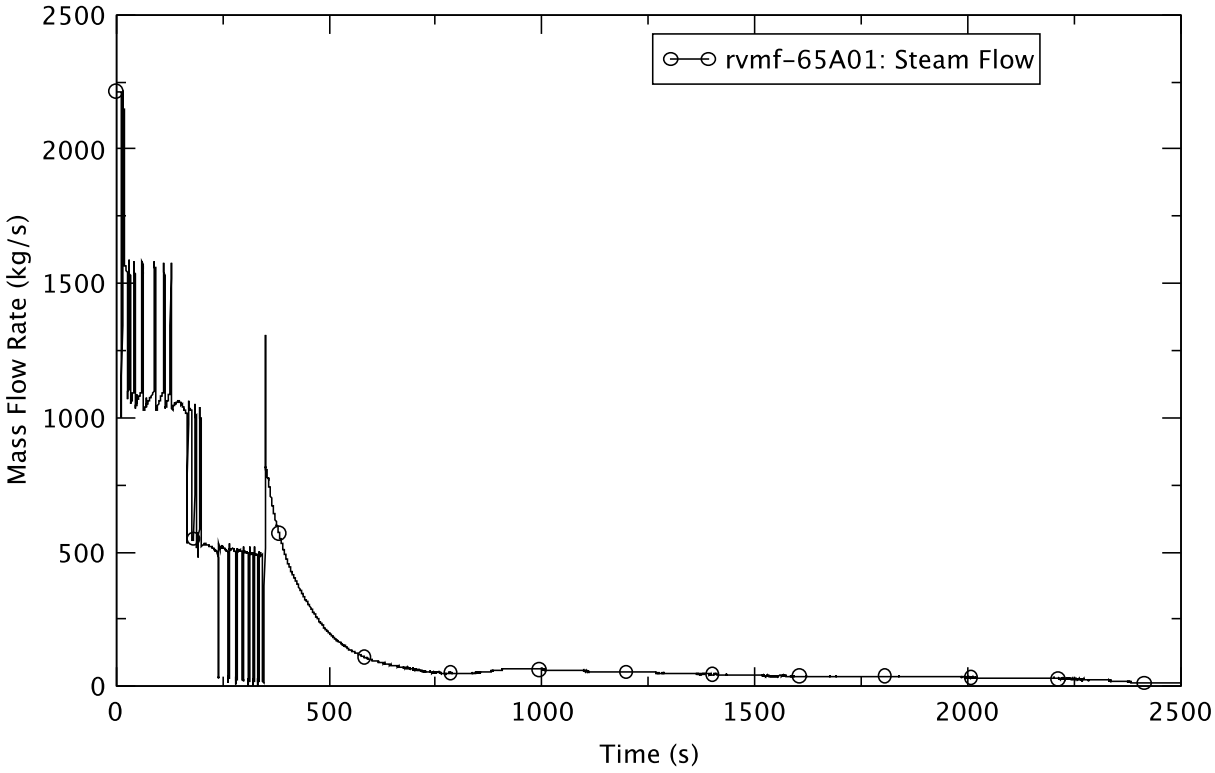

Figure 4.3 Steamline Flow - BOC, TAF

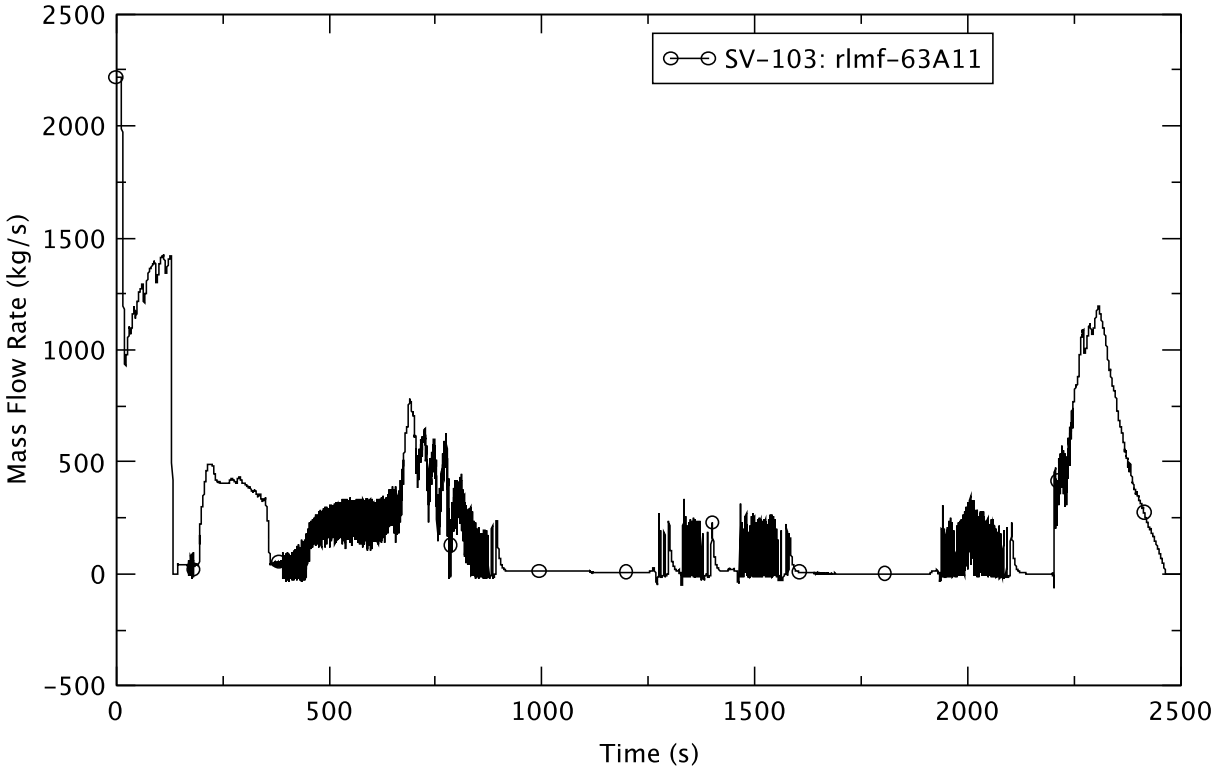

Figure 4.4 Feedwater Flowrate - BOC, TAF

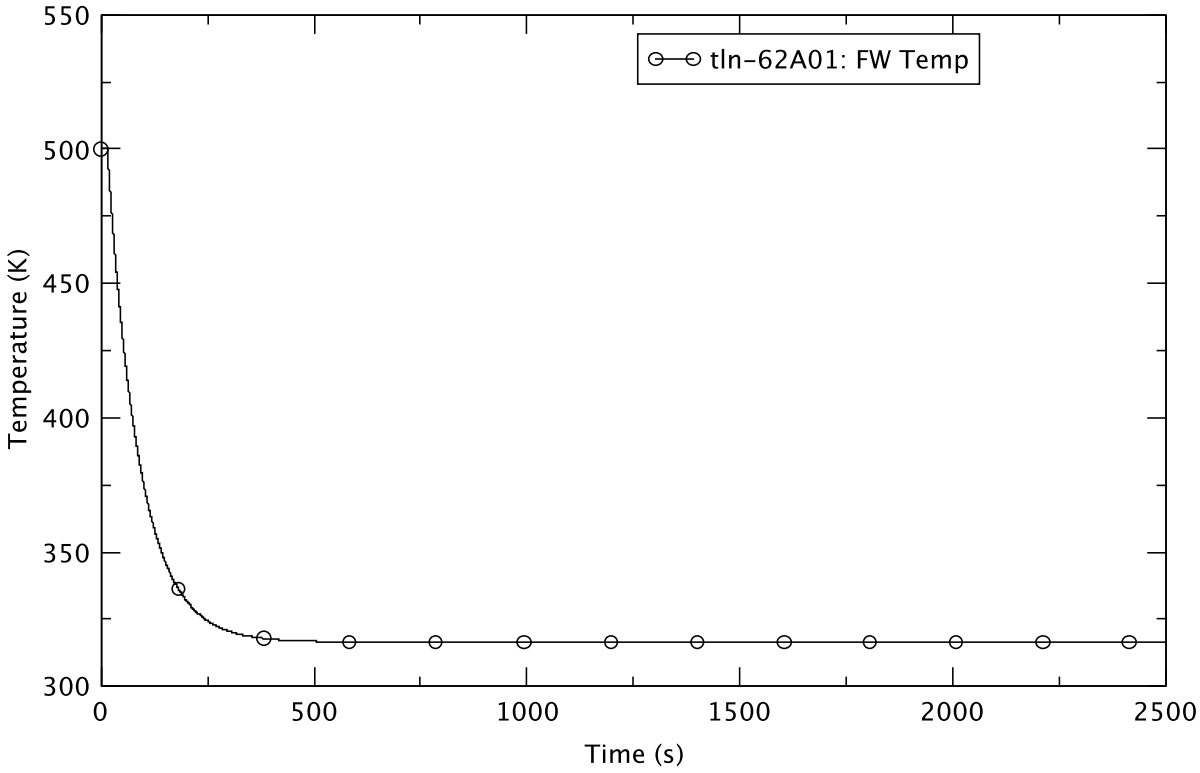

Figure 4.5 Feedwater Temperature - BOC, TAF

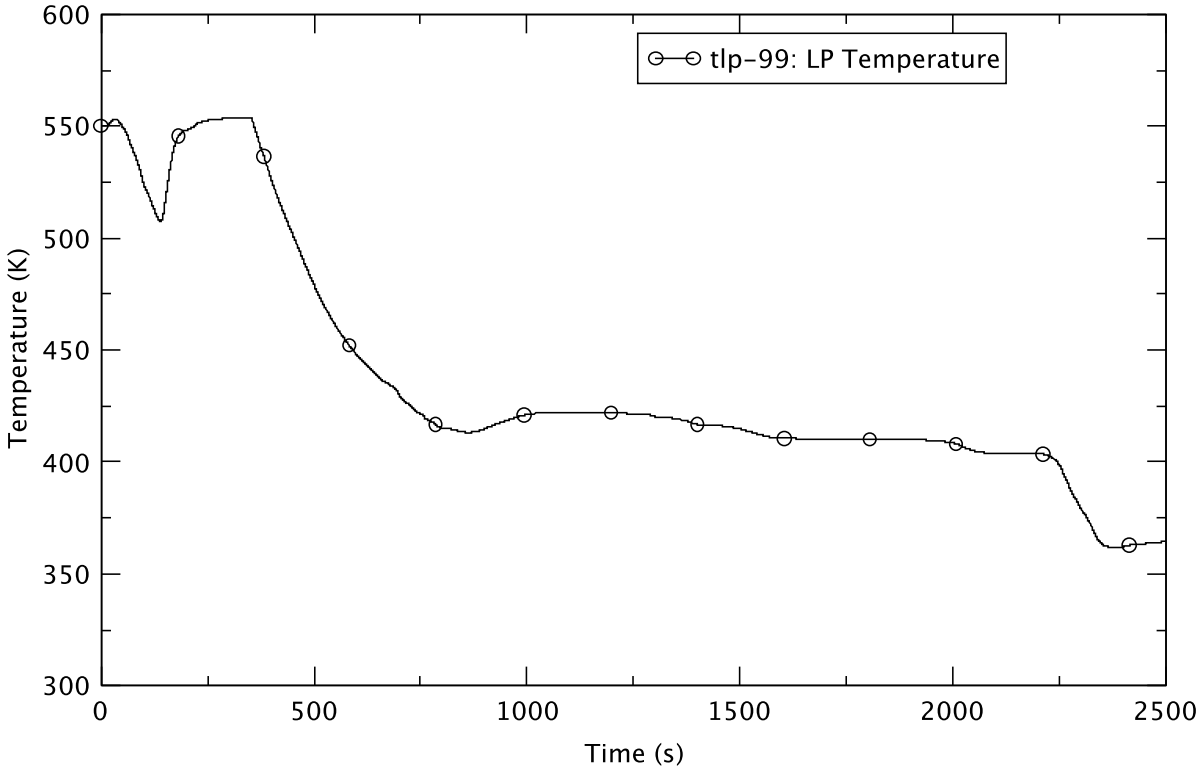

Figure 4.6 Lower Plenum Temperature - BOC, TAF

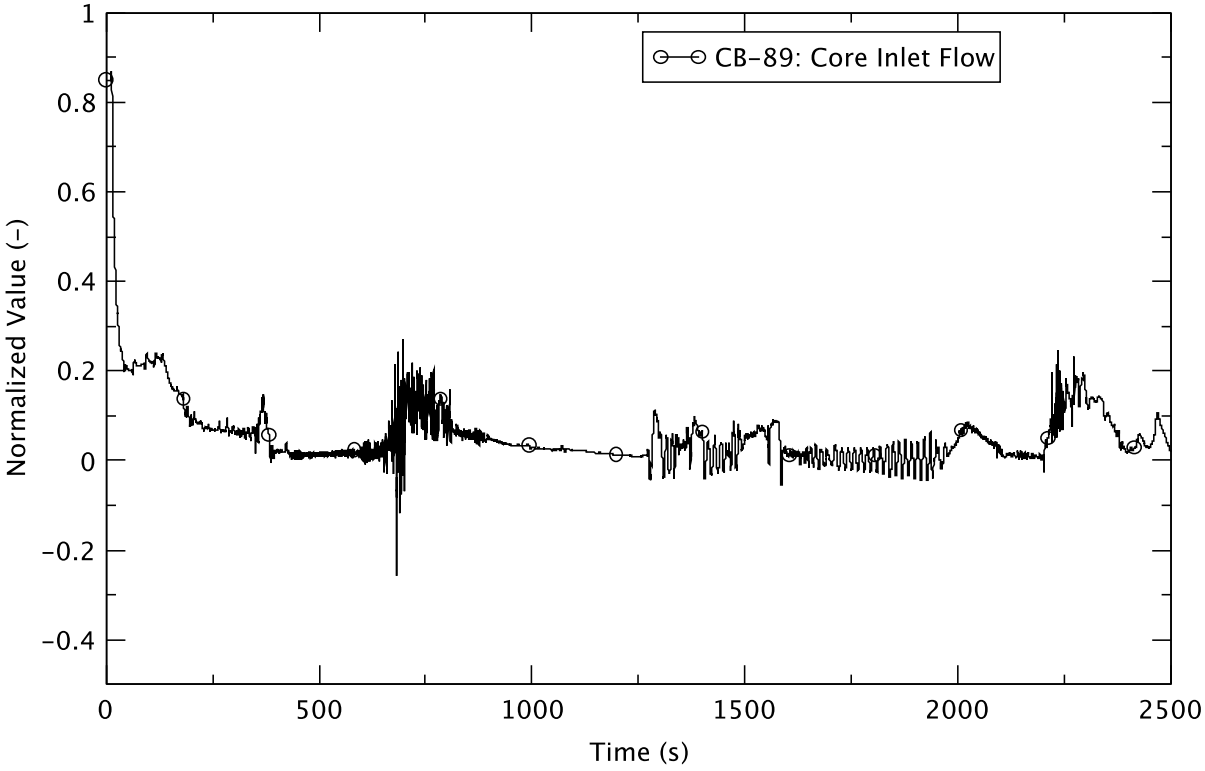

Figure 4.7 Core Flow - BOC, TAF

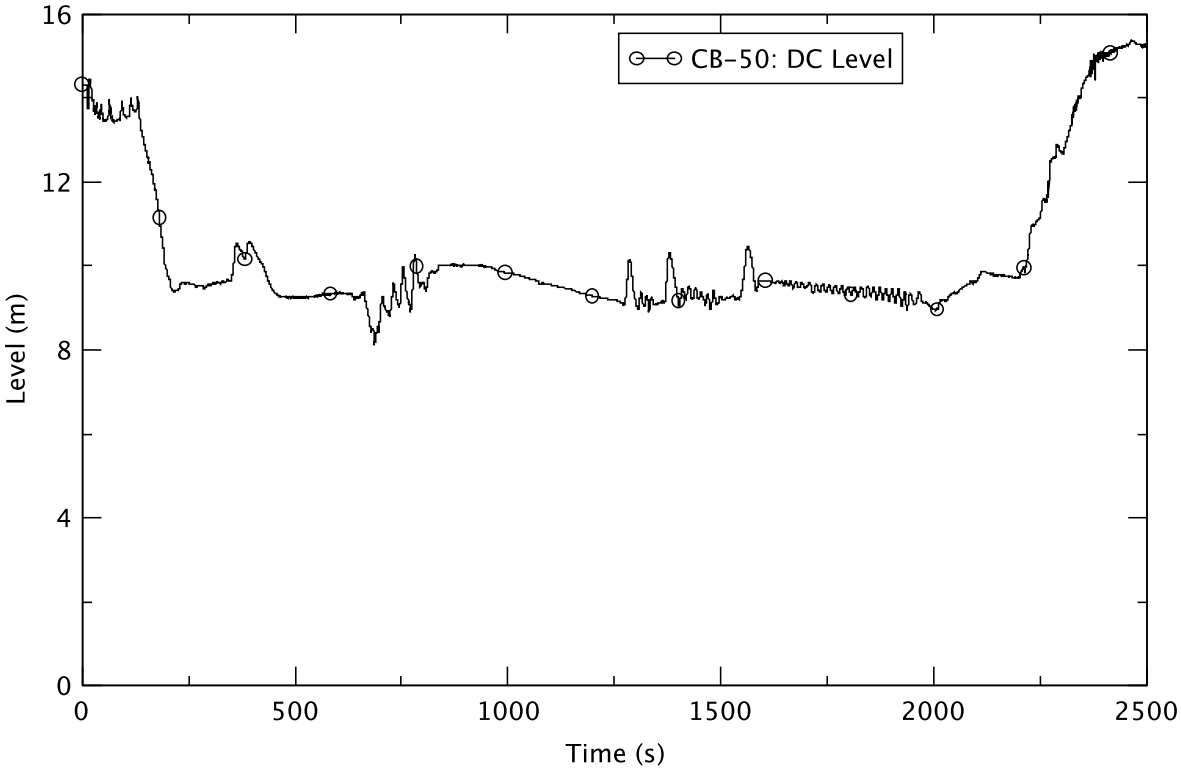

Figure 4.8 Downcomer Water Level - BOC, TAF

TRACE/PARCS simulates the manual operator action to reduce water level to TAF at 130 s. The impact of this is to immediately reduce the feedwater flow into the vessel downcomer; consequently, the level of downcomer water begins to drop. A lower level entails a smaller density-head driving force for core flow and, therefore, the core flowrate decreases as the downcomer water level declines. The lowering of water level is seen to be effective in lowering the reactor power. In turn, the demand for feedwater also declines, causing a corresponding increase in the temperature of the lower plenum that further depresses the reactor power. Notably, part of the increase in the lower plenum temperature after the lowering of the water level, arises from the discharge of saturated water from the steam separators.

The TRACE/PARCS analysis demonstrates that the reactor power does respond to 2RPT and water level control as designed, and a quasi-steady-state is approached with the release of steam to the suppression pool via the safety/relief valves. However, due to high power following the RPT, the heatup of the suppression pool causes the containment to approach its heat capacity temperature limit (HCTL). Figure 4.9 shows that at 349 s the suppression pool reaches its HCTL of 344 K. At that point, the operators are assumed to manually actuate the automatic depressurization system (ADS) to blow down the RPV.

The effect of the ED is most visible in the rapid decrease in the reactor pressure and the sudden surge in steam flow through the open ADS valves in bank D (Figure 4.10). Several other effects are observed after ED: a swell in the downcomer water level, a surge in the core flow, and a drop in feedwater flow. However, the most significant impact on the core's thermal-hydraulics due to the ED is the flashing of the coolant in the core and, to a lesser extent, in the lower plenum. This is evident in the plots of void fractions in the core bypass, Figure 4.11 for ring 1 and Figure 4.12 for ring 2, and in the lower plenum, Figure 4.13 (ring 1) and Figure 4.14 (ring 2). Notably, the extent of voiding in rings 1 and 2 in the the lower plenum differs because of differences in the pressure and temperature of the coolant in the respective rings. The refilling of the vessel lower plenum, completed at about 700 s, is preceded by a slight drop in water level as the source of the water is from the downcomer. This then increases feedwater flow and core flow.

Between 600 s and 1000 s, the core power fluctuates due to perturbations in the core flow and the downcomer water level as the feedwater control system attempts to maintain water level to TAF. After 1000 s, these disturbances in core flow and water level, reflecting periodic flashing in the core region because the core inlet temperature is hovering around saturation, have little effect on the reactor power as the depressurization, together with boron injection, shuts down the reactor and the total power drops to that due to decay heat (Figure 4.1).

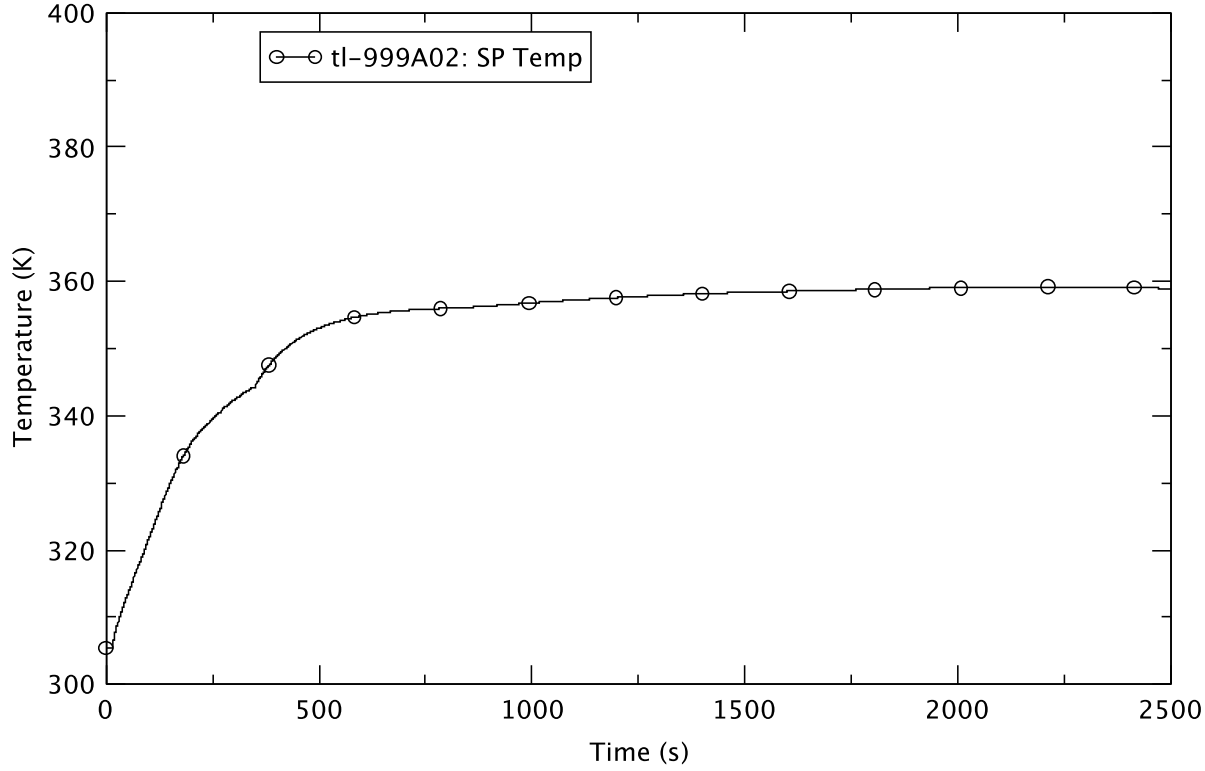

Figure 4.9 Suppression Pool Temperature - BOC, TAF

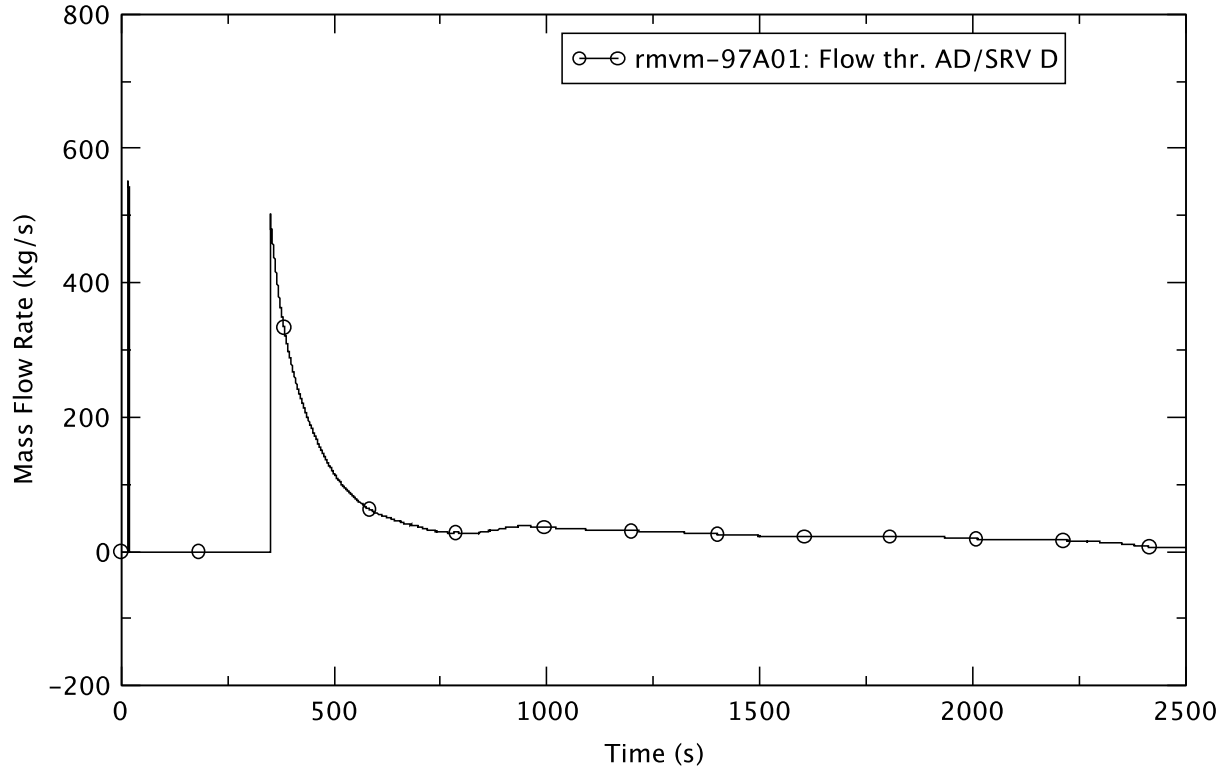

Figure 4.10 Mass Flow Through SRV/ADS Bank D - BOC, TAF

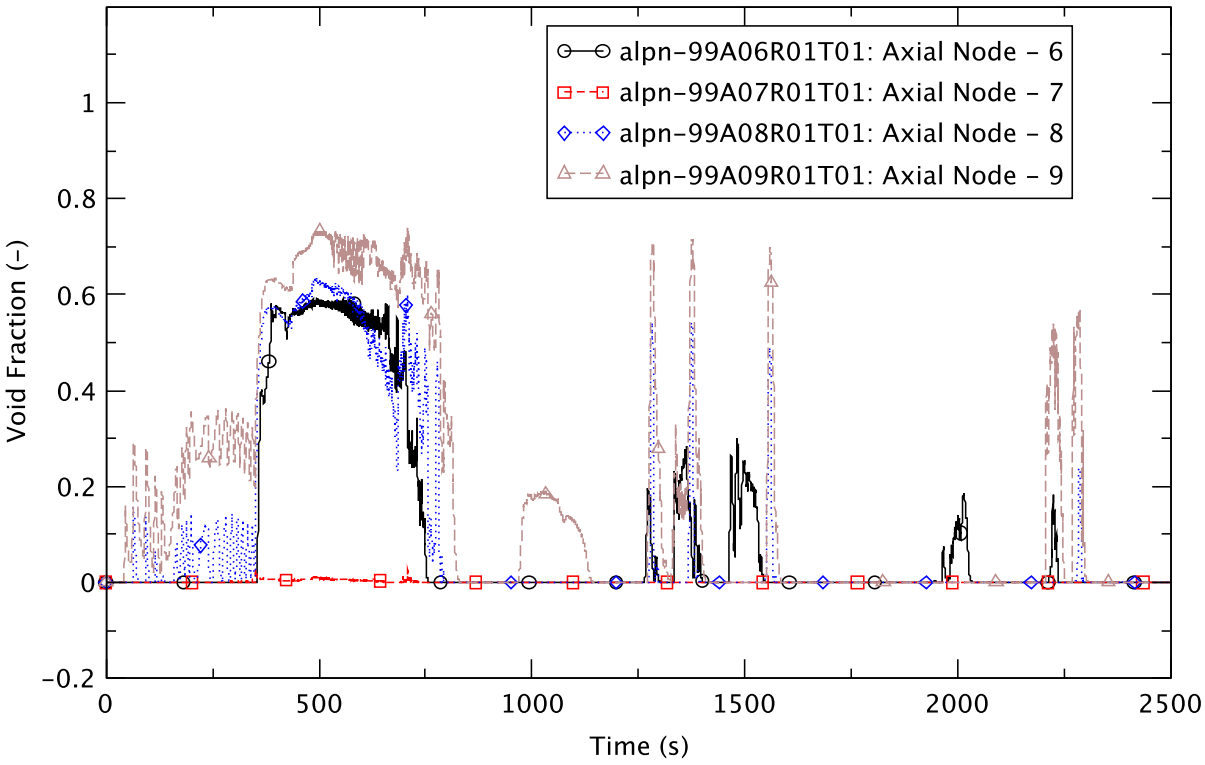

Figure 4.11 Void Fraction in Core Bypass (Ring-1) - BOC, TAF

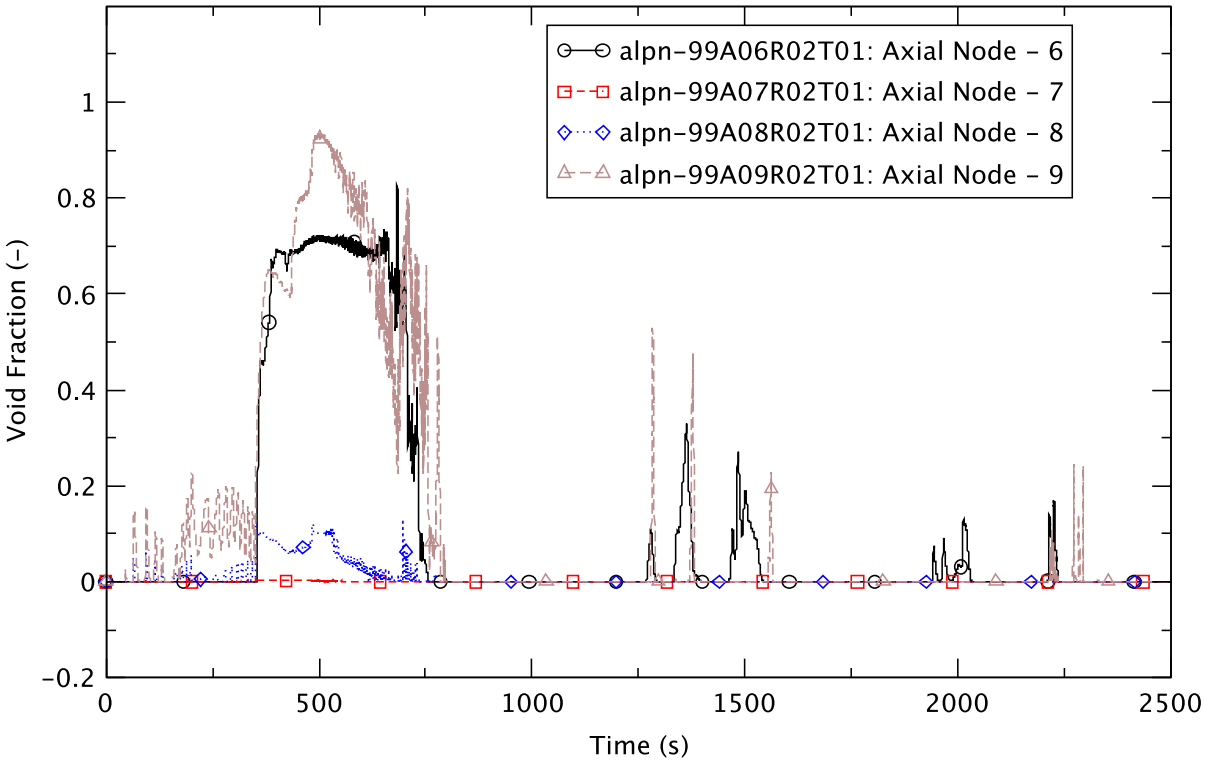

Figure 4.12 Void Fraction in Core Bypass (Ring-2) - BOC, TAF

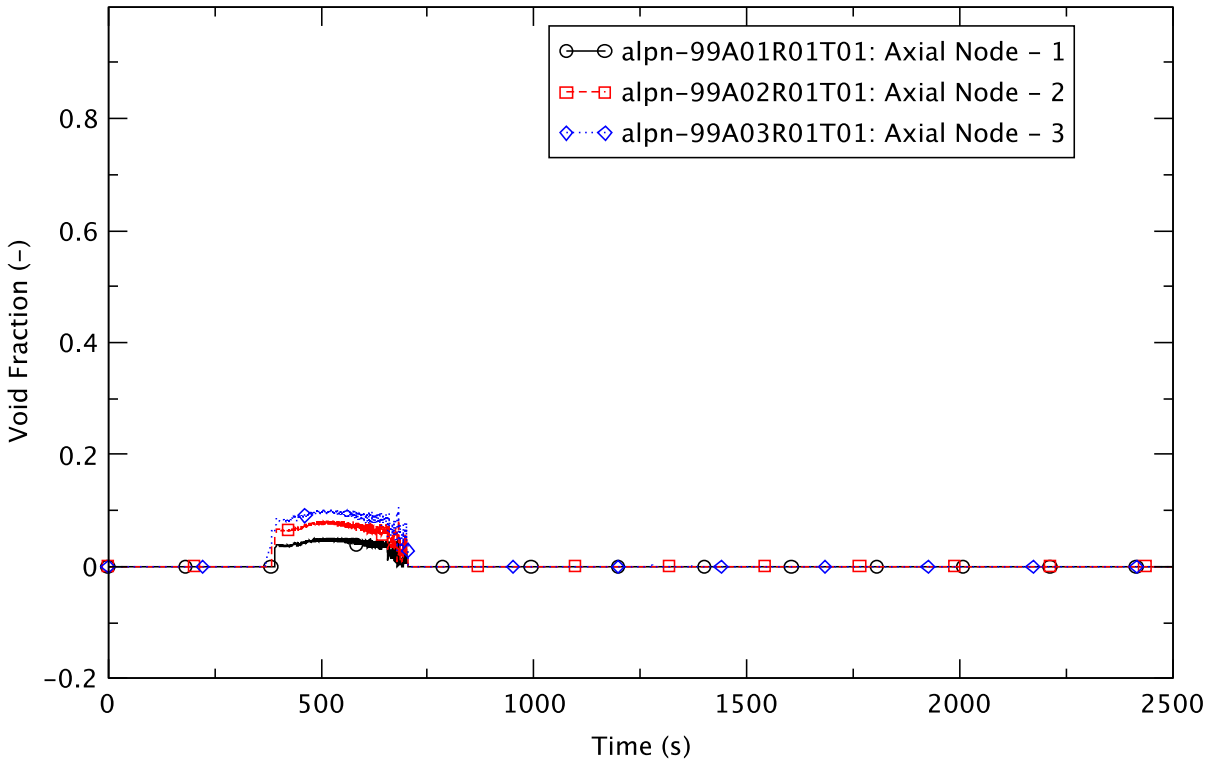

Figure 4.13 Void Fraction in Lower Plenum (Ring-1) - BOC, TAF

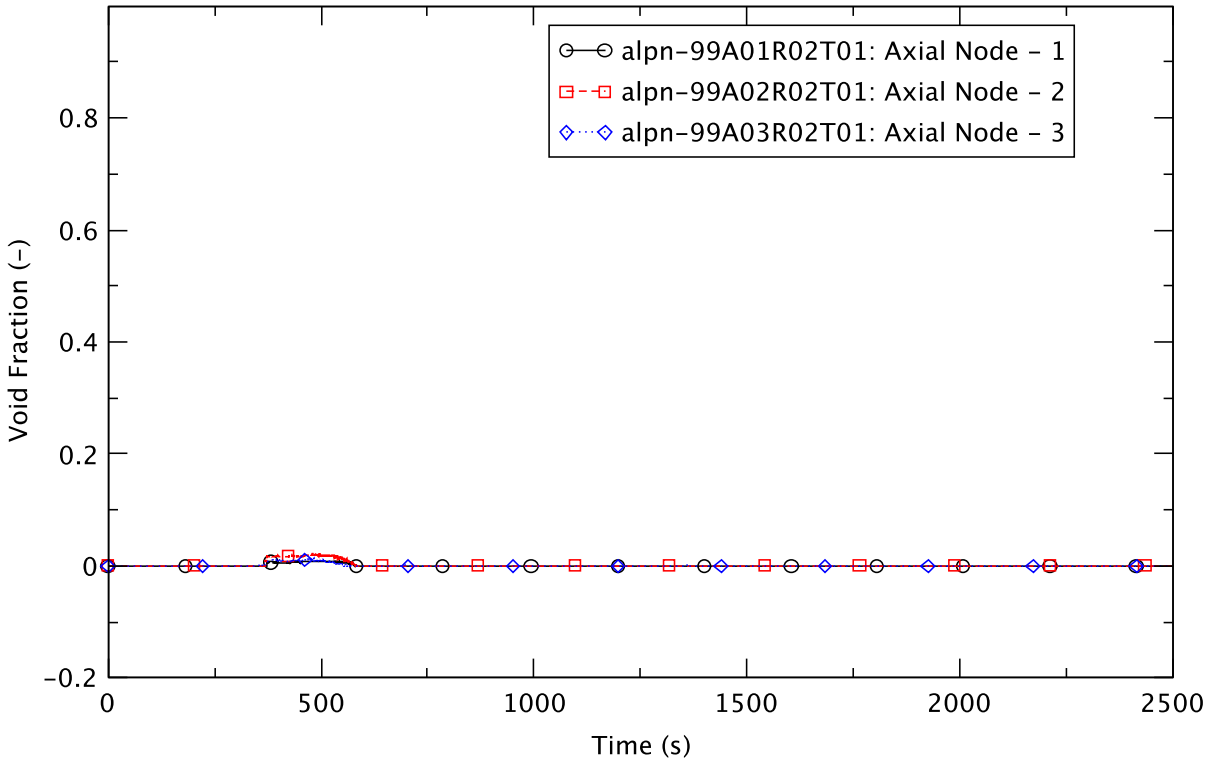

Figure 4.14 Void Fraction in Lower Plenum (Ring-2) - BOC, TAF

The core average void fraction, as inferred from the moderator density calculated by PARCS, is shown in Figure 4.15. It is around 0.6 for the early part of the transient, and becomes about 0.4 after quasi-steady natural circulation is established at about 1000 s. The core void drops to zero after the reactor water level is restored to its normal level.

Boron injection is an important action the operator undertakes to mitigate reactor power in an ATWS-ED transient. In the TRACE/PARCS model, boron is injected to the lower plenum of the VESSEL component with an effective concentration that accounts for mixing and remixing (Section 2.3.7 and Appendix A have more details). The boron inventory in the core region is plotted in Figure 4.16 as a function of time. The boron injection starts at 211 s, and it takes 30-40 seconds for it to reach the core region. In general, the boron inventory tracks with the liquid fraction in the core, as is inferred from the core average void fraction (Figure 4.15). The increase at about 700 s coincides with the refilling of the lower plenum along with rising downcomer water level from a higher feedwater flow, causing an increase in core flow. A later rise in boron inventory occurs after recovery of the water level, commencing at 2180 s.

The boron concentration in the lower plenum is shown in Figure 4.17 and Figure 4.18, respectively, for ring 1 and ring 2 of the vessel. The initial buildup of boron is consistent with its path, entering the vessel at axial node 4 and then being carried sequentially by coolant flow to axial nodes 3, 2, and 1. Thus initially, concentration is highest in axial node 3 and lowest in axial node 1. There is a drop in boron concentration in the lower plenum around 400 s. This is due to the effective boron concentration at the injection point becoming zero as shown in Figure 4.19. The reduction in boron concentration at the injection point is a feature of the boron transport model when stratification is predicted. The model tracks the stratified boron for later delivery into the coolant when the flow condition again supports its remixing.

There are three other distinct times when the model predicts zero boron concentration at the injection point. Around them, at ~1100 s, ~1700 s, and ~2100 s, the boron concentration in axial node 3 in ring 1 dips below the concentration predicted in nodes 1 and 2. It takes time for the boron to build up to sufficient concentration in the core, overcoming positive reactivity components, to enable the reactor to shutdown.

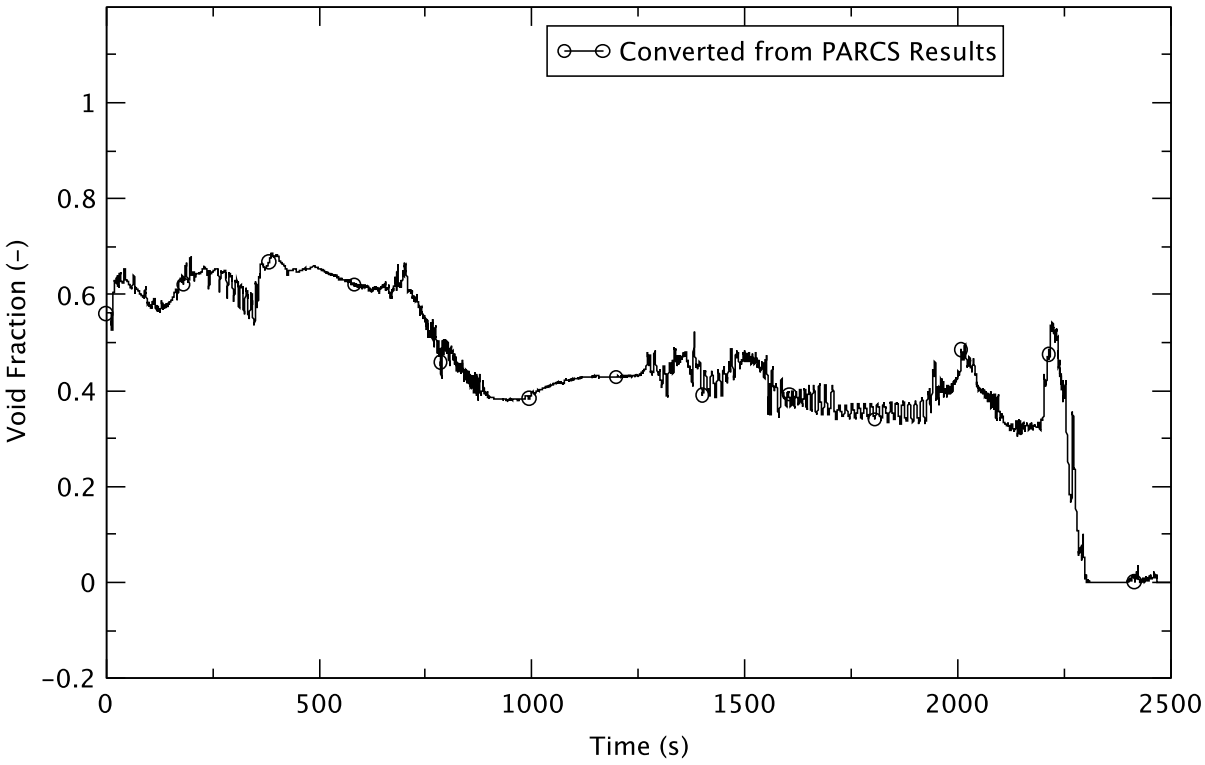

Figure 4.15 Core Average Void Fraction - BOC, TAF

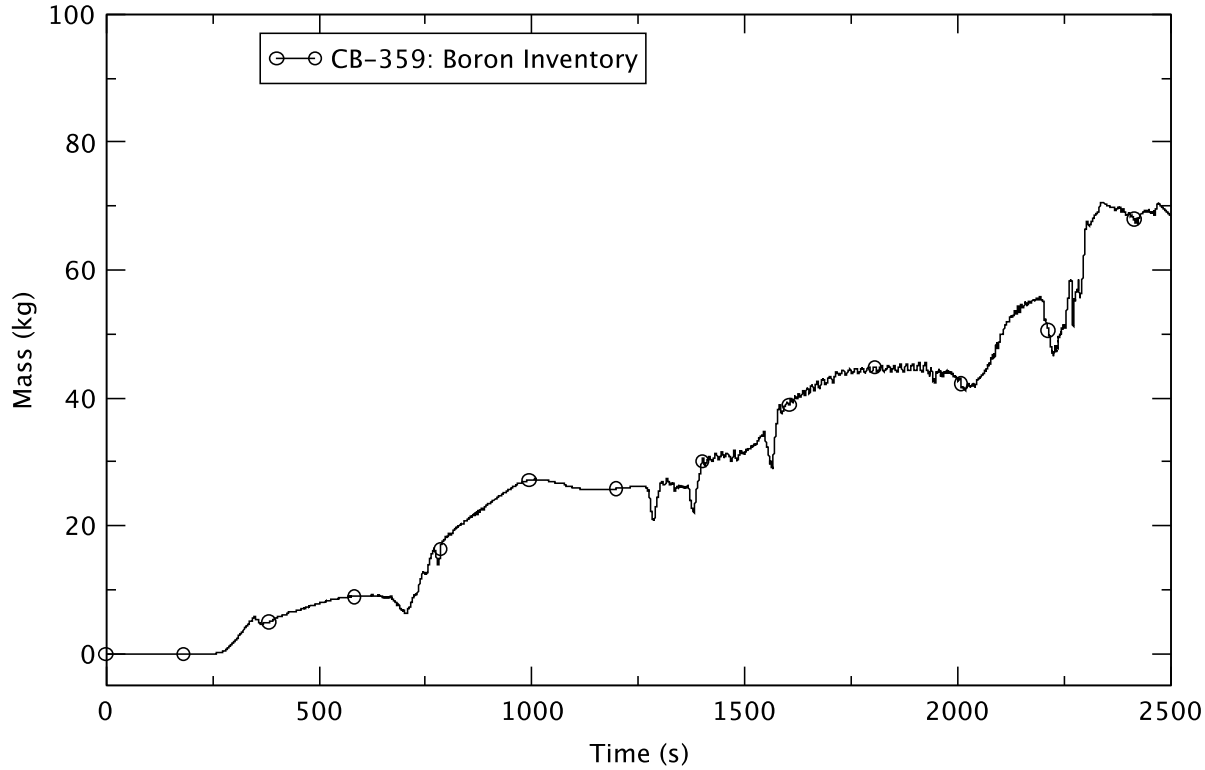

Figure 4.16 Boron Inventory in the Core - BOC, TAF

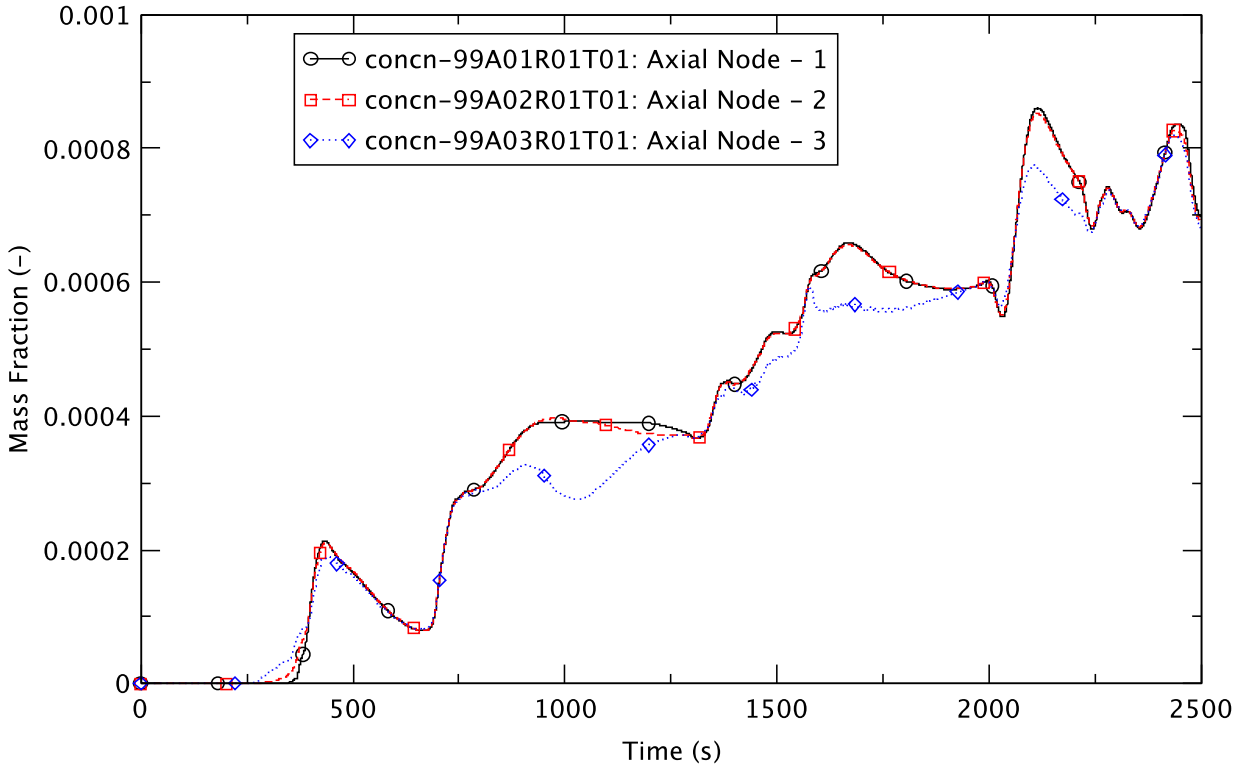

Figure 4.17 Boron Concentration in Ring 1 - BOC, TAF

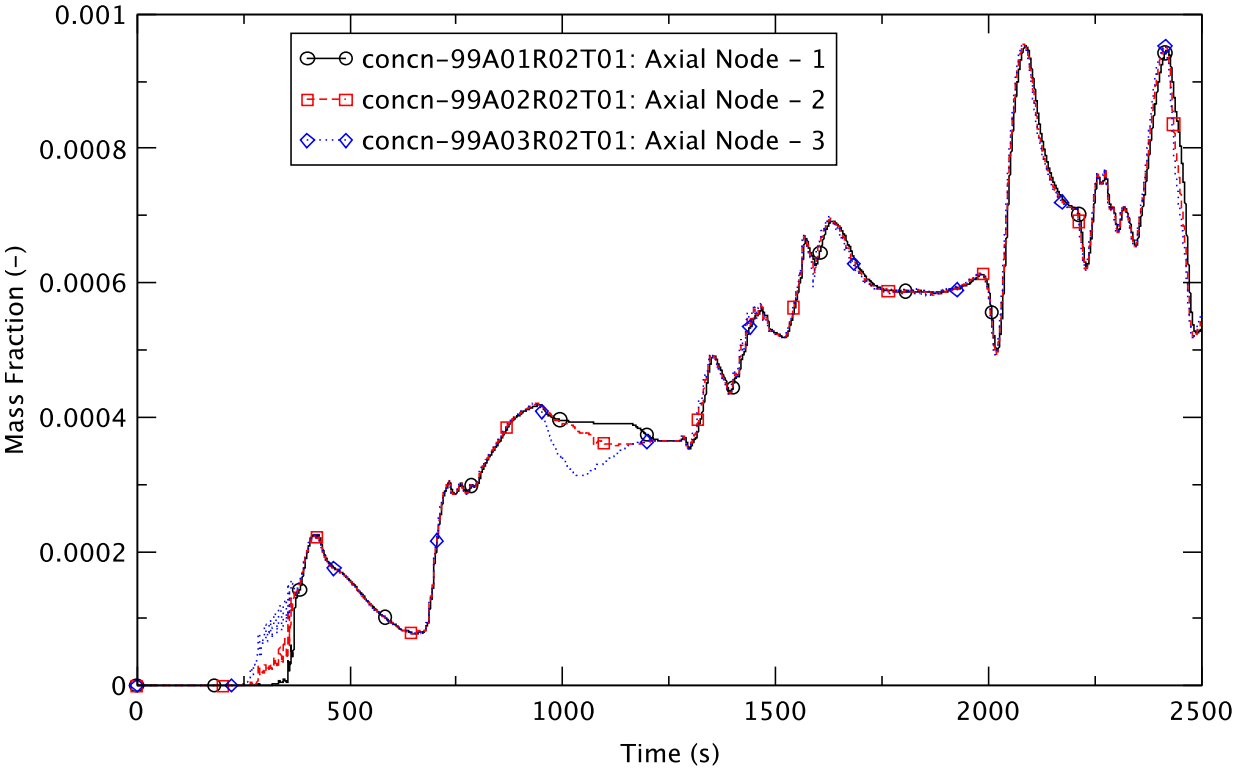

Figure 4.18 Boron Concentration in Ring 2 - BOC, TAF

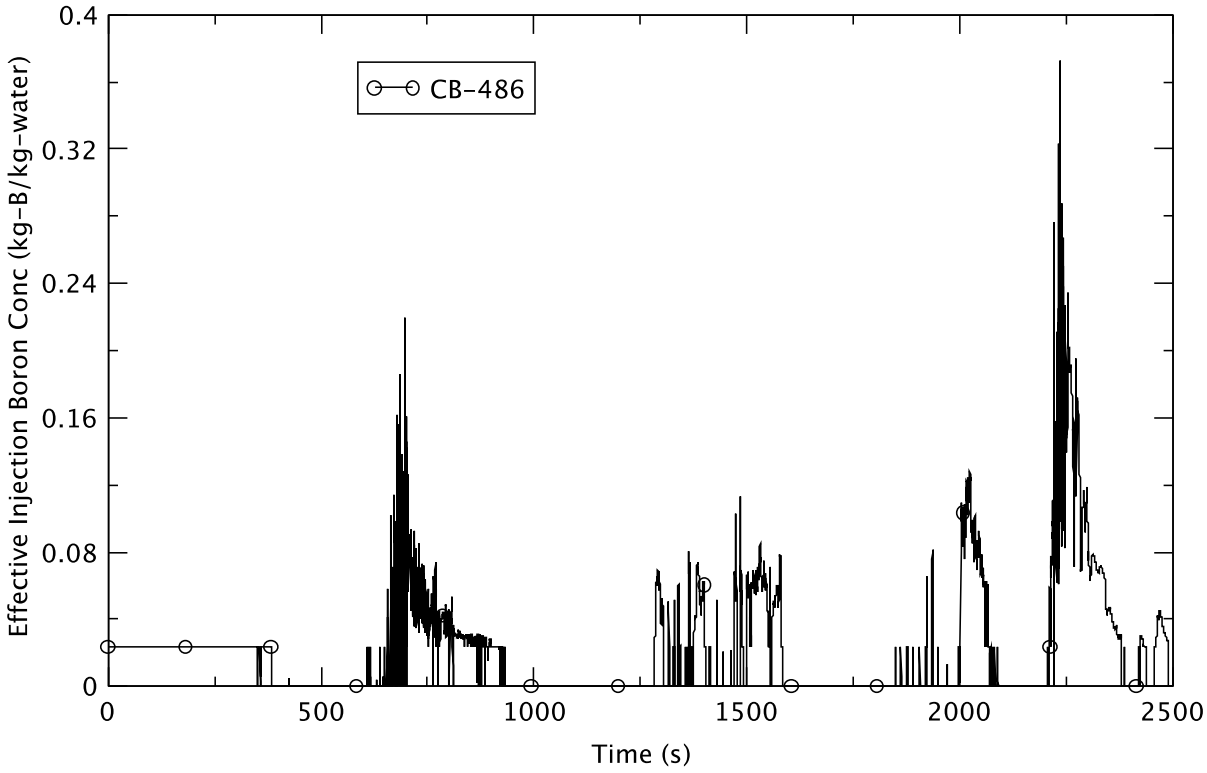

Figure 4.19 Effective Injection Boron Concentration - BOC, TAF

Figure 4.20 shows that the net reactivity of the core stays negative after around 1000 s; indicative of sufficient buildup of negative boron reactivity to sustain a reactor shutdown. This figure also shows all components of reactivity feedback calculated by PARCS; fuel temperature (T_f or Doppler), moderator density (dm), and boron (Boron). It depicts that the restoration of water level at 2180 s elicits a positive increase in the moderator density reactivity, but that is more than compensated for by a corresponding increase in the negative contribution from boron reactivity.

A key assumption in modeling boron transport is to relate the core flowrate to the effective entrainment of the borated solution. The normalized core flow at the exit of the jet pump was shown earlier in Figure 4.7. It is also interesting to show the mass flow in the recirculation line. After 2RPT, the core flow is under natural circulation and the flow in the recirculation line is expected to decay to zero. Figure 4.21 reveals that the latter reaches a quasi-steady value of ~500 kg/s after the 2RPT. It then declines to zero only after water level control is initiated at 130 s. The figure also illustrates that actuation of feedwater flow (Figure 4.4) and the ensuing perturbations to the downcomer water level also induce flow in the recirculation line.

The outcome of the ATWS-ED BOC TAF transient for the four figures-of-merit discussed in Section 1.2 is explained next.

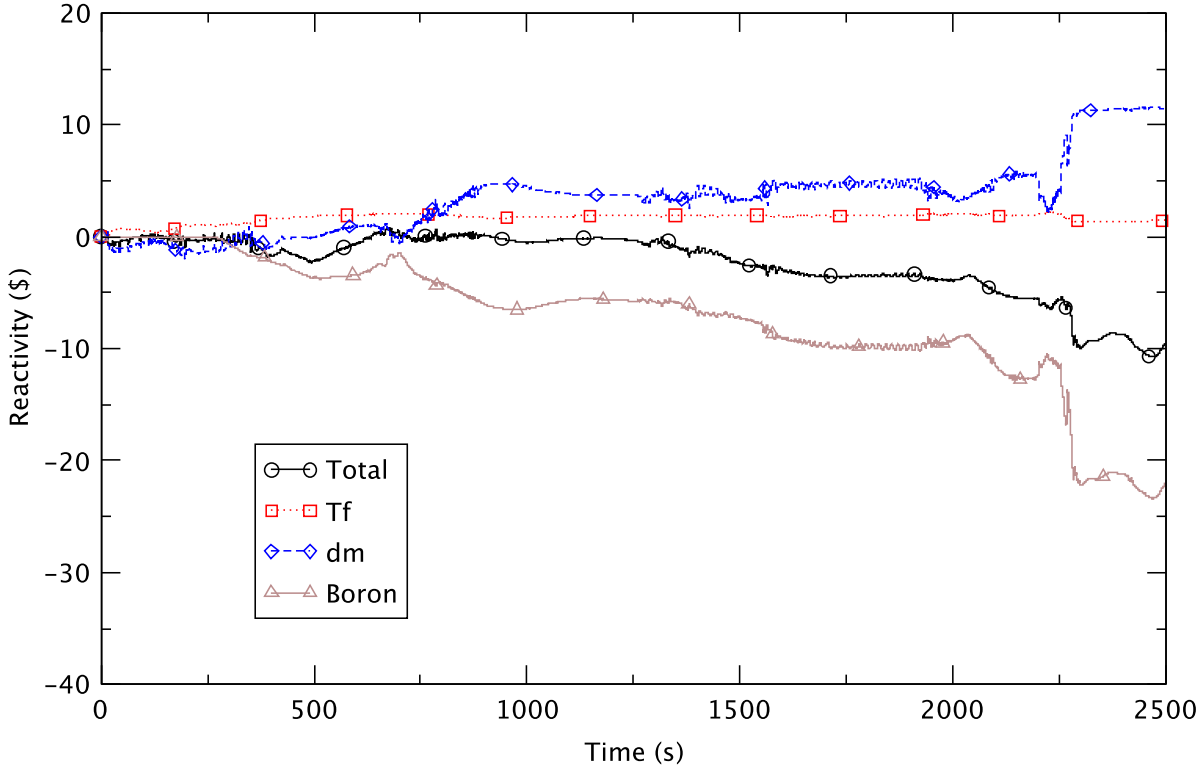

Figure 4.20 Core Reactivity - BOC, TAF

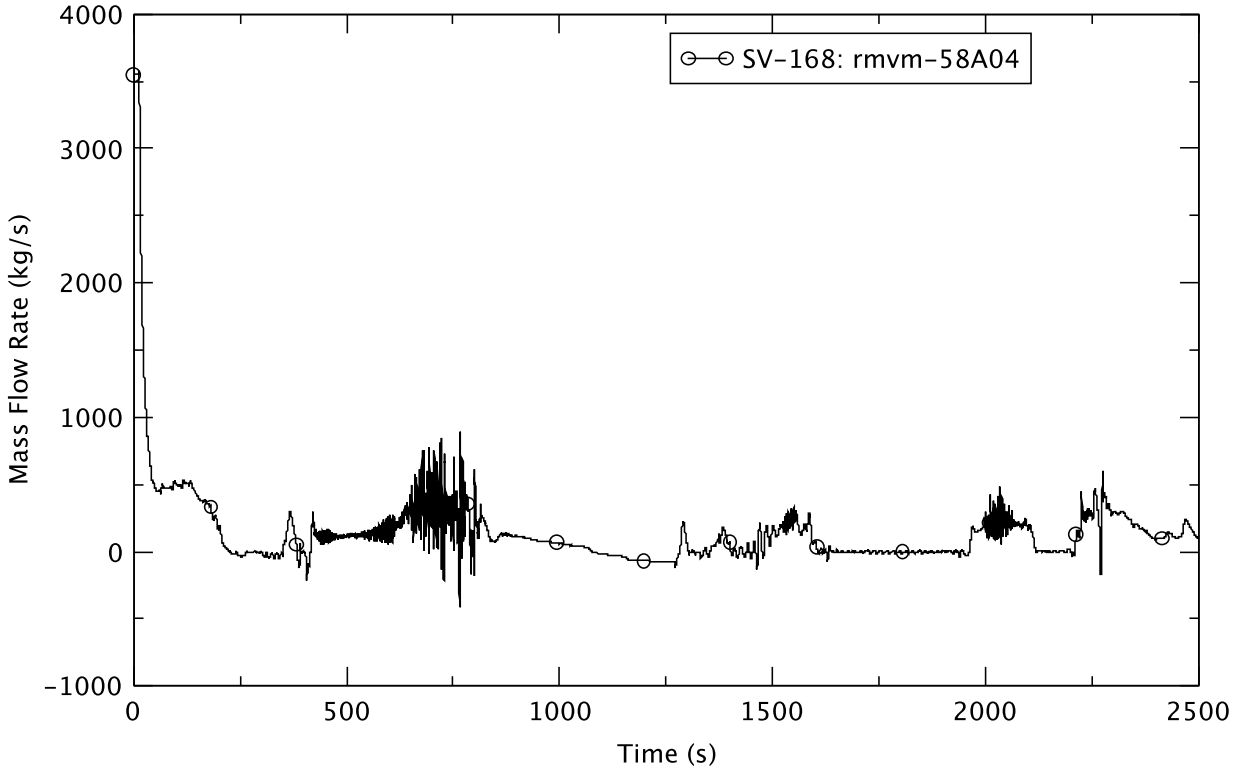

Figure 4.21 Recirculation Line Flow - BOC, TAF

1) Peak clad temperature (PCT)

Figure 4.22 plots the core-wide PCT as a function of time. The maximum PCT occurs at 137.4 s when the power still is relatively high after the 2RPT, and the core flow starts to drop responding to water level control. There is no overheating of the clad; the PCT stays well below 1478 K (2200°F). The axial clad temperature, shown in Figure 4.23, displays fairly uniform temperature profile(s) for longer than 500 s, as did the fuel centerline temperature (Figure 4.24).

2) Recriticality

The TRACE/PARCS calculation shows that there is no recriticality due to either choking in the SRVs, or dilution of boron in the coolant. The steam flow through the SRVs is choked but the SRVs have sufficient capacity that there is no significant repressurization of the RPV. The choking condition (Figure 4.25) is calculated for the SRV/ADS bank D for almost the whole duration of the transient. It is eliminated when the steaming rate is reduced by injecting feedwater at 2180 s to raise the water level.

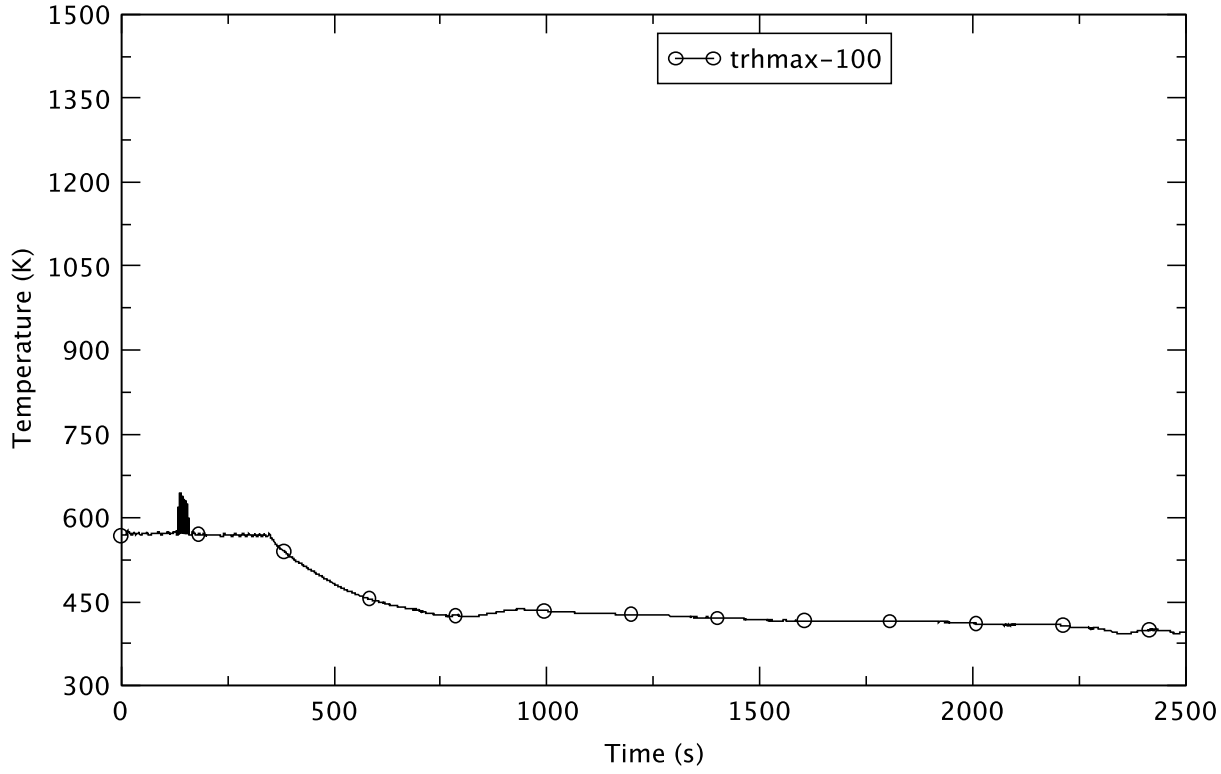

Figure 4.22 Peak Clad Temperature - BOC, TAF

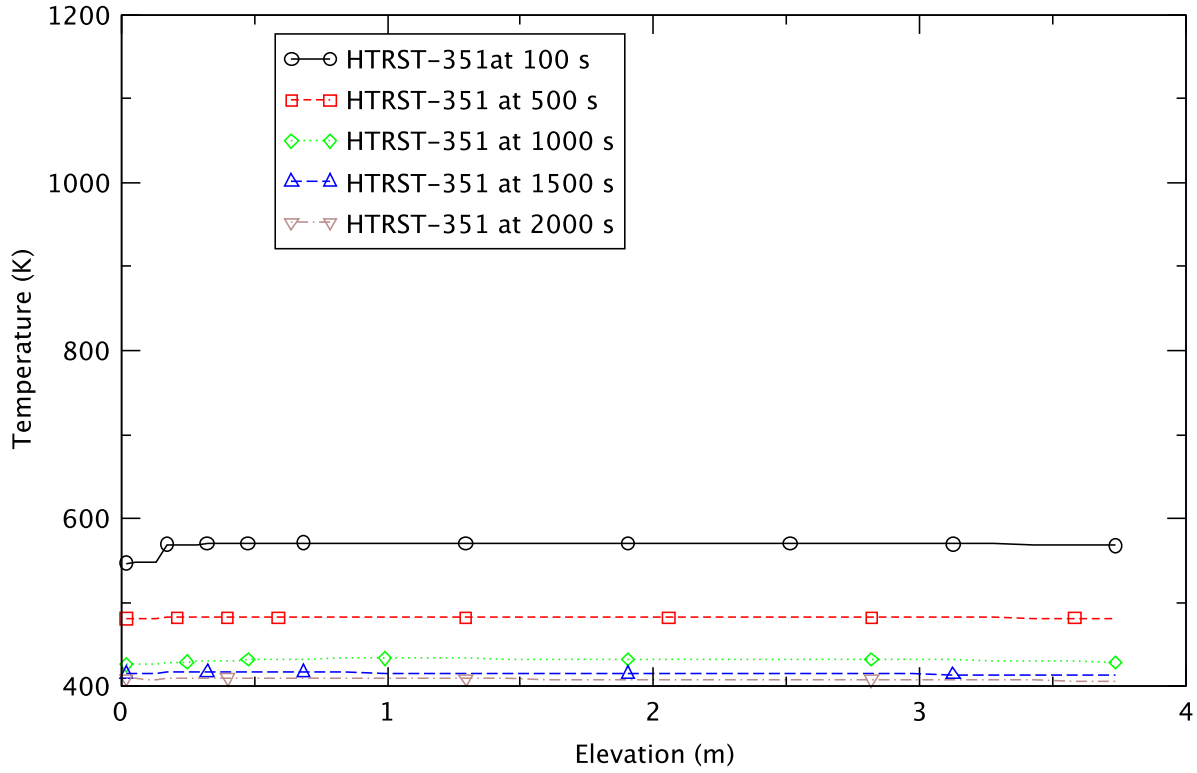

Figure 4.23 Axial Profile of Clad Temperature - BOC, TAF

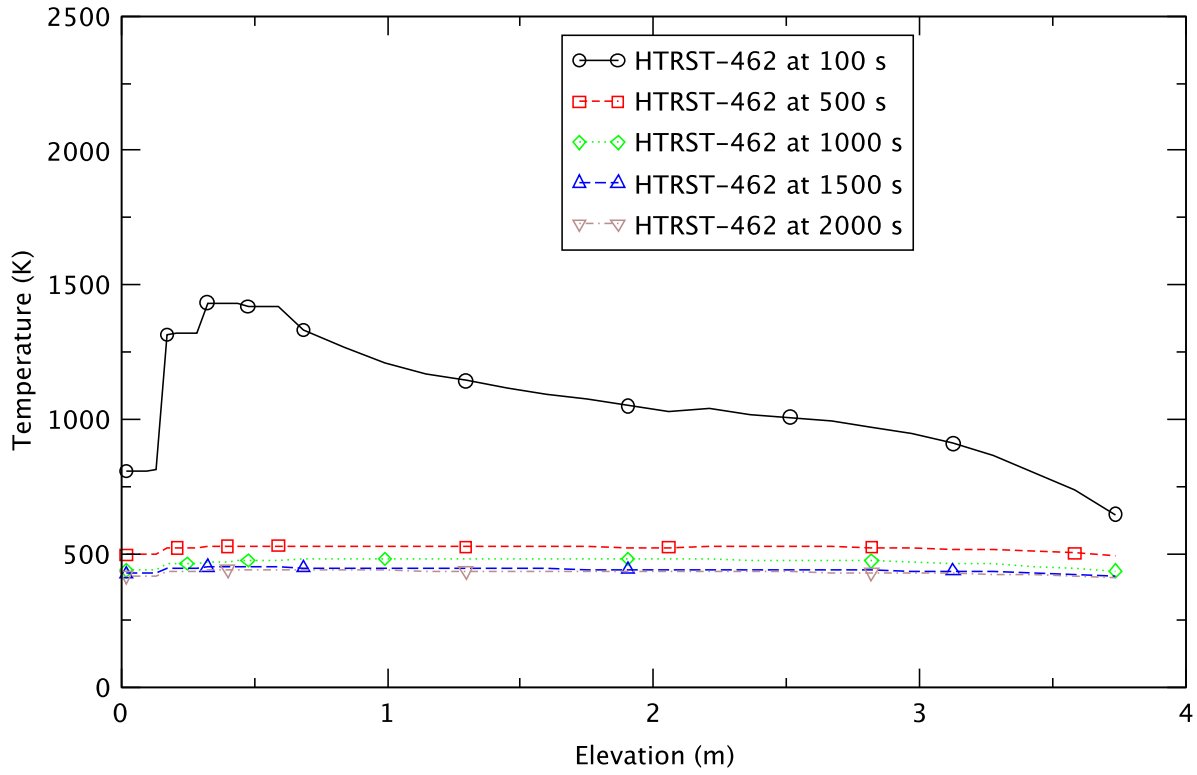

Figure 4.24 Axial Profile of Fuel Centerline Temperature - BOC, TAF

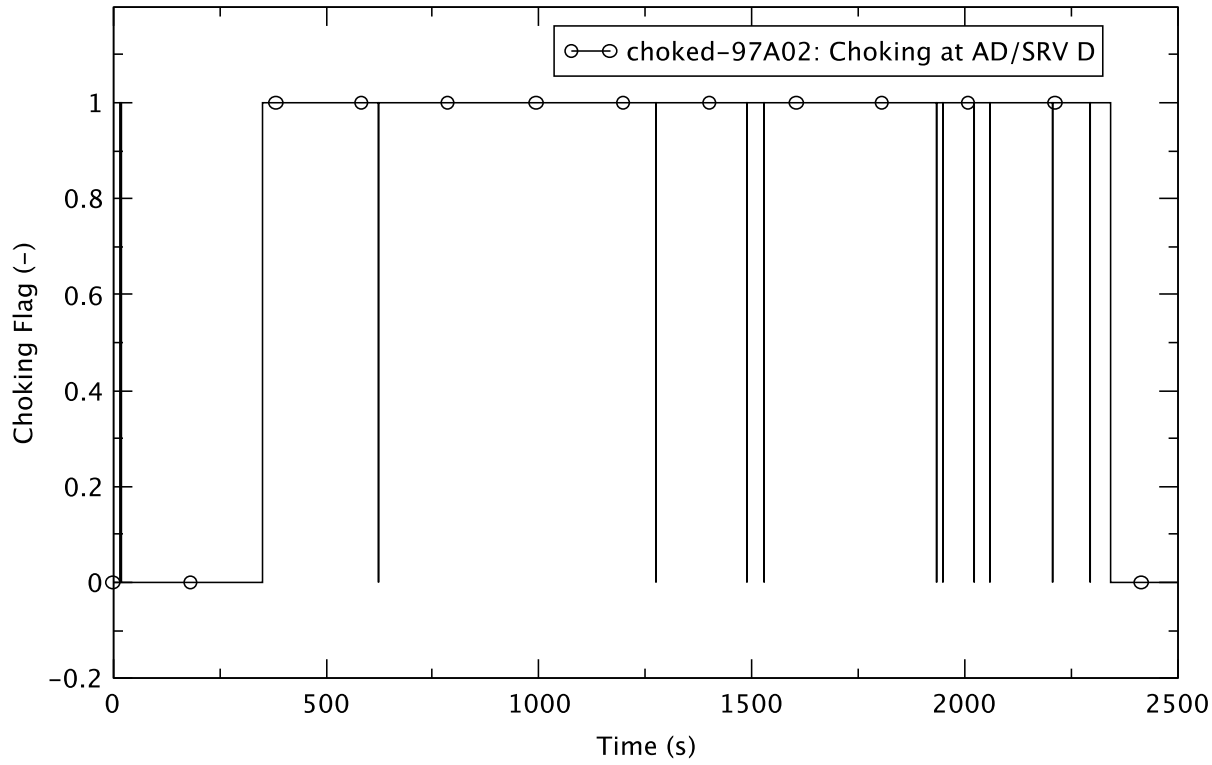

Figure 4.25 Choking Flag for SRV/ADS Bank D - BOC, TAF

Analyses undertaken during the review of the MELLLA+ licensing topical report [1] did not simulate the manual cycling of the valves by the operator, and so the current analysis did not (i.e., the ADS valves remain open). Depending on the plant's specific emergency-operating procedures (EOPs), the operator may cycle the valves to control the reactor pressure between 50 psi and 100 psi after the emergency depressurization is completed (i.e., reactor pressure < 135 psi). In the current analysis, recriticality is not evident, but plant-specific EOPs should be accounted for in plant-specific analyses.

Another potential cause of recriticality is the dilution of boron concentration in the core that can result from boron stratification in the lower plenum due to a low flow-rate, and/or an increase in water density due to ED and the addition of feedwater. The TRACE/PARCS calculation does not indicate any instance of recriticality. Therefore, the analysis demonstrates that the effects of ED and feedwater injection are not sufficient to cause recriticality due to boron dilutiion. The effect of boron dilution is observed only briefly between 500 s and 700 s in Figure 4.20, a time plot showing different reactivity components. In the figure, boron reactivity is seen to be the dominant contributor maintaining the reactor shutdown from ~1000 s onward.

3) Wetwell temperature

The temperature in the suppression pool reaches its maximum of 359.2 K at about 2208 s. The TRACE/PARCS calculations simulate two equivalent residual heat removal (RHR) loops in the suppression pool cooling mode. Additionally, the TRACE/PARCS calculations treat the passive heat structures in the suppression pool and wetwell airspace. The results from them demonstrate that these features suffice to prevent excessive heat-up of the suppression pool to its limit of 373 K, that is defined as the boiling temperature at atmospheric pressure.

4) Containment pressure

In Figure 4.26, the pressure in the drywell is seen to approach the maximum of 0.162 MPa at 538 s, shortly after the ED. The maximum pressure is low enough not to challenge the integrity of the containment.

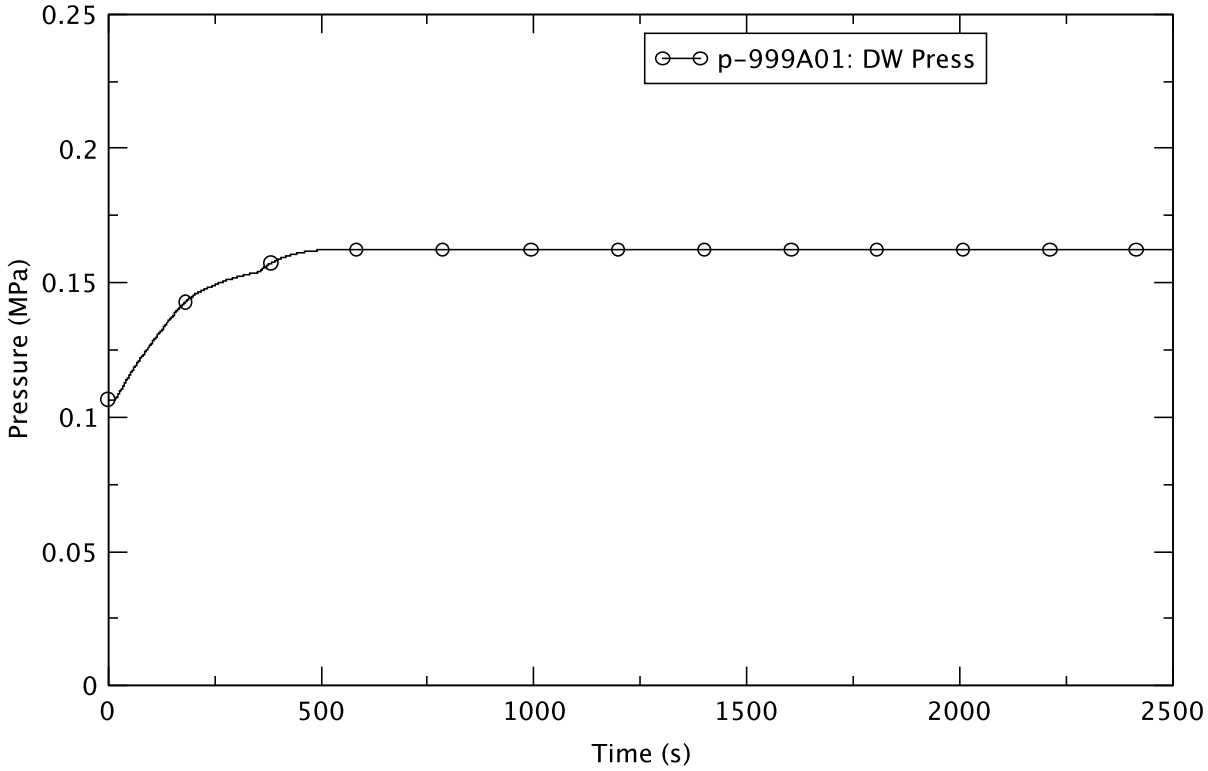

Figure 4.26 Drywell Pressure - BOC, TAF

In summary, the TRACE/PARCS analysis demonstrates that the ATWS-ED transient initiated by MSIV closure is mitigated successfully by a combination of the 2RPT and the operator actions that depressurized the RPV, reduced power by controlling water level, and injected boron as the secondary shutdown mechanism.

4.2.3 Effect of Level Control at BOC

In an ATWS-ED event, level control is an operator action to reduce core power. When the core is cooled by natural circulation (after 2RPT), lowering the downcomer water level translates to less hydrostatic head available to drive core flow. With a lower core flow, the core void fraction increases, so resulting in a higher negative void (moderator density) reactivity feedback, and a lower core power. However, boron reactivity also contributes to the core reactivity and contributes reactivity in the opposite direction of the void reactivity under these conditions. With an increasing core void fraction, the boron inventory in the core declines, leading to a lower negative boron reactivity.

The results of the TRACE/PARCS analysis suggest that a lower water level does not always result in a lower power if the feedback from boron reactivity becomes non-negligible. Another observation derived from the TRACE/PARCS results is that voiding in the core can influence two competing effects that determine the core flow; it can increase the buoyancy to drive the

natural circulation flow, while at the same time increase flow resistance due to two-phase frictional losses. The TRACE/PARCS results suggest that at relatively high core flow (e.g., with water level at TAF+5), voiding in the core helps to promote higher flow while the opposite is true when the core flow is relatively low (e.g., with water level at TAF-2). A third observation from the TRACE/PARCS results is that an ED initiated at a relatively high reactor power (e.g., with water level at TAF+5) will engender slower depressurization and a milder transient response in many of the thermal-hydraulic parameters.

A select set of plots (Figure 4.27 to Figure 4.36) is used to compare and contrast the transient responses of three BOC cases when the water level is controlled to TAF, TAF-2, and TAF+5.

In general, as seen in Table 4.4, the responses of the TAF and TAF-2 cases are quite similar as compared to the responses of the TAF+5 case. The only exception is in the maximum PCT (TRACE output parameter trhmax). For the TAF+5 and the TAF cases, the maximum occurs early, right after the initiation of water level control when core flow is still relatively high. For TAF-2 there is a delayed heat-up of the core at a time when the reduction in water level has caused the core flow to approach a lower quasi-steady value, and the corresponding maximum PCT is more limiting than in the other two cases.

The reactor power (Figure 4.27), generally exhibits similar responses for all three cases. However, there appears to be a break point in the power response for the TAF+5 case at about 500 s. A review of the total reactivity (Figure 4.32) reveals that it fluctuates very close to zero (null reactivity) until 500 s, and thereafter, total reactivity stays negative, and the reactor finally is on the way to being shutdown.

The TAF+5 case with a higher water level (Figure 4.30) that supports a higher core flow (Figure 4.29) has a higher power than the other cases before 500 s. Around 500 s, the reactor power is decreasing. This finding indicates the effectiveness of the operator actions to reduce the level of core power and put the plant on a trajectory to hot shutdown.

The higher power with TAF+5 control leads to an earlier depressurization (at 297 s) relative to the other two cases (Figure 4.28). With the reactor still critical, the decline in power is small, and the rate of depressurization is reduced for the TAF+5 case. Correspondingly, the decrease in core flow (Figure 4.29) and level swell (Figure 4.30) are much subdued in this case compared to the other two cases.

Table 4.4 Comparison of Key Results for BOC Base Cases

Key Event	BOC TAF	BOC TAF-2	BOC TAF+5
Maximum PCT (trhmax-100)	646 K (137 s)	707 K (588 s)	639 K (146 s)
Core Boron Inventory (CB 359) > 0.01 kg	248 s	252 s	245 s
Emergency Depressurization	349 s	345 s	297 s
Maximum Drywell Pressure	0.162 MPa (538 s)	0.162 MPa (536 s)	0.170 MPa (772 s)
Reactor Shutdown (Stayed < 3.25% Initial Power)	1001 s	1075 s	975 S
Maximum Suppression Pool Temperature	359.2 K (2208 s)	357.9 K (2203 s)	368.0 K (2156 s)

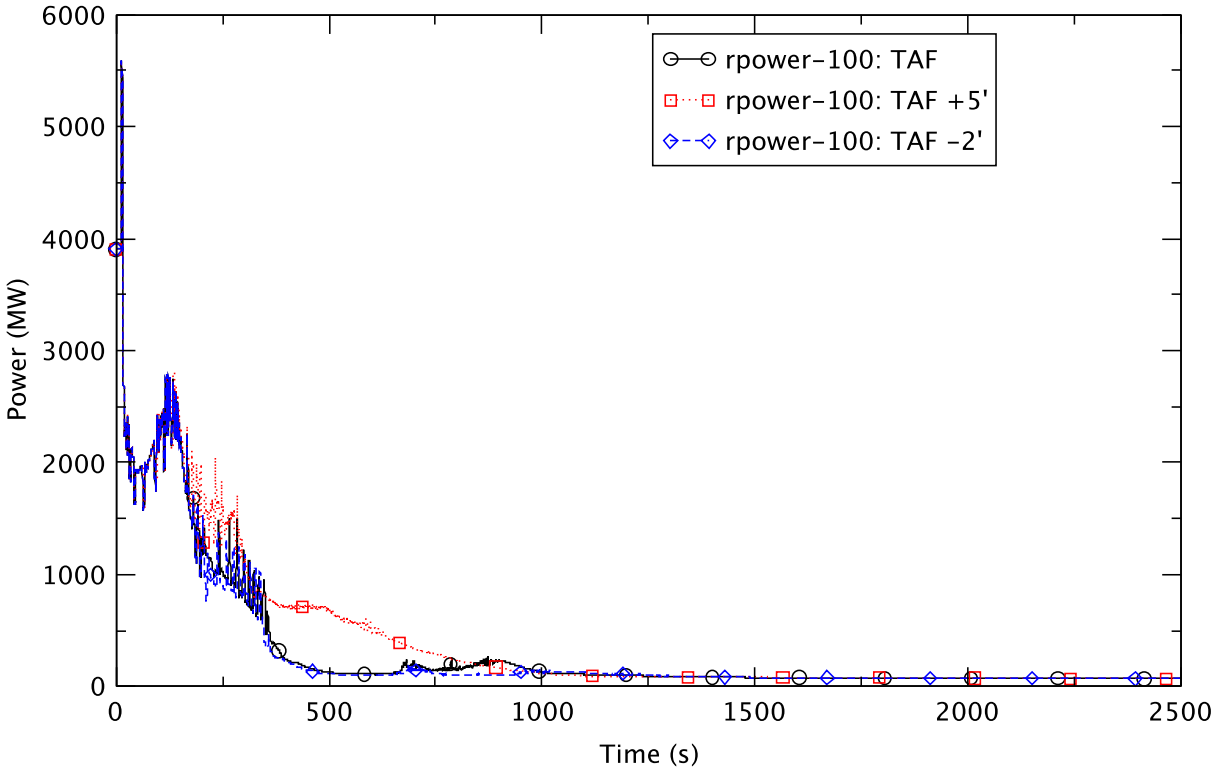

Figure 4.27 Reactor Power - BOC Base Cases

The timing of the ED for the TAF and TAF-2 cases is close. It is a little counter-intuitive to observe the TRACE/PARCS result indicating a slightly earlier depressurization time for TAF-2. The expectation is that the TAF case, with its higher water level, should have a higher power. The explanation for the observed trend lies in the boron reactivity. In the TAF-2 case, during the early phase of the transient (i.e., before the ED), a higher core-average void results in a lower boron inventory in the core relative to the TAF case. The boron reactivity appears to be more dominant than the moderator density reactivity; hence, the net result is a higher power for TAF-2 .

After depressurization (at ~350 s) for both the TAF and TAF-2 cases there is voiding in the lower plenum and natural circulation flow is “broken” resulting in a reduction in core flow (Figure 4.29). Subsequent refilling of the lower plenum and the core region lowers the water level (Figure 4.30) and causes fluctuations in core flow around 750 s. For the TAF+5 case between 1000 s and 1500 s the core power has dropped sufficiently for the core region to be refilled with water; evidenced by the fluctuations in water level and a general decreasing trend in the core flow during that period.

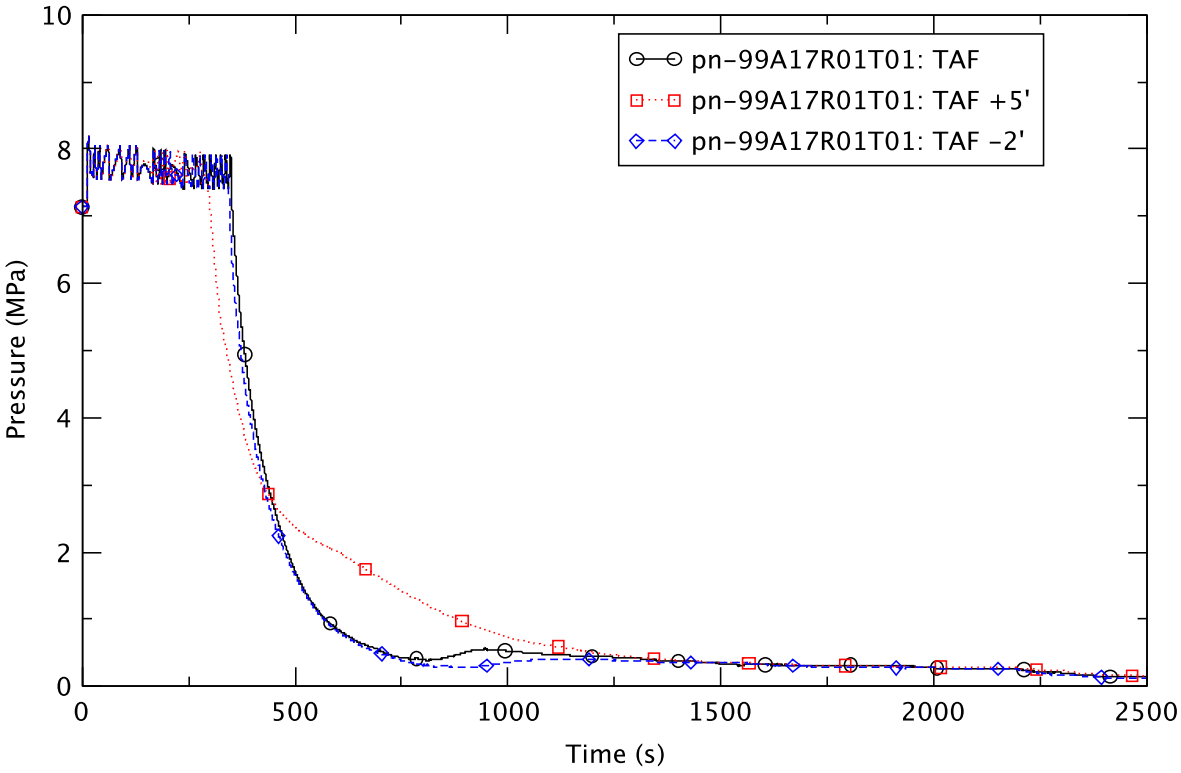

Figure 4.28 Reactor Pressure - BOC Base Cases

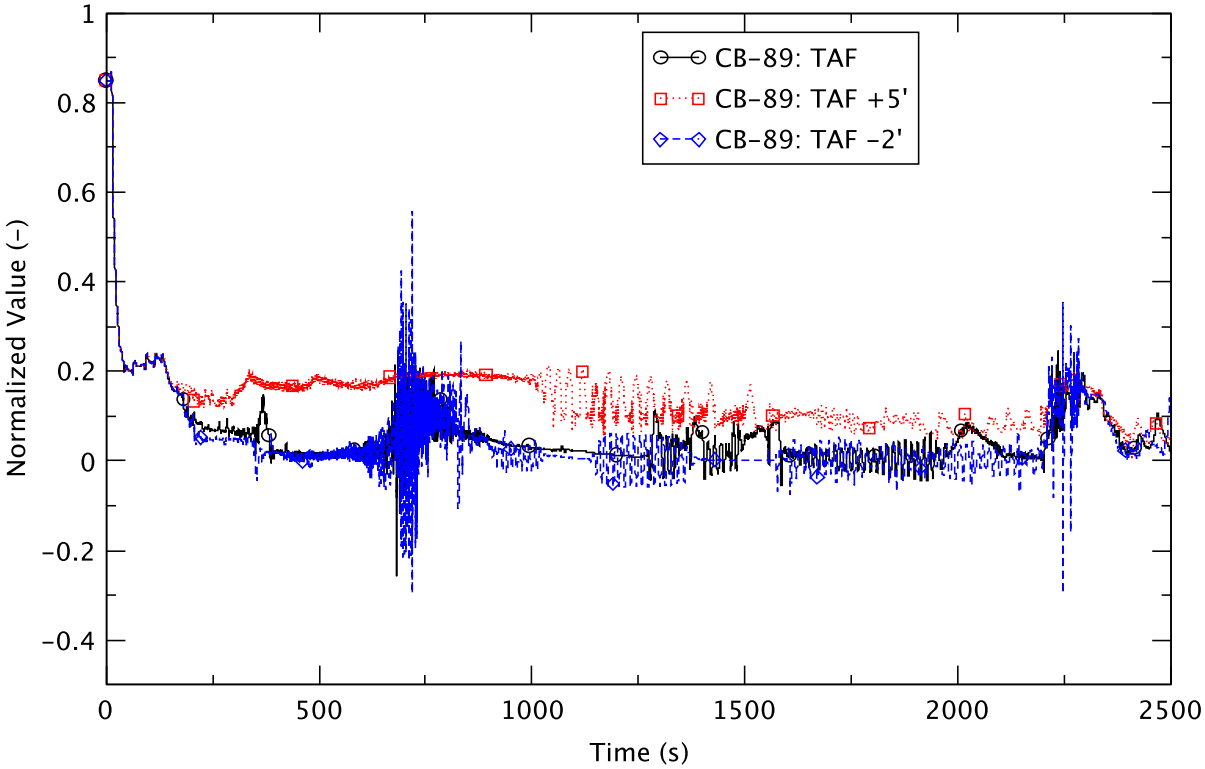

Figure 4.29 Core Flow - BOC Base Cases

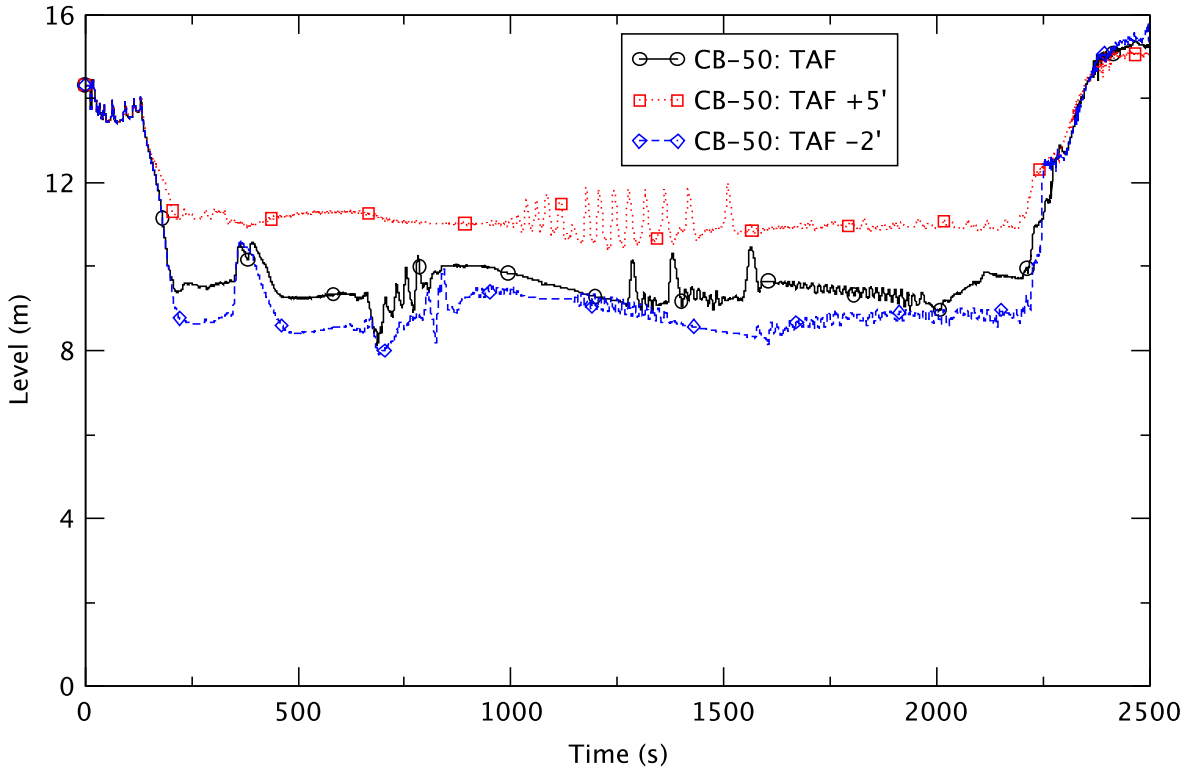

Figure 4.30 Downcomer Water Level - BOC Base Cases

A distinguishing trend in the TAF+5 case is the boron inventory in the core region. As evident from Figure 4.31, the core inventory is generally increasing with time because the higher water level is able to support a healthy core flow that entrains all the boron injected into the lower plenum. The core reactivity (Figure 4.32), also depicts a monotonic increase in boron negative reactivity for the TAF+5 case. The boron reactivity with TAF-2 control is similar to that of the TAF case, and exhibits a temporary decrease in the boron negative reactivity between ~500 s and 700 s (Figure 4.33) that can be attributed to the boron transport logic predicting its stratification due to low core flow.

Results of the TRACE/PARCS analysis indicate that in all three BOC cases, the reactor remains shutdown by the injected boron. There is no recriticality due to either repressurization of the reactor vessel, or the dilution of boron.

As indicated earlier, the maximum PCT for the TAF-2 case is more limiting than for the other two cases. Figure 4.34 shows the maximum PCT for the TAF-2 case and the clad temperatures for two fuel rods in two separate core channels. The figure shows that the location of the PCT changes with time. Channel 281 is closer to the center of the core than is Channel 461, and it is in the former that the maximum PCT is close to that for the core-wide value. The heatup of axial node 33 takes about 100 s, and, during that period, multiple axial nodes experience a high void condition in the channel. As the figure shows, once the cladding surface quenches (and rewets), the rate of temperature decrease outpaces the initial rate of heat-up.

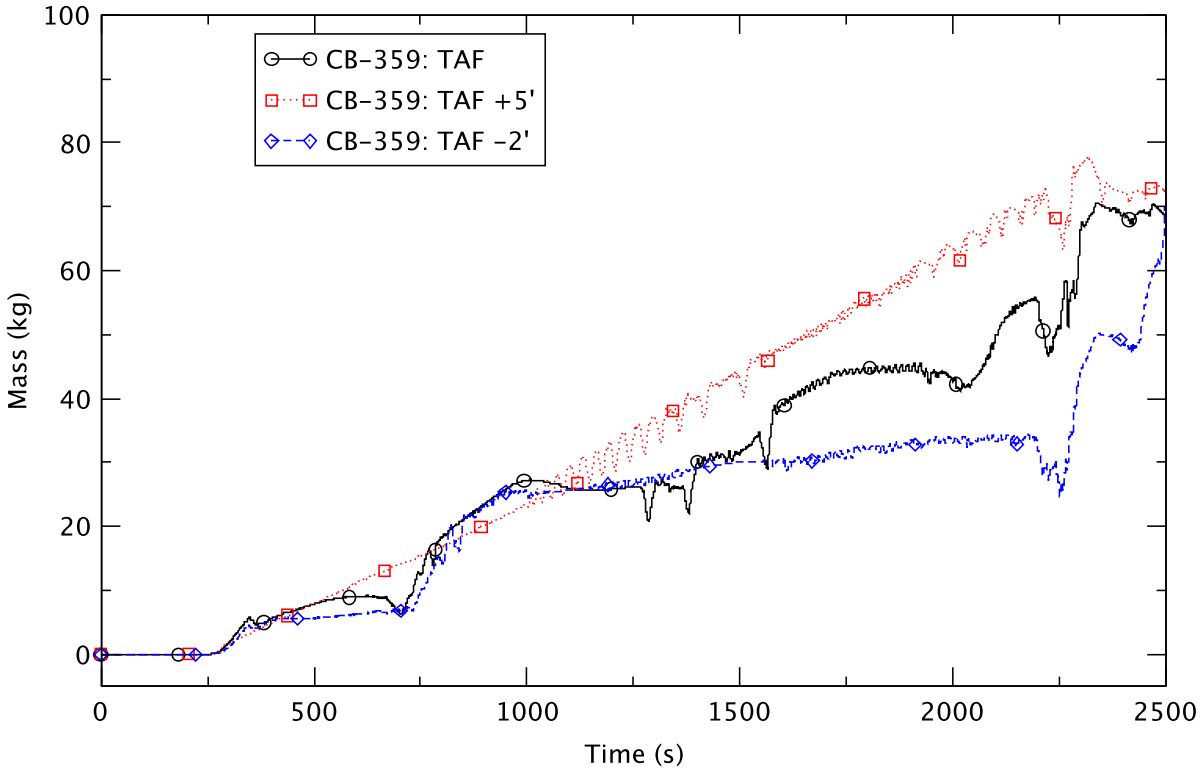

Figure 4.31 Boron Inventory in the Core - BOC Base Cases

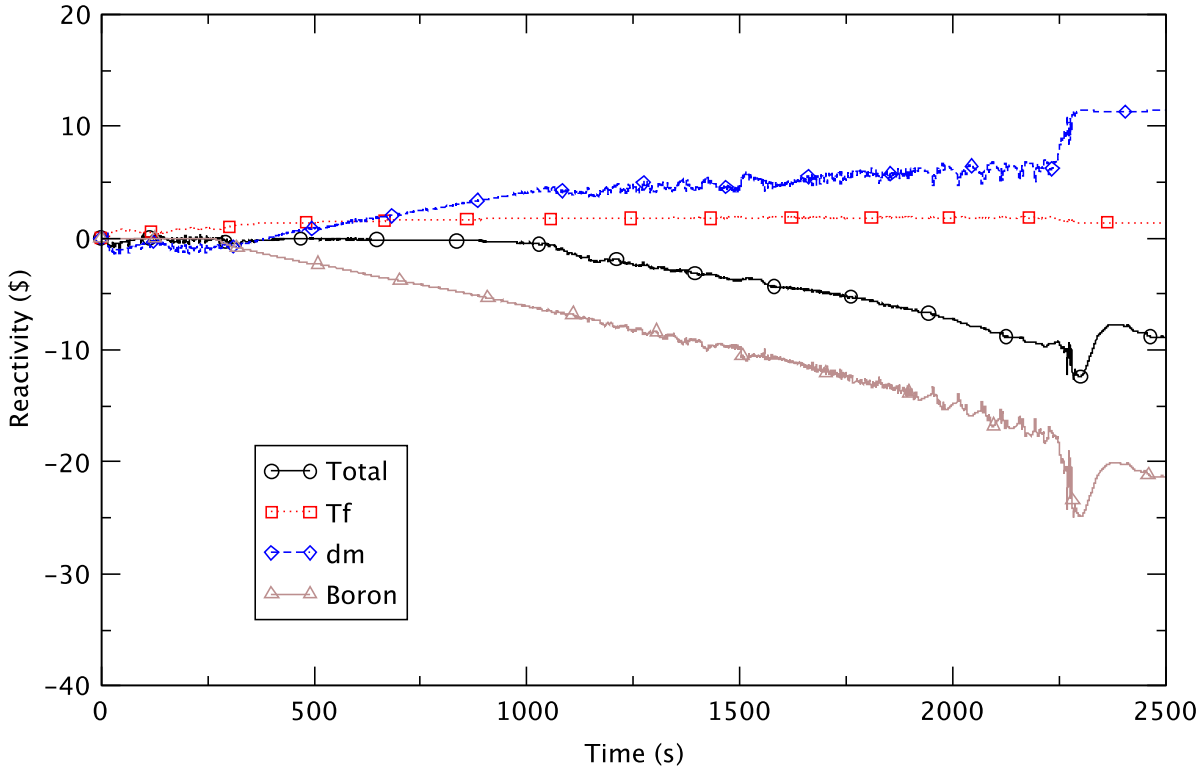

Figure 4.32 Core Reactivity - BOC, TAF+5

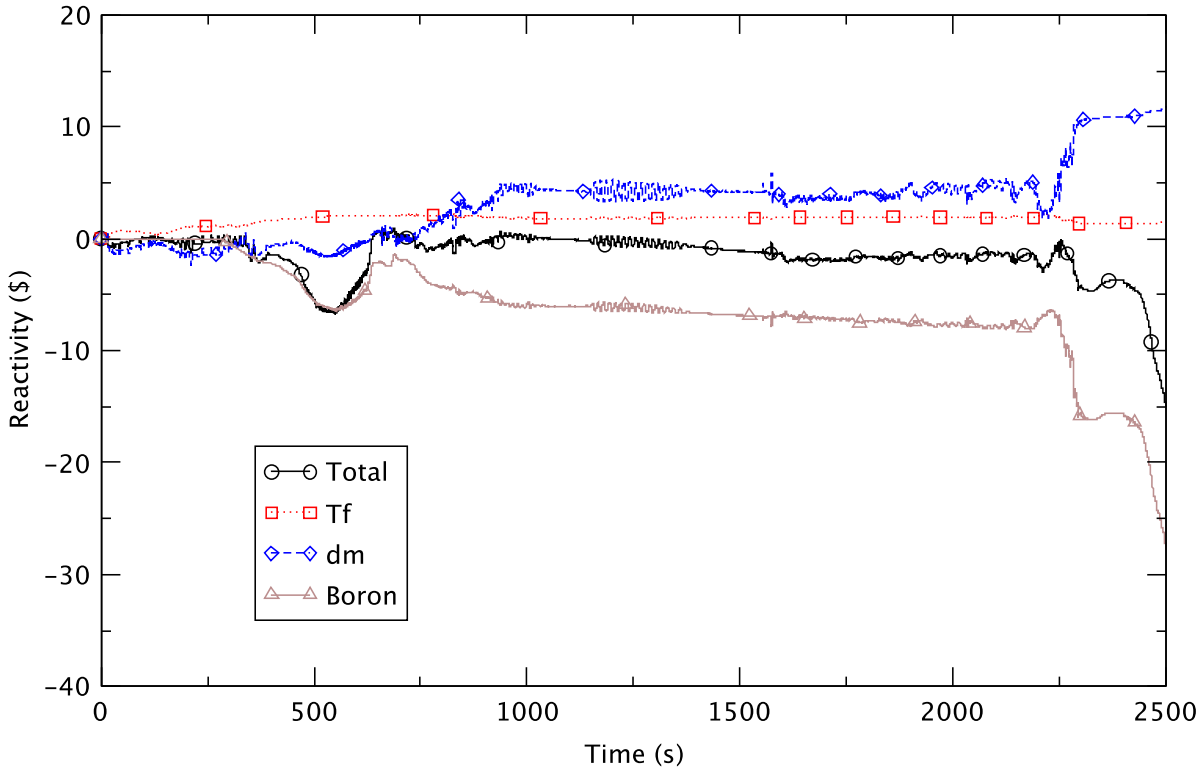

Figure 4.33 Core Reactivity - BOC, TAF-2

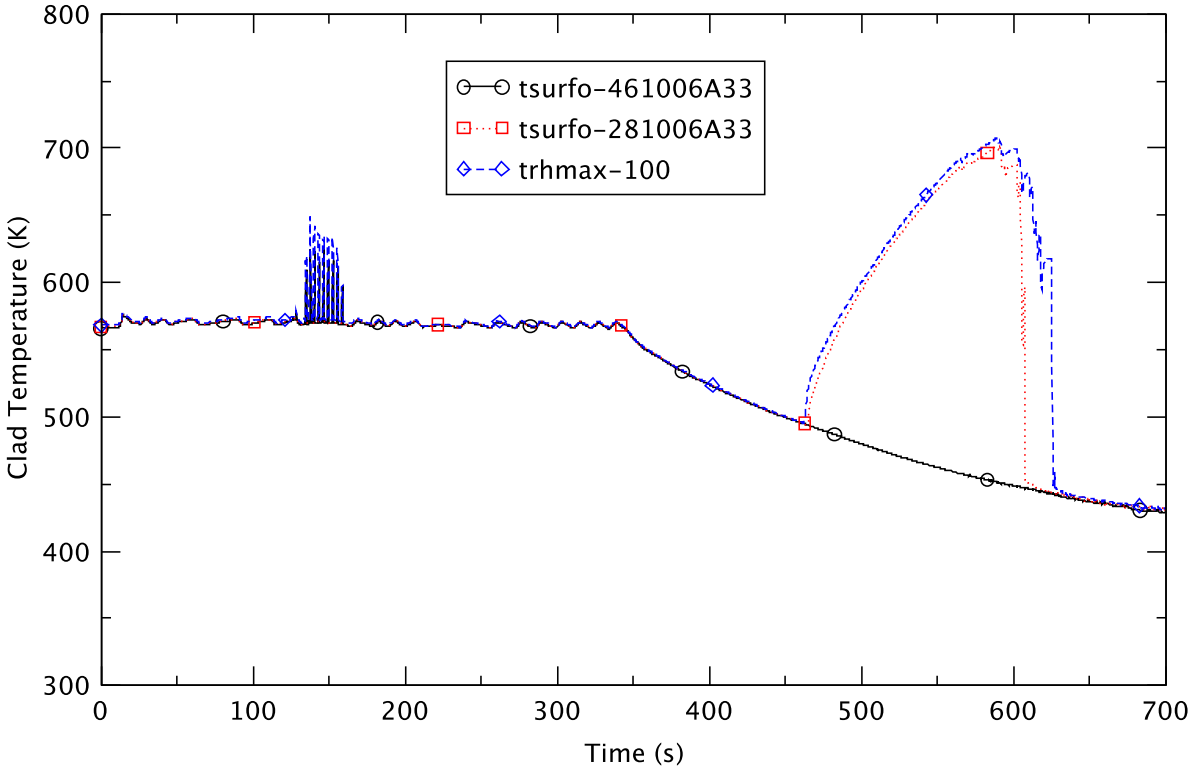

Figure 4.34 Peak Clad Temperature - BOC, TAF-2

The temperature of the suppression pool water (Figure 4.35) is an indication of energy discharged to the pool via the SRVs. The TAF+5 case certainly has the highest pool temperature of the three cases considered. The TAF case has a slightly higher peak pool temperature than the TAF-2 case. In all three cases the pool temperature stays much below the boiling point at atmospheric pressure, and thus, is not expected to impact the safe shutdown of the reactor.

The transient response of the drywell pressure (Figure 4.36) again is as expected, with the highest calculated for the TAF+5 case. In all three cases, the maximum drywell pressure is low enough so as not to be a concern for the containment integrity.

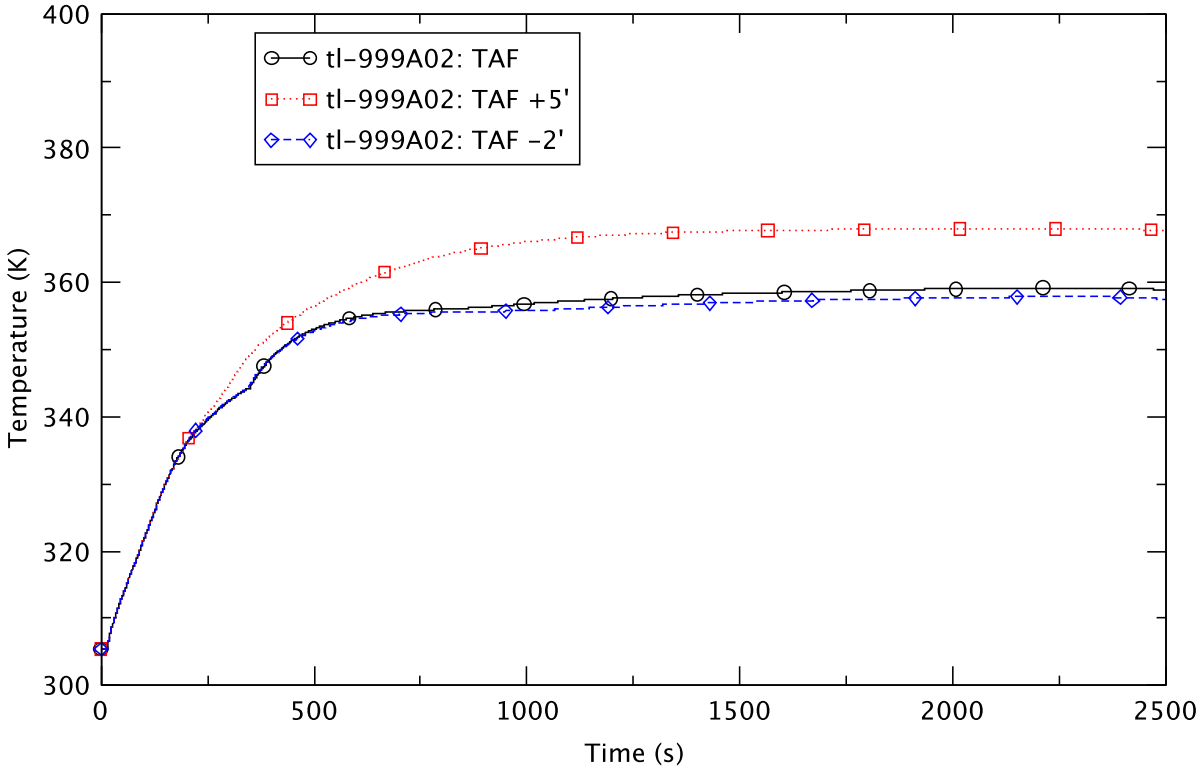

Figure 4.35 Suppression Pool Temperature - BOC Base Cases

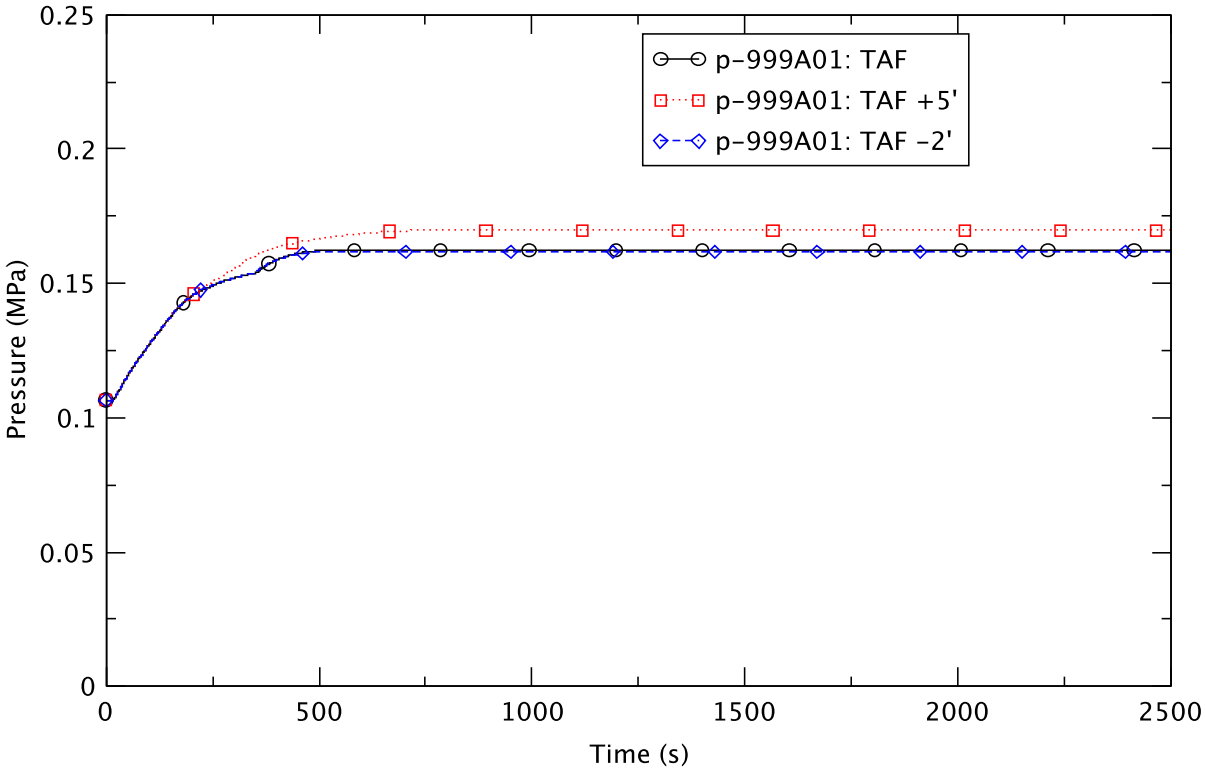

Figure 4.36 Drywell Pressure - BOC Base Cases

4.2.4 Effect of Numerical Scheme at BOC

The analysis of ATWS-ED transients utilized two numerical schemes, stability-enhanced two-step (SETS) and semi-implicit (SI). The obvious advantage of SETS is its ability to use time-step sizes larger than that required by the material Courant limit. However, one of its weaknesses is the likelihood of incurring numerical diffusion in the solution of field equations. This deficiency is of some concern in simulating boron transport in the reactor since numerical diffusion could overpredict the mixing and transport of boron in the coolant flow. An alternate numerical scheme available in TRACE/PARCS for the numerical solution of the thermal-hydraulic equations is the SI scheme that limits the size of the time-step to the material Courant limit but is more amenable to minimizing numerical diffusion. To assess the sensitivity of the results to the numerical scheme used to solve the thermal-hydraulic field equations, the BOC-TAF case is reanalyzed using the SI scheme. This section uses a select set of plots (Figure 4.37 through Figure 4.46) to compare and contrast the transient results obtained from the two numerical schemes.

In general, as seen in Table 4.5, most of the key parameters of the TRACE/PARCS analysis are quite similar for the two cases. The most striking difference between them lies in the prediction of core flow immediately after emergency depressurization and that impacts the power response of the reactor (Figure 4.37).

Table 4.5 Comparison of Key Results for BOC TAF Cases - SETS and SI

Key Event	BOC TAF (SETS)	BOC TAF (EDSI)
Maximum PCT (trhmax-100)	646 (137 s)	657 (136 s)
Core Boron Inventory (CB 359) > 0.01 kg	248 s	248 s
Emergency Depressurization	349.2 s	343.9 s
Maximum Drywell Pressure	0.162 MPa (538 s)	0.162 MPa (538 s)
Reactor Shutdown (Stayed < 3.25% Initial Power)	1001 s	839 s
Maximum Suppression Pool Temperature	359 K (2208 s)	361 K (2168 s)

The timing of ED for the two cases almost is identical as is the rate of depressurization (Figure 4.38). However, for the SI case, the core flow is maintained high after the ED, while the SETS case predicts a break in natural circulation, resulting in practically zero core flow (Figure 4.39)[2]. Both cases control water level via the feedwater system. Both experience level swell after the ED (Figure 4.40) with the SETS case lasting a little longer. Between roughly 300 s and 700 s the feedwater flow for the SI case (Figure 4.41) is higher than the flow for the SETS case (Figure 4.4). This finding is consistent with the higher reactor power and core pressure exhibited by the SI case during this period.

[2] The sensitivity of the natural circulation flow through the core and the downcomer was explored in regard to the numerical scheme and initial conditions. Details of the study will be discussed in a later report. Those additional analyses suggest that the numerical solution for the core flow is mathematically chaotic, and that there is more than one possible solution (i.e., the transient outcome depends heavily on the initial conditions).

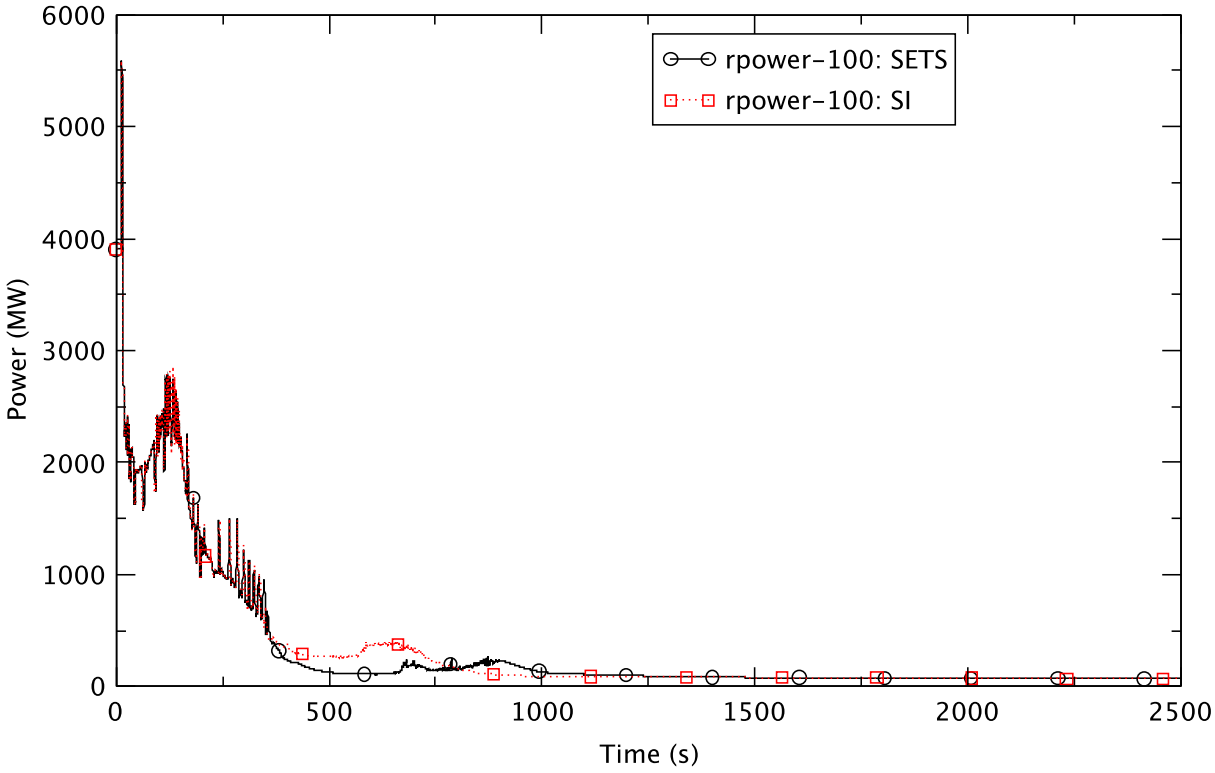

Figure 4.37 Reactor Power - BOC-TAF, SETS & SI

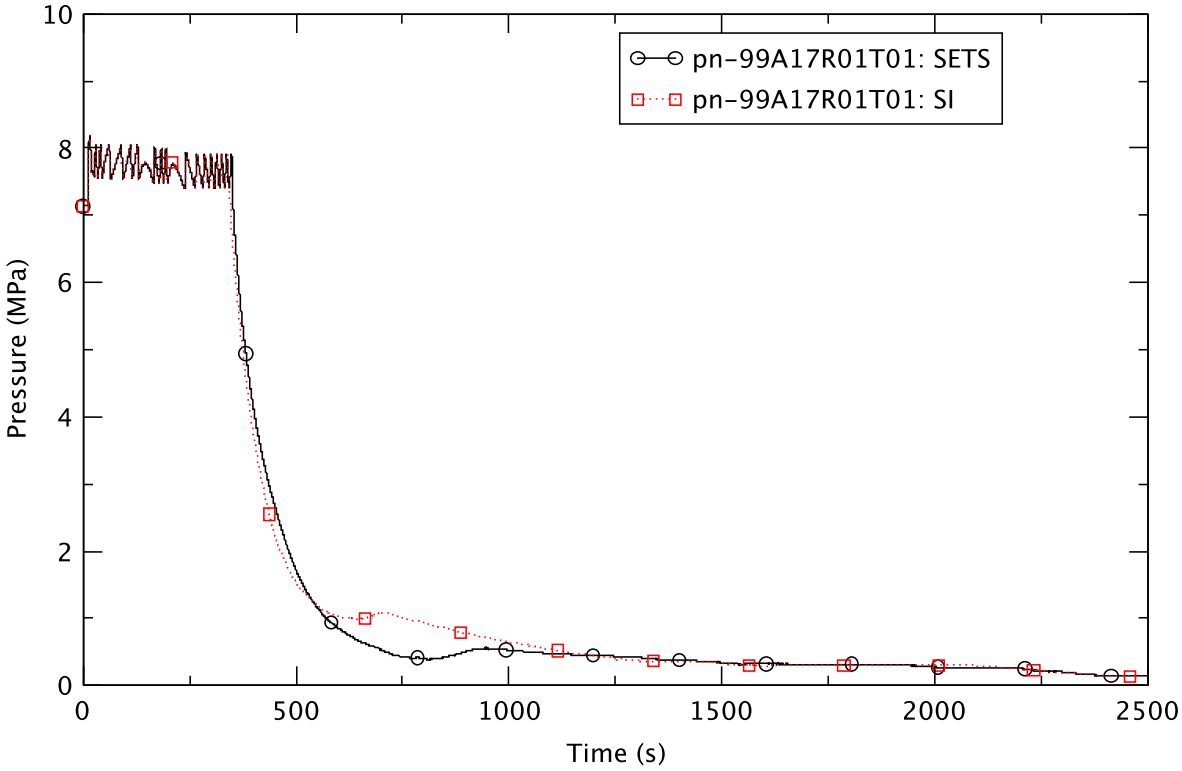

Figure 4.38 Reactor Pressure - BOC-TAF, SETS & SI

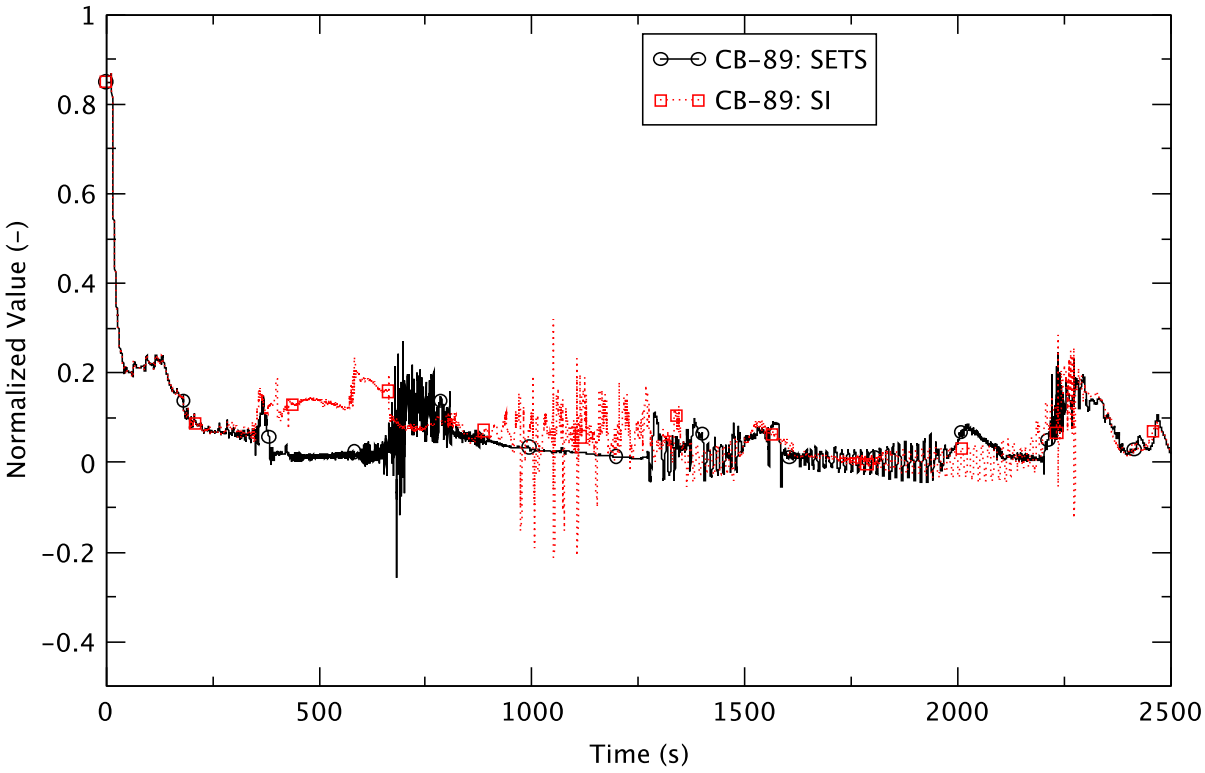

Figure 4.39 Core Flow - BOC-TAF, SETS & SI

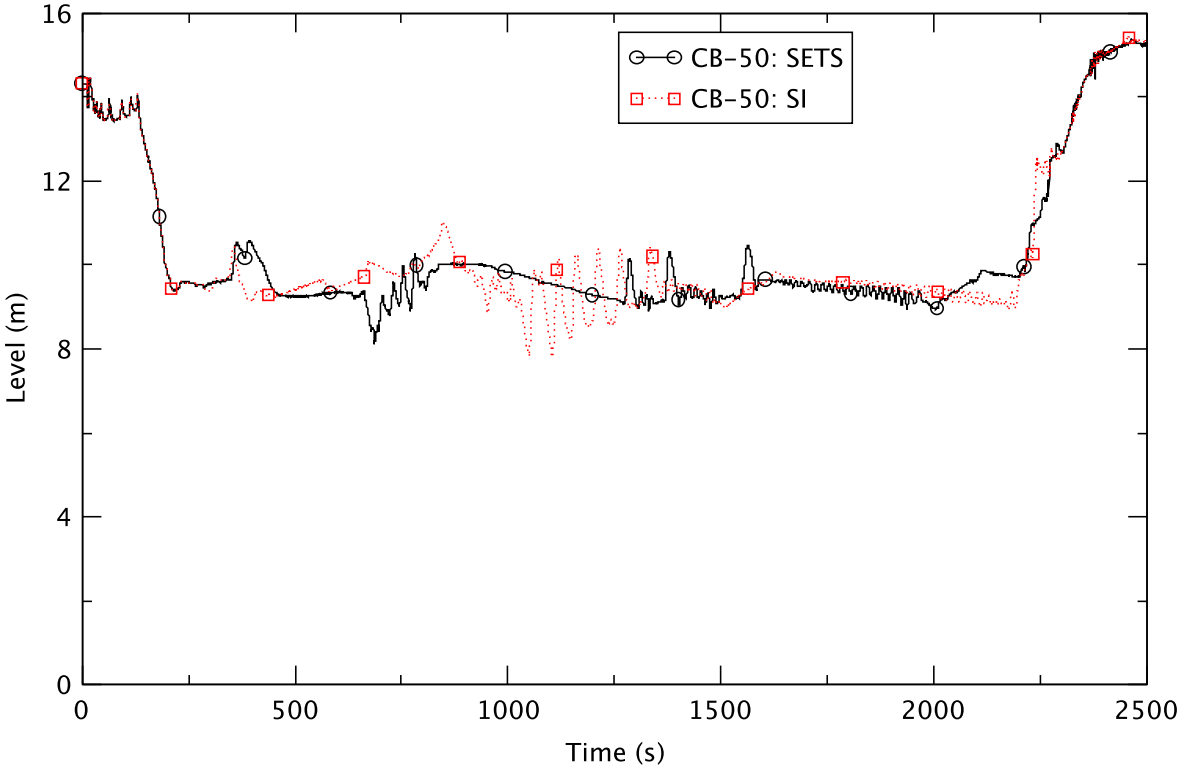

Figure 4.40 Downcomer Water Level - BOC-TAF, SETS & SI

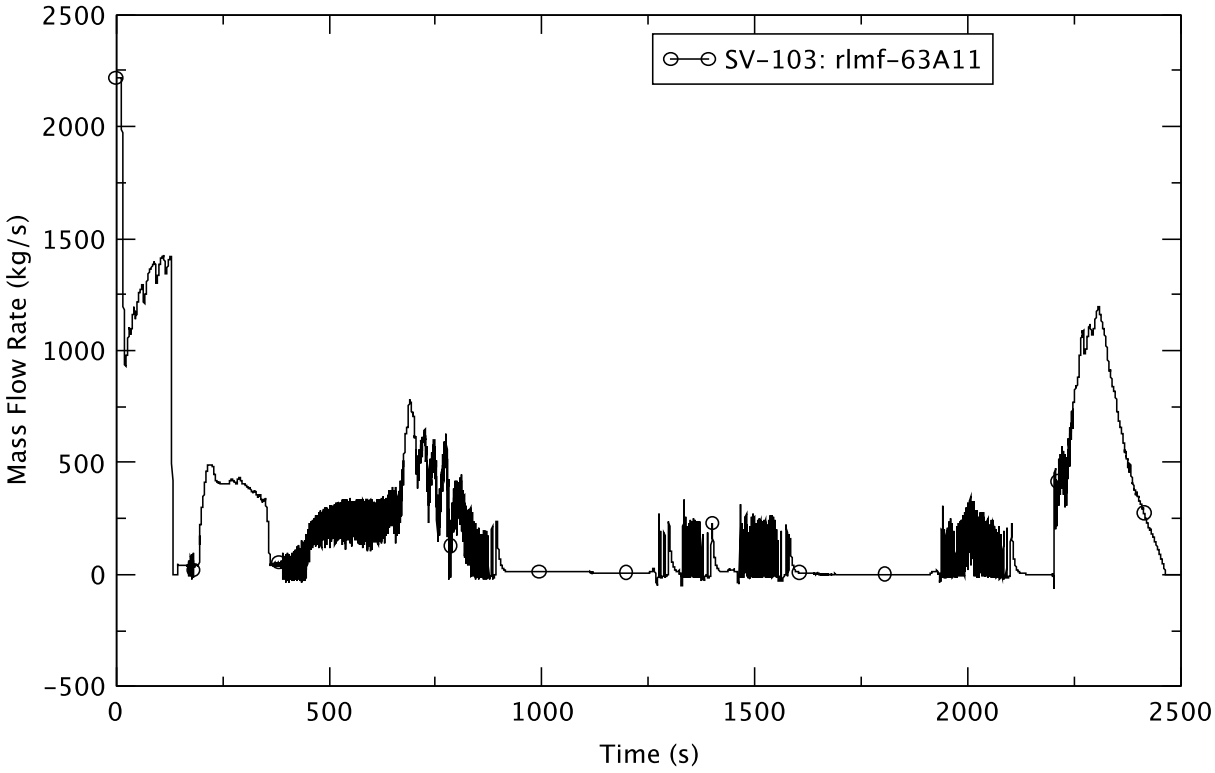

Figure 4.41 Feedwater Flowrate - BOC-TAF, SI

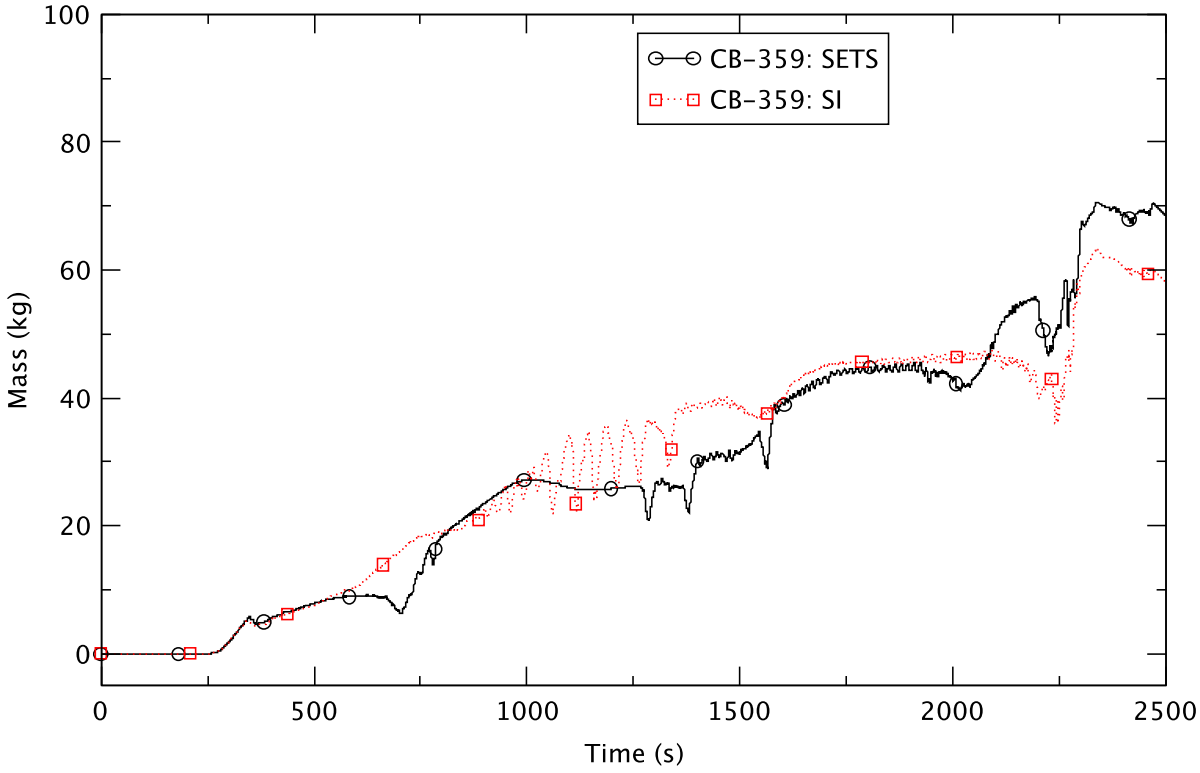

Figure 4.42 Boron Inventory in the Core - BOC-TAF, SETS & SI

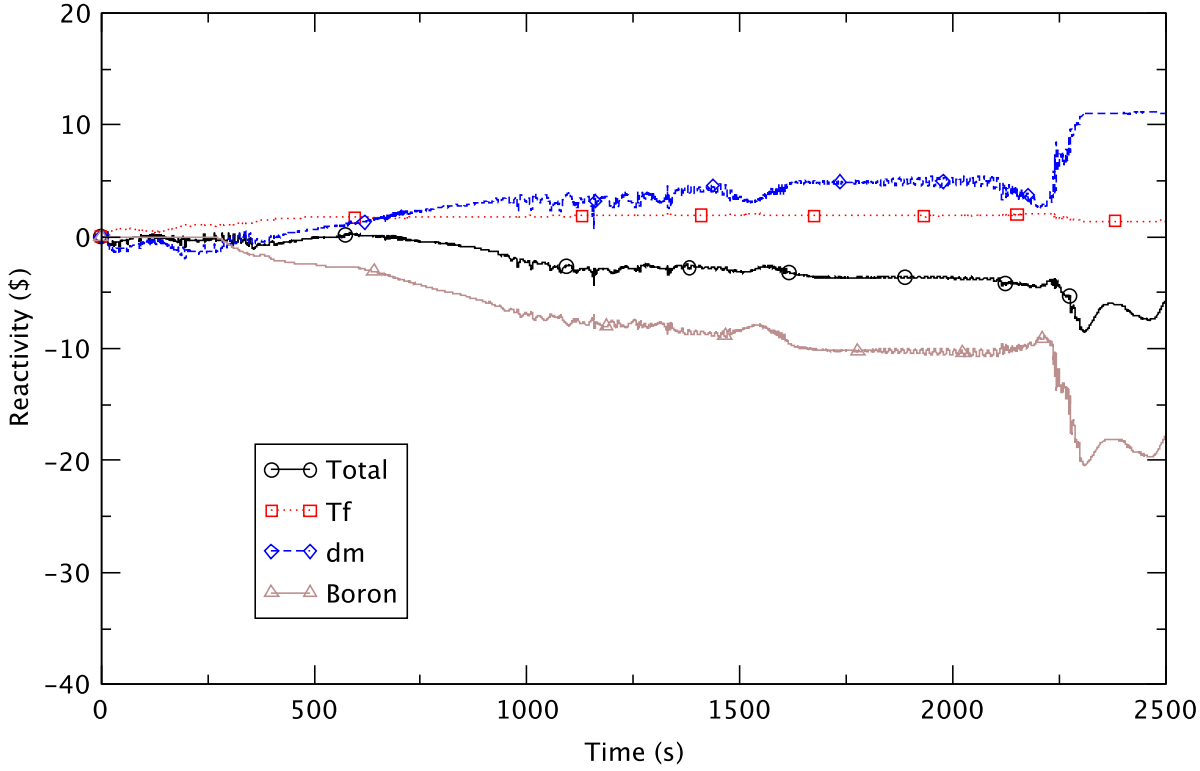

Figure 4.43 Core Reactivity - BOC-TAF, SI

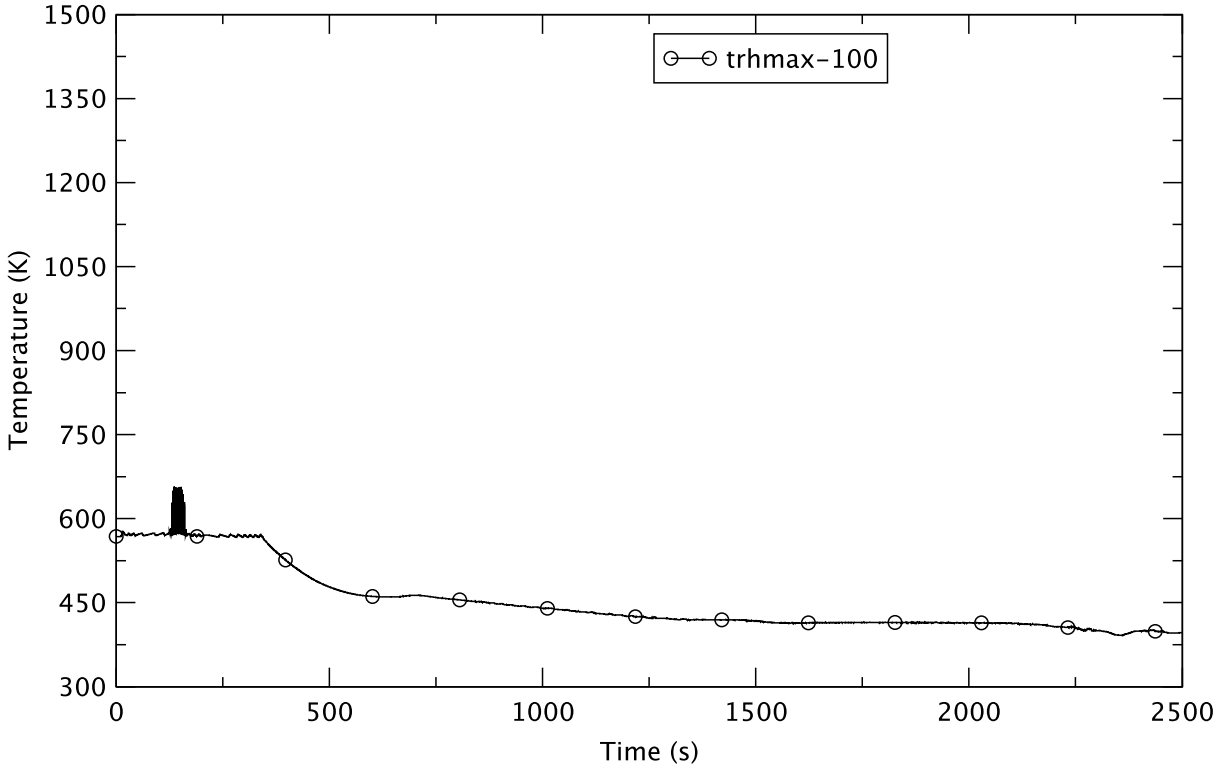

Figure 4.44 Peak Clad Temperature - BOC-TAF, SI

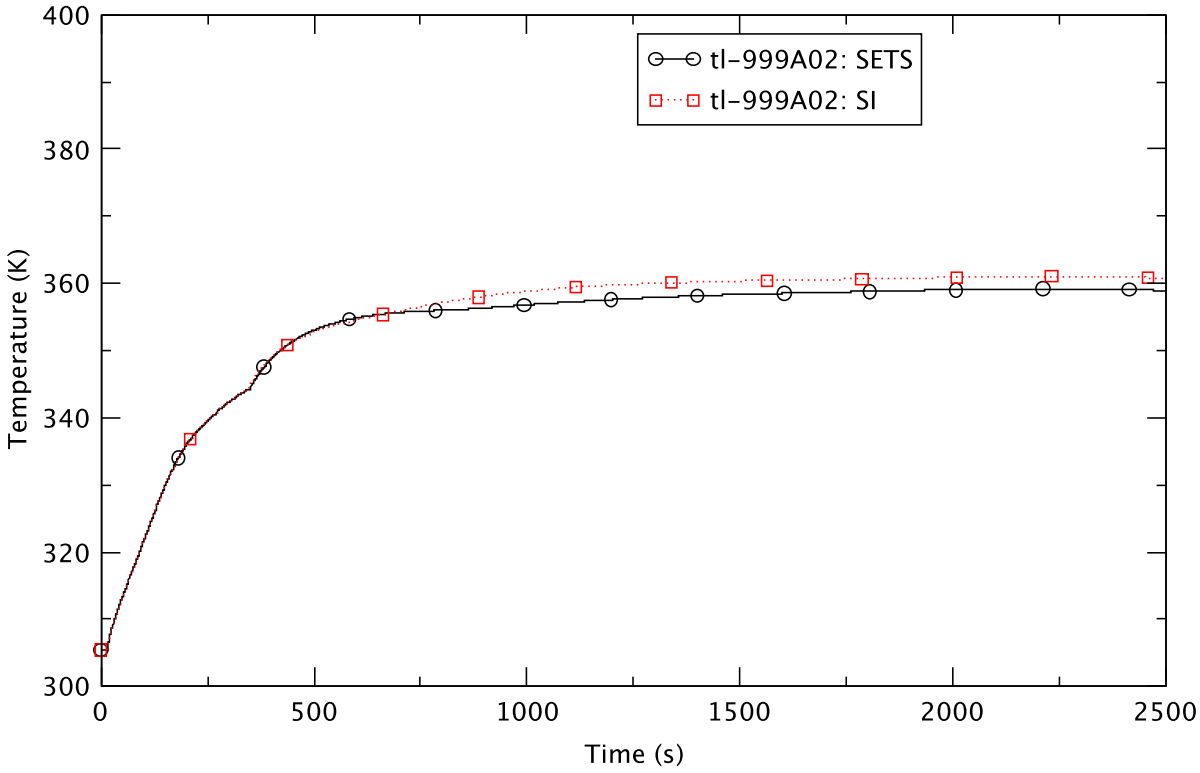

Figure 4.45 Suppression Pool Temperature - BOC-TAF, SETS & SI

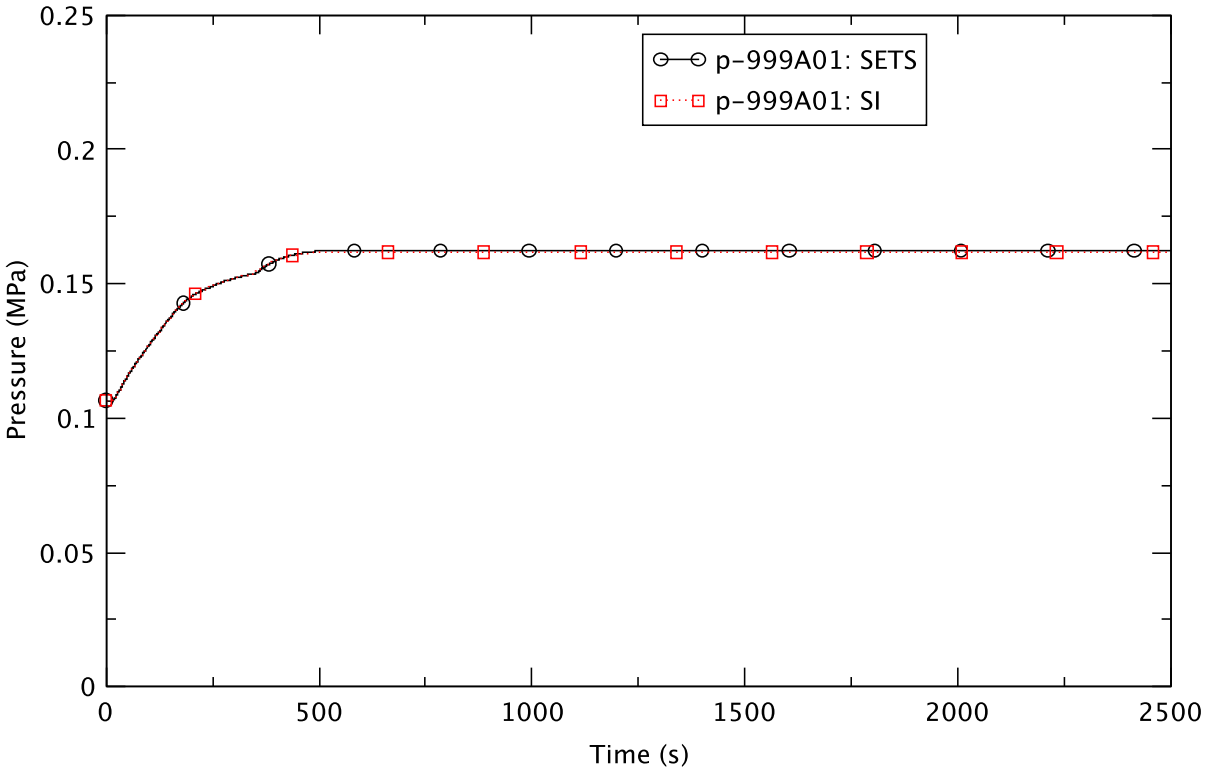

Figure 4.46 Drywell Pressure - BOC-TAF, SETS & SI

4.3 Peak-Hot-Excess-Reactivity (PHE) Cases

There are four ATWS-ED cases at the PHE exposure condition. Three of them evaluate different strategies for reactor water level control (RWLC). These base cases represent controlling water level to TAF, TAF+5, and TAF-2, sometime after the transient is initiated. The TAF+5 case was selected as the representative case; Section 4.3.1 summarizes the timing of events from the TRACE/PARCS simulation of this case, which is discussed further in Section 4.3.2. The parametric effects of controlling the reactor water level to TAF-2, TAF, and TAF+5 are considered in Section 4.3.3. Section 4.3.4 compares upper-plenum boron injection with the lower-plenum injection.

4.3.1 Sequence of Events for the PHE Representative Case

The progression of this transient, ATWS-ED at PHE with RWLC to TAF+5, generally follows the generic description in Section 4.1 but with a few deviations. Notably after the ED, the level swell is less pronounced and there is no flashing in the lower plenum; the reactor stays critical for a bit longer. Table 4.6 shows the time sequence for this event; detailed discussions of the system behavior are in the next section.

Table 4.6 Sequence of Events at PHE with RWLC to TAF+5

Time (s)	Event
0.0	• Null transient simulation starts
10.0	• Null transient simulation ends • Trip initiates an MSIV closure
13.4	• High RPVpressure trips recirculation pumps
13.8	• First lift of SRV
14.4	• Maximum PCT of 577 K (trhmax-100)
14.6	• MSIV completely closed.
130	• Initiation of reactor water level control
211	• Initiation of boron injection
~245	• Boron starts accumulating in the core (CB 359 > 0.01 kg).
300	• Initiation of emergency depressurization.
783	• Drywell reaches a maximum pressure of 0.170 MPa.
2092	• Suppression pool reaches maximum temperature of 368 K.
2180	• Initiation of restoring reactor water level over 100 seconds.
2500	• Simulation ends.

4.3.2 Transient Response of the PHE Representative Case

The overall transient response of this representative case at PHE is very similar to the corresponding case at BOC, discussed in Section 4.2.3. For the early phase of the transient the reactor power responds to 2RPT and operator actions to lower the water level (Figure 4.47). The pressure response of the reactor to emergency depressurization is shown in Figure 4.48, and the rate of steam flow through the steamline is shown in Figure 4.49. From the latter, it can be inferred that just before the ED, two banks of SRVs are required to relieve the pressure inside the reactor vessel. The break point in the power response at about 500 s is related to the core reactivity. A review of the total reactivity (Figure 4.67) reveals that it fluctuates very close to zero (null reactivity) until ~500 s, and then stays negative and the reactor is on the way to being shutdown.

Feedwater flow and feedwater temperature, respectively, are shown in Figure 4.50 and Figure 4.51. The effect of the gradual ramp-down in feedwater flow between ~400 s and 600 s is evident in a change at ~500 s in the rate of temperature change in the lower plenum (Figure 4.52).

The ED appears to have only a small impact on core flow, Figure 4.53, and downcomer water leve, Figure 4.54. These two parameters remain relatively stable between roughly 500 s and 1000 s, while the reactor power continues to decline.

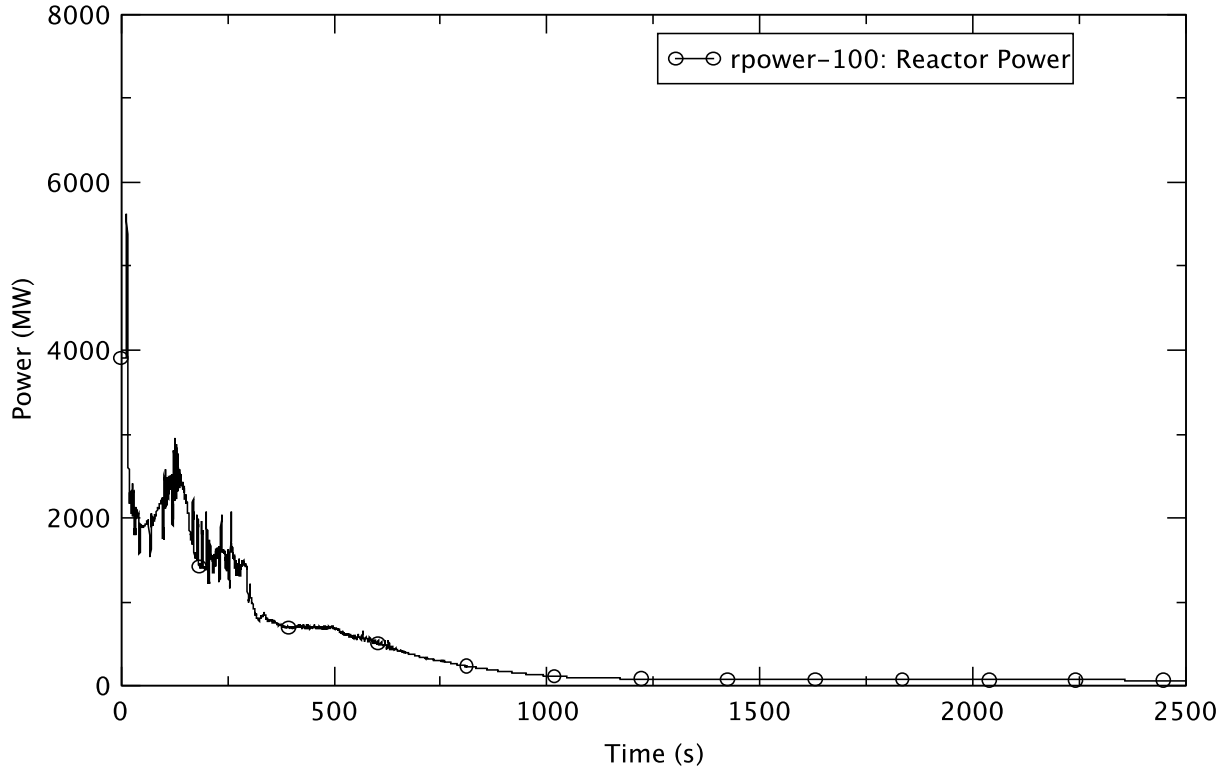

Figure 4.47 Reactor Power - PHE, TAF+5

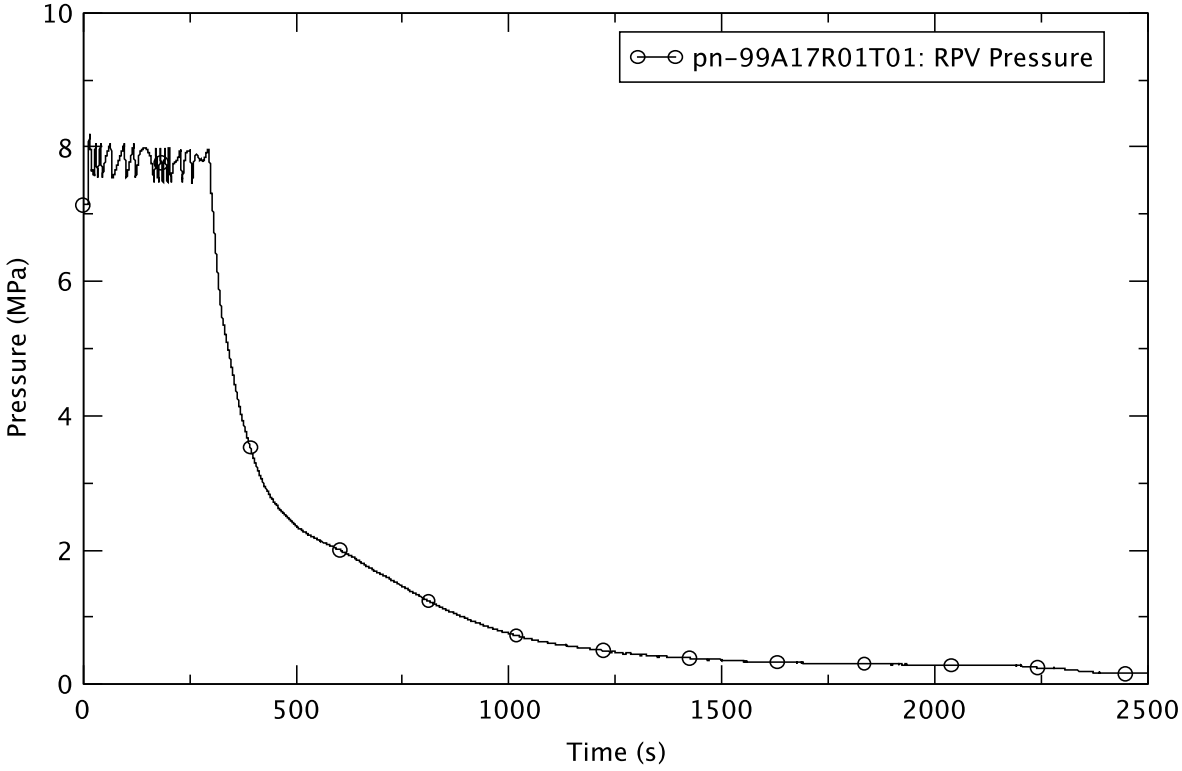

Figure 4.48 Reactor Pressure - PHE, TAF+5

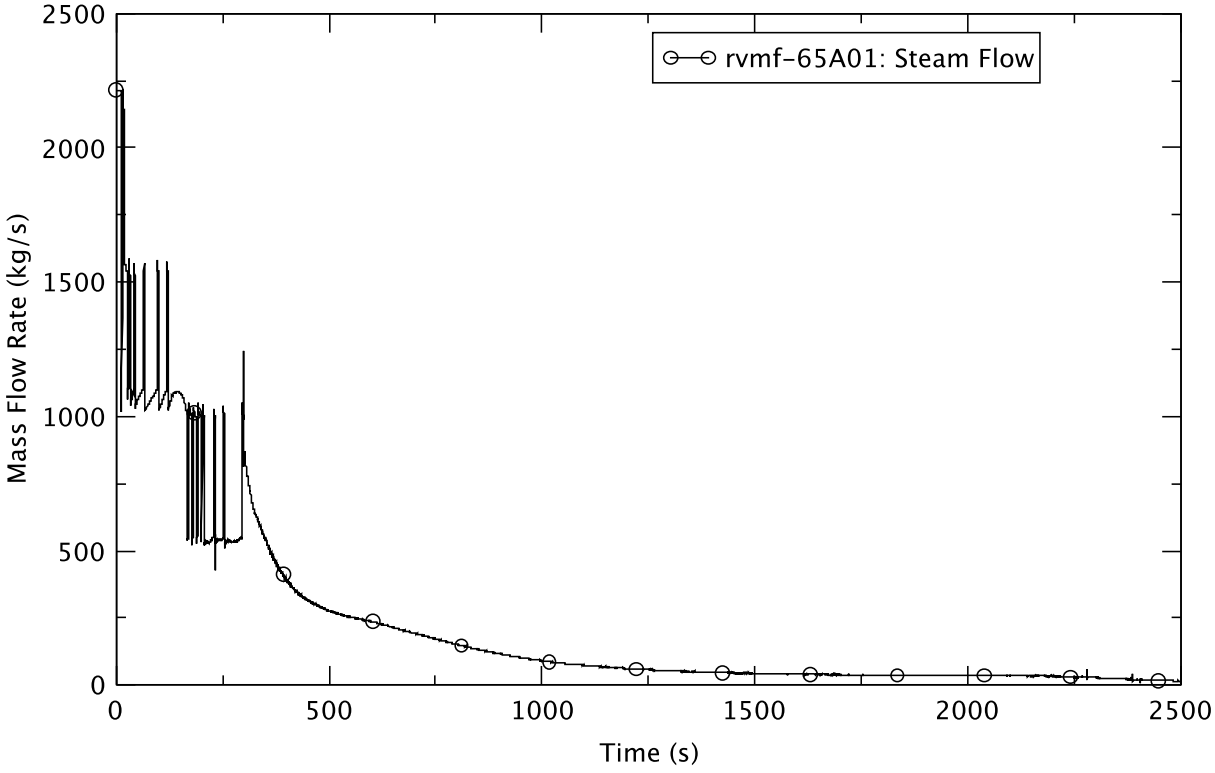

Figure 4.49 Steamline Flow - PHE, TAF+5

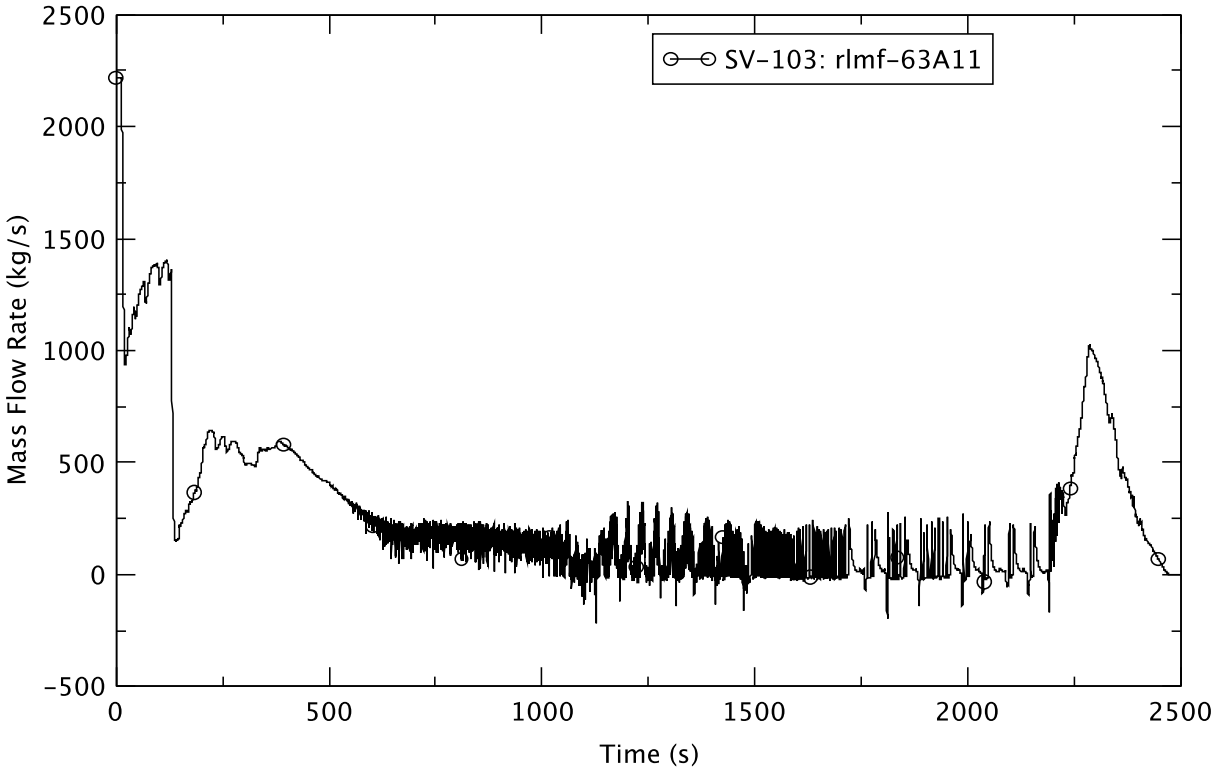

Figure 4.50 Feedwater Flowrate - PHE, TAF+5

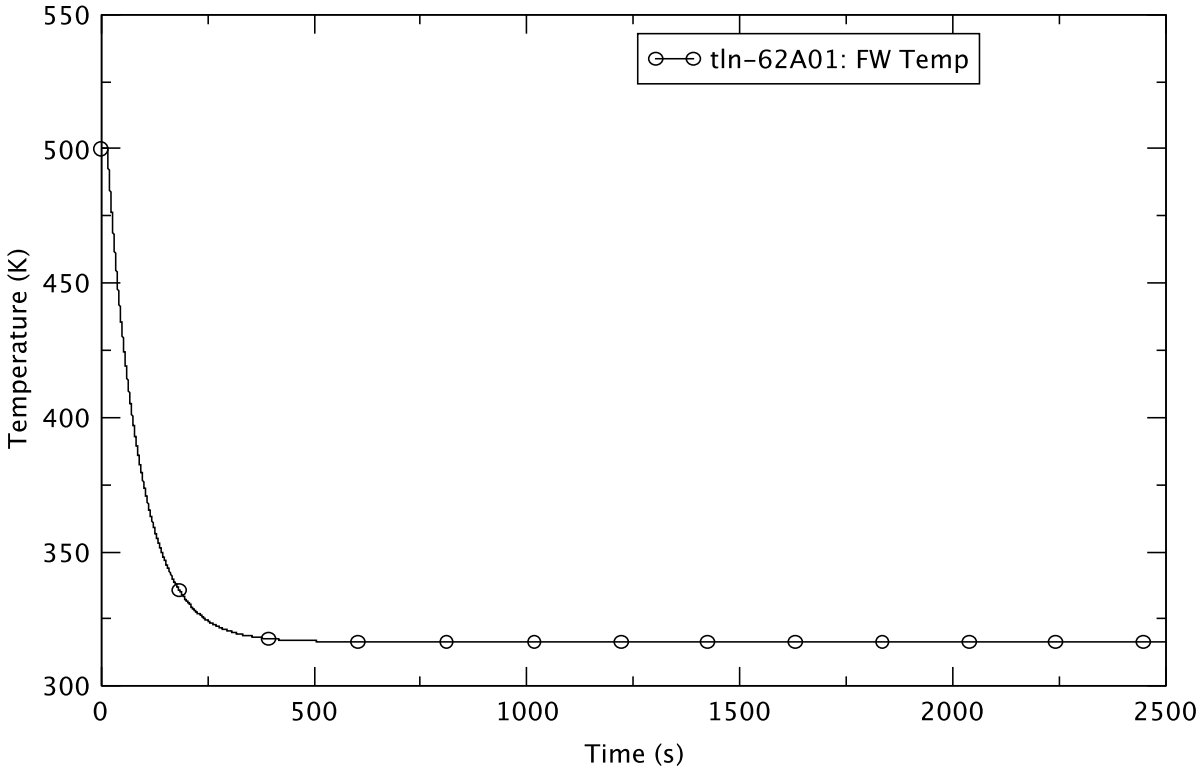

Figure 4.51 Feedwater Temperature - PHE, TAF+5

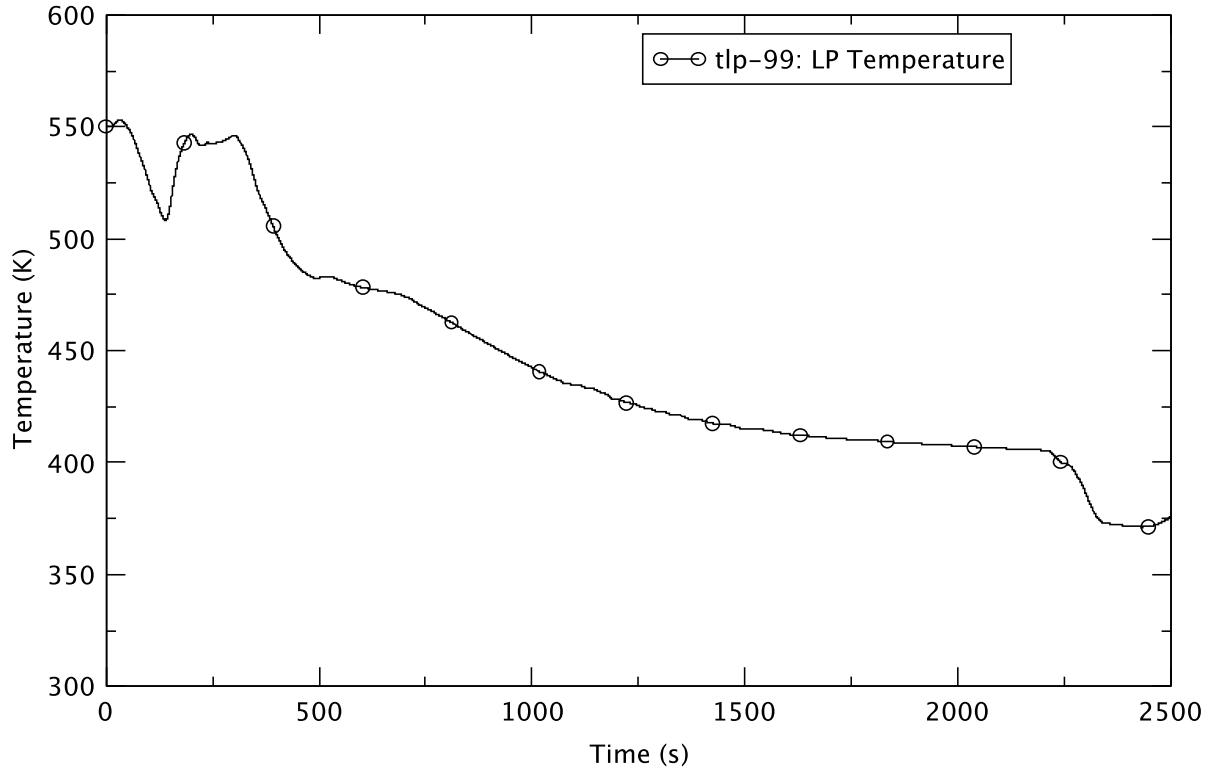

Figure 4.52 Lower Plenum Temperature - PHE, TAF+5

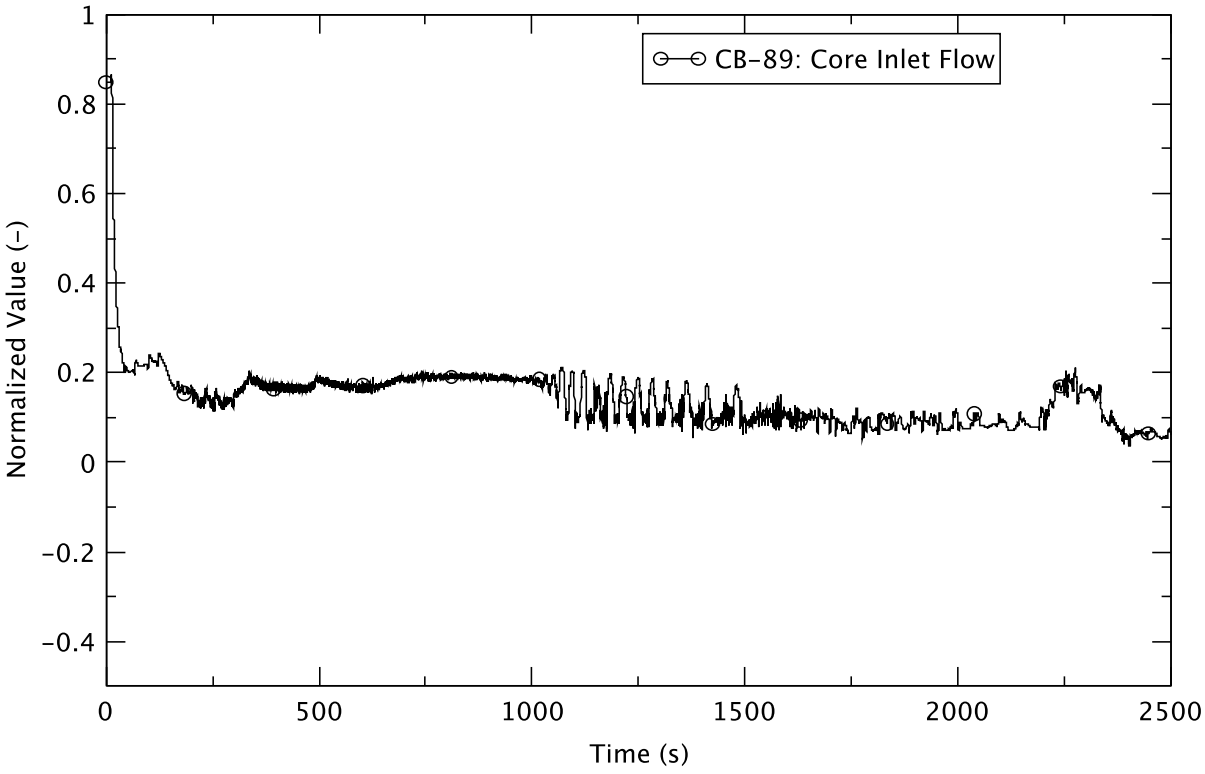

Figure 4.53 Core Flow - PHE, TAF+5

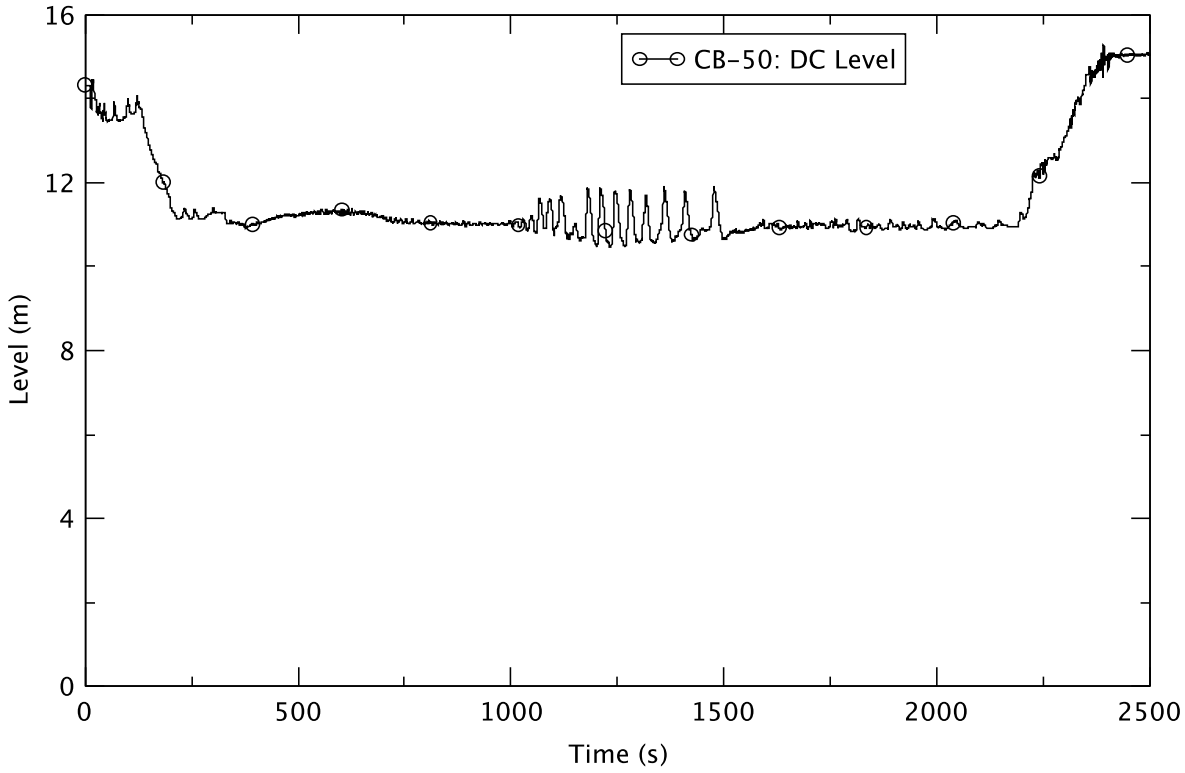

Figure 4.54 Downcomer Water Level - PHE, TAF+5

The effect of ED is evident in the response of other parameters. In Figure 4.52, the temperature of the lower plenum exhibits a downturn immediately after the ED. However, the temperature of the suppresion pool, shown in Figure 4.55, shows an increase in the rate of change after the ED at ~300 s. The mass flow through the open SRV/ADS in bank D is illustrated in Figure 4.56, and the flow decay has a time constant of several hundred seconds.

Flashing in the core bypass region is observed after ED (plots of void fraction are shown in Figure 4.57 and Figure 4.58). However, there is no flashing in the lower plenum (see plots of void fraction in Figure 4.59 and Figure 4.60). With decreasing reactor power, the refilling of the core region begins at ~1000 s and is completed at ~1500 s. Cyclic fluctuations in the core flow and in the downcomer water level during that period are observed and at the same time, the feedwater flow cycles up and down in attempting to maintain a constant water level at TAF+5.

The core average void fraction, derived from the average coolant density from the PARCS output, is shown in Figure 4.61. In general, the trend is for the core to accumulate more and more liquid as the reactor power falls to the decay-heat level.

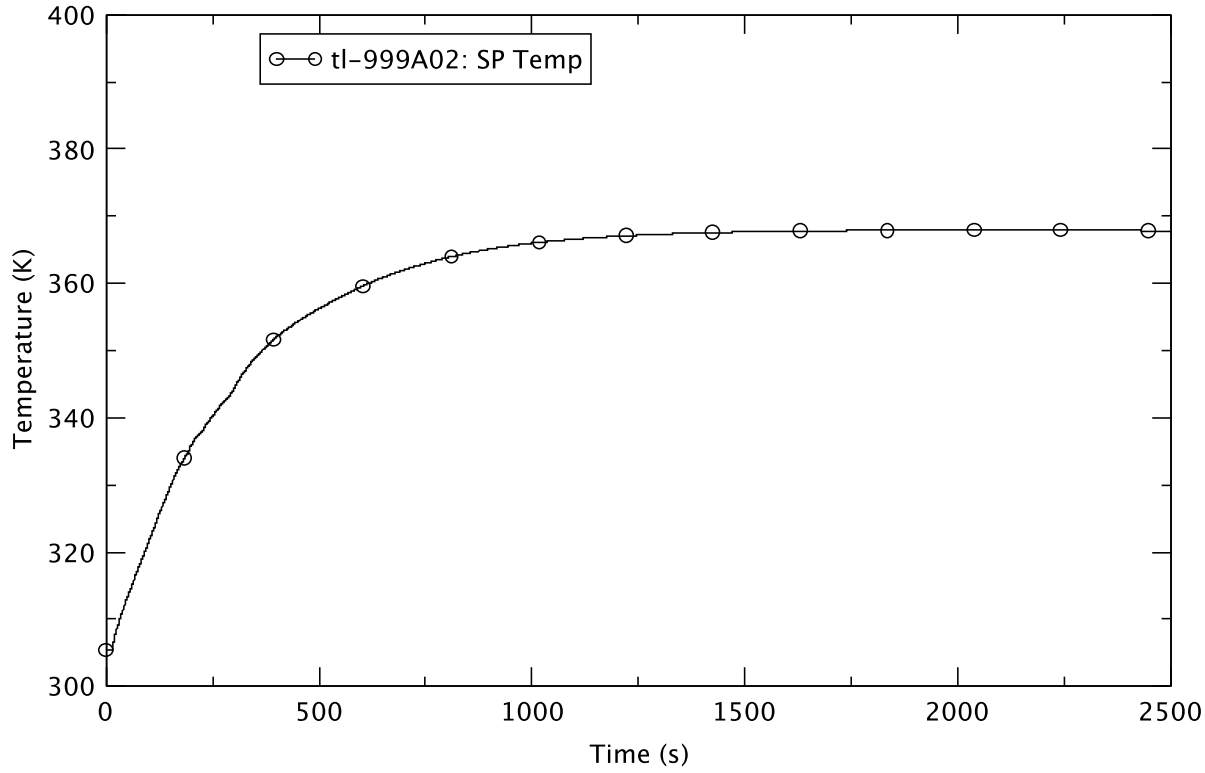

Figure 4.55 Suppression Pool Temperature - PHE, TAF+5

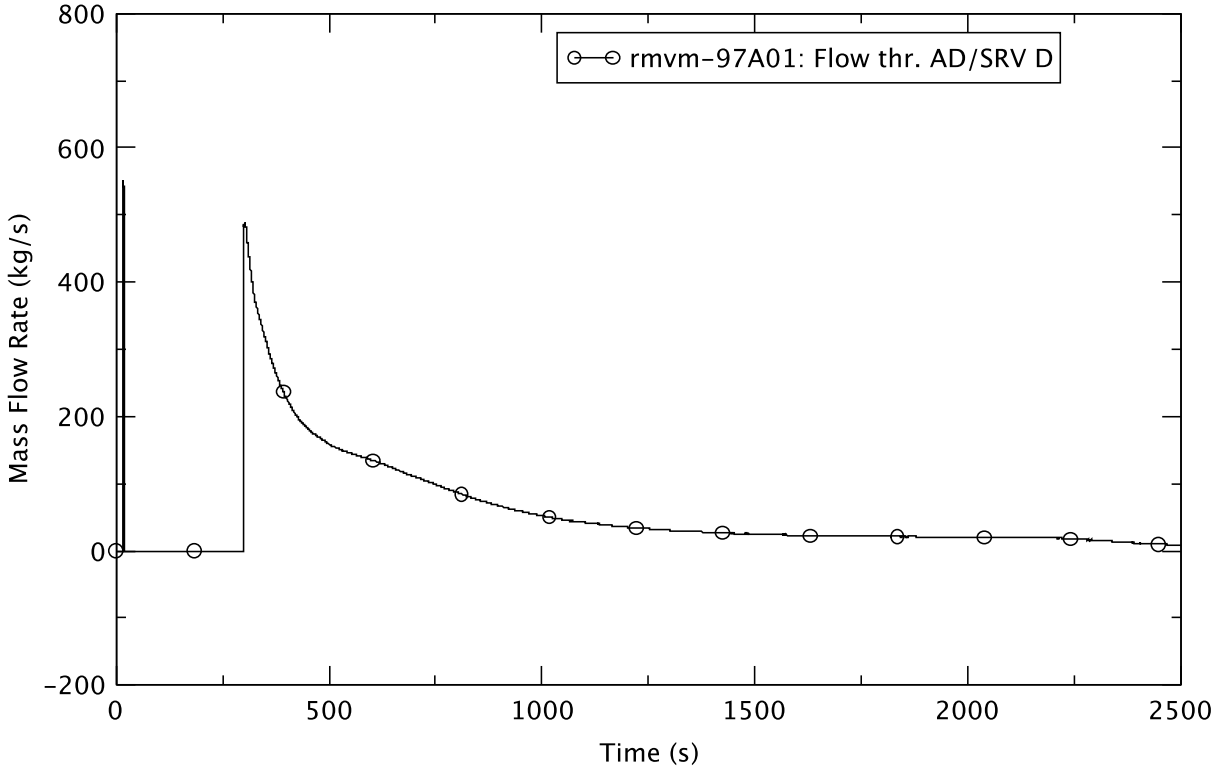

Figure 4.56 Mass Flow Through SRV/ADS Bank D - PHE, TAF+5

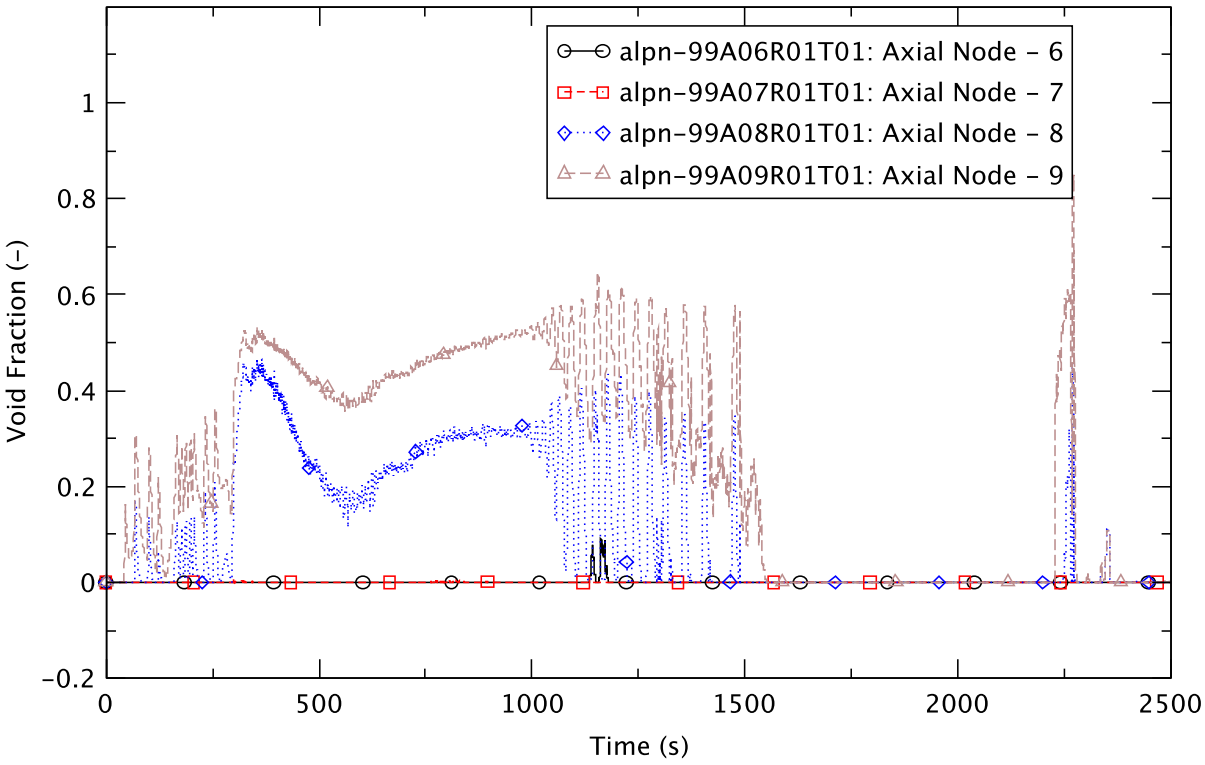

Figure 4.57 Void Fraction in Core Bypass (Ring-1) - PHE, TAF+5

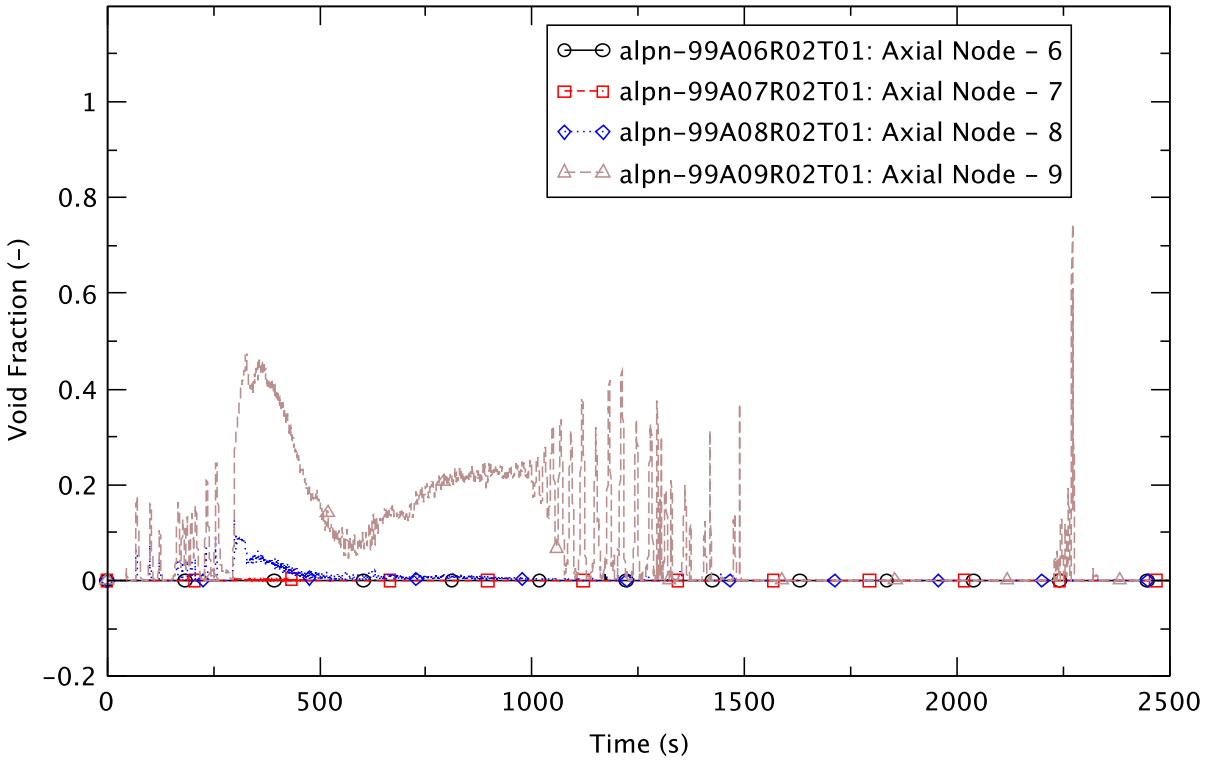

Figure 4.58 Void Fraction in Core Bypass (Ring-2) - PHE, TAF+5

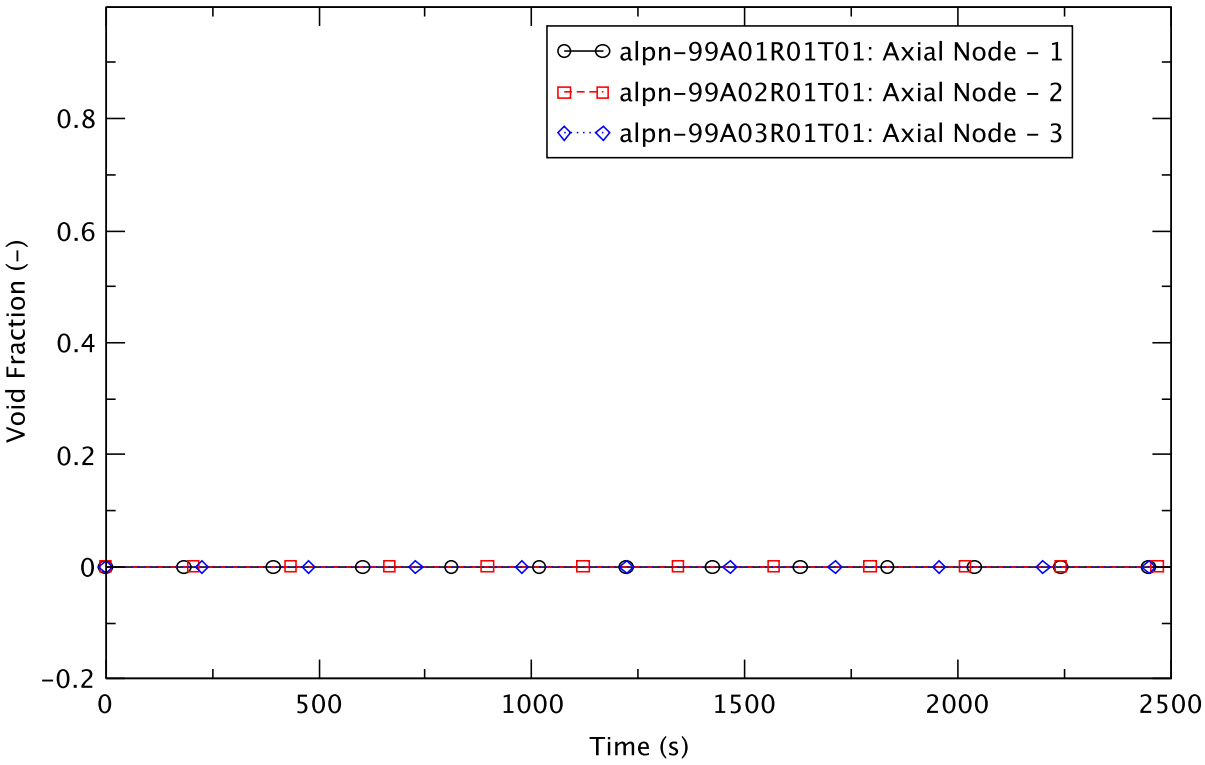

Figure 4.59 Void Fraction in Lower Plenum (Ring-1) - PHE, TAF+5

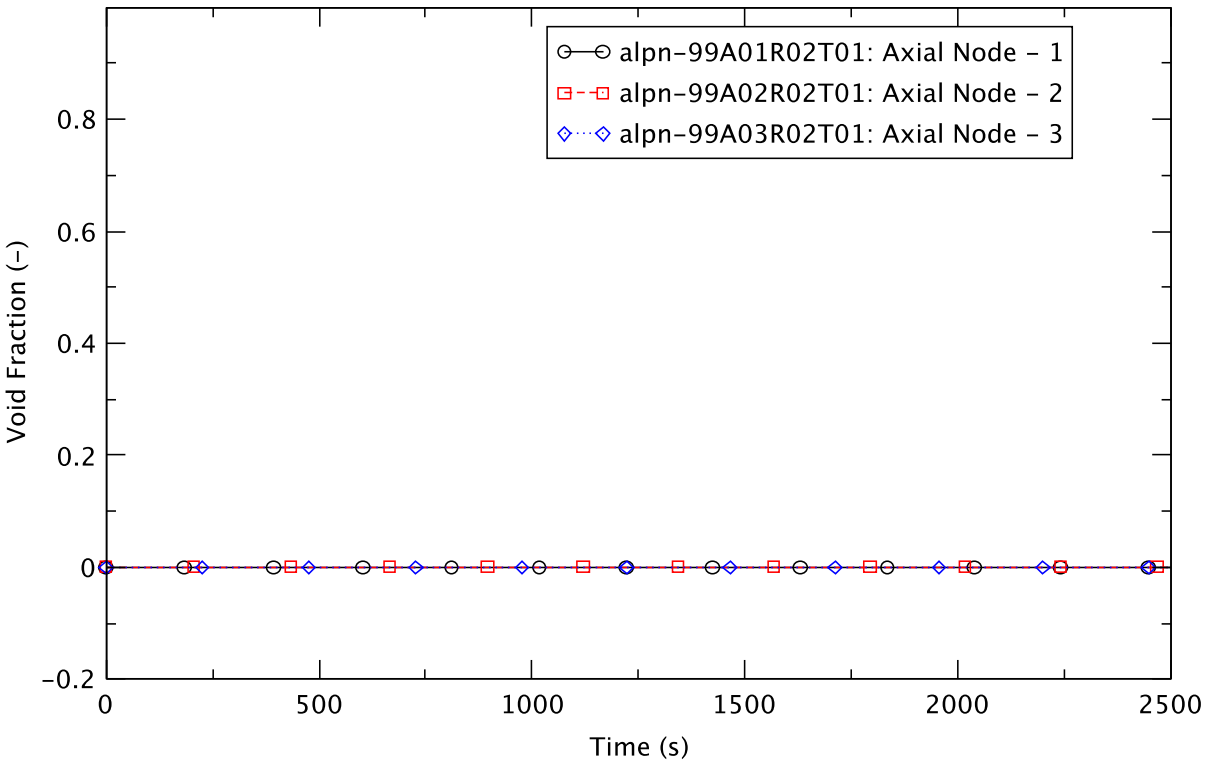

Figure 4.60 Void Fraction in Lower Plenum (Ring-2) - PHE, TAF+5

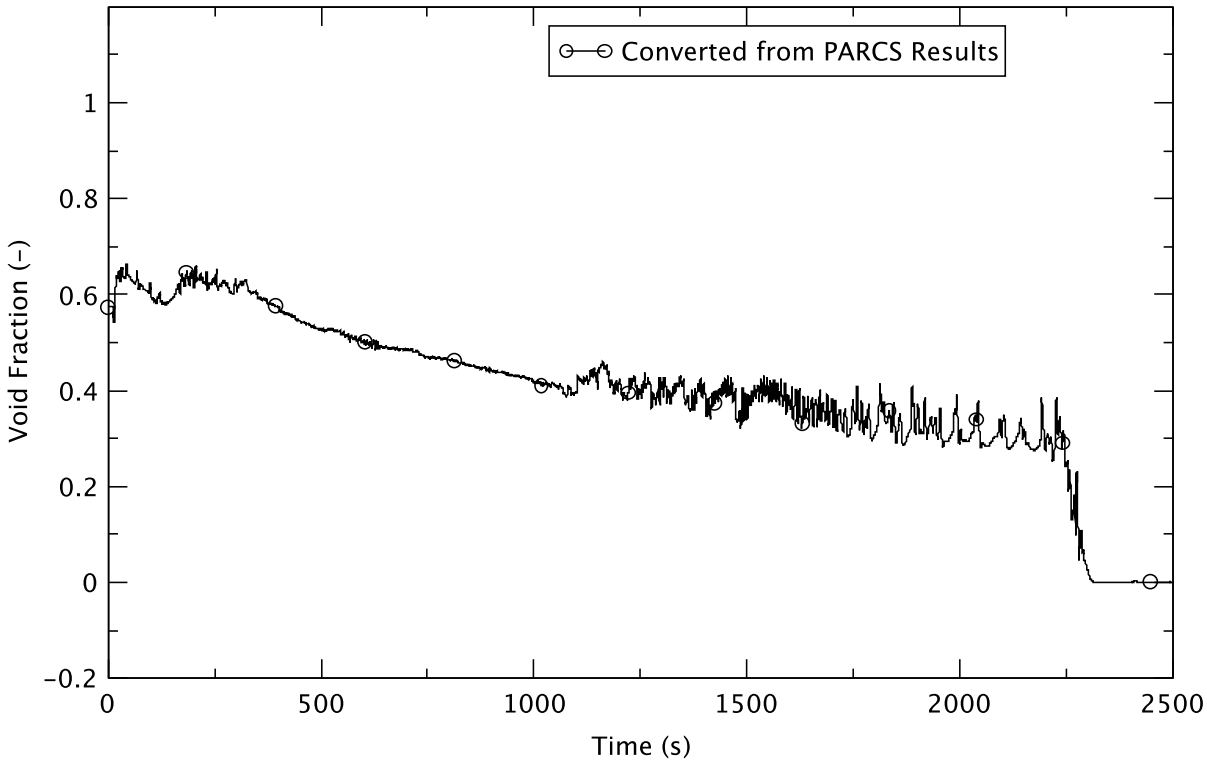

Figure 4.61 Core Average Void Fraction - PHE, TAF+5

With no break in the natural circulation core flow, the boron inventory in the core increases monotonically (Figure 4.62); the same trend is observed in the boron concentration in the lower plenum (Figure 4.63 and Figure 4.64). The effective boron concentration injected into the reactor vessel is shown in Figure 4.65. The concentration is seen to remain constant throughout the transient (except for a momentary drop at ~2400 s) and is indicative of the full entrainment of boron in the lower plenum. According to the boron mixing model (Section 2.3.7), entrainment drops from full to zero when the normalized core flow falls below a threshold value. At ~2400 s, the core flow (Figure 4.53) crosses the threshold briefly and the mixing drops to zero for a short time. This corresponds to the mixing coefficient becoming zero briefly at ~2400 s (Figure 4.66).

The core reactivity, Figure 4.67, reveals that the reduction of core power does not engender a major change in the fuel temperature (Doppler) reactivity, and the changes in the moderator densitiy reactivity are a reflection of the average core void (Figure 4.61). Overall, the monotonic increase in the boron reactivity far exceeds that of the other reactivity components, and hence, the net core reactivity remains substantially negative keeping the reactor shutdown.

The more or less continual operation of the feedwater system (Figure 4.50) appears to suggest a connection to the non-zero flow in the recirculation line (Figure 4.68).

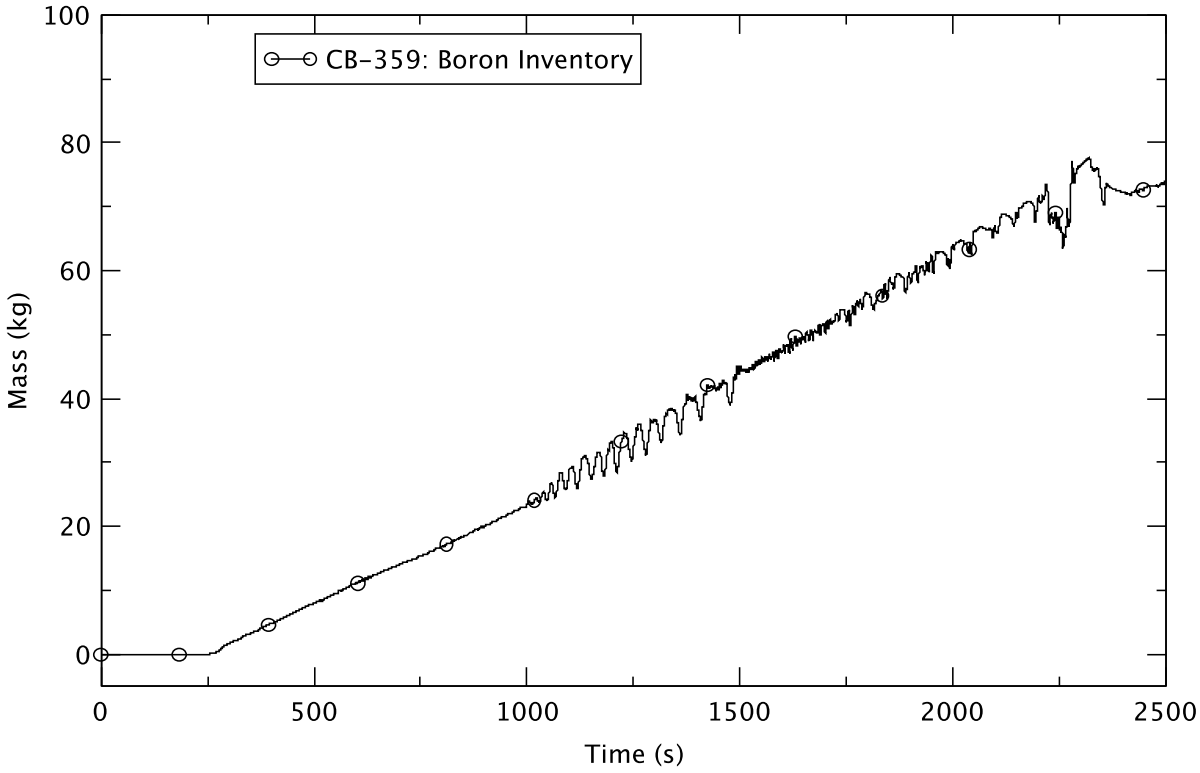

Figure 4.62 Boron Inventory in the Core - PHE, TAF+5

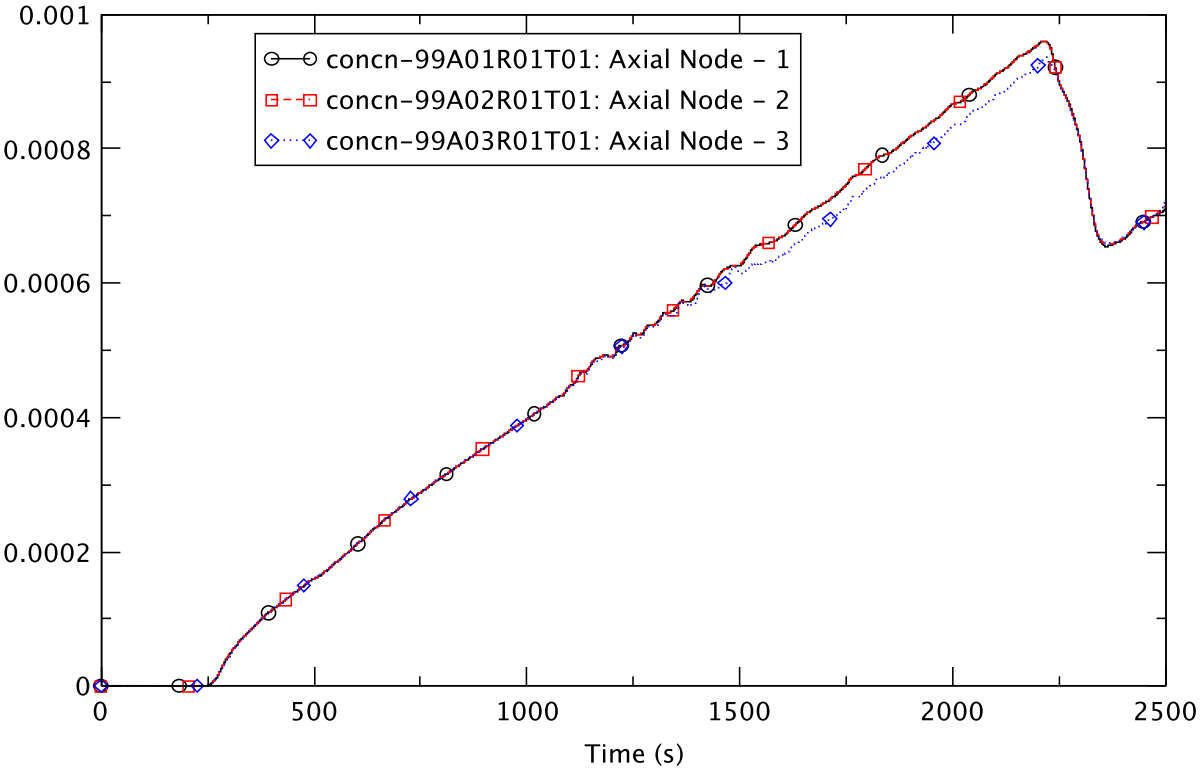

Figure 4.63 Boron Concentration in Ring 1 - PHE, TAF+5

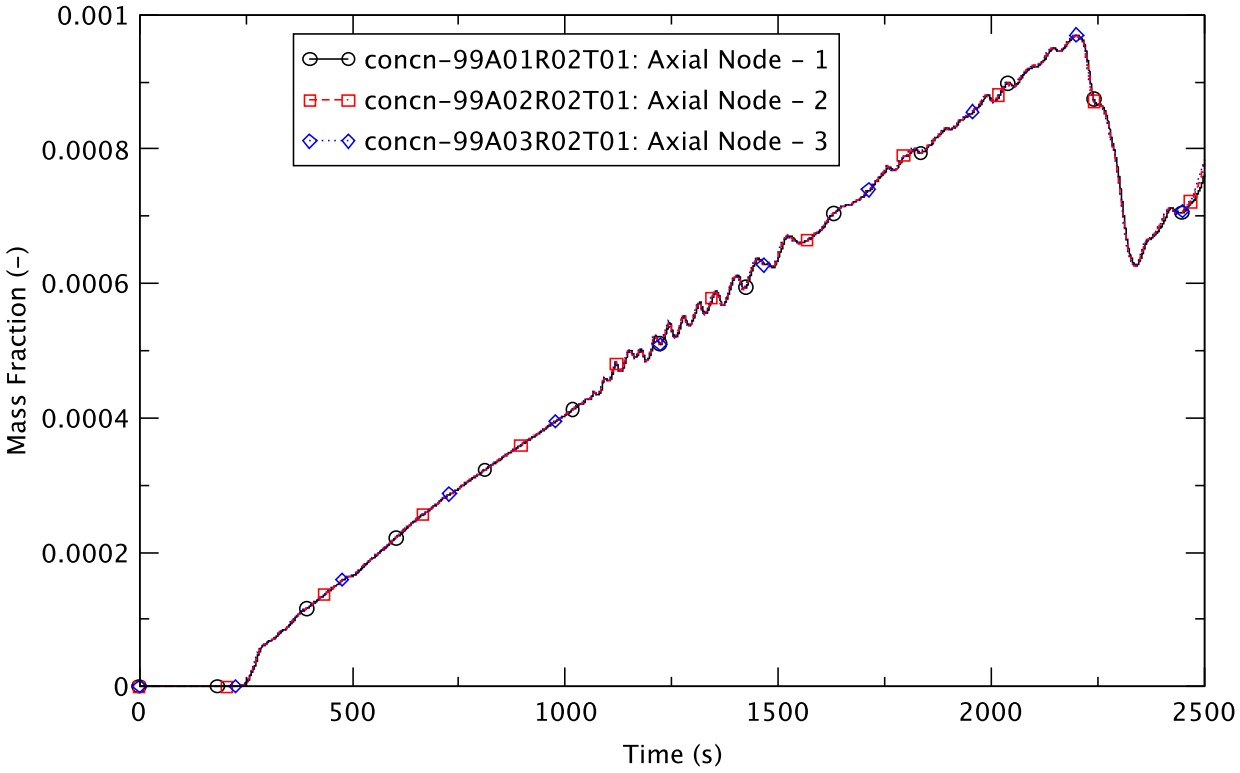

Figure 4.64 Boron Concentration in Ring 2 - PHE, TAF+5

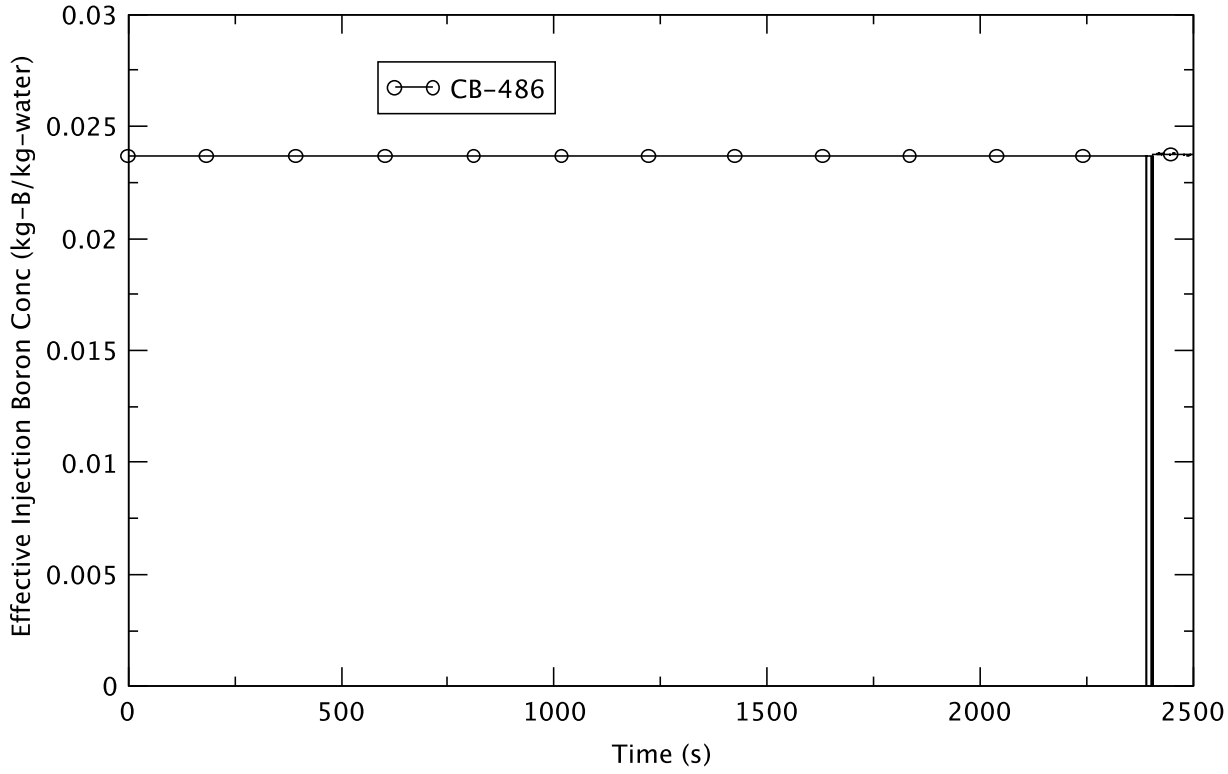

Figure 4.65 Effective Injection Boron Concentration - PHE, TAF+5

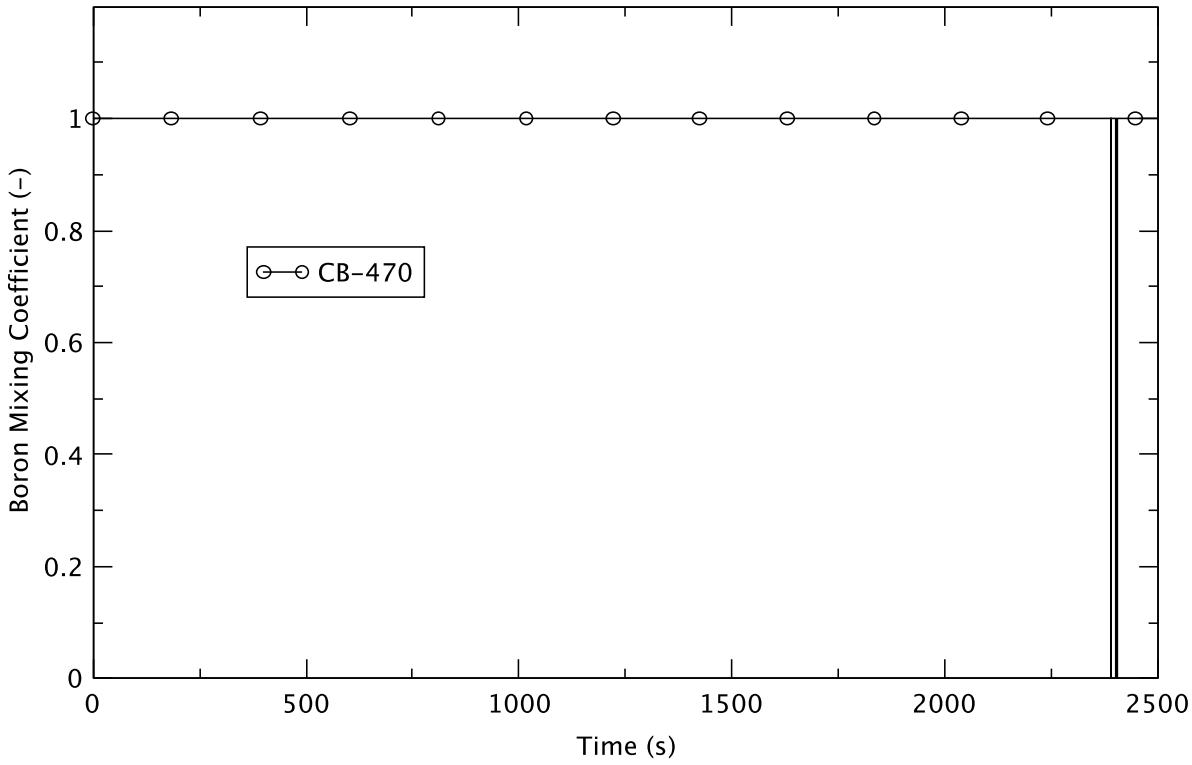

Figure 4.66 Boron Mixing Coefficient - PHE, TAF+5

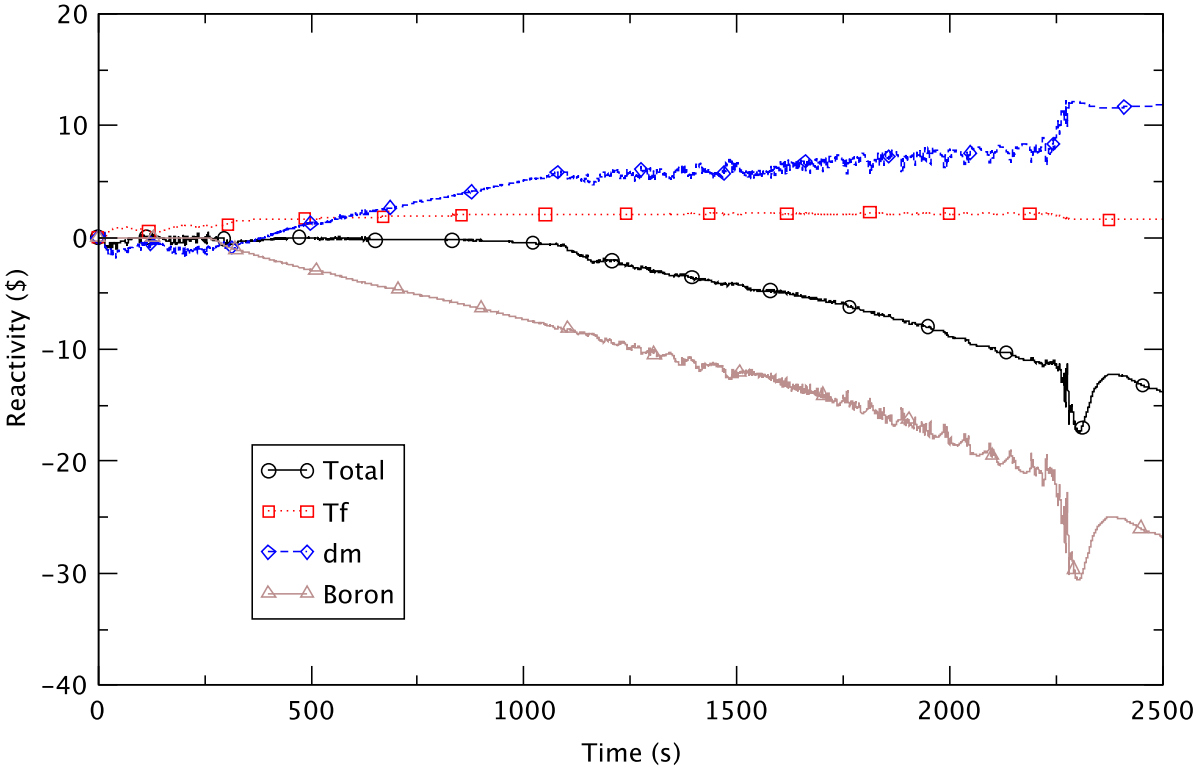

Figure 4.67 Core Reactivity - PHE, TAF+5

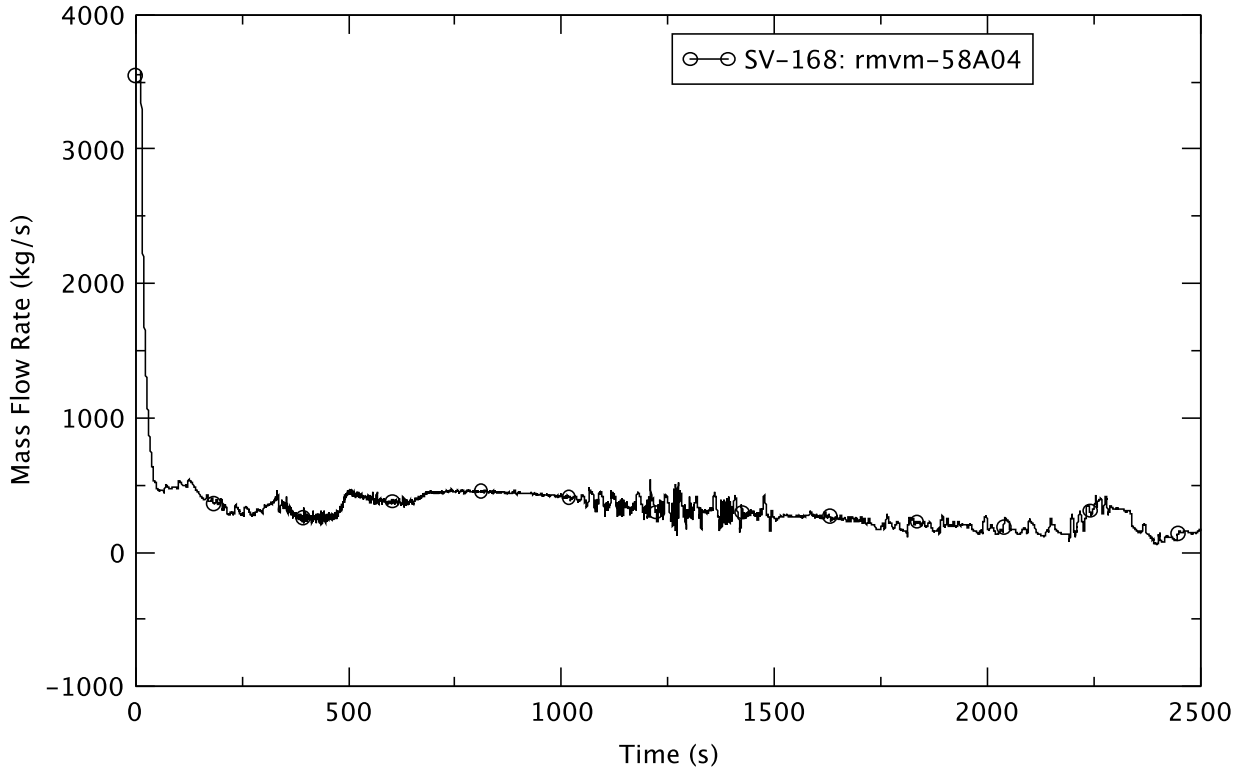

Figure 4.68 Recirculation Line Flow - PHE, TAF+5

The outcome of the PHE TAF+5 transient with respect to the four figures-of-merit is discussed next.

1) Peak clad temperature (PCT)

Figure 4.69 depicts the core-wide PCT as a function of time. The maximum PCT occurs at 14.4 s when the reactor still is undergoing pressurization, that is, before the MSIV is fully closed. The maximum PCT is only a few degrees K higher than the initial PCT, when the reactor is at full power. The axial clad temperature (Figure 4.70), displays a fairly uniform profile at different times during the transient. The transient response of the clad temperature is consistent with heat transfer by nucleate boiling wherein the clad temperature tends to track with the liquid saturation temperature during pressure transients. The profile of the fuel centerline temperature (Figure 4.71) exhibits a bottom peak initially but it becomes progressively more uniform over time.

2) Recriticality

The TRACE/PARCS calculation shows that there is no recriticality due to choking in the SRVs. The steam flow through the SRV is choked but the capacity of the SRVs is sufficient such that there is no significant repressurization of the RPV. The choking condition (Figure 4.72) is calculated for the SRV/ADS bank D for almost the whole duration of the transient. It is eliminated at around 2370 s when the steaming rate is reduced by the injection of feedwater at 2180 s to raise the water level, and the upstream pressure falls.

For this transient the boron reactivity basically increases monotonically (Figure 4.67) and there is no evidence of any dilution effect and hence, any potential for recriticality.

3) Wetwell temperature

The suppression pool reaches the maximum temperature of 368 K at about 2092 s (Figure 4.55). The TRACE/PARCS analysis shows that using the equivalent of two RHR loops in the suppression pool cooling mode, and incorporating heat structures in both the suppression pool and the airspace in the wetwell suffice to prevent the suppression pool from approaching boiling .

4) Containment pressure

Figure 4.73 shows that the drywell pressure reaches a maximum of 0.17 MPa at about 500 s after the ED, and then remains almost constant. The maximum pressure is low enough that the integrity of the containment is not challenged.

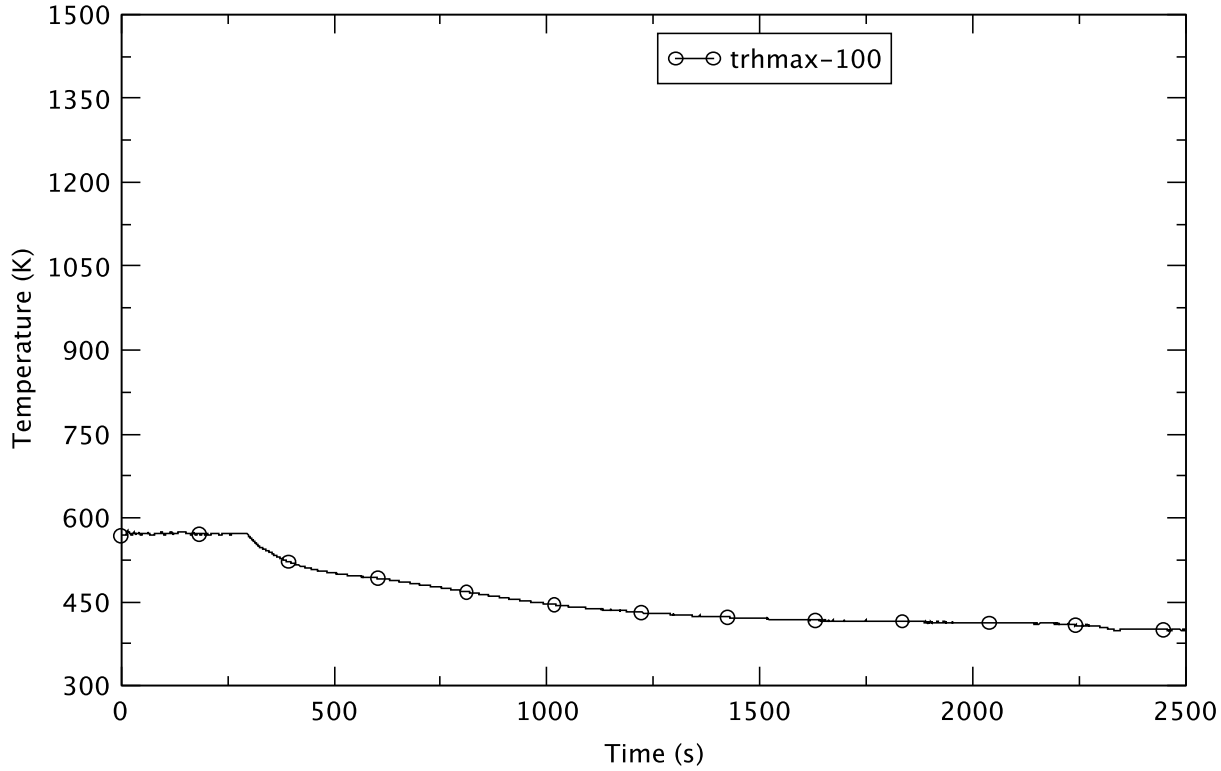

Figure 4.69 Peak Clad Temperature - PHE, TAF+5

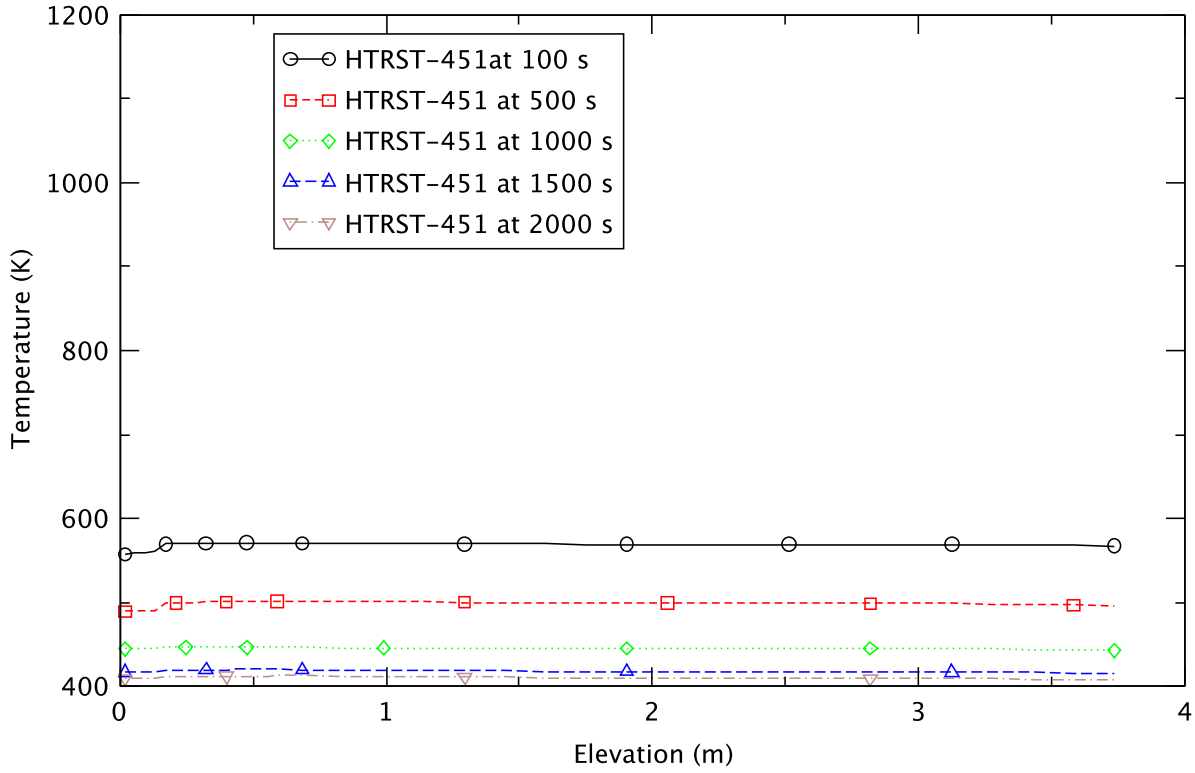

Figure 4.70 Axial Profile of Clad Temperature - PHE, TAF+5

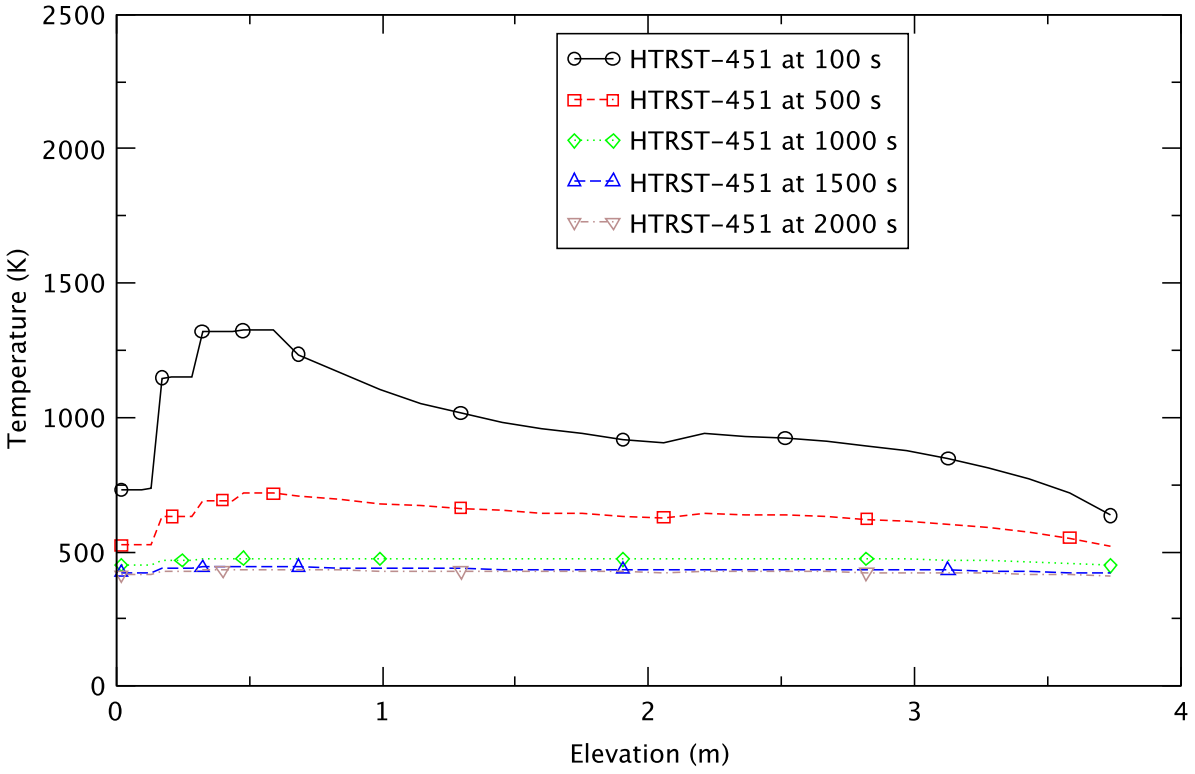

Figure 4.71 Axial Profile of Fuel Centerline Temperature - PHE, TAF+5

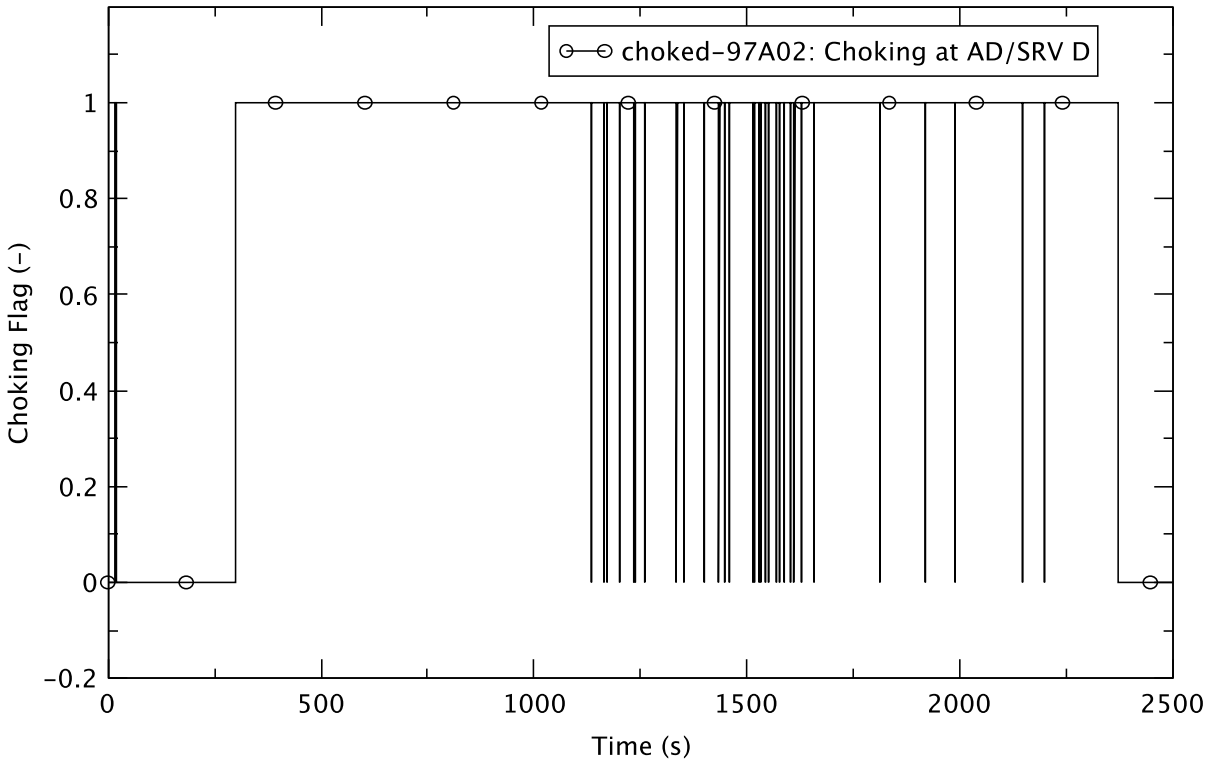

Figure 4.72 Choking Flag for SRV/ADS Bank D - PHE, TAF+5

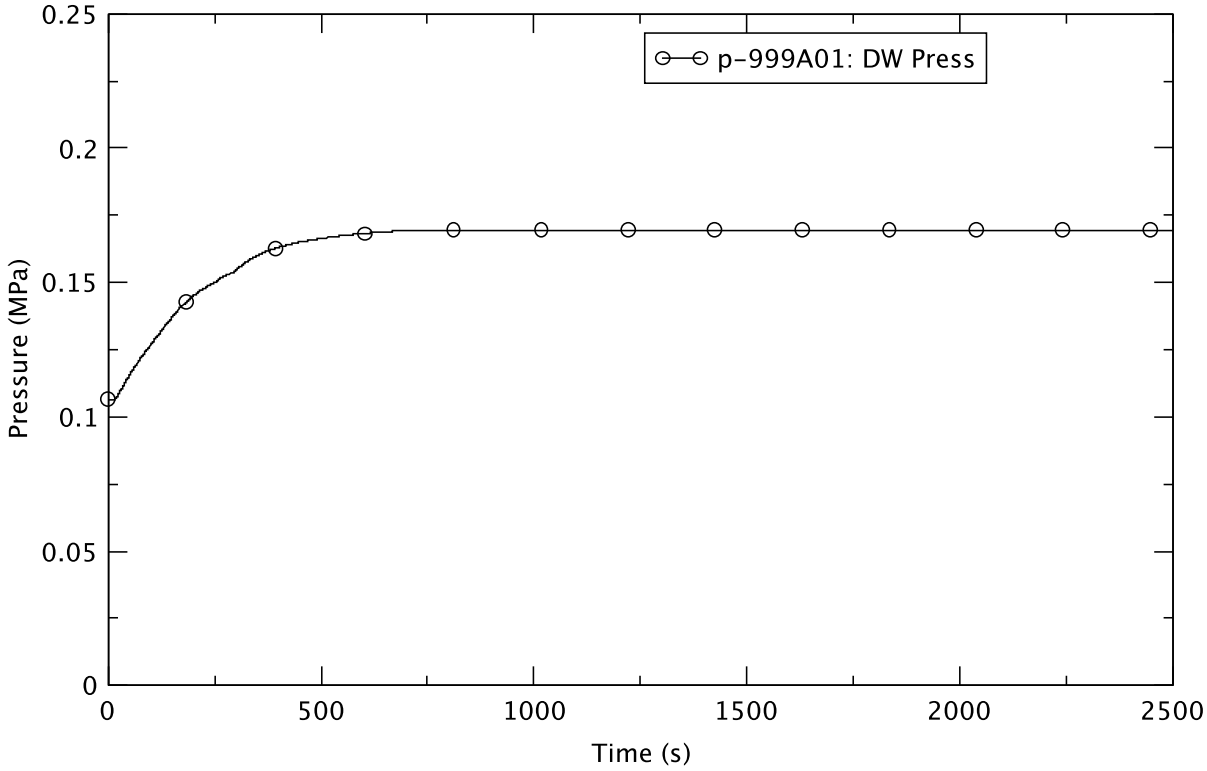

Figure 4.73 Drywell Pressure - PHE, TAF+5

4.3.3 Effect of Level Control at PHE

In general, the transient responses to water level control for the PHE exposure condition are very similar to the responses at BOC discussed in Section 4.2.3. This is evident by comparing key results from the former, shown in Table 4.7, with those in Table 4.4 for the latter. In all cases, the maximum PCT is higher for BOC than for PHE.

A select set of plots (Figure 4.74 to Figure 4.84) is used to compare and contrast the transient responses of three PHE cases when the water level is controlled to TAF, TAF-2, and TAF+5.

As observed in the BOC cases, the responses of the TAF and TAF-2 cases at PHE again are quite similar. However, they exhibit different behavior in the maximum PCT. For TAF+5 and TAF, the maximum occurs early, immediately after MSIV closure is initiated when the core flow still is relatively high. For TAF-2, there is delayed heat-up of the core at a time when the reduction in water level causes the core flow to approach a lower quasi-steady value, and the corresponding maximum PCT is more limiting than in the other two cases.

The reactor power (Figure 4.74) generally exhibits similar responses for all three cases. However, unlike the TAF+5 case, there is no leveling off of the reactor power for TAF and TAF-2 immediately after emergency depressurization (ED); instead the power continues to decrease.

With a higher reactor power after the initiation of level control, the TAF+5 case has the earliest ED time. For the same reasons detailed in Section 4.2.3, the TAF-2 case has a slightly earlier ED time than does the TAF case.

Table 4.7 Comparison of Key Results for PHE Base Cases

Key Event	PHE TAF	PHE TAF-2	PHE TAF+5
Maximum PCT (trhmax-100)	577 K (14 s)	671 K (599 s)	577 K (14 s)
Core Boron Inventory (CB 359) > 0.01 kg	247 s	253 s	245 s
Emergency Depressurization	352 s	348 s	300 s
Maximum Drywell Pressure	0.162 MPa (542 s)	0.162 MPa (542 s)	0.170 MPa (783 s)
Reactor Shutdown (Stayed < 3.25% Initial Power)	995 s	1068 s	986 s
Maximum Suppression Pool Temperature	359 K (2220 s)	358 K (2209 s)	368 K (2092 s)

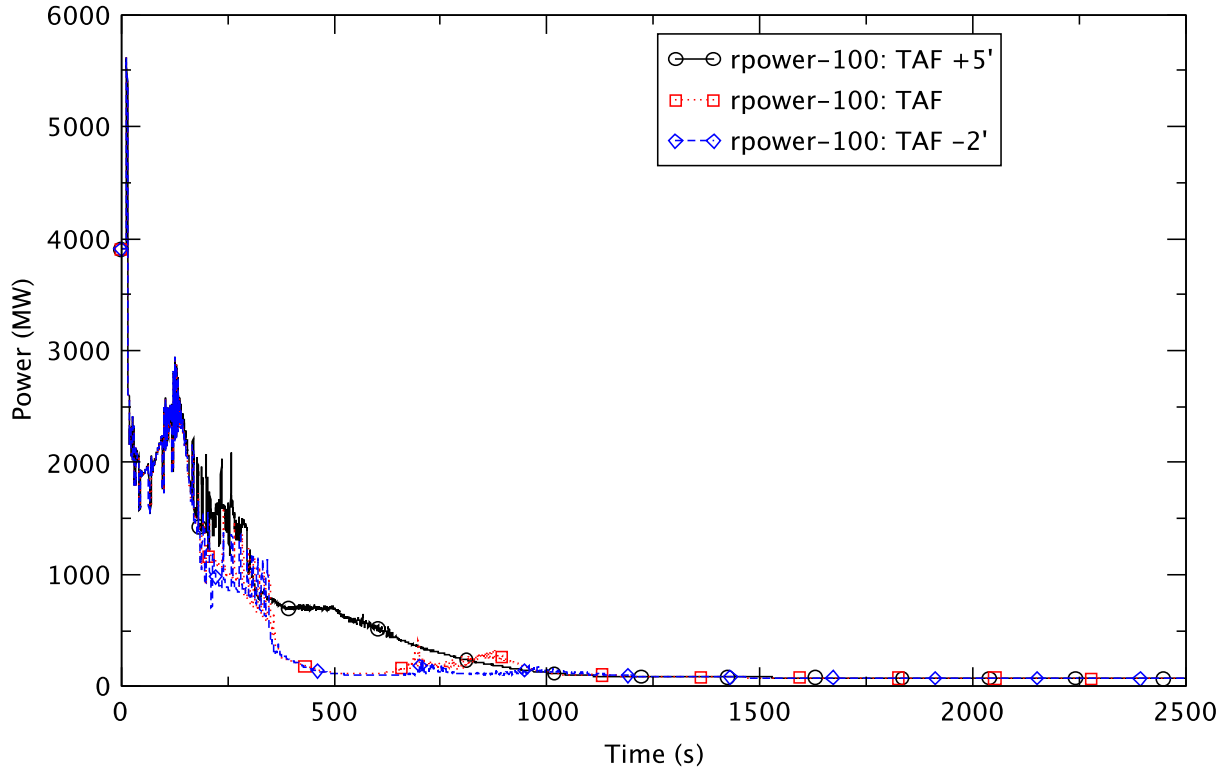

Figure 4.74 Reactor Power - PHE Base Cases

The pressure response after the ED is shown in Figure 4.75. With a more rapid depressurization in the TAF and TAF-2 cases there is voiding in the lower plenum and natural circulation flow is "broken," thereby reducing core flow (Figure 4.76). There also is a significant level swell in the downcomer after the ED for TAF and TAF-2 control (Figure 4.77). Subsequent refilling of the lower plenum and the core region causes a decrease in the water level and fluctuation in the core flow around 750 s. For TAF+5, between 1000 s and 1500 s the core bypass region begins refilling with water. This is evident in the fluctuating but decreasing void fractions shown earlier in Figure 4.57 and Figure 4.58. During refilling, there are oscillations in the water level and a general decreasing trend in the oscillating core flow.

The core boron inventories, shown in Figure 4.78, are similar to those for the BOC cases (Figure 4.31). Though the final inventory at 2500 s is almost the same for all of the BOC and PHE cases, the rate of delivery is a little faster for the latter.

The core reactivity for TAF and TAF-2 are shown in Figure 4.79 and Figure 4.80, respectively. The positive net reactivity occurring roughly between 750 s and 1000 s is responsible for the power perturbations observed in Figure 4.74 for both TAF and TAF 2. In all three PHE cases, the reactor remains shutdown by the injected boron; no recriticality is observed after either repressurization of the reactor vessel or the dilution of boron.

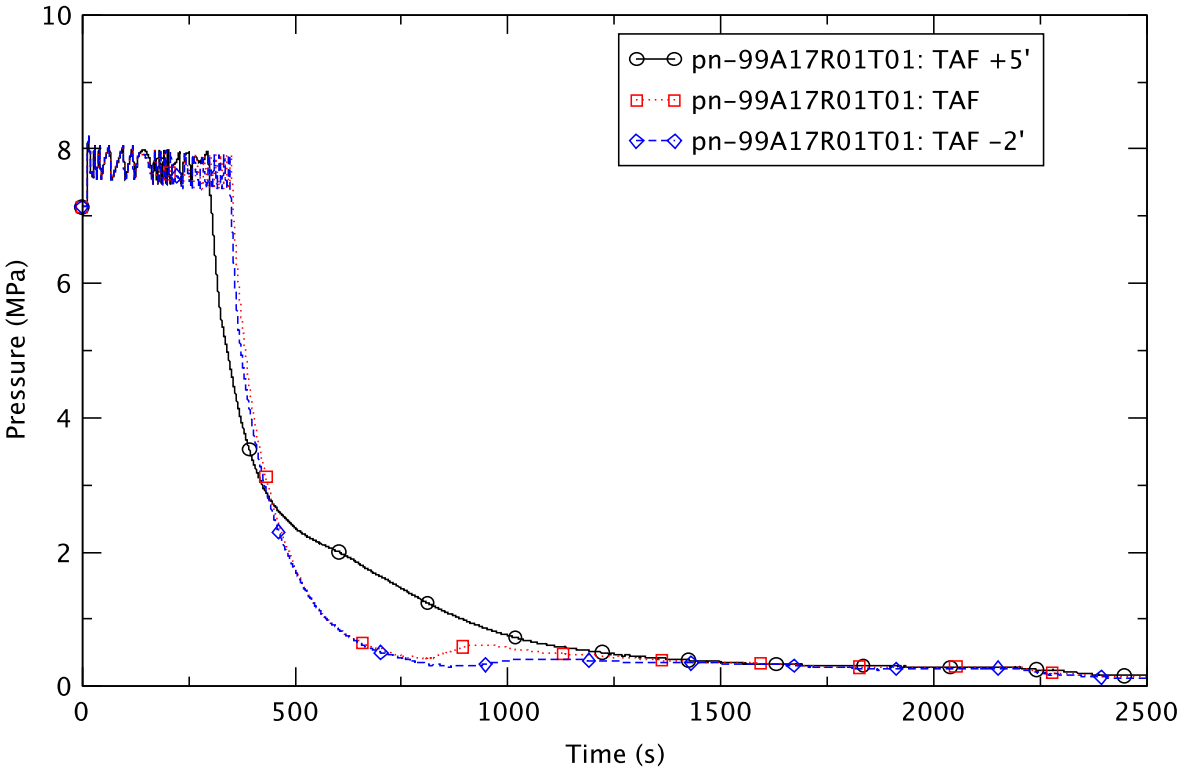

Figure 4.75 Reactor Pressure - PHE Base Cases

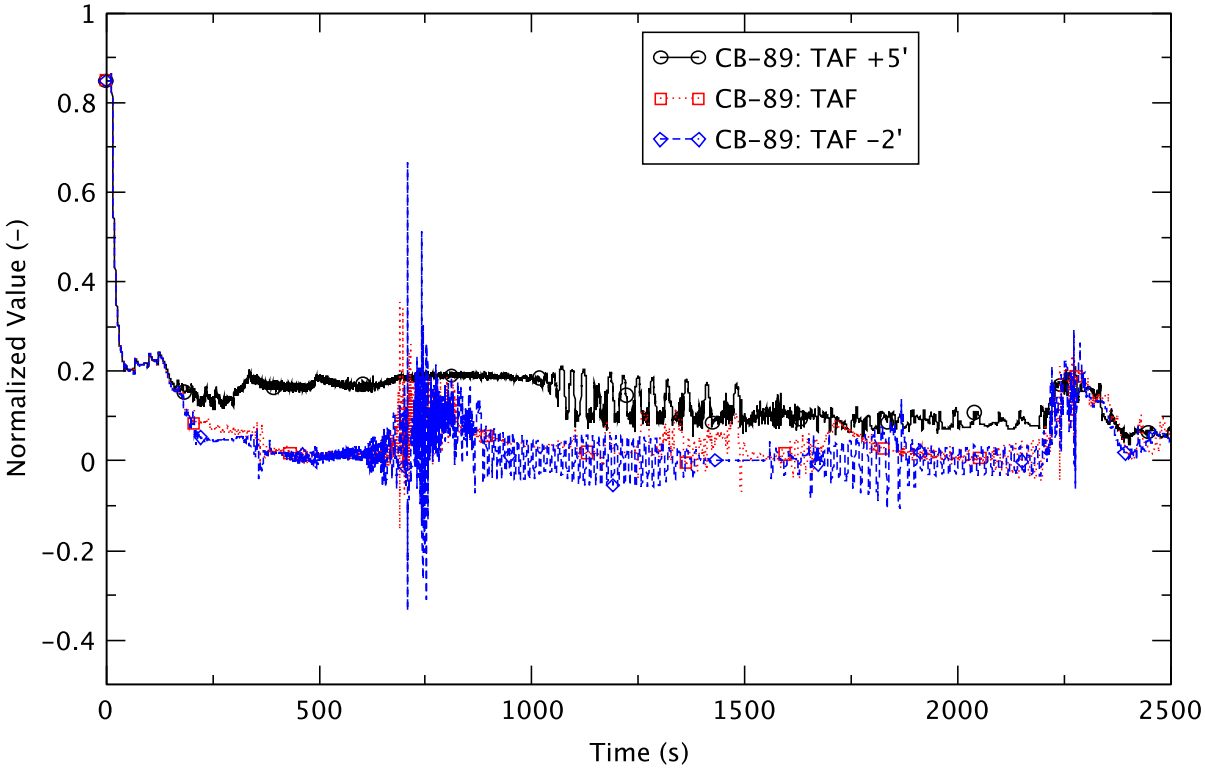

Figure 4.76 Core Flow - PHE Base Cases

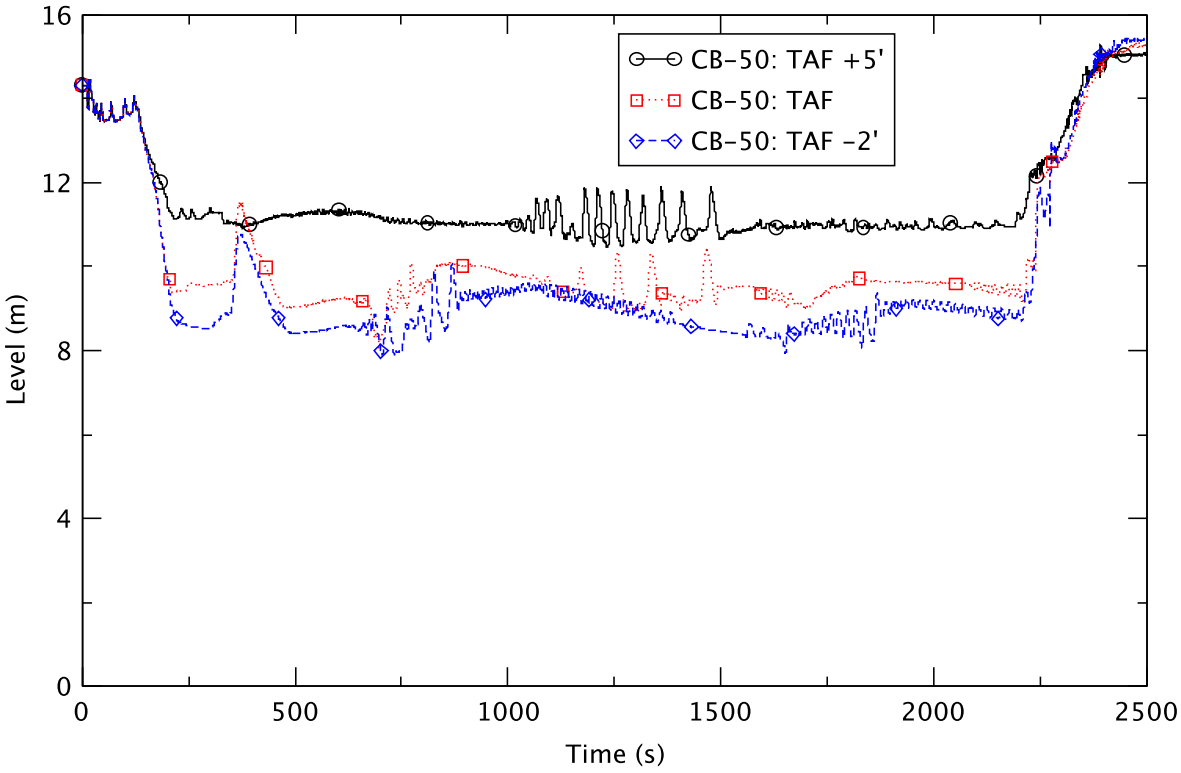

Figure 4.77 Downcomer Water Level - PHE Base Cases

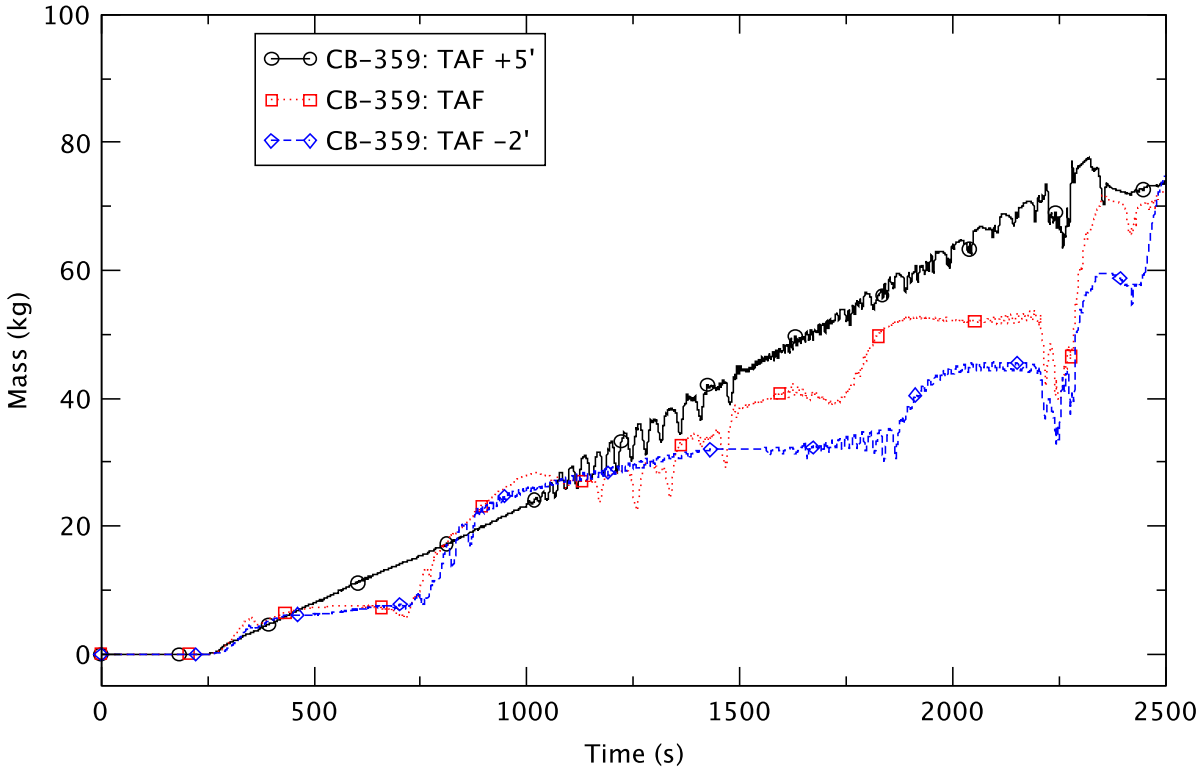

Figure 4.78 Boron Inventory in the Core - PHE Base Cases

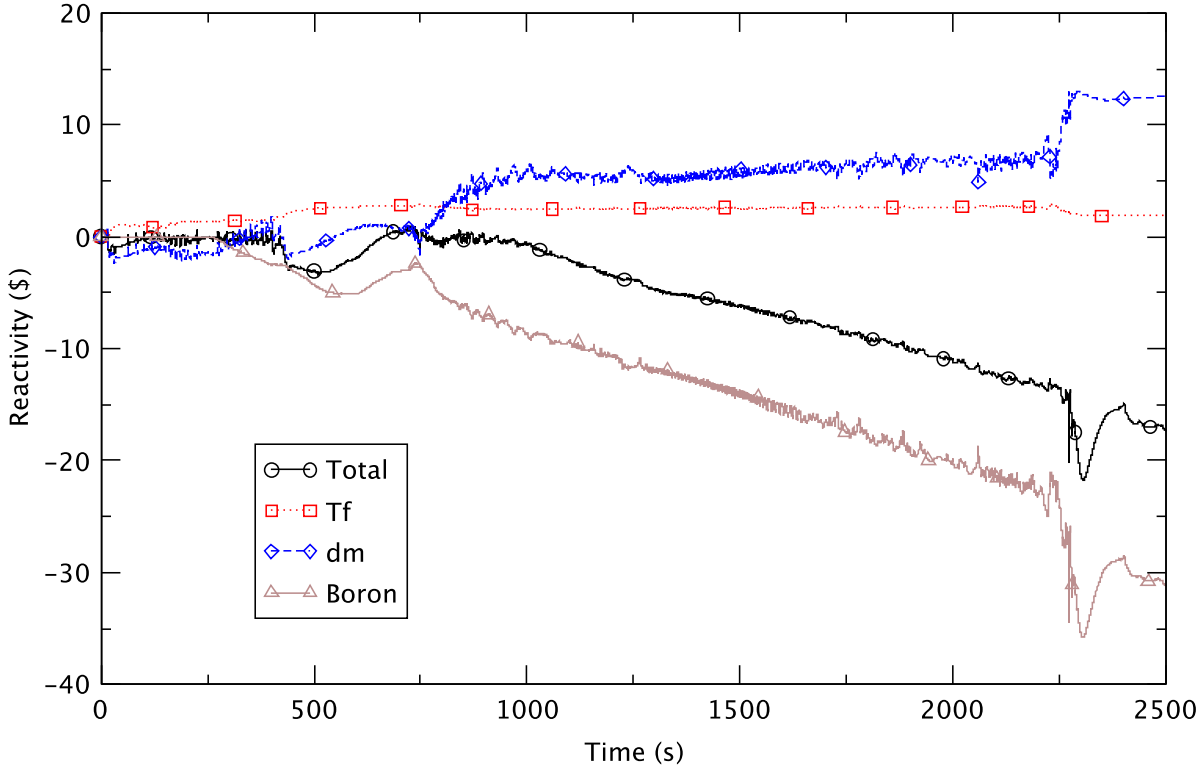

Figure 4.79 Core Reactivity - PHE, TAF

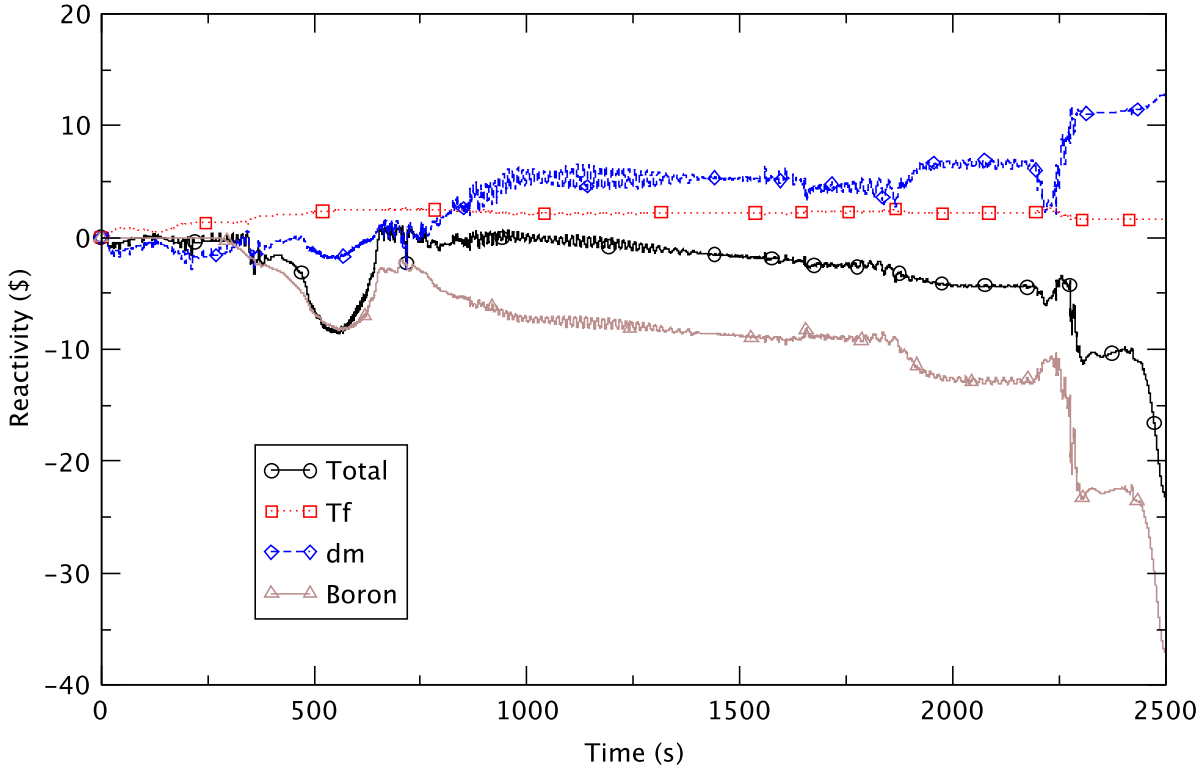

Figure 4.80 Core Reactivity - PHE, TAF-2

As discussed earlier, the maximum PCT for the TAF-2 case is more limiting than for the other two cases; Figure 4.81 shows this maximum PCT (~671 K) occurring at ~600 s, the time when the core voiding also reaches a maximum (Figure 4.82).

The temperature of the suppression pool water (Figure 4.83) is an indication of the energy discharged to the pool via the SRVs. The TAF+5 case had the highest peak pool temperature of the three cases considered; the TAF case has a slightly higher peak temperature than the TAF-2. In all three, the pool temperature stays much below 373 K and thus, is not expected to affect the reactor's safe shutdown.

The transient response of the drywell pressure (Figure 4.84) is as expected, with TAF+5 having the highest pressure. In all three cases, the maximum drywell pressure is sufficiently low as not to be a concern for the containment's integrity.

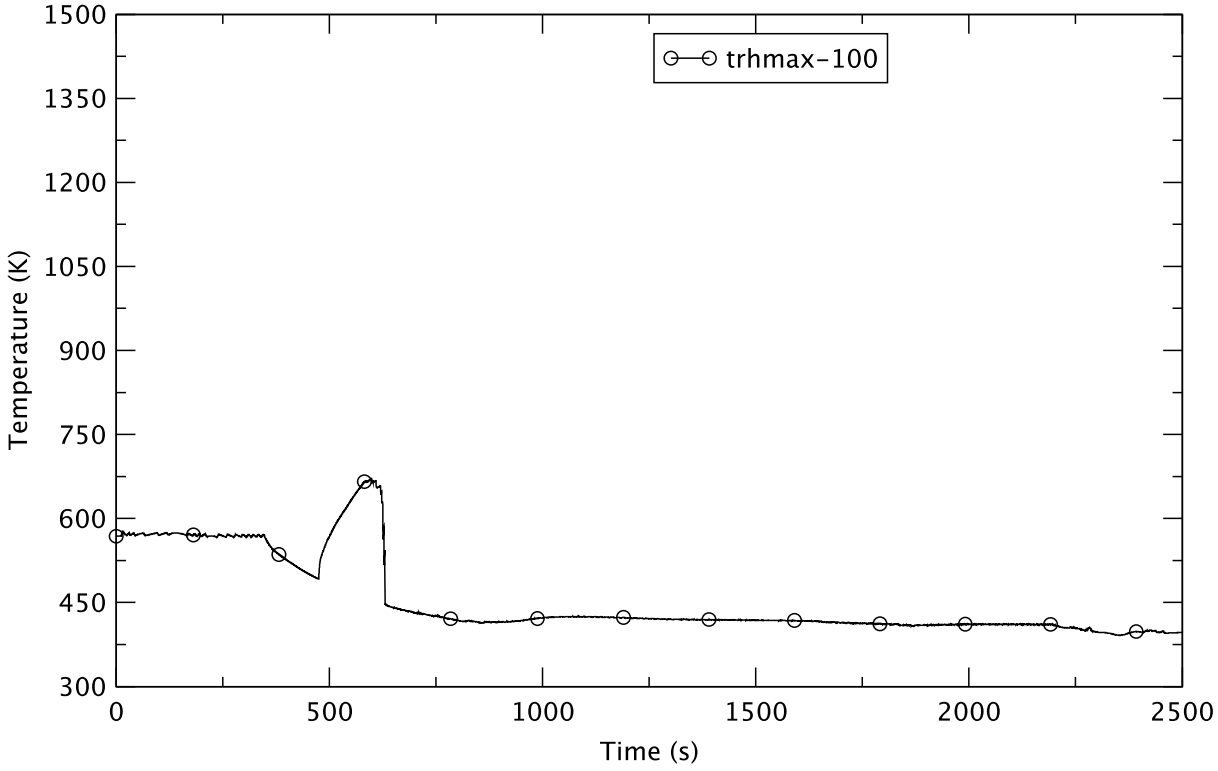

Figure 4.81 Peak Clad Temperature - PHE, TAF-2

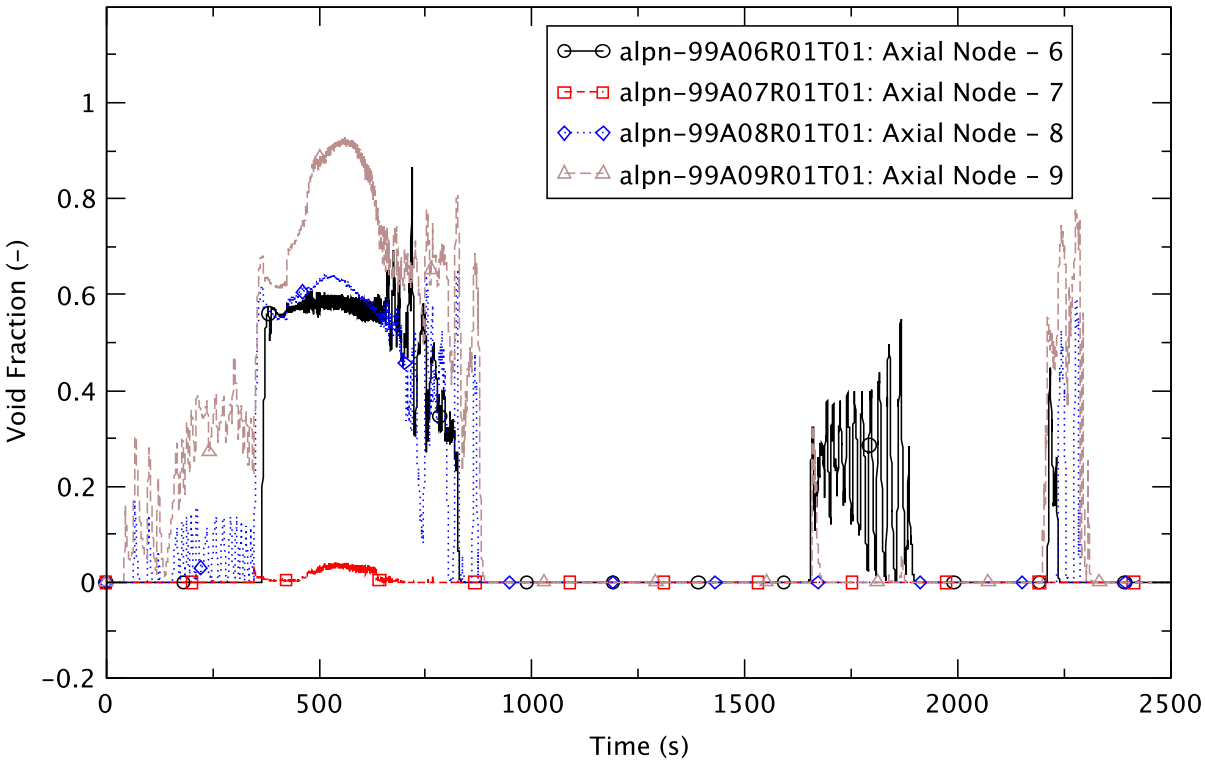

Figure 4.82 Void Fraction in Core Bypass (Ring-1) - PHE, TAF-2

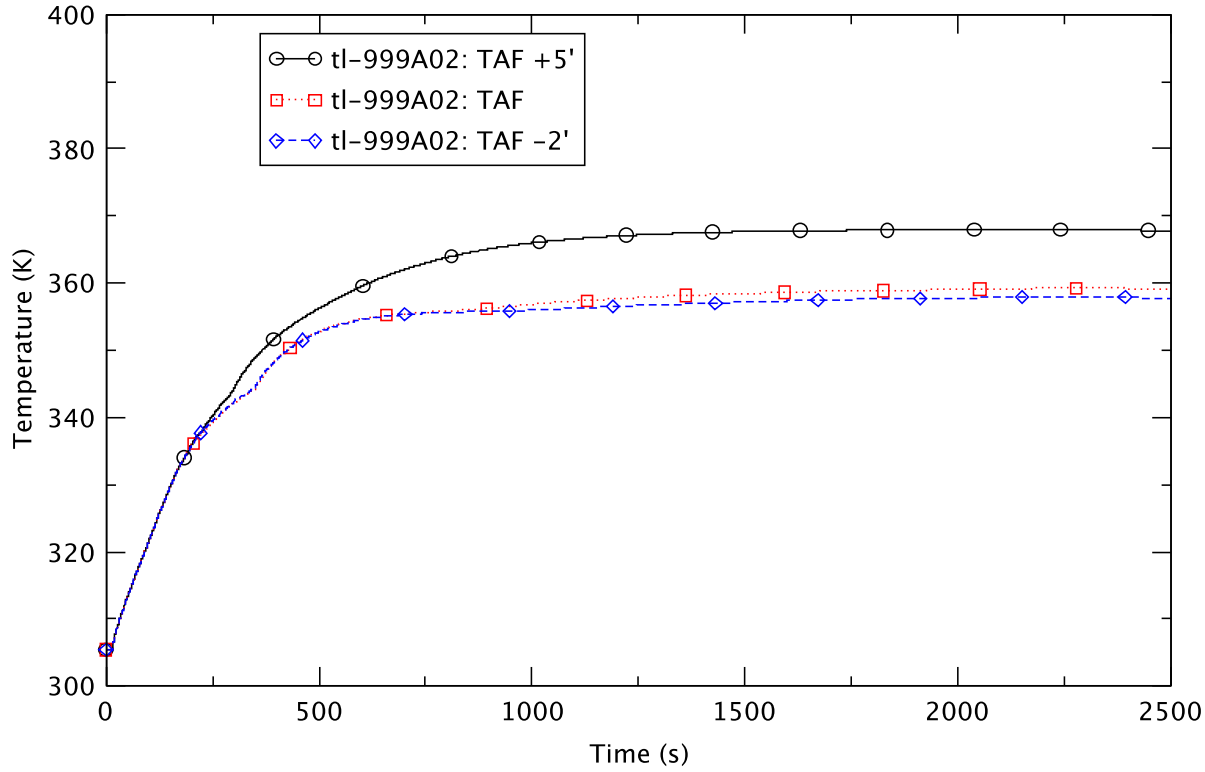

Figure 4.83 Suppression Pool Temperature - PHE Base Cases

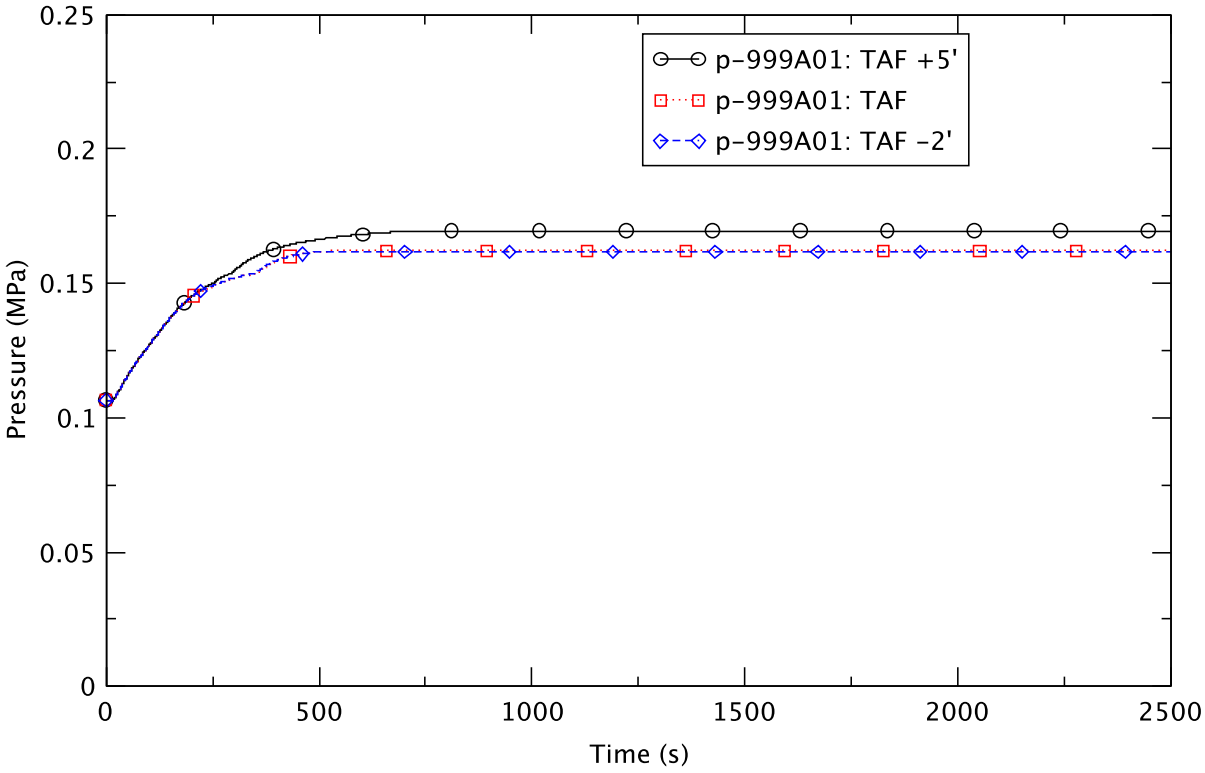

Figure 4.84 Drywell Pressure - PHE Base Cases

4.3.4 Effect of SLCS Injection Point at PHE

One of the design differences between a BWR/4 and a BWR/5 is the location of the injection point for the standby liquid control system (SLCS). For this analysis of the ATWS-ED transient, a lower-plenum injection (applicable to a BWR/4) is nominally assumed for all cases. A case was run to assess the sensitivity of the transient response to an injection point located in the upper plenum of the reactor vessel, as would occur for a BWR/5. In such a case, boron is delivered to the upper plenum via the high-pressure core spray line. In the TRACE/PARCS model, this is simulated by delivering the boron solution from a pipe with an interface on the outer surface of ring 2 of the vessel at axial level 10. The two-phase flow in the upper plenum is highly turbulent (unlike the nearly stagnant lower plenum), and therefore, boron injected into the upper plenum is presumed to be well mixed. For this scenario, the internal TRACE/PARCS boron tracking model (equivalent to the 100% mixing scenario of the boron transport model described in Appendix A) is sufficient; no special treatment of mixing and/or remixing is required [5].

Table 4.8 compares some key parameters derived from the results of the TRACE/PARCS analysis. The initial buildup of boron in the core is a little bit faster when the injection is into the upper plenum than when it is injected into the lower plenum because the injection point is inside the control volume used to account for the core boron inventory.

Table 4.8 Comparison of Key Results at PHE - Boron Injection Location

Key Event	PHE TAF+5 (Lower Plenum)	PHE TAF+5 (Upper Plenum)
Maximum PCT (trhmax-100)	577 K (14 s)	577 K (14 s)
Core Boron Inventory (CB 359) > 0.01 kg	245 s	221 s
Emergency Depressurization	300 s	304 s
Maximum Drywell Pressure	0.170 MPa (783 s)	0.170 MPa (801 s)
Reactor Shutdown (Stayed < 3.25% Initial Power)	986 s	1030 s
Maximum Suppression Pool Temperature	368 K (2092 s)	369 K (2109 s)

In the reference case where the injection is to the lower plenum, Figure 4.66 shows that boron mixing, as predicted by the boron transport model, is 100% (except for the momentary drop to zero at 2400 s). Thus, boron is completely entrained with the coolant flow and the mechanism for the boron transport in the lower plenum is identical for the two cases, lower and upper plenum injection respectively. As expected, with injection into the upper plenum, the arrival of boron in the lower plenum is delayed by the transit time of the coolant flow between the core and the lower plenum via the steam separator and the downcomer: Figure 4.85 shows that there is about a 35 s delay. Overall, the location of the injection point has little impact on the transient response (Figure 4.86 through Figure 4.92).

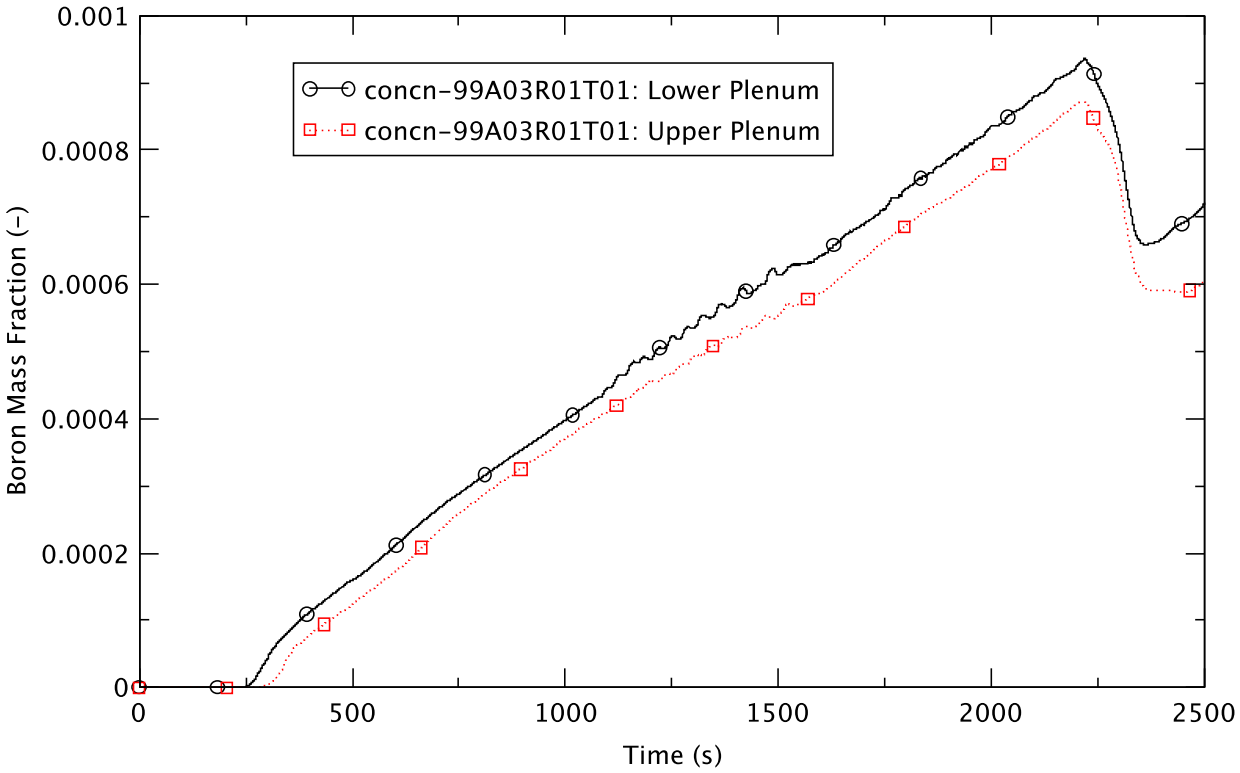

Figure 4.85 Boron Concentration in Ring 1 - TAF+5, Lower & Upper Plenum Injection

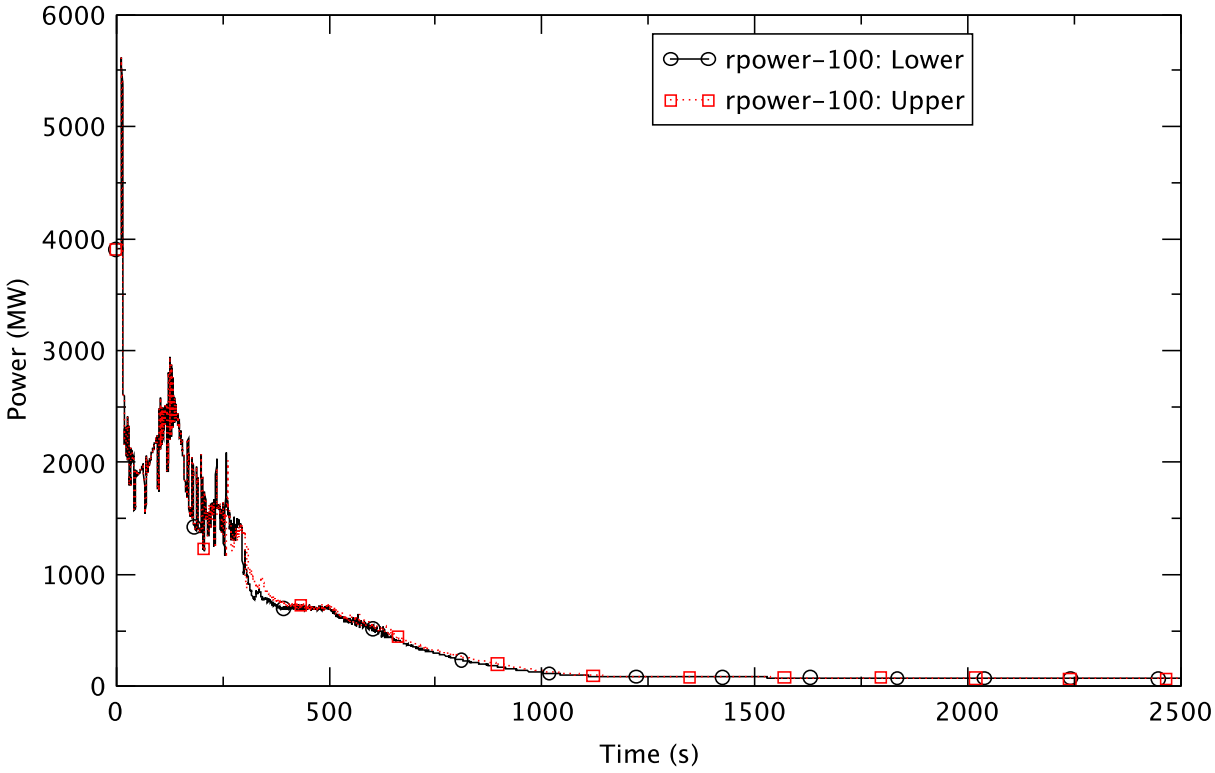

Figure 4.86 Reactor Power - TAF+5, Lower & Upper Plenum Injection

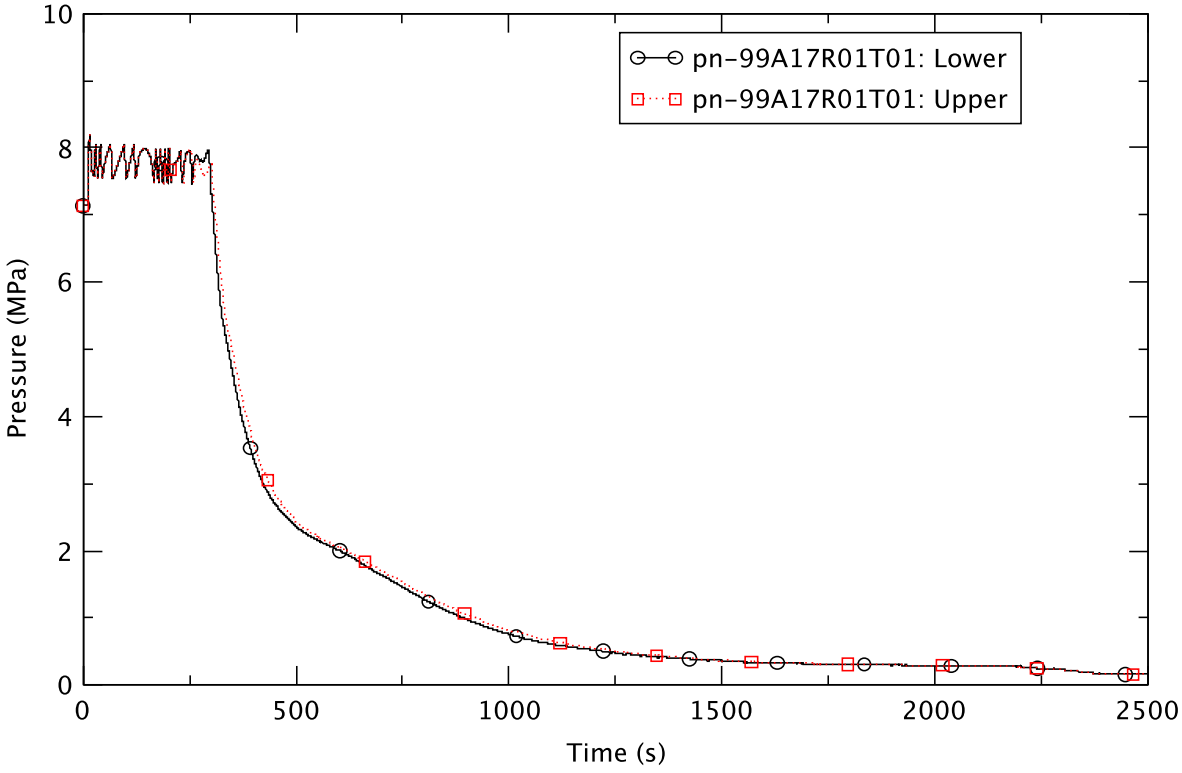

Figure 4.87 Reactor Pressure - TAF+5, Lower & Upper Plenum Injection

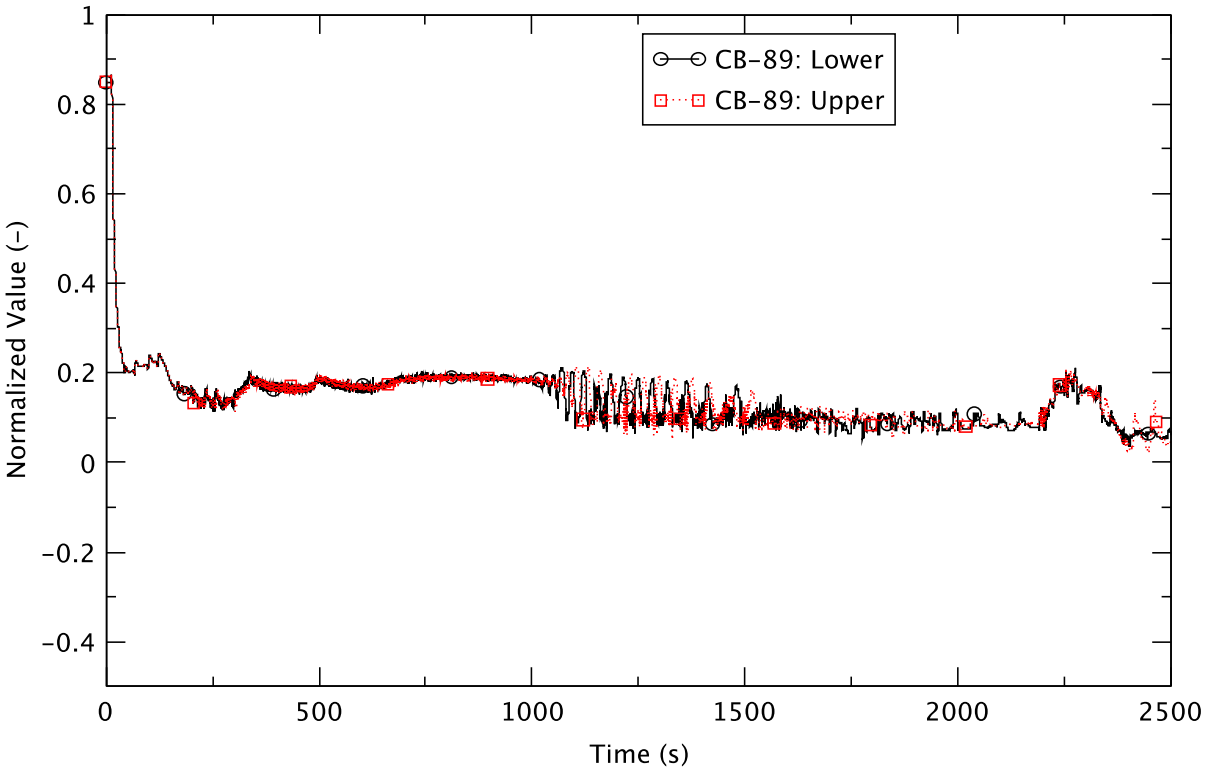

Figure 4.88 Core Flow - TAF+5, Lower & Upper Plenum Injection

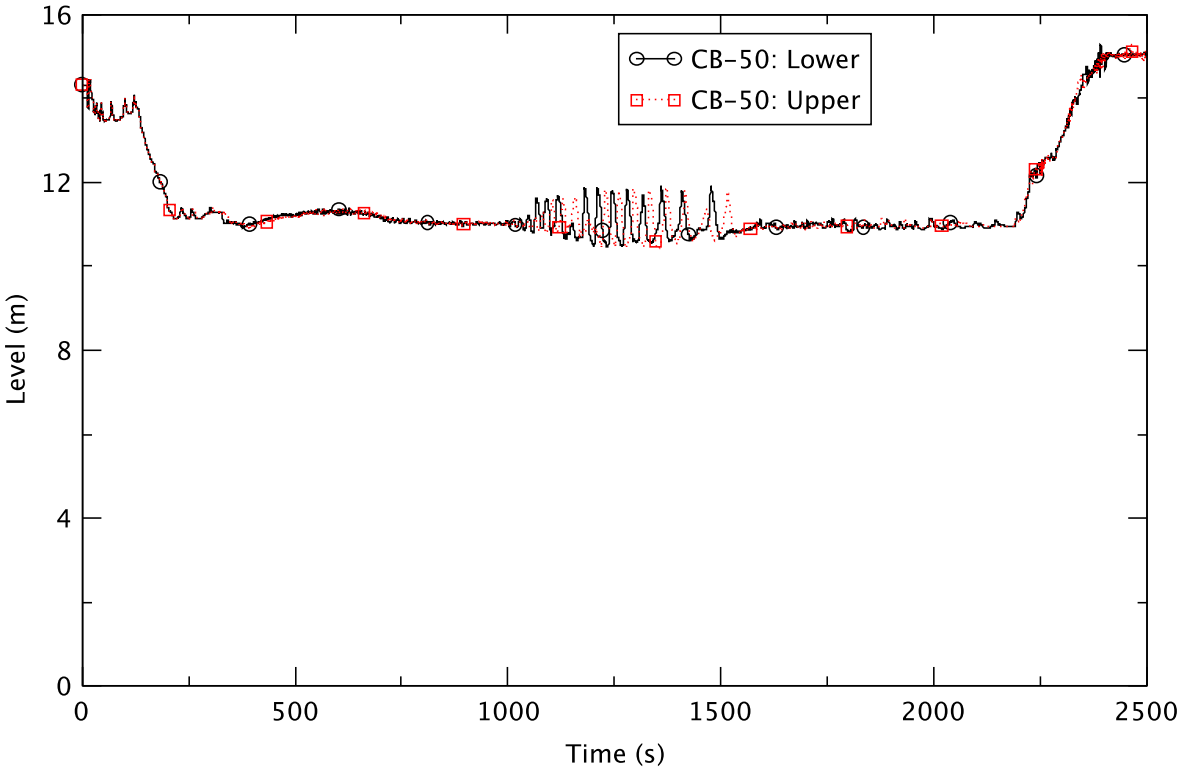

Figure 4.89 Downcomer Water Level - TAF+5, Lower & Upper Plenum Injection

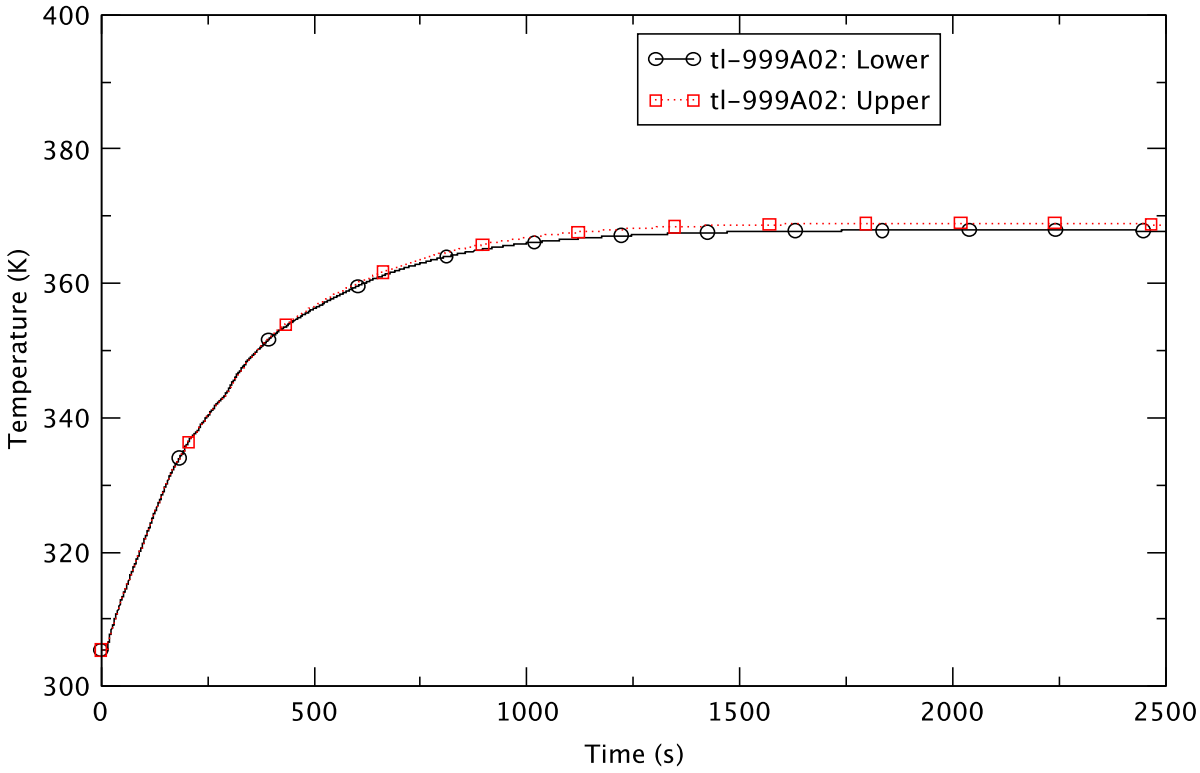

Figure 4.90 Suppression Pool Temperature - TAF+5, Lower & Upper Plenum Injection

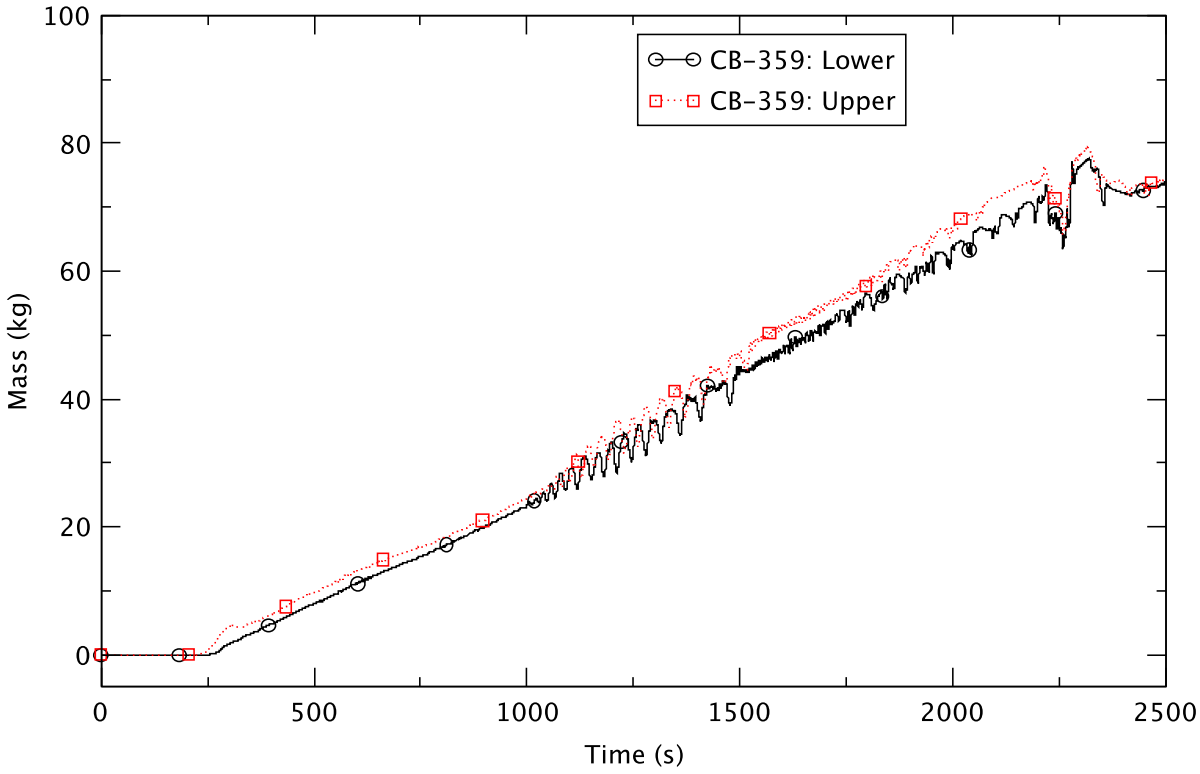

Figure 4.91 Boron Inventory in the Core - TAF+5, Lower & Upper Plenum Injection

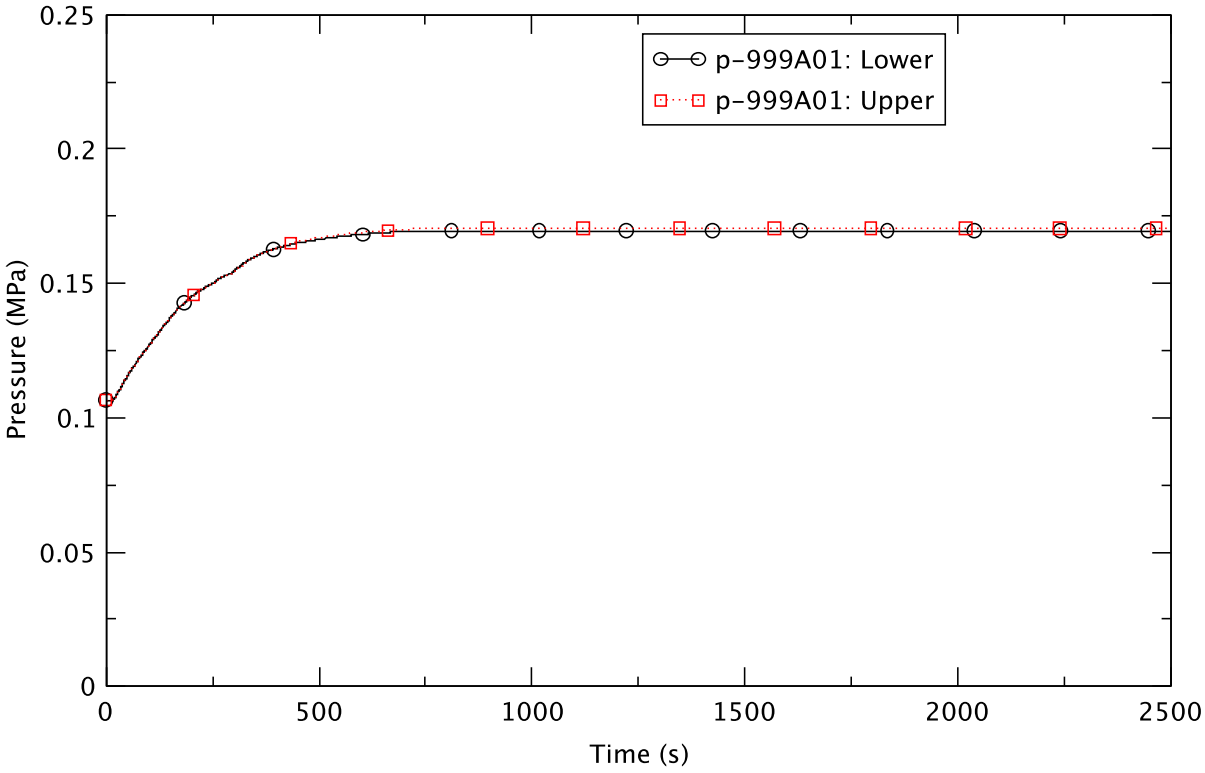

Figure 4.92 Drywell Pressure - TAF+5, Lower & Upper Plenum Injection

4.4 End-of-Full-Power-Life (EOFPL) Cases

There are eight ATWS-ED cases at EOFPL. Three of them are for evaluating different strategies of reactor water level control (RWLC). These "base" cases represent controlling water level to TAF, TAF+5, and TAF-2, 120 s after the transient starts. The TAF-2 case was selected as the representative case; Section 4.4.1 summarizes the timing of events from the TRACE/PARCS simulation of the representative case. A detailed discussion of the representative case is given in Section 4.4.2. The parametric effects of controlling the reactor water level to TAF+5, TAF, and TAF-2 are discussed in Section 4.4.3. The remaining five cases are sensitivity cases and will be covered in a subsequent report as part of this series of ATWS analyses. One of them is a 75% flow case (with level control to TAF-2); it represents a scenario with an eigenvalue offset for criticality based on low-low core flow. Three sensitivity cases are at 85% flow (with level control to TAF, TAF+5, and TAF-2) and they serve to simulate a condition of top-peaked power shape achievable within the allowable operating domain. The last sensitivity case examines the effect of using a spectrally corrected void-history (with level control to TAF+5).

4.4.1 Sequence of Events for the EOFPL Representative Case

The progression of this transient, ATWS-ED at EOFPL with RWLC to TAF-2, generally follows the generic description in Section 4.1. Table 4.9 shows the time sequence for this event; the system behavior is detailed in the next section.

Table 4.9 Sequence of Events at EOFPL with RWLC to TAF-2

Time (s)	Event
0.0	• Null transient simulation starts
10.0	• Null transient simulation ends • Trip initiates an MSIV closure
13.4	• High RPV pressure trips recirculation pumps
13.7	• First lift of SRV
14.6	• MSIV closes completely
130	• Initiation of reactor water level control
211	• Initiation of boron injection
~264	• Boron starts accumulating in the core (CB 359 > 0.01 kg)
450	• Initiation of emergency depressurization
648	• Drywell reaches a maximum pressure of 0.160 MPa
699	• Maximum PCT of 639 K (trhmax-100)
2180	• Initiation of restoring reactor water level over 100 seconds
2191	• Suppression pool reaches maximum temperature of 357 K
2500	• Simulation ends.

4.4.2 Transient Response of the EOFPL Representative Case

In many respects, the transient response of the EOFPL TAF-2 case is similar to the BOC TAF case described in Section 4.2.1. For example, the reactor power response (Figure 4.93) follows the general trend of all other ATWS-ED transients analyzed in this work. However, the amplitude of the power oscillation after the 2RPT appears to be larger than in the corresponding cases at BOC and PHE.

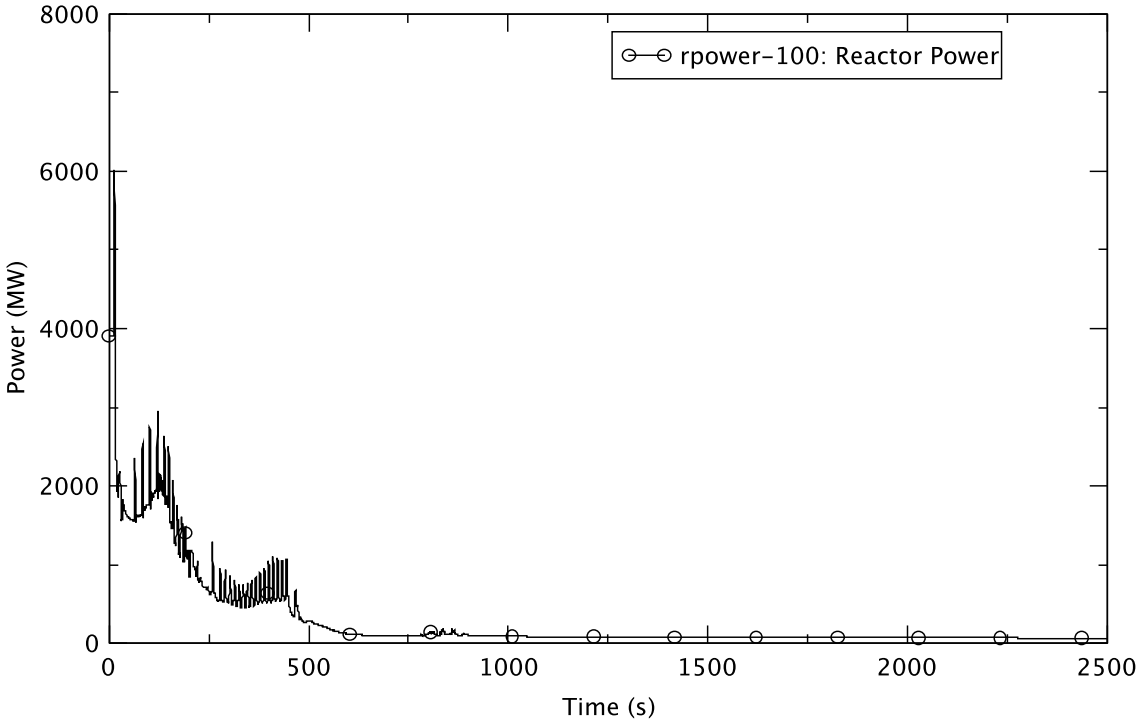

Figure 4.93 Reactor Power - EOFPL, TAF-2

With water level dropping to TAF-2, the reactor power is reduced further, and this delays the need to exercise emergency depressurization until 450 s. Figure 4.94 illustrates this rapid depressurization. The actuation of the SRVs to relieve pressure prior to the ED is evident in the steamline flow shown in Figure 4.95. With the ADS valves deployed, the steam flow decreases in response to the reactor's depressurization .

As steam is vented through the SRV/ADS valves, make-up water is delivered to the reactor vessel via the feedwater system to maintain water level. The flowrate and temperature of the feedwater are shown, respectively in Figure 4.96 and Figure 4.97. After lowering the water level to TAF-2, the feedwater spargers are exposed to the steam in the reactor vessel. As depicted in Figure 4.98, the coolant temperature in the lower plenum begins to increase right after the initiation of level control at 130 s. The increase results from the discharge of saturated water from the steam separator. The feedwater flow, shown in Figure 4.96, includes the RCIC flow that feeds into the feedwater line. The RCIC flow is shown in Figure 4.99; since the RCIC's pump is driven by steam from the reactor, its operation is hampered by a depressurized reactor.

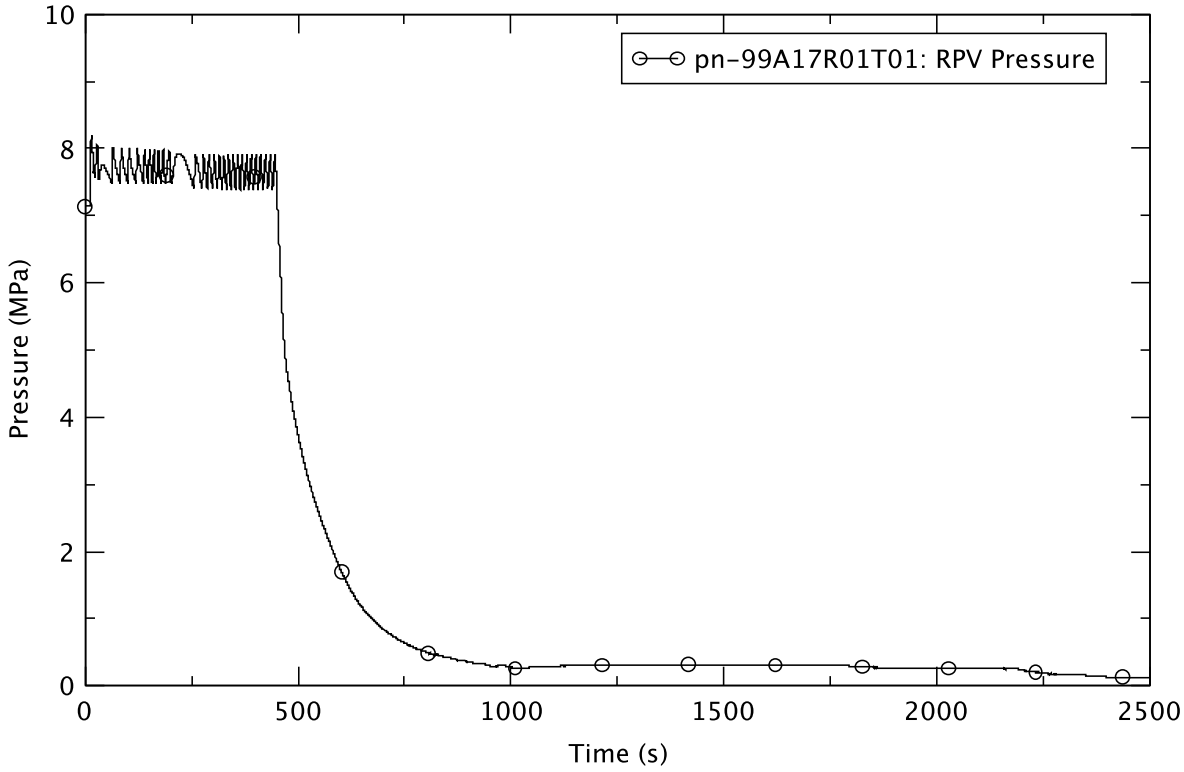

Figure 4.94 Reactor Pressure - EOFPL, TAF-2

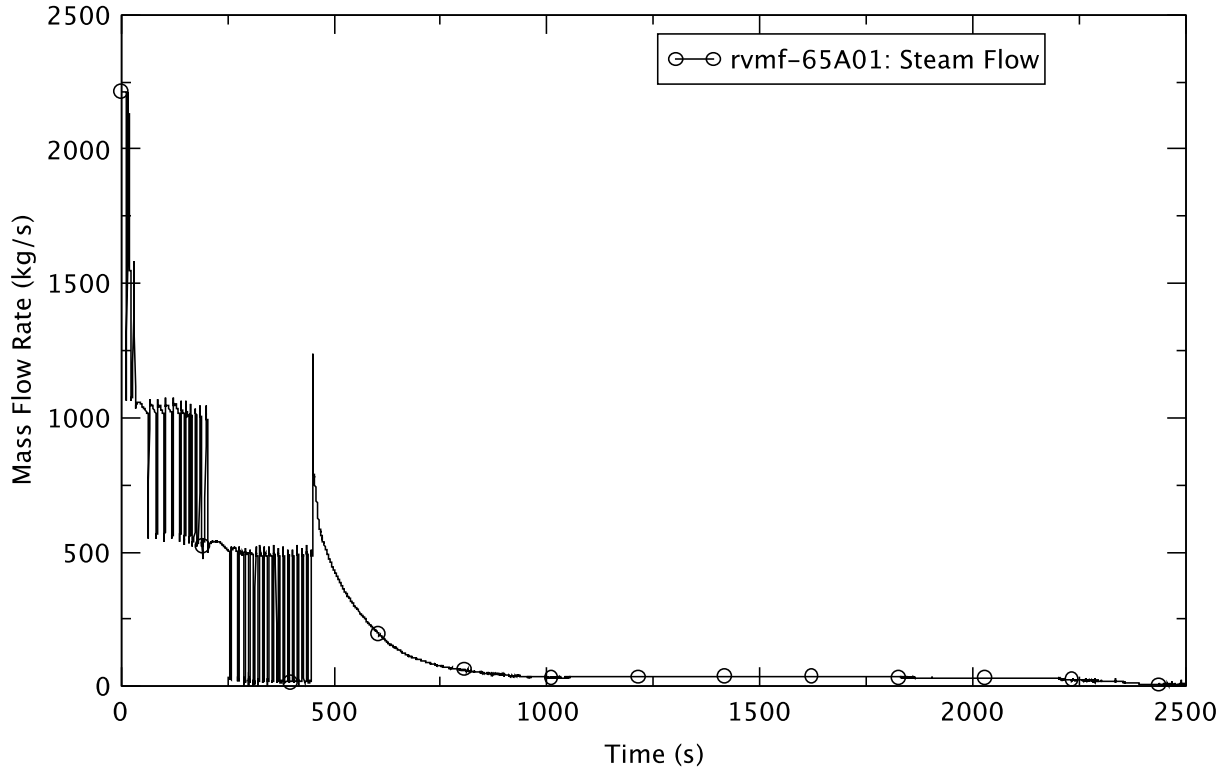

Figure 4.95 Steamline Flow - EOFPL, TAF-2

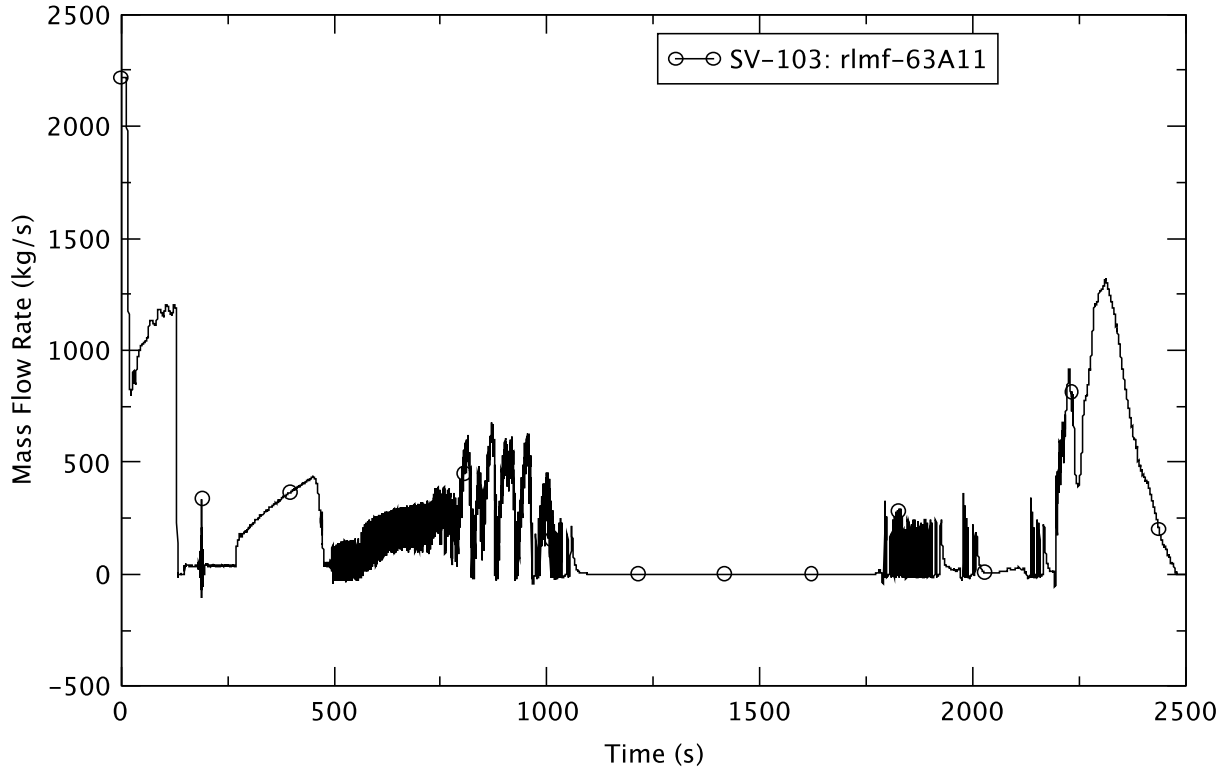

Figure 4.96 Feedwater Flowrate - EOFPL, TAF-2

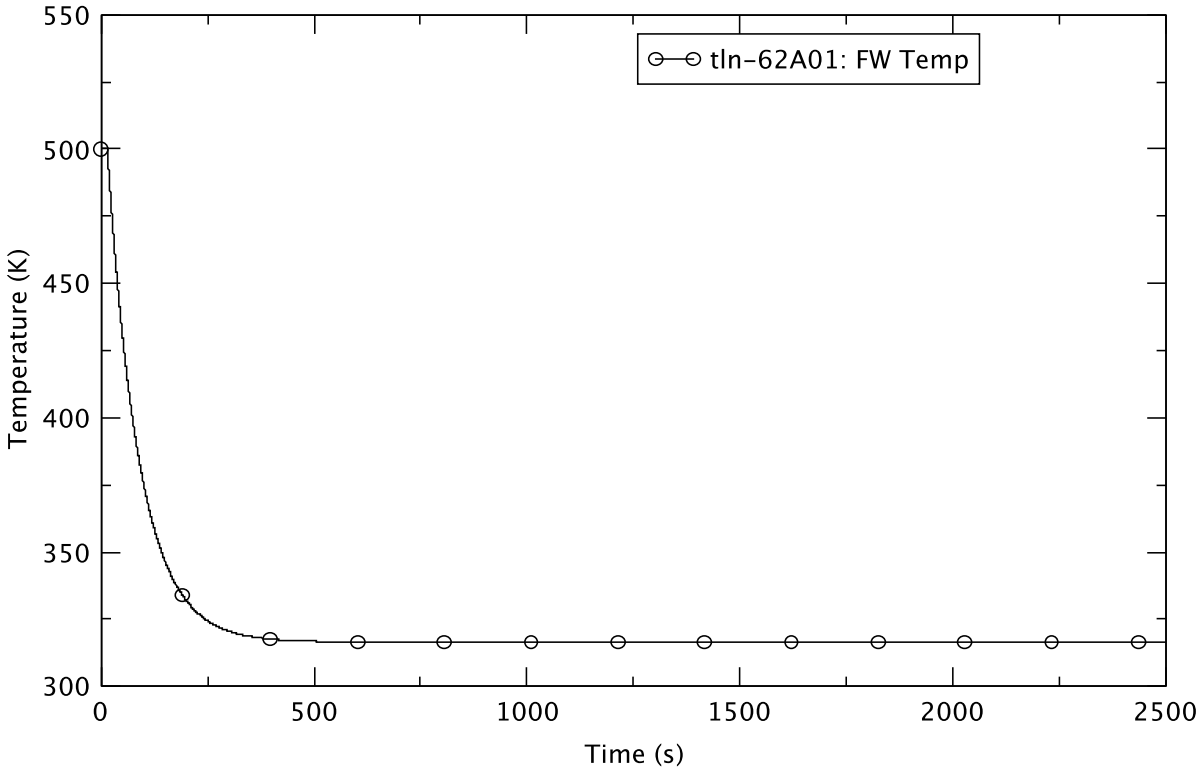

Figure 4.97 Feedwater Temperature - EOFPL, TAF-2

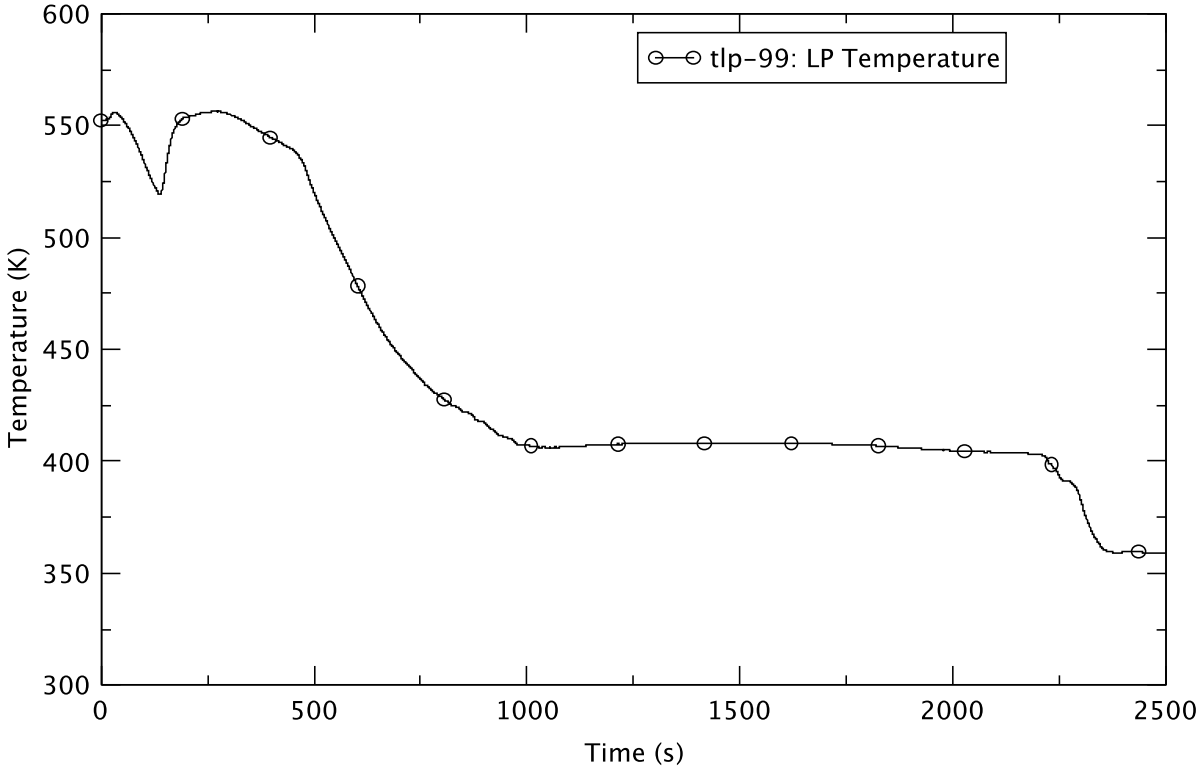

Figure 4.98 Lower Plenum Temperature - EOFPL, TAF-2

The approach to the heat capacity temperature limit (HCTL) that requires an ED is demonstrated in Figure 4.100 that shows the suppression pool temperature. The change in the rate of temperature increase at 450 s is an indication of opening of the ADS valves. The immediate effect of depressurization is observed in a ~1.7 m swell in downcomer water level (Figure 4.101). This rise in level rise also momentarily increases the core flow (Figure 4.102).

The sudden surge in steam flow through the open ADS valves in Bank D is shown in Figure 4.103. Accompanying the ED is flashing of the coolant in the core and in the lower plenum, as illustrated in the plots of the void fraction in the core bypass, Figure 4.104 (for ring 1) and Figure 4.105 (ring 2), and the lower plenum, Figure 4.106 (ring 1) and Figure 4.107 (ring 2). Notably, the extent of voiding in rings 1 and 2 in the the lower plenum differs because of differences in the pressure and temperature of the coolant in the respective rings. The refilling of the lower plenum, completed at about 1000 s, is preceded by oscillations in water level as the source of the refilling water is the downcomer, and is accompanied by oscillations in feedwater flow and core flow. Between 1000 s and 1500 s, a damping of oscillations in the core flow and the downcomer water level is apparent and a quasi-steady condition persists for the next few hundred seconds.

The core average void fraction (Figure 4.108) is inferred from the moderator density calculated by PARCS. It is noted that with an initially top-peaked axial power distribution for the EOFPL, the core-average void fraction is lower than the cases analyzed at BOC and PHE.

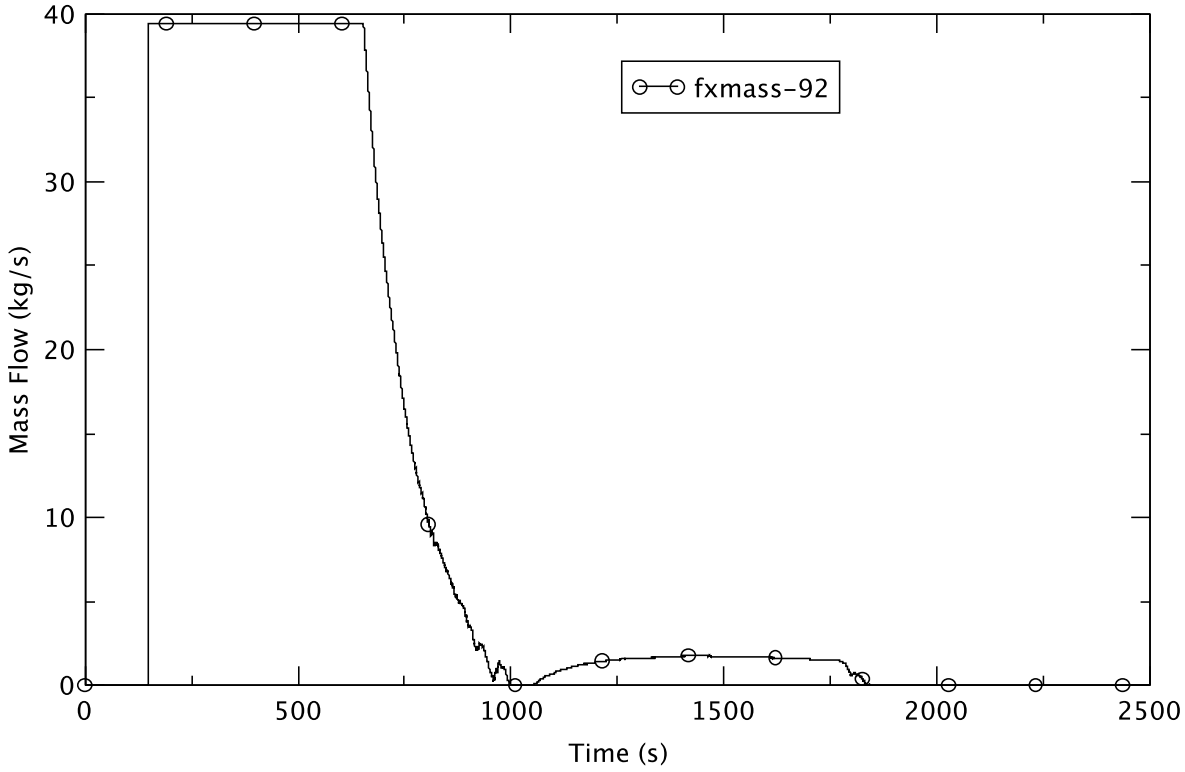

Figure 4.99 RCIC Flow

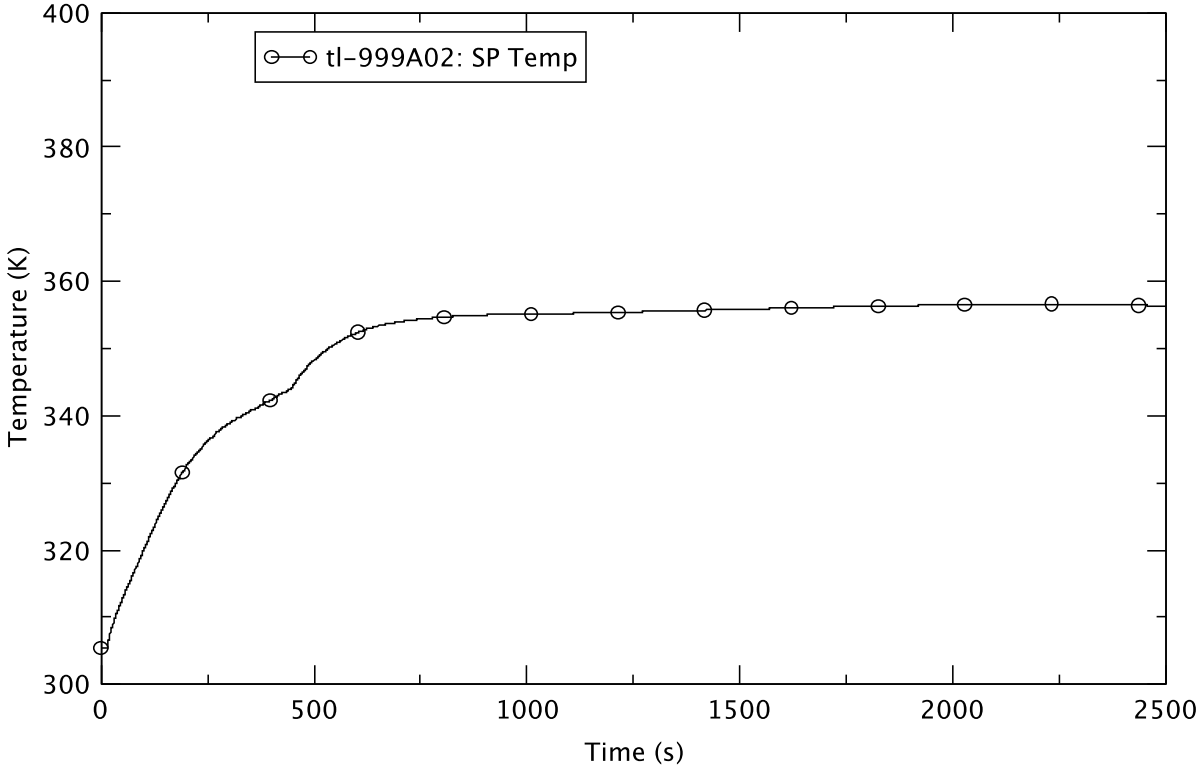

Figure 4.100 Suppression Pool Temperature - EOFPL, TAF-2

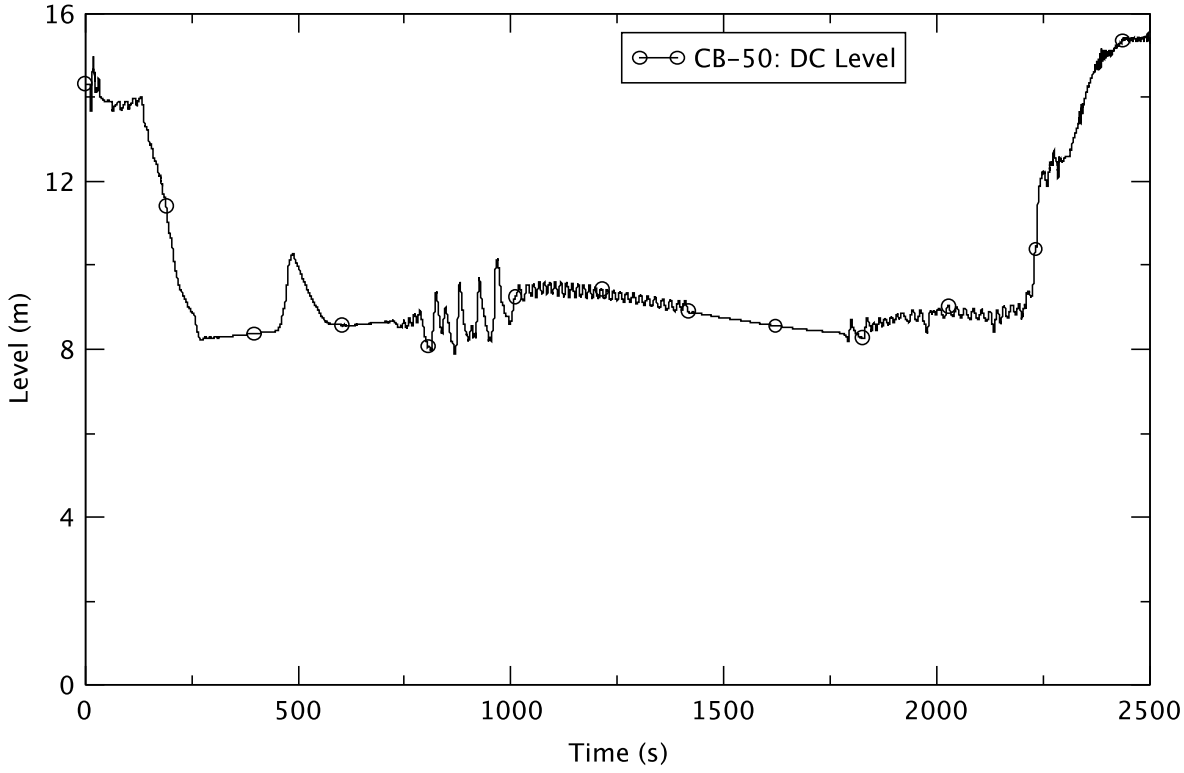

Figure 4.101 Downcomer Water Level - EOFPL, TAF-2

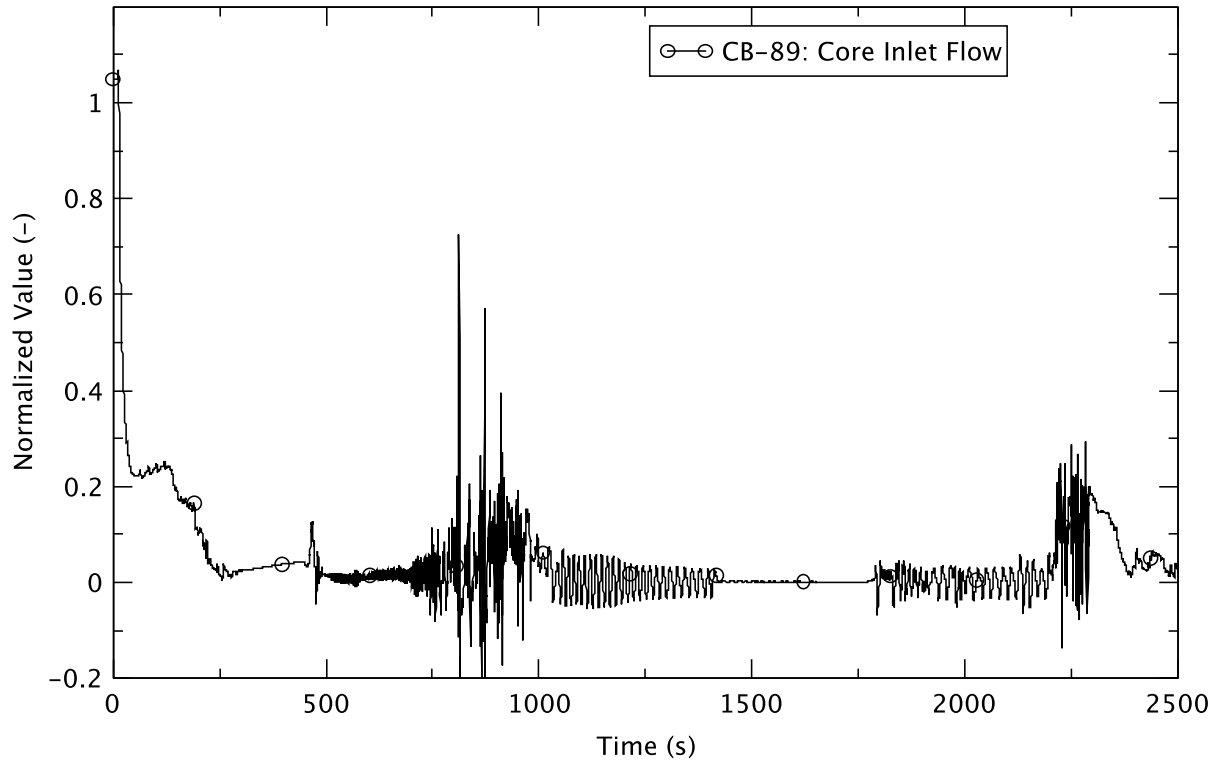

Figure 4.102 Core Flow - EOFPL, TAF-2

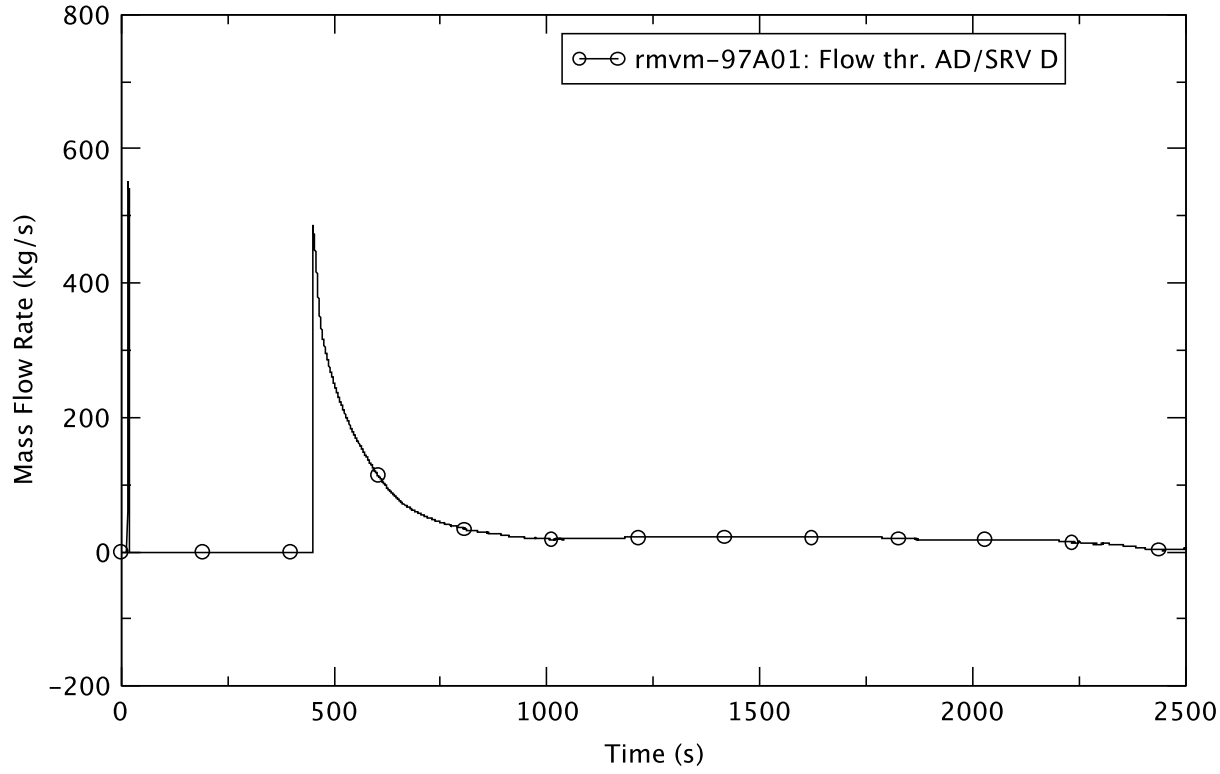

Figure 4.103 Mass Flow Through SRV/ADS Bank D - EOFPL, TAF-2

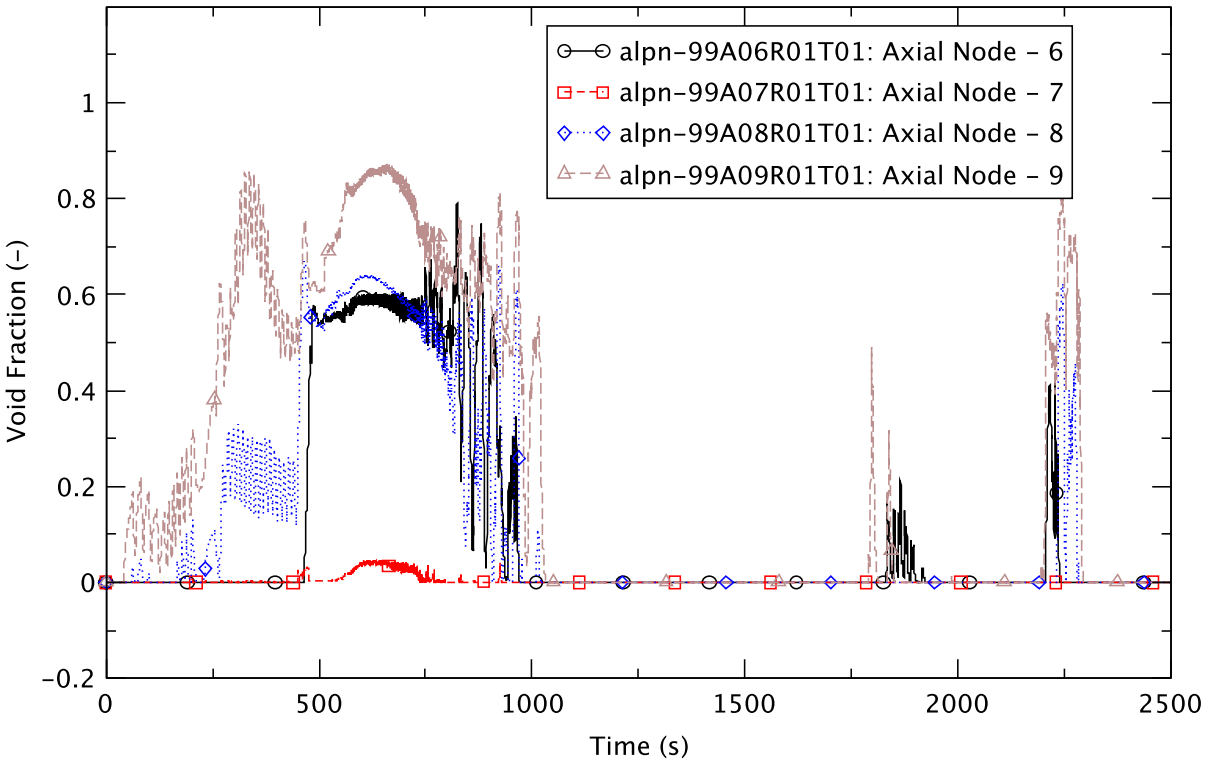

Figure 4.104 Void Fraction in Core Bypass (Ring-1) - EOFPL, TAF-2

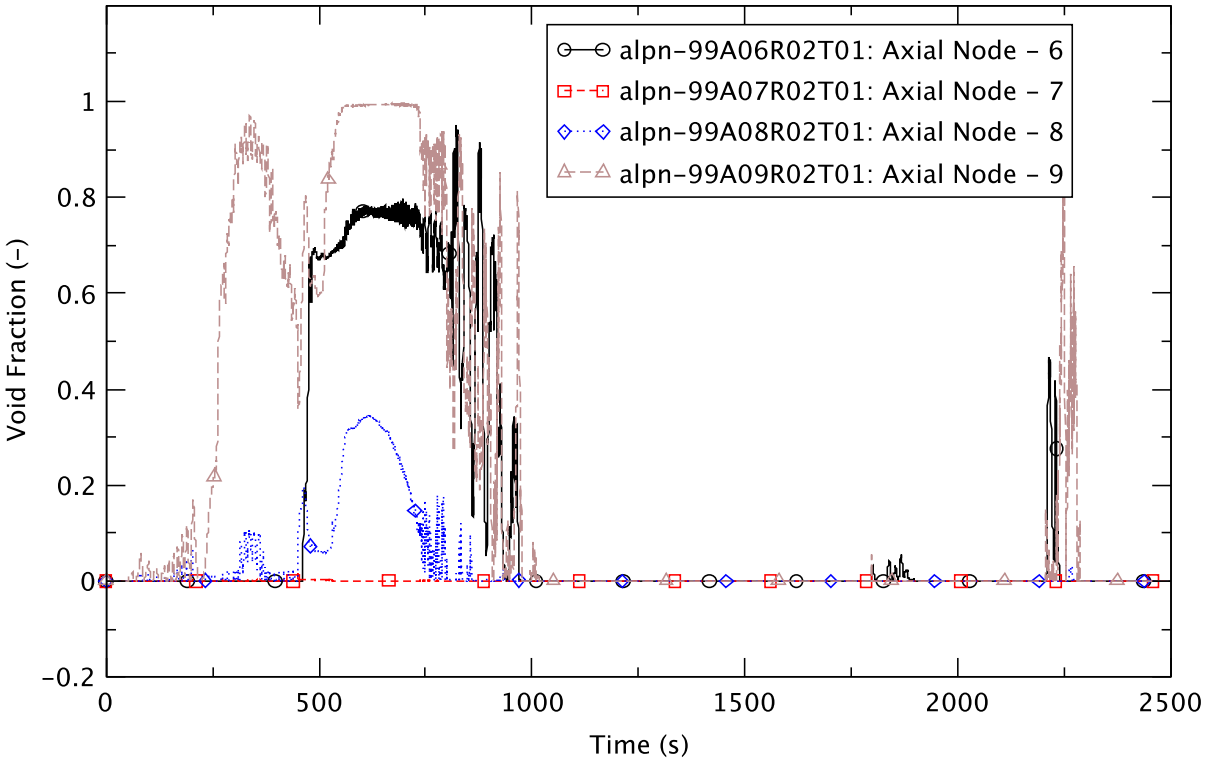

Figure 4.105 Void Fraction in Core Bypass (Ring-2) - EOFPL, TAF-2

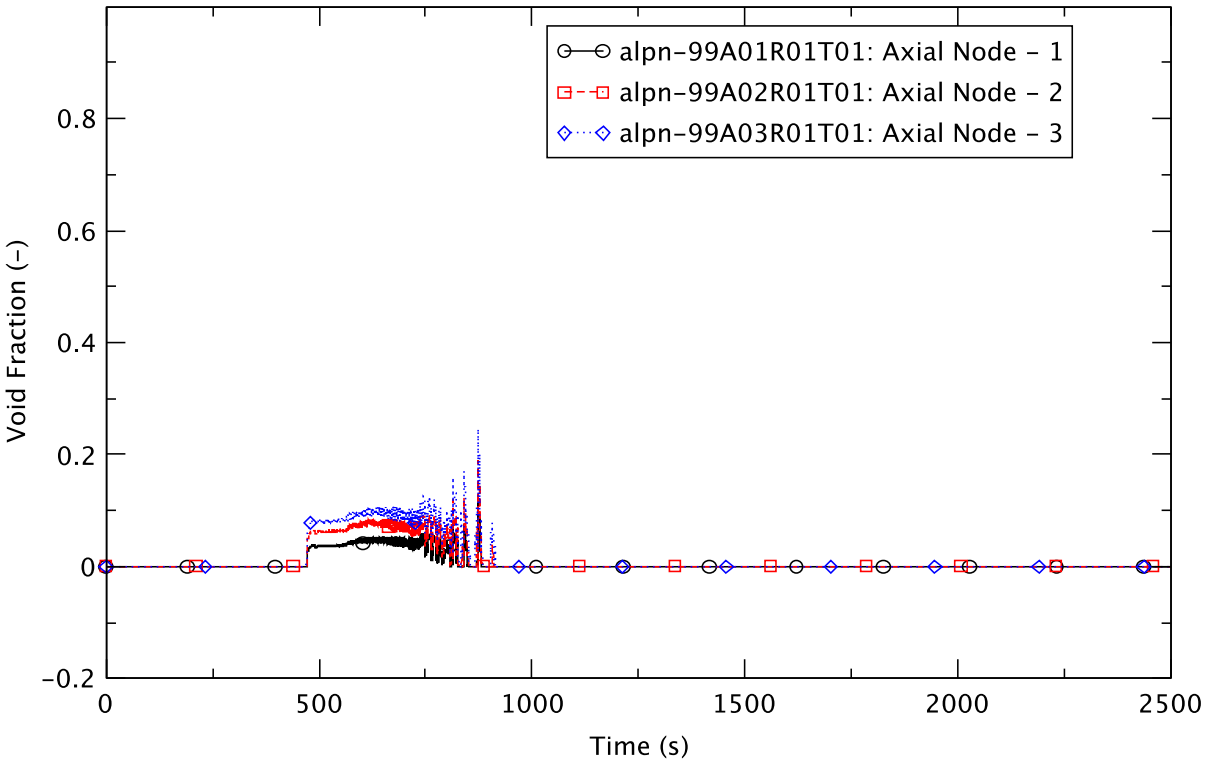

Figure 4.106 Void Fraction in Lower Plenum (Ring-1) - EOFPL, TAF-2

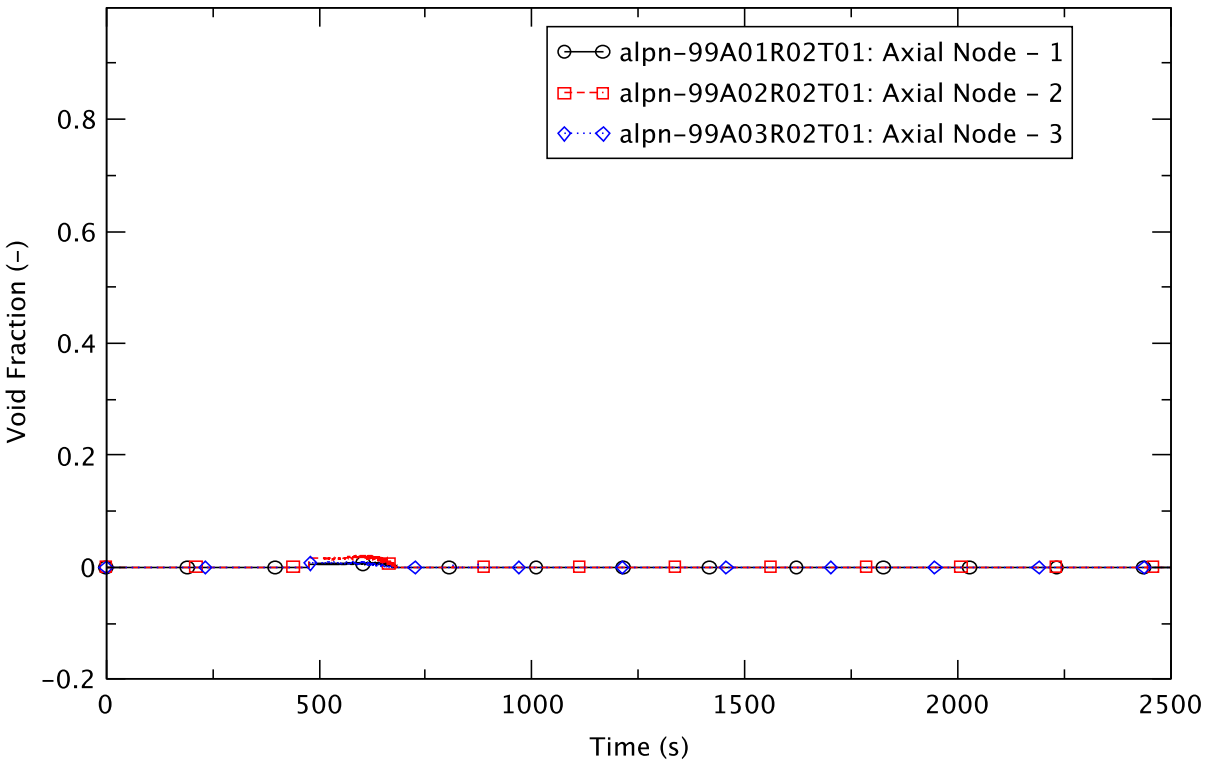

Figure 4.107 Void Fraction in Lower Plenum (Ring-2) - EOFPL, TAF-2

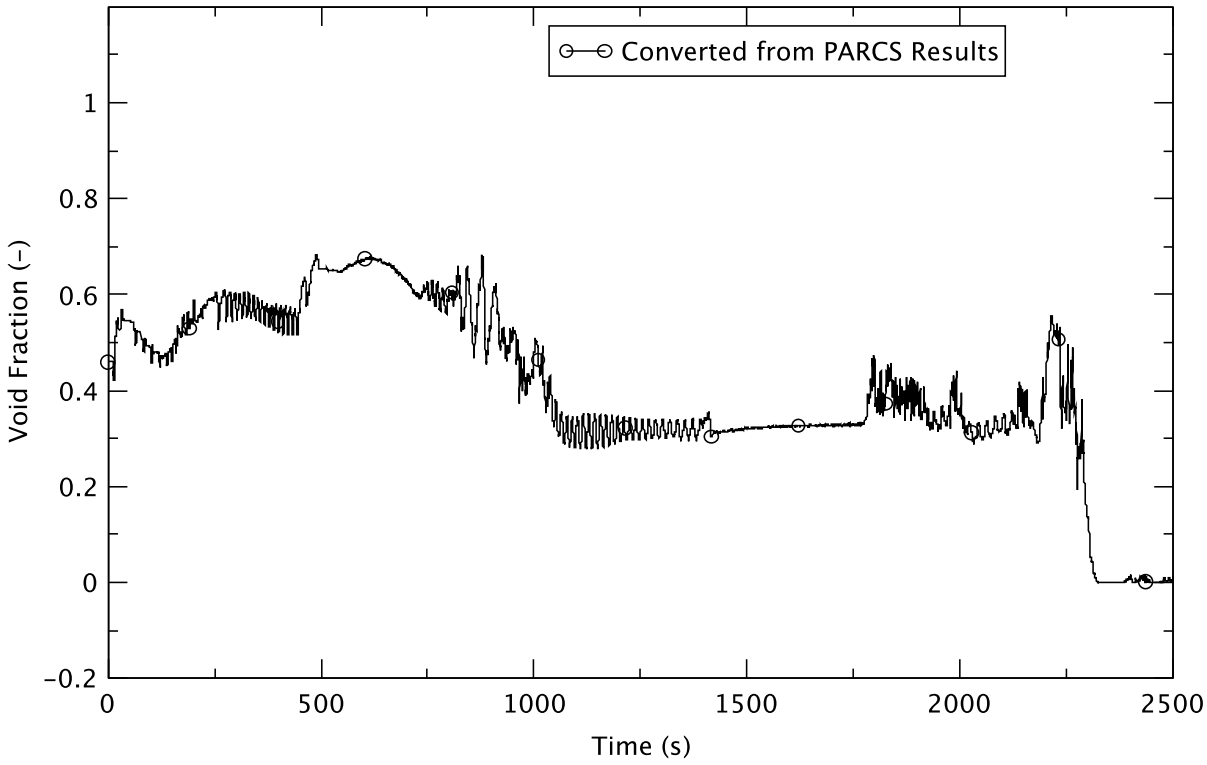

Figure 4.108 Core Average Void Fraction - EOFPL, TAF-2

The boron inventory in the core region is plotted in Figure 4.109. The injection starts at 211 s and it takes ~50 s for the boron to reach the core region in the EOFPL TAF-2 case. In general, the boron inventory tracks with the liquid fraction in the core as is inferred from the core average void fraction (Figure 4.108). The increase in boron inventory at about 800 s coincides with the refilling of the lower plenum. Along with rising downcomer water level from increased feedwater flow, the core flow also rises. A later increase in boron inventory occurs after water level recovery, which begins at 2180 s. The boron concentration in the lower plenum is shown in Figure 4.110 and Figure 4.111 for rings 1 and 2 of the vessel, respectively. The rises and dips in boron concentration in the lower plenum are correlated with the effective boron concentration at the injection point (Figure 4.112). The reactivity components, Figure 4.113, reveals that boron reactivity has a higher magnitude than the reactivity components for fuel temperature (Doppler), and moderator density (void).

The mass flowrate in the recirculation line is shown in Figure 4.114. Seemingly, perturbations in the core flow (jet pump exit flow, shown in Figure 4.102) and the downcomer water level also propagate into the recirculation line. Between ~1400 s and ~1800 s, the recirculation flow is clearly negative (~100 kg/s) when the flow from the core inlet varies close to zero, while the downcomer level slowly and steadily declines.

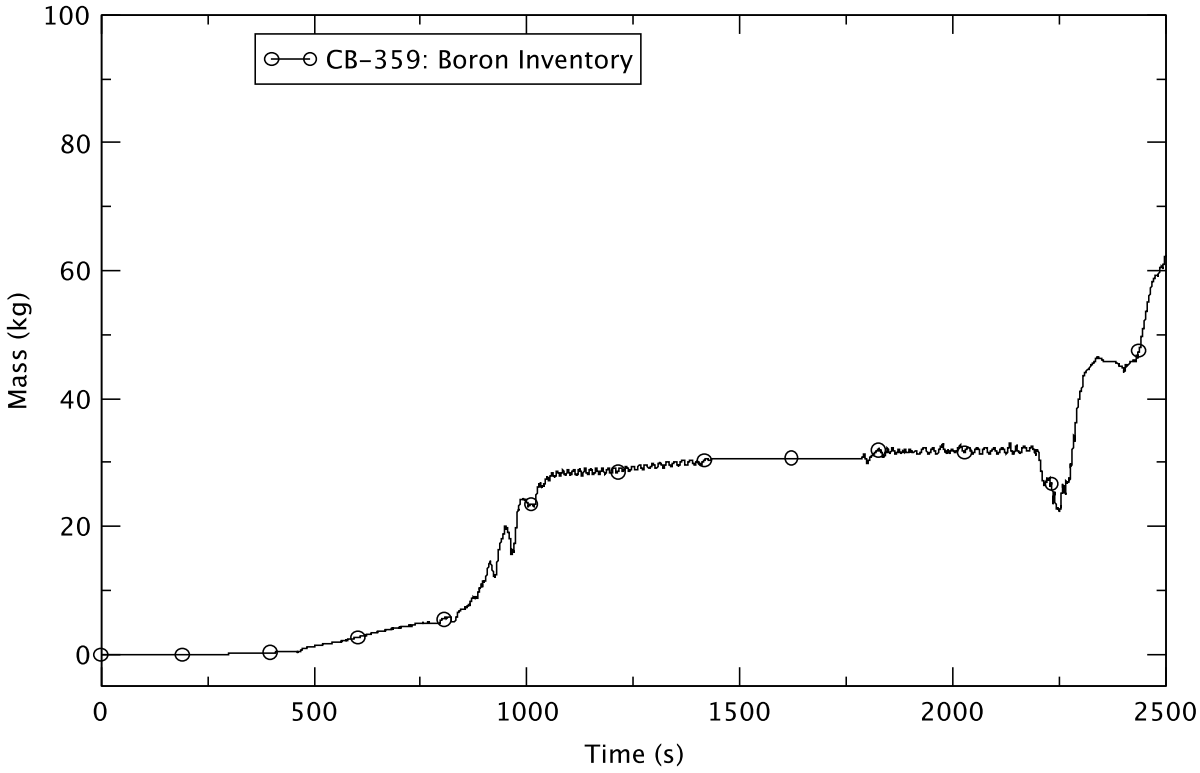

Figure 4.109 Boron Inventory in the Core - EOFPL, TAF-2

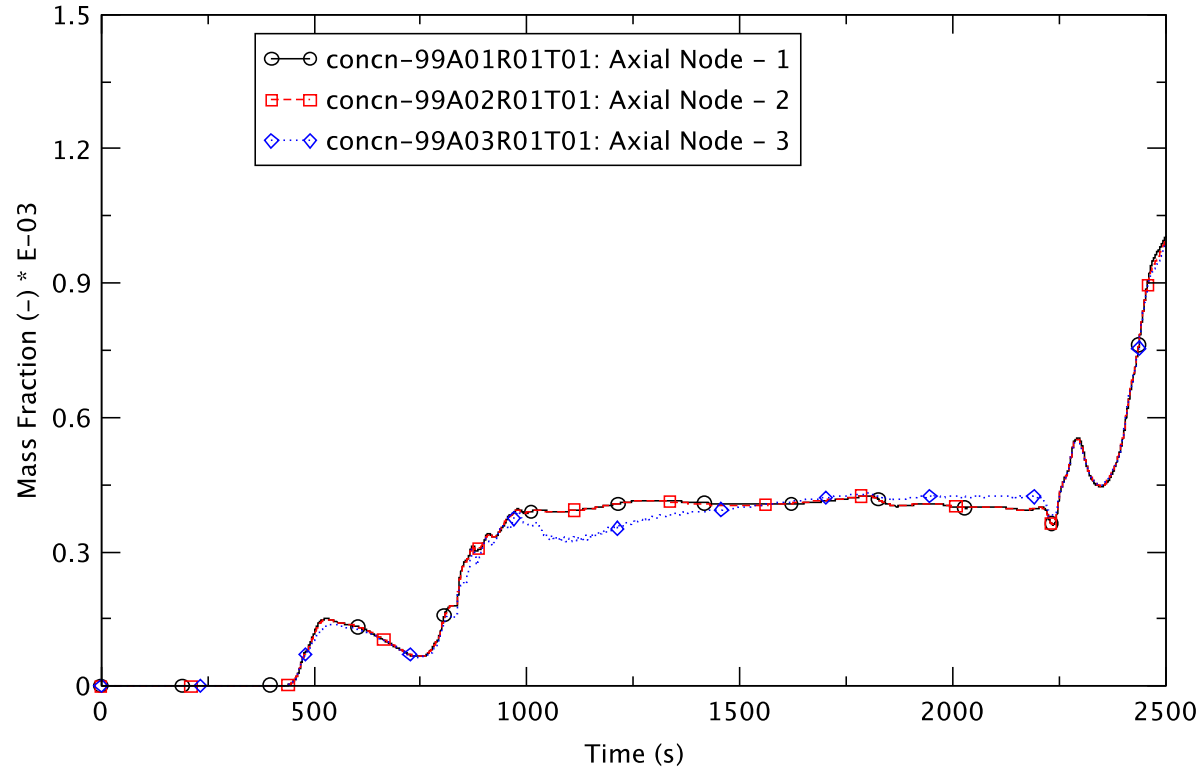

Figure 4.110 Boron Concentration in Ring 1 - EOFPL, TAF-2

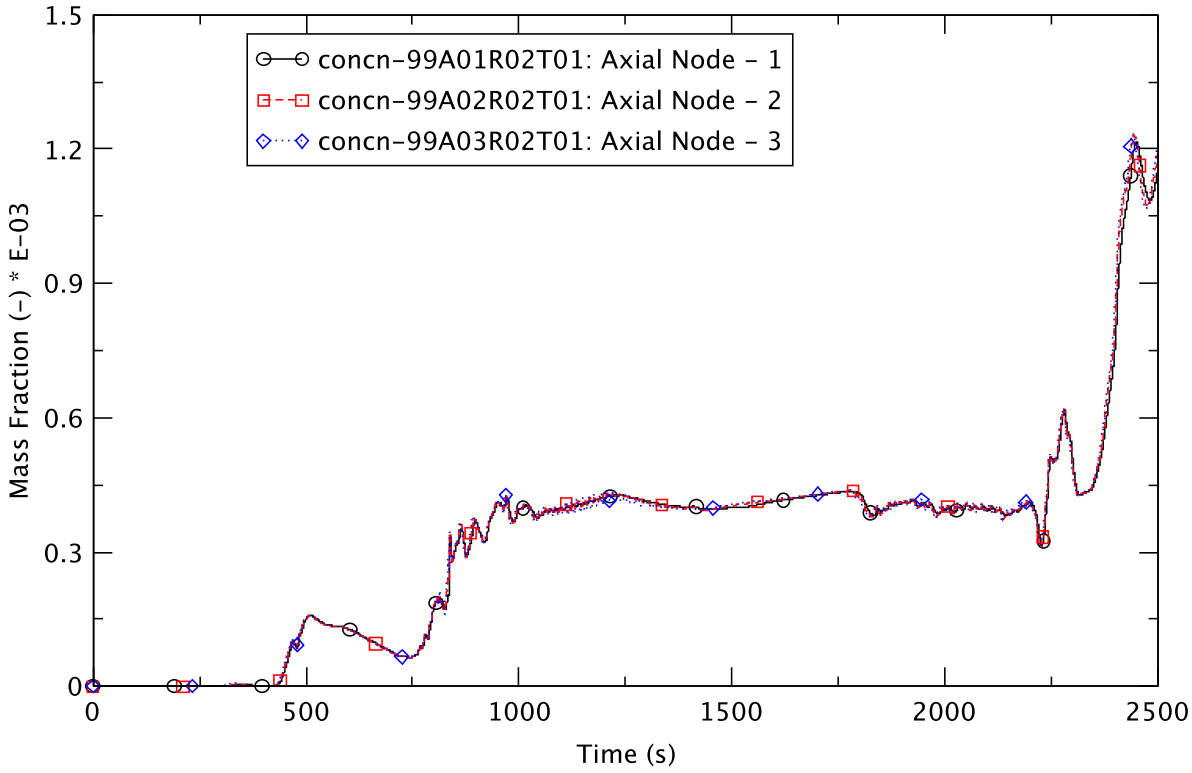

Figure 4.111 Boron Concentration in Ring 2 - EOFPL, TAF-2

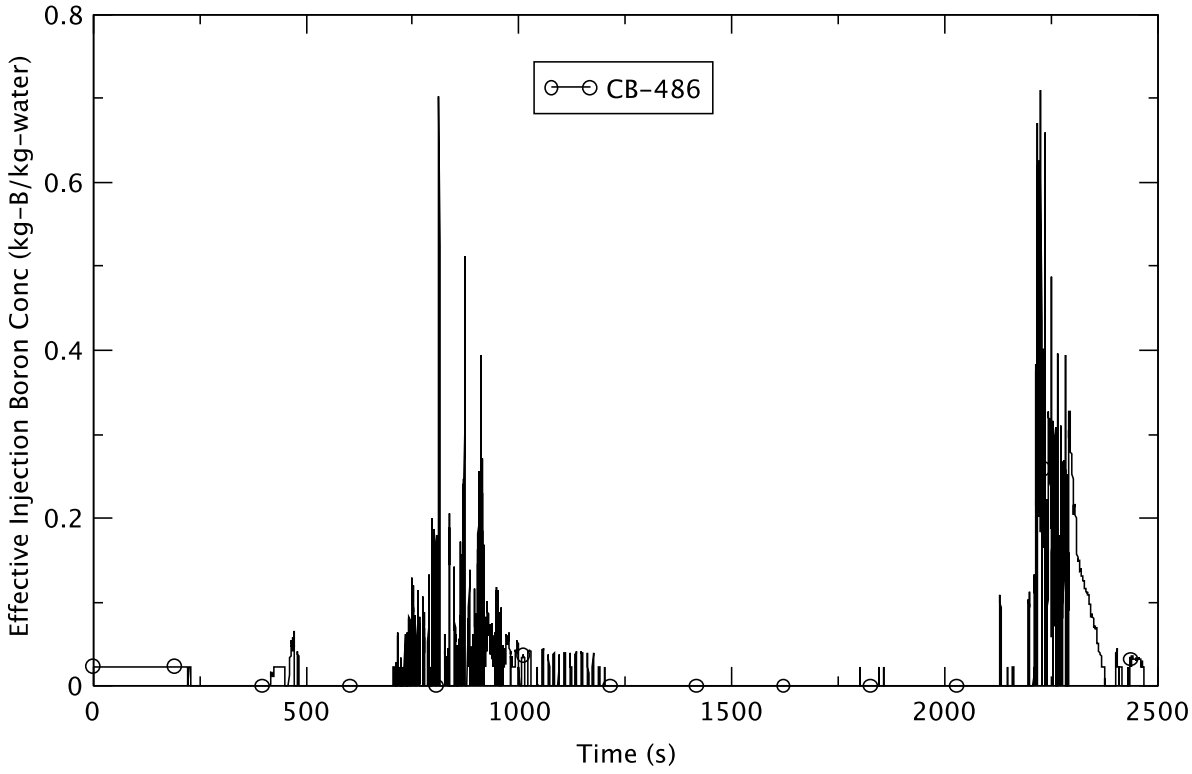

Figure 4.112 Effective Injection Boron Concentration - EOFPL, TAF-2

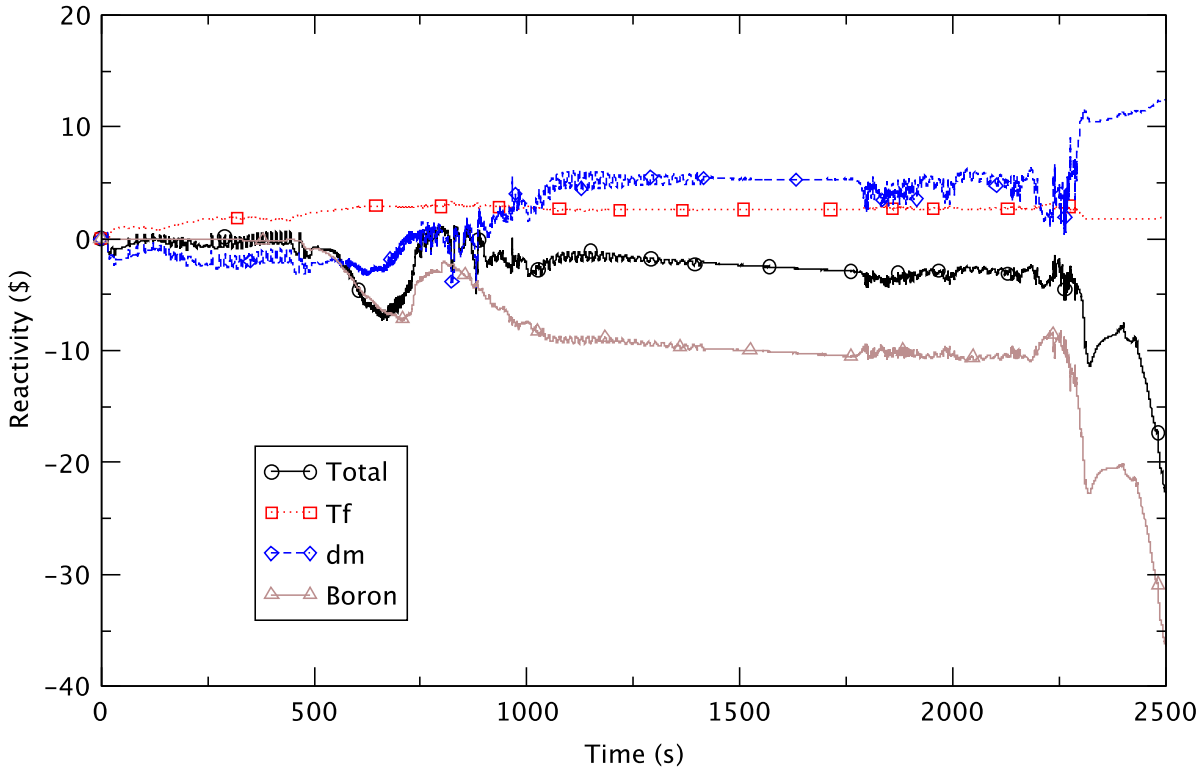

Figure 4.113 Core Reactivity - EOFPL, TAF-2

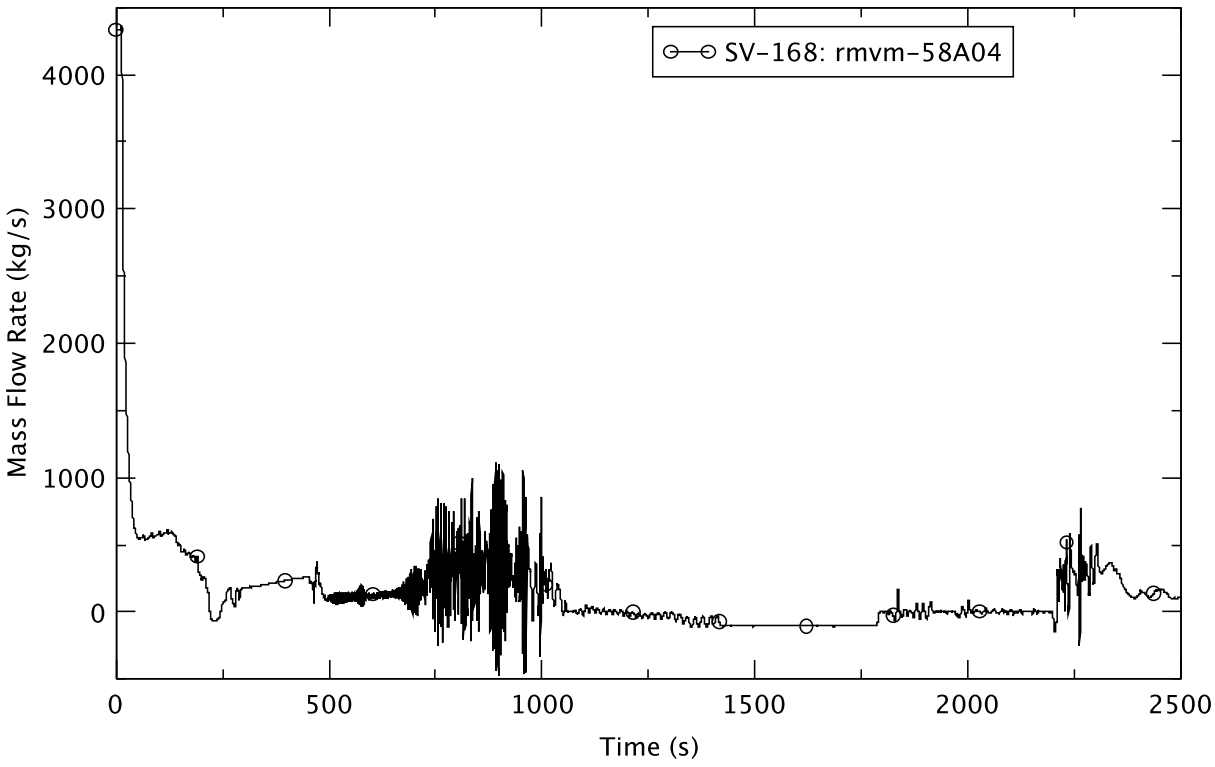

Figure 4.114 Recirculation Line Flow - EOFPL, TAF-2

The outcome of the ATWS-ED EOFPL TAF-2 transient with respect to the four figures-of-merit is discussed next.

1) Peak clad temperature (PCT)

The core-wide PCT is plotted in Figure 4.115. The maximum PCT occurs at 700 s when the core is voided. The clad is not overheated; its maximum, at 639 K, is well below 1478 K (2200°F). The axial clad temperature, Figure 4.116, displays a fairly uniform profile for times longer than 500 s. The fuel centerline temperature, Figure 4.117, exhibits a similar trend.

2) Recriticality

The TRACE/PARCS calculation shows that there is no recriticality due to choking in the SRVs. The steam flow through the SRV is choked but the SRVs have sufficient capacity that there is no significant repressurization of the RPV. The choking condition (Figure 4.118) is calculated for the SRV/ADS Bank D for almost the entire duration of the transient. The choking condition is eliminated when upstream pressure is reduced as the steaming rate is lowered by the injection of feedwater at 2180 s.

The effect of boron dilution is observed only briefly, between 700 s and 800 s in Figure 4.113, that shows different reactivity components. It demonstrates that boron reactivity is the dominant contributor in keeping the reactor shutdown from ~800 s onward and no recriticality is possible.

3) Wetwell temperature

The suppression pool reaches the maximum temperature of 357 K at about 2191 s. The TRACE/PARCS analysis shows that using the equivalent of two RHR loops in the suppression-pool cooling mode and adding heat structures in both the suppression pool and the airspace in the wetwell suffice to prevent the water in the suppression pool from approaching boiling .

4) Containment pressure

Figure 4.119 shows that the drywell pressure approaches a maximum of 0.16 MPa shortly after the ED; a value low enough that the integrity of the containment is not challenged.

In summary, the TRACE/PARCS analysis demonstrates that the ATWS-ED transient initiated by the MSIV closure is mitigated successfully by a combination of 2RPT and the operator actions that depressurized the RPV, reduced power by controlling water level, and injected boron.

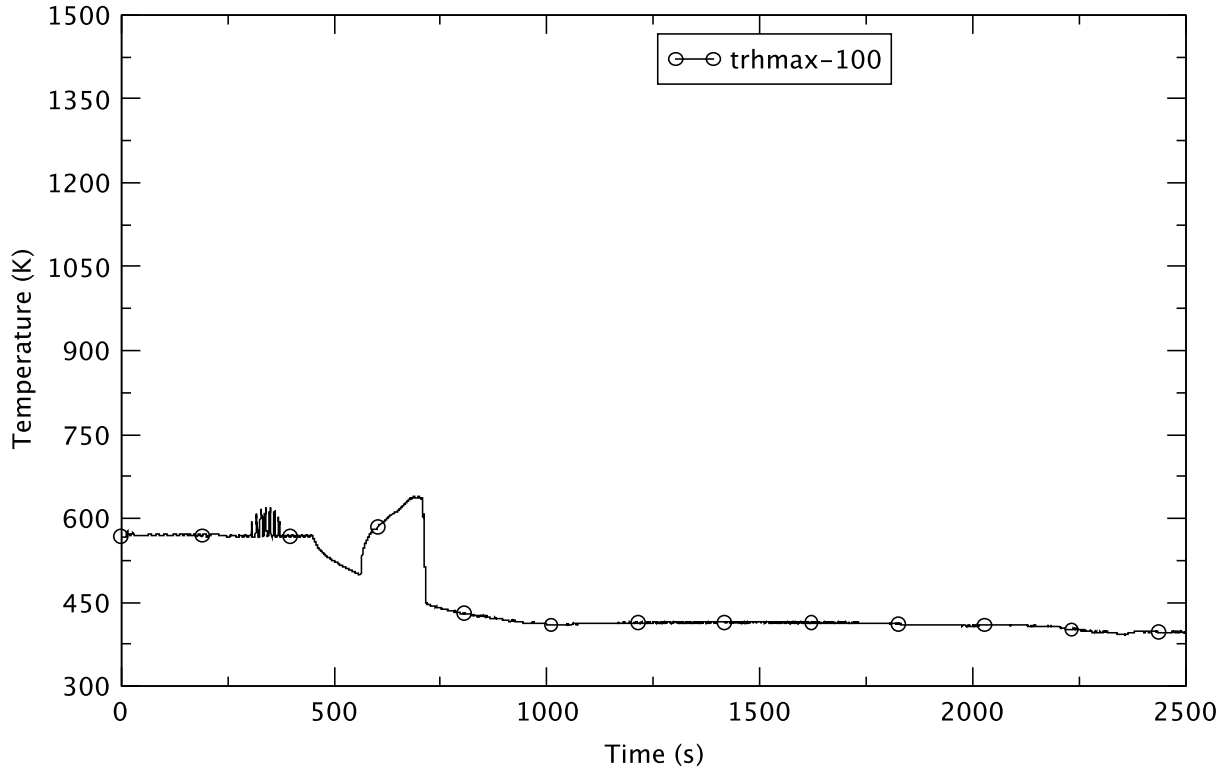

Figure 4.115 Peak Clad Temperature - EOFPL, TAF-2

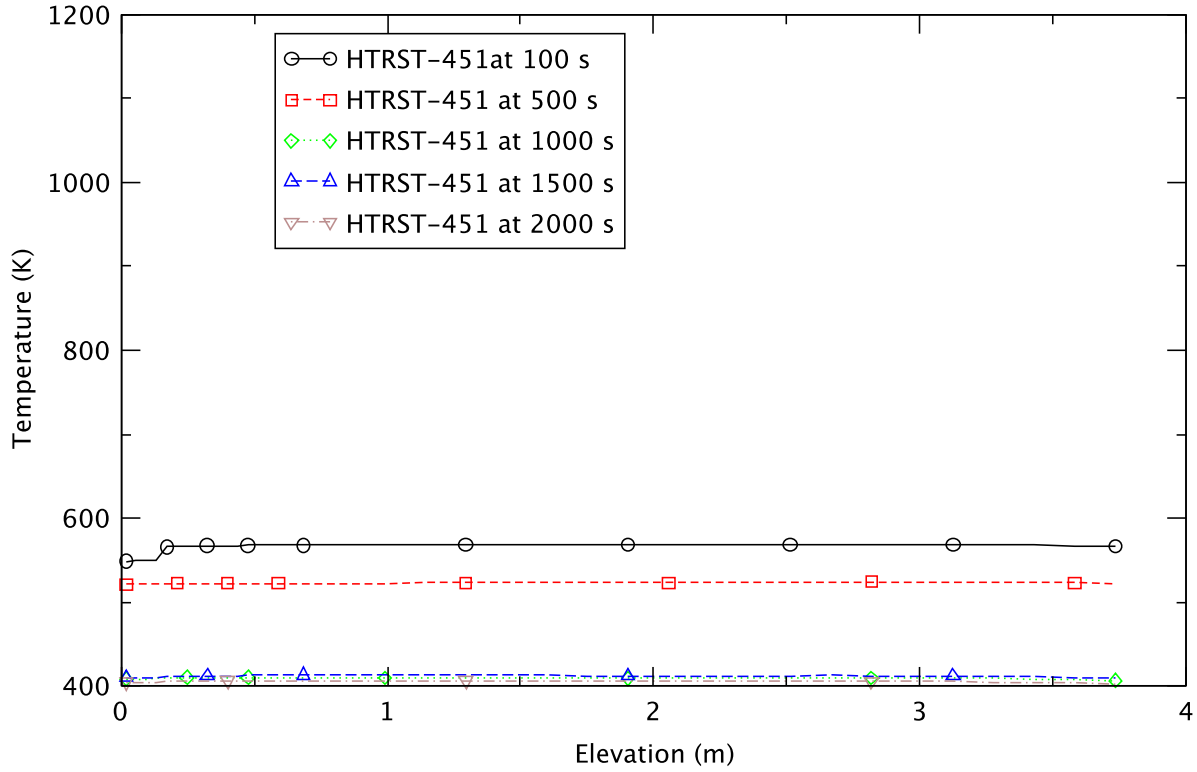

Figure 4.116 Axial Profile of Clad Temperature - EOFPL, TAF-2

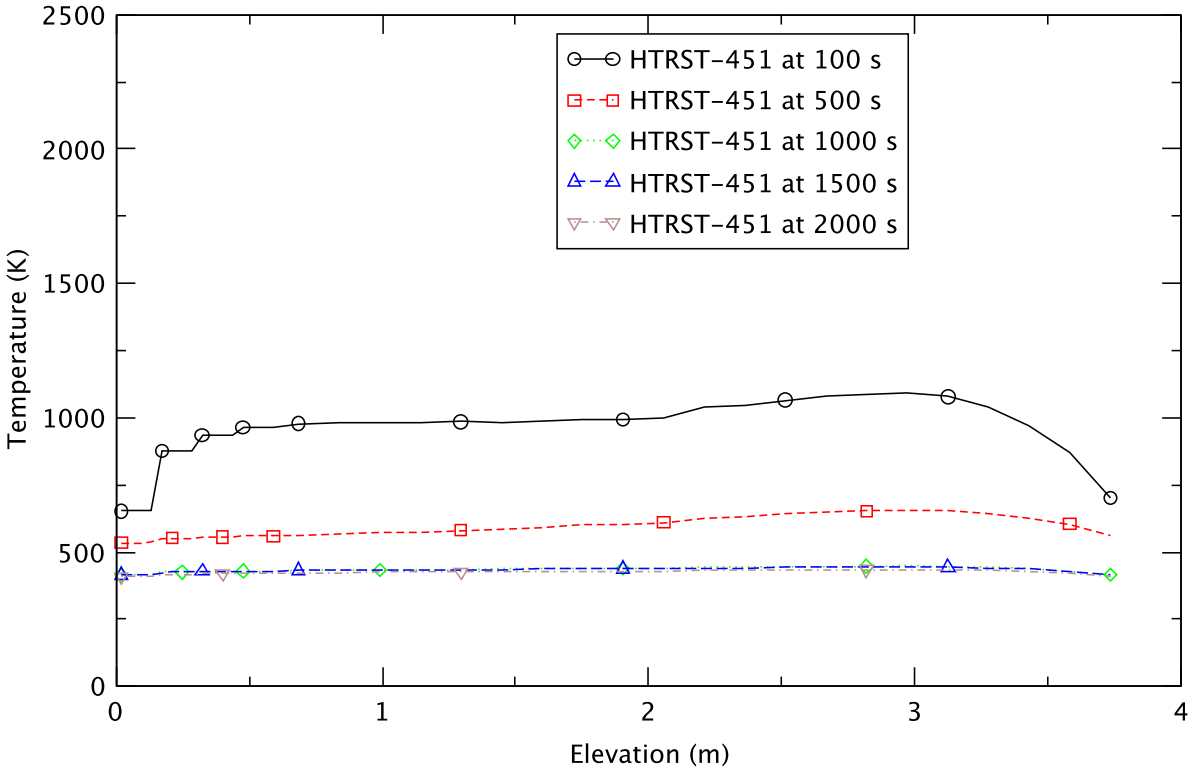

Figure 4.117 Axial Profile of Fuel Centerline Temperature - EOFPL, TAF-2

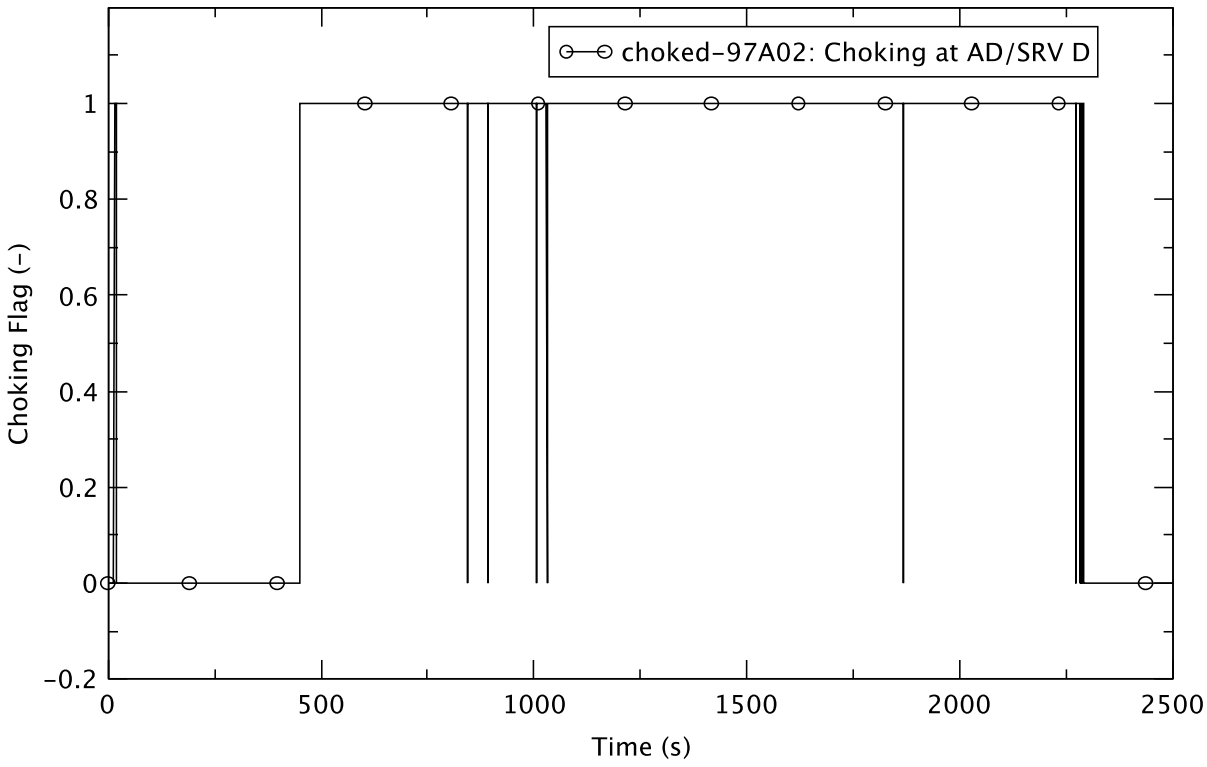

Figure 4.118 Choking Flag for SRV/ADS Bank D - EOFPL, TAF-2

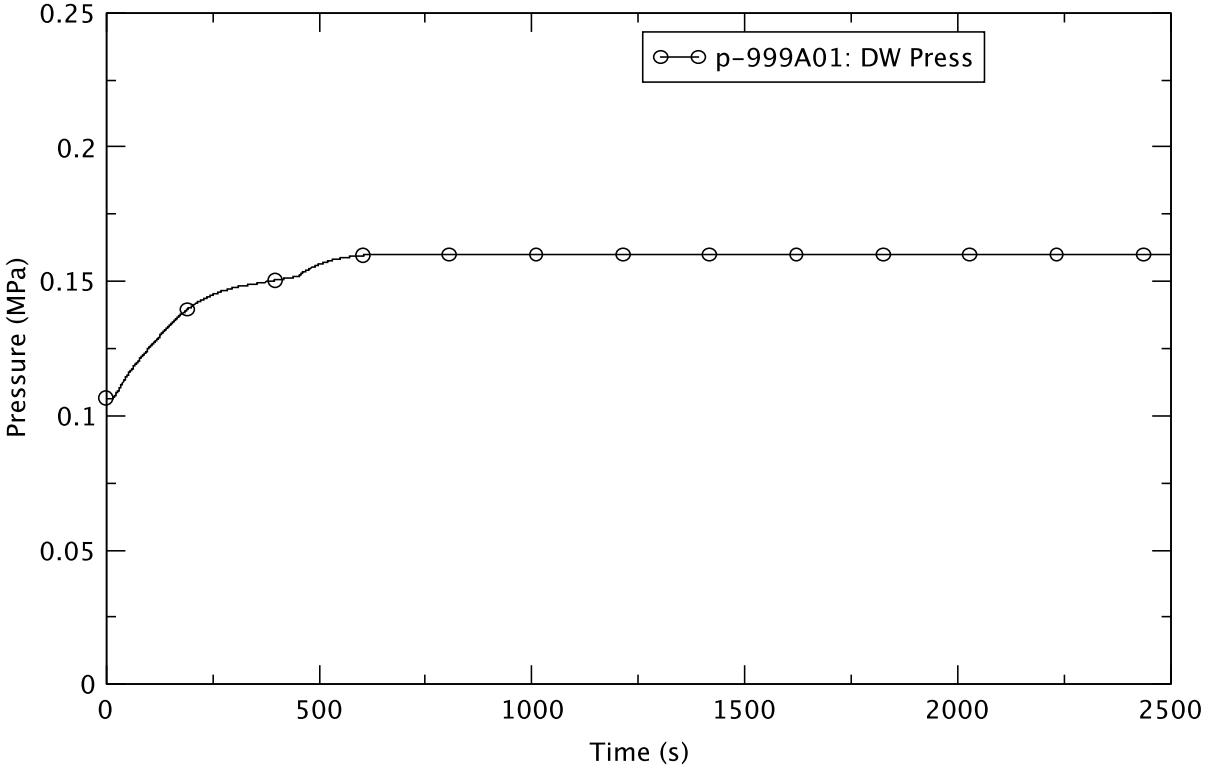

Figure 4.119 Drywell Pressure - EOFPL, TAF-2

4.4.3 Effect of Level Control at EOFPL

In general, the transient responses to controlling water level for the EOFPL exposure condition are very similar to those for the BOC and PHE conditions discussed in Sections 4.2.3 and 4.3.3. This is evident by comparing key results at EOFPL in Table 4.10, with those in Table 4.4 and Table 4.7 for the corresponding BOC and PHE cases. However, there are several characteristics of the EOFPL TAF+5 case that differ from the corresponding case at the other two exposures :

- after ED, natural circulation is broken and reactor power decreases further
- there is flashing in the lower plenum after ED
- boron dilution is observed during refilling of the lower plenum and the core

The following select set of plots (Figure 4.120 to Figure 4.128) is used to compare and contrast the transient responses of three EOFPL cases when the water level is controlled to TAF, TAF-2, and TAF+5.

All three cases exhibit similar responses. Exceptions are in the timing of the maximum PCT and the accumulation of boron in the core region. For the TAF+5 and the TAF cases, the maximum PCT occurs early, immediately after MSIV closure is initiated when core flow still is still relatively high. For TAF-2, there is a delayed heat-up of the core at a time when the reduction in water level has caused the core flow to approach a lower quasi-steady value, and the corresponding maximum PCT is more limiting than the other two cases. For boron build-up in the core region, the TAF+5 case shows a monotonic increase after natural circulation is established sometime after the ED, while the boron inventory remains relatively unchanged for more than 1000 s for TAF and for TAF-2.

Table 4.10 Comparison of Key Results for EOFPL Base Cases

Key Event	EOFPL TAF	EOFPL TAF-2	EOFPL TAF+5
Maximum PCT (trhmax-100)	577 K (14.3 s)	639 K (699 s)	577 K (14.3 s)
Core Boron Inventory (CB 359) > 0.01 kg	243 s	264 s	246 s
Emergency Depressurization	485 s	450 s	403 s
Maximum Drywell Pressure	0.160 MPa (674 s)	0.160 MPa (648 s)	0.162 MPa (588 s)
Reactor Shutdown (Stayed < 3.25% Initial Power)	805 s	887 s	937 s
Maximum Suppression Pool Temperature	356 K (2182 s)	357 K (2191 s)	359 K (2288 s)

The transient response of the reactor power (Figure 4.120) is similar for all three cases, viz., a power spike after the MSIV closure, and a power decrease after lowering the water level and depressurization. With a higher reactor power after the initiation of level control, the TAF+5 case has the earliest ED time. For the reasons explained earlier in Section 4.2.3, the TAF-2 case has a slightly earlier ED time than does the TAF case. In all three cases, the ED occurs later than the corresponding cases at BOC and PHE.

Figure 4.121 shows the pressure response after the ED. The rate of depressurization is similar for all of them, and there is voiding in the lower plenum and natural circulation flow is “broken,” thereby reducing core flow (Figure 4.122). There also is a significant level swell in the downcomer after the ED for the TAF and TAF-2 cases (Figure 4.123) but only a minor one for TAF+5.

In the TAF case, both the core flow and the downcomer level oscillate between 250 s and 500 s. For all three cases. subsequent refilling of the lower plenum and the core region after the ED results in decreases in the water level and fluctuations in core flow around 750 s. Then, between 1000 s and 2000 s all three exhibit periodic fluctuations in water level and a general decreasing trend in the core flow.

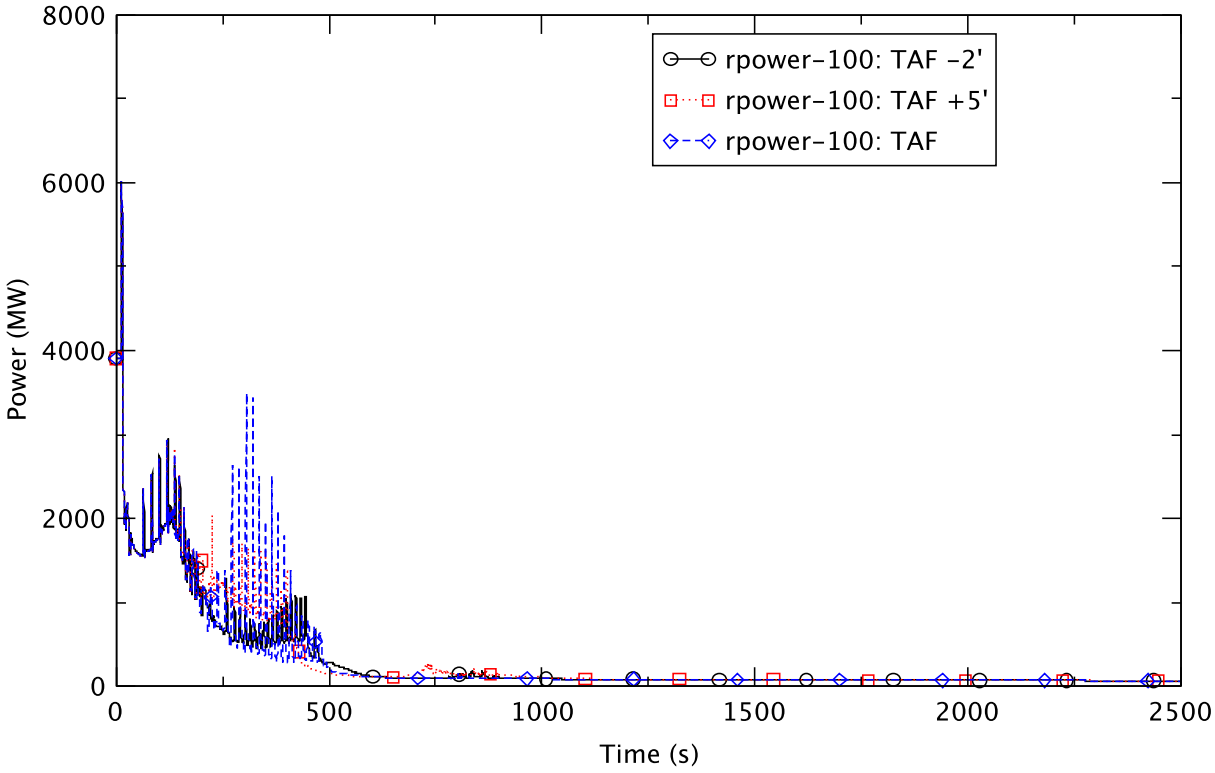

Figure 4.120 Reactor Power - EOFPL Base Cases

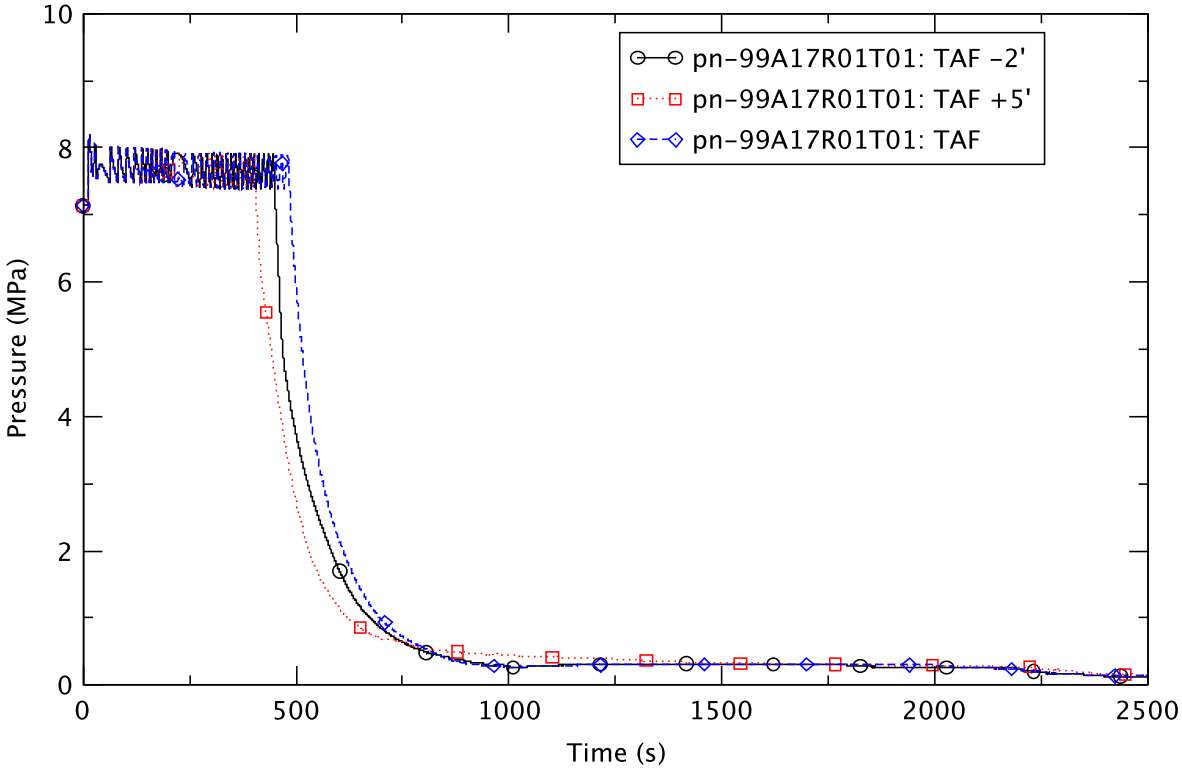

Figure 4.121 Reactor Pressure - EOFPL Base Cases

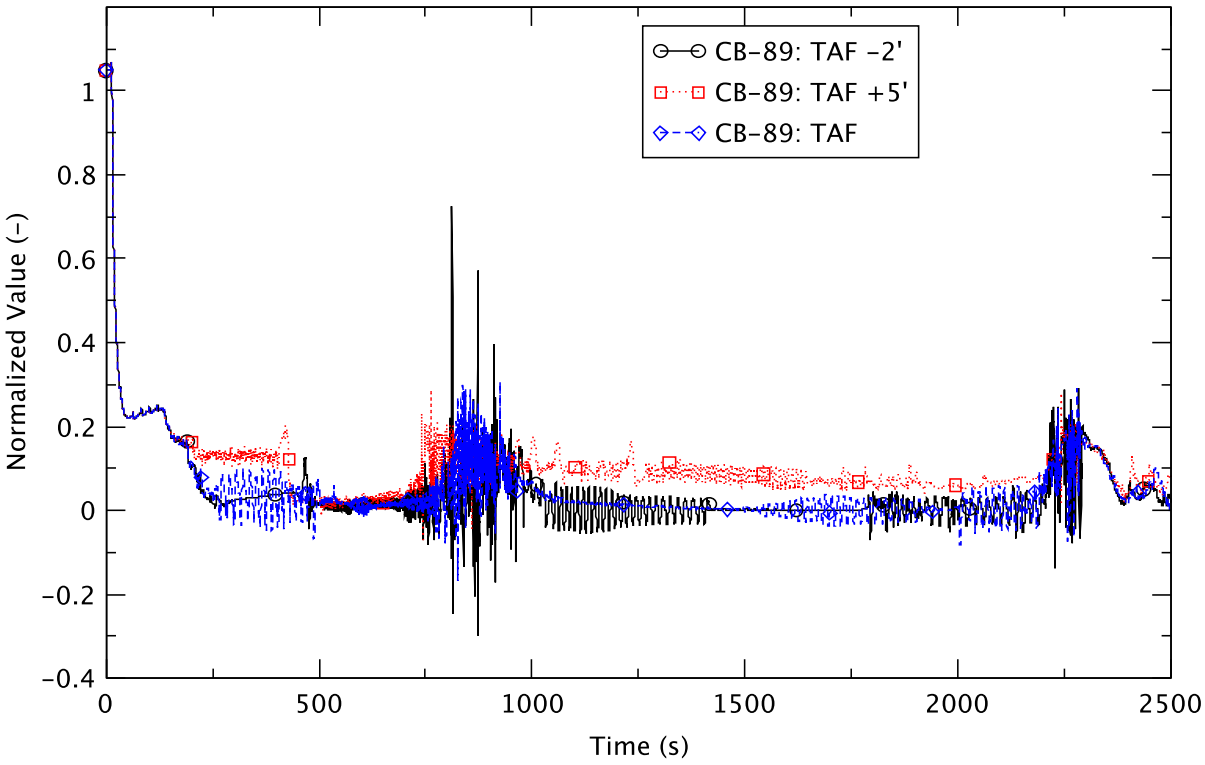

Figure 4.122 Core Flow - EOFPL Base Cases

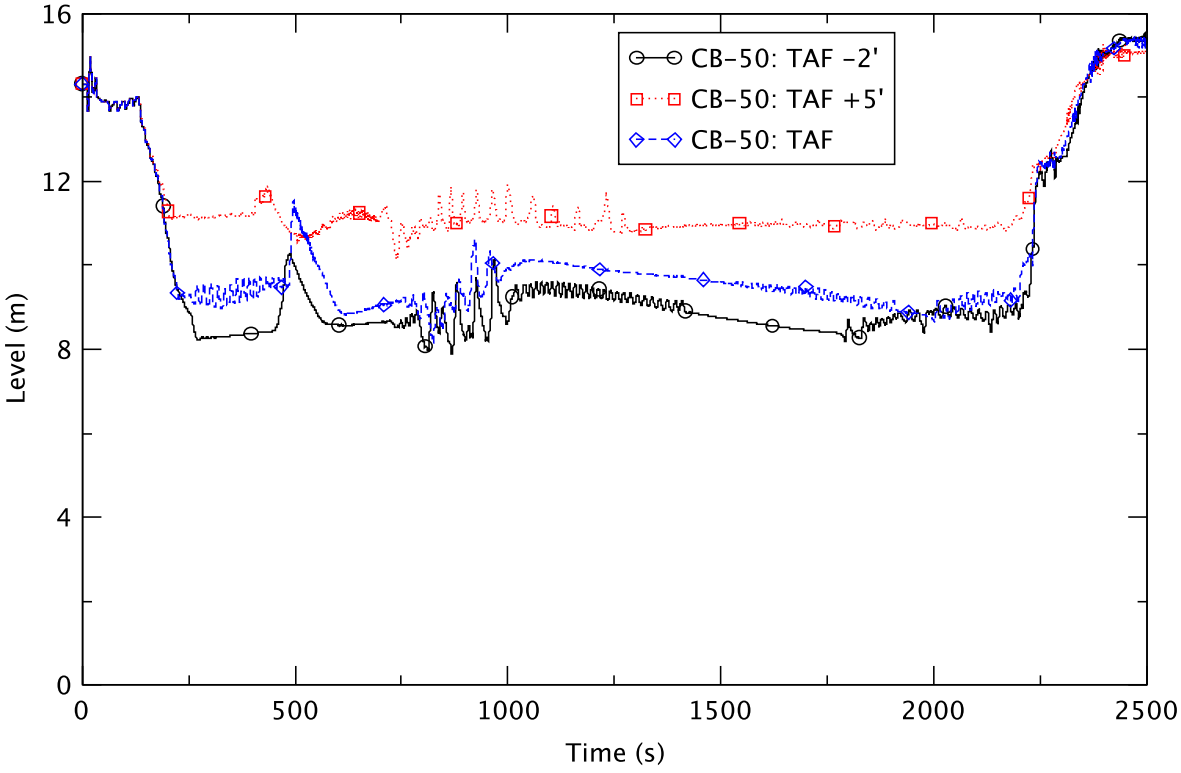

Figure 4.123 Downcomer Water Level - EOFPL Base Cases

The core boron inventory, shown in Figure 4.124, generally reflects the transport of boron by mixing, a process which requires a minimum coolant flow of 4% to begin entraining boron. The reactivity components for the TAF+5 and TAF cases are shown in Figure 4.125 and Figure 4.126, respectively. The positive net reactivity occurring roughly at 750 s is responsible for the power perturbations observed in Figure 4.120 for the TAF+5 case. The dilution of boron is seen in Figure 4.125 for the TAF+5 case when boron reactivity declines between 500 s and 750 s. In all three EOFPL cases the reactor remains shutdown by the injected boron; no recriticality is observed due to either repressurization of the reactor vessel or dilution of the boron.

As indicated earlier, the maximum PCT for the TAF-2 case is more limiting than for the other two cases. Figure 4.115 shows the maximum PCT for this case occurring at ~700 s, a time when the core voiding also reaches its maximum (Figure 4.104).

The temperature of the suppression pool water (Figure 4.127) is an indication of energy discharged to the pool via the SRVs. The TAF+5 case has the highest temperature of the three cases considered. The other two have almost identical peak pool temperatures. In all three cases, the pool temperature stays much below the boiling point and is not expected to impact the safe shutdown of the reactor.

The transient response of the drywell pressure (Figure 4.128) again is as expected, with the highest pressure for the TAF+5 case. In all three, the maximum drywell pressure is low enough not to be a concern for the containment's integrity.

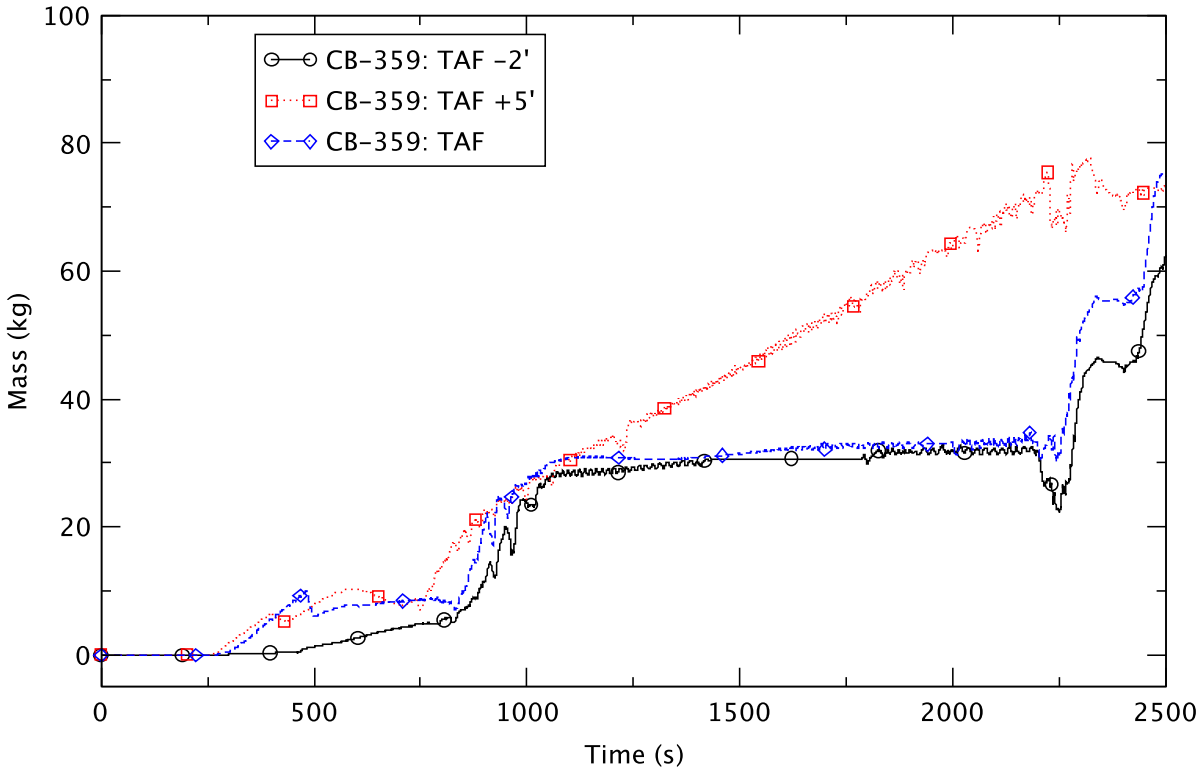

Figure 4.124 Boron Inventory in the Core - EOFPL Base Cases

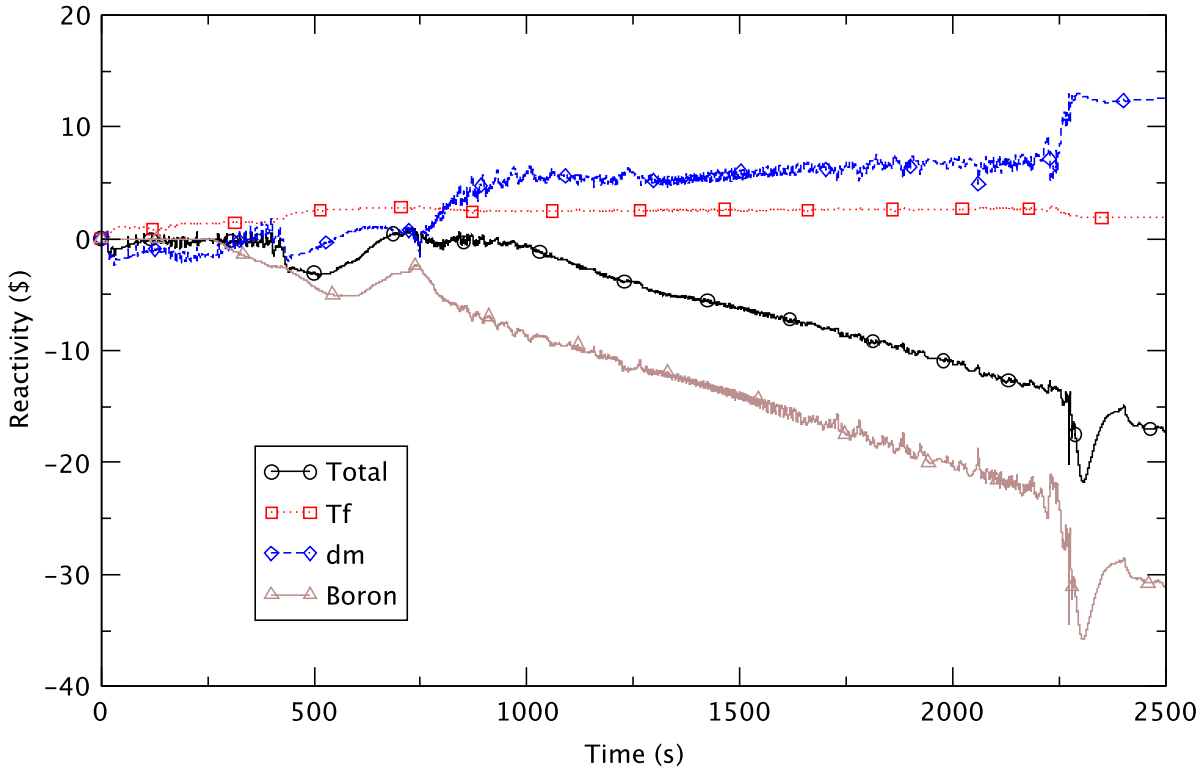

Figure 4.125 Core Reactivity - EOFPL, TAF+5

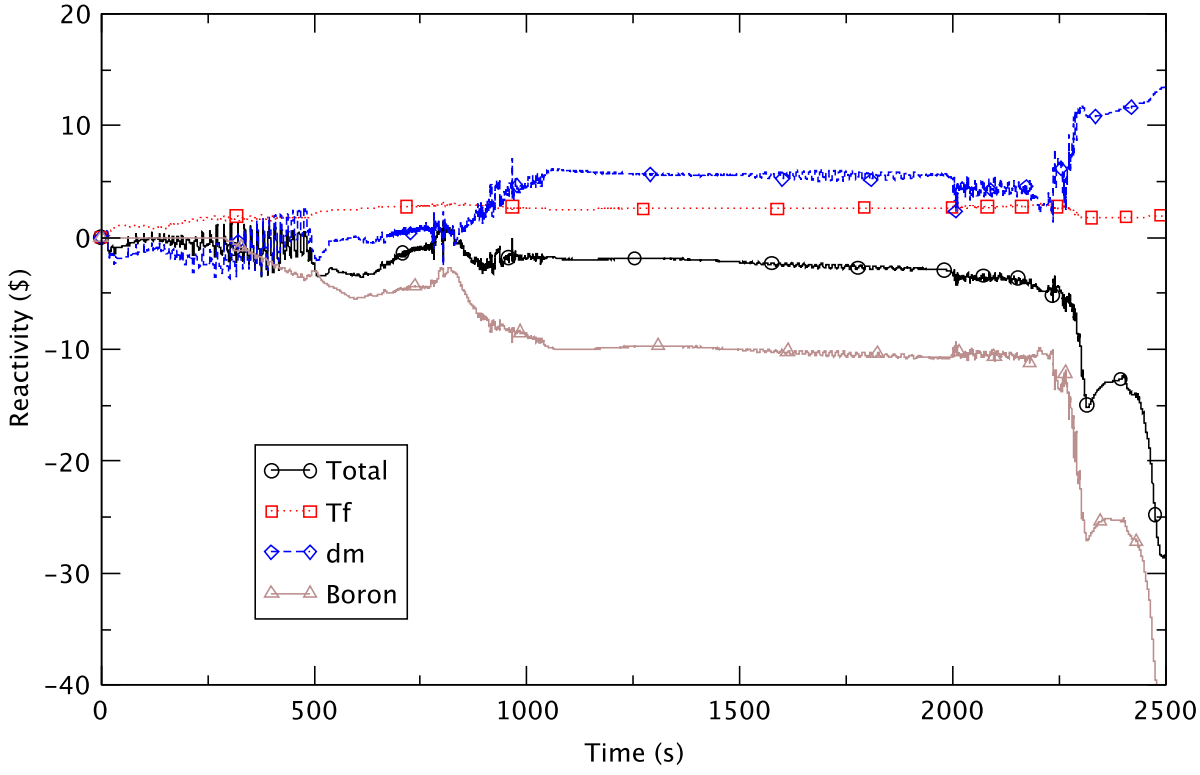

Figure 4.126 Core Reactivity - EOFPL, TAF

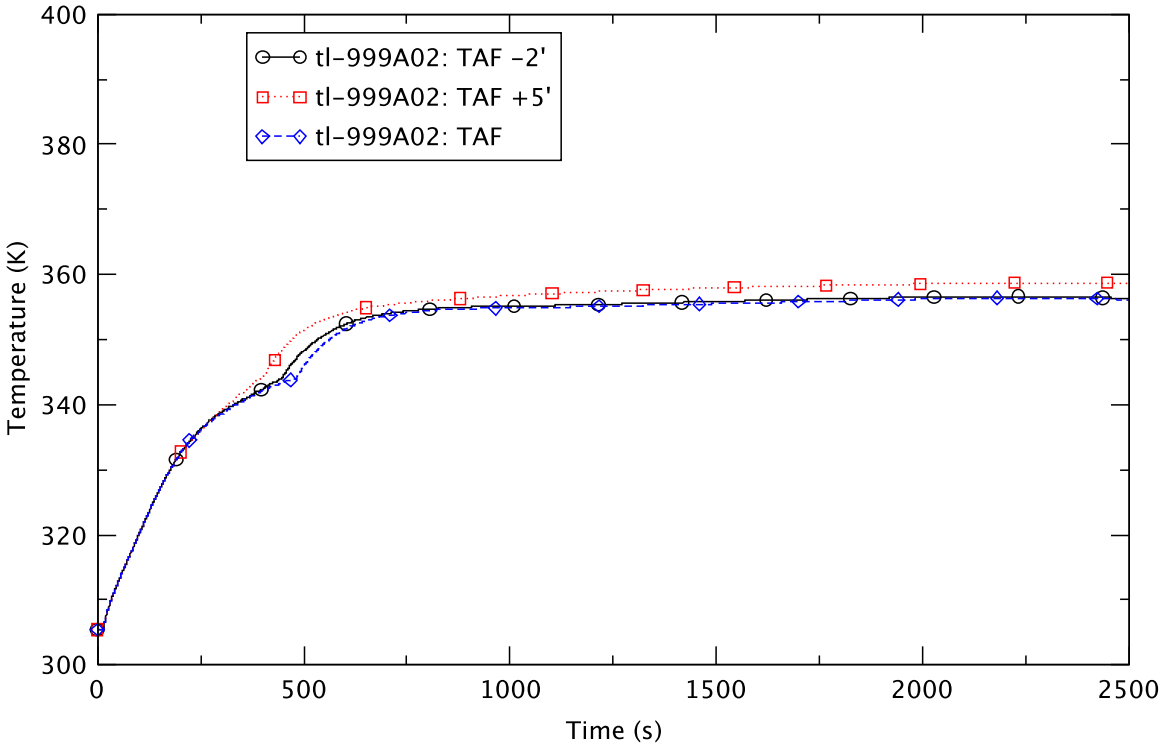

Figure 4.127 Suppression Pool Temperature - EOFPL Base Cases

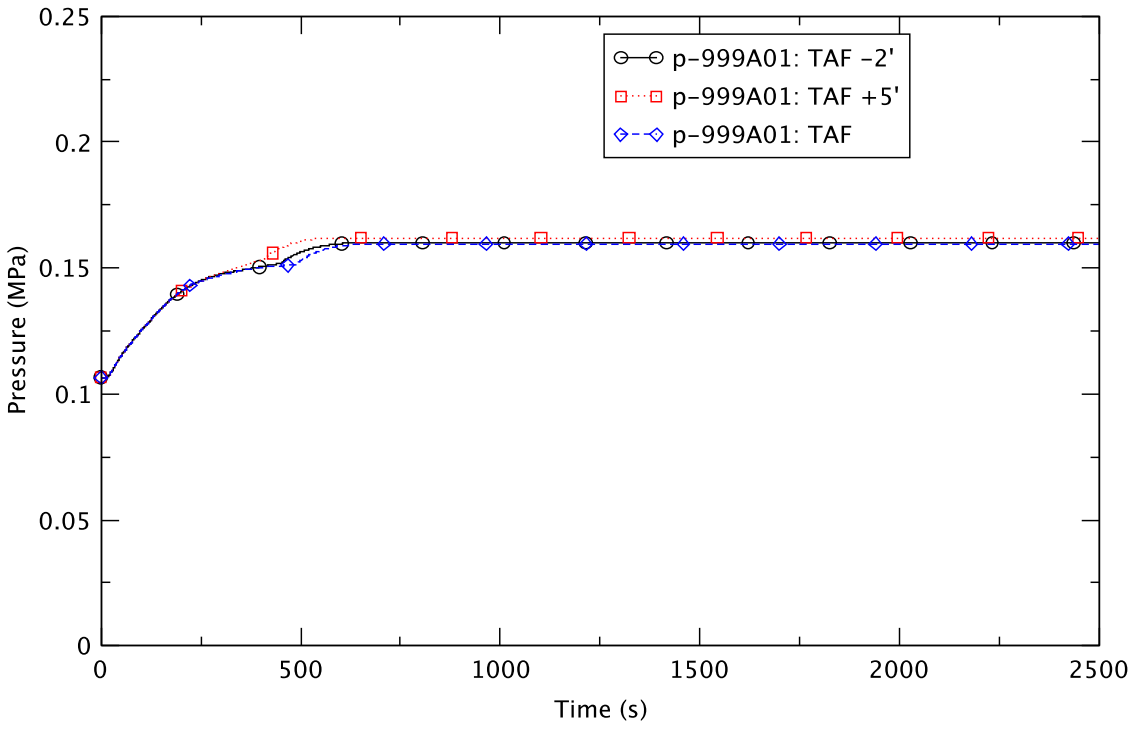

Figure 4.128 Drywell Pressure - EOFPL Base Cases

5 SUMMARY AND CONCLUSIONS

The first objective of this work is to develop TRACE/PARCS models supporting ATWS confirmatory analyses at MELLLA+ operating conditions for scenarios initiated by closure of main steam isolation valves (MSIVs) that lead to emergency depressurization (ED) once the heat capacity temperature limit (HCTL) of the suppression pool is exceeded. The second objective is the analysis of these ATWS-ED scenarios with different assumptions about plant conditions and/or modeling. An ancillary objective is to assess the capabilities of the TRACE/PARCS code to calculate the thermal-hydraulic and neutronic phenomena associated with these events.

These objectives were met, and this report provides the details. The BWR/5 TRACE/PARCS model used in the analysis of ATWS-ED transients is an updated version of the model described in a previous report for ATWS events initiated by a turbine trip [2]. In this chapter, the most significant conclusions are given. The chapter is divided into 1) a section on how the study generally met the objectives, 2) a section on what was learned about ATWS-ED events, and, 3) a section related to the calculational tool that was used. In the current study, TRACE/PARCS was used to analyze a BWR/4-like model derived from a BWR/5 model for the ATWS application.

5.1 TRACE/PARCS Application to ATWS-ED Events

The BWR model used with TRACE/PARCS to simulate the ATWS-ED events is updated from an earlier model [2]. It encompasses plant components needed for simulating an ATWS initiated by MSIV closure. The systems/components include the following:

- standby liquid control system (SLCS) with different injection points and control logic to simulate the transport of boron in the coolant
- recirculation loop with pump and flow-control valve
- feedwater line with an associated water level control system
- reactor core isolation cooling system (RCIC)
- safety- and relief-valves (SRVs) and automatic depressurization system (ADS)
- containment with passive heat structures and suppression pool cooling

The core, containing GE14 fuel, is represented by 27 thermal-hydraulic channels wherein each channel represents a group of similar fuel assemblies in terms of burnup and proximity to inserted control rod banks. Four different types of fuel rods are represented within a channel. The model can be used for many ATWS applications and for other accidents and operational transients. A MATLAB script was developed for generating input for the CHAN components in TRACE. The script includes a feature to use FRAPCON results to develop inputs for the dynamic gap model in TRACE. The exposure data required to interpolate the FRAPCON results are imported by the script from a PARCS input-data file. Thus, the script can generate cycle-specific inputs for the CHAN components.

5.2 ATWS Events Initiated by MSIV Closure

Using the TRACE/PARCS coupled-code system, results were obtained for ATWS events initiated by an MSIV closure in a BWR/5 operating in an expanded operating domain under MELLLA+ conditions. The calculations provide the reactor response under different initial and

boundary conditions. The range of conditions utilized in the eleven cases calculated includes the following:

- three fuel exposure conditions, beginning-of-cycle (BOC), peak-hot-excess-reactivity (PHE), and end-of-full-power-life (EOFPL)
- three water level control strategies, top-of-active-fuel plus five feet (TAF+5), TAF, and TAF-2
- two initial flows within the MELLLA+ operating range, 105% and 85% of nominal
- two numerical schemes, SETS and semi-implicit (SI)
- two locations for boron injection, upper and lower plenum

The results show the following:

- In all cases considered, the ATWS-ED transient initiated by MSIV closure is mitigated successfully by a combination of an automatic recirculation pump trip (2RPT), and operator actions that depressurize the reactor pressure vessel using the ADS, and reduce power by water level control and injection of boron using the SLCS.

- Early action to lower the downcomer water level is effective in mitigating a power increase as a result of increasing subcooling of the core inlet.

- The cycling of SRVs before the emergency depressurization causes power oscillations. No substained power oscillations related to density-wave oscillations (and core instability) were observed.

- After 2RPT, lowering the water level reduces reactor power through a decrease in core flow that engenders more voiding in the core.

- Emergency depressurization results in decreasing reactor power towards the decay heat level.

- The effect of ED, flashing of reactor coolant, and the swelling of downcomer water level is less pronounced when the rate of depressurization is reduced.

- The rate of depressurization is a function of the steaming rate, that is, the reactor power. A higher power generally leads to a slower depressurization rate.

- Subsequent to the ED, oscillations in core flow and water level are due to periodic voiding and refilling of the core and the cycling of the feedwater system in an attempt to maintain water level.

- Maximum peak clad temperature (PCT) occurs either very early or much later. When early, it occurs either right after the MSIV closure or shortly after initiation of water level reduction when the reactor power is still ~50%. When late, it happens after the ED when the core is nearly voided and the reactor power is at or near decay-heat level. The high void condition usually results in more limiting PCT even though the reactor may be at a lower power level than during the case with a higher core flow. However, all of the predicted PCTs are below 1478 K (2200°F).

- In all cases analyzed, there is no re-pressurization, and the reactor stays sub-critical after sufficient boron has built up in the core[3].

- Injection of boron is effective in overcoming the effects of positive reactivity due to fuel temperature decreasing, and moderator density increasing.

- There is about a 30 s to 50 s delay before the injected boron reaches the core. The delivery of boron is consistent with the boron transport model implemented in the TRACE/PARCS BWR/5 model.

- An increase in the density of liquid water due to ED or to adding feedwater has no observable impact on the dilution of the boron concentration.

- Boron stratification in the lower plenum due to low core flow is the principal cause of the reduction in boron reactivity during the ATWS-ED transient.

- Restoring the water level to its normal elevation substantially increases the core boron inventory.

- The implementation of two-loop cooling and passive heat sinks in the wetwell of the containment is effective in mitigating the heat-up of the suppression pool and prevents boiling.

- The drywell pressure in all cases is low compared to the design pressure of a typical BWR/5 containment.

- In comparing the nine "base" cases (three cycle conditions x three level control strategies) the following trends are observed:

    - For each cycle condition, the TAF and TAF-2 cases are closer in their transient response relative to the TAF+5 case.
    - Level control affects core flow and the core average void fraction.
    - Qualitatively, the core boron reactivity is inversely proportional to the average void fraction.
    - A higher core void fraction implies a higher void reactivity. However, the lower liquid fraction in a high void situation means a lower boron inventory in the core. These two counter-acting effects both contribute to the determination of the reactor power.
    - At relatively high core flow (e.g., in the case of water level at TAF+5) voiding in the core helps to promote higher flow, while the opposite is true when the core flow is relatively low (e.g., with the water level at TAF-2).
    - An ED initiated at a relatively high reactor power (e.g., with water level at TAF+5) will result in a slower depressurization and a milder transient response in many of the thermal-hydraulic parameters, such as level swell in the downcomer.
    - For the TAF+5 and the TAF cases, the maximum PCT occurs early. At the PHE and the EOFPL conditions, it occurs during the initial power spike caused by the MSIV closure. At the BOC condition, it occurs right after water level control is initiated when core flow still is relatively high.

[3] However in plant-specific applications the analysis should include emergency operating procedures that would call for reclosing all ADS/SRV valves after successful depressurization, an action that could lead to repressurization and recriticality.

- For the TAF-2 cases, there is a delayed heat-up of the core at a time when the reduction in water level has caused the core flow to approach a lower quasi-steady value, and the maximum PCT is more limiting when compared to the other two level-control strategies.
- In general, the maximum PCT is the highest at BOC and the lowest at EOFPL.
- In general, the timing of the ED is earlier for the BOC and PHE cases (with the former ahead by only a few seconds) than the EOFPL cases. The difference in timing between the BOC and EOFPL cases are in excess of 100 seconds.
- For each statepoint, the TAF+5 case has the earliest ED timing, followed by the TAF-2 case, and then the TAF case. The TAF-2 case is ahead of the TAF case by a few seconds for the BOC and PHE conditions, but the difference widens to 35 seconds for the EOFPL condition.
- For all cases, reactor power falls after the ED. However, the decrease in power is less rapid for the TAF+5 cases at BOC and PHE. In those cases, natural circulation flow is maintained while in the cases where rapid power decay is observed, natural circulation is broken.
- The rate of boron transport to the core depends upon the core flow (as determined by modeling assumptions). At lower core-flow conditions (e.g., with the water level at TAF and TAF-2), there are long periods when the flow is less than the entrainment threshold, and no entrainment of boron is calculated by the model.
- At higher core flowrates (e.g., with the water level at TAF+5), boron is more effectively mixed and delivered to the active core region at a higher rate, resulting in a continuous build up of boron inventory in the core.
- In all TAF and TAF-2 cases, the maximum suppression pool temperatures are all less than 360 K, but within a few degrees of it. For the TAF+5 cases, the maximum is 372 K at BOC and PHE, and 359 K at EOFPL.
- In all cases, the maximum drywell pressure falls between 0.16 MPa and 0.17 MPa.

- In comparing the results of using the SETS and SI numerical schemes the following is observed:

  - Most key parameters as a function of time are quite similar for the two cases.
  - The most striking difference between the two is in predicting the core flow immediately after the emergency depressurization. In the SI case, the core flow is maintained high after the ED while the SETS case predicts a break in the natural circulation resulting in practically zero core flow[4].
  - The differences in the prediction of core flow affect the evolution of the core power and boron transport in the core. However, the impact on the containment response is insignificant.
  - The maximum PCT is about 10 K higher in the case of SI than that of SETS .

- In comparing the results of different locations for boron injection, the following is observed:

  - The initial buildup of boron in the core is a little bit faster when the injection is into the upper plenum. However, there is little noticeable difference in the transient response between the two cases.
  - With the slightly earlier arrival of boron in the core, the ED occurs about three seconds later for the case with injection into the upper plenum.

[4] See footnote 2.

- The maximum PCT, maximum suppression pool temperature, and the maximum drywell pressure basically are identical for the two cases.

5.3 Modeling in TRACE/PARCS

TRACE/PARCS was shown to be an extremely useful tool for analyzing ATWS events. However, in some areas of the code the capabilities and/or modeling could be improved as explained below.

Coordination and Knowledge Management

One of the lessons learned from the current project is that close coordination is beneficial between the analyst (i.e., BNL) and code developer (i.e., NRC) when undertaking complex transient calculations (e.g., ATWS) using the TRACE/PARCS code system. Due to the complexity of this application of TRACE/PARCS, significant effort was expended throughout the course of this work to improve the code and document the relevant user-experience.

Numerical Scheme/Time-Step Size

TRACE/PARCS has a comprehensive set of models to handle a multitude of thermal-hydraulic phenomena that are crucial to the understanding of the reactor system response to different initial and boundary conditions. Successful completion of an ATWS-ED simulation often has depended on carefully considering the reactor conditions and phenomena when determining the appropriate time-step sizes and numerical-solution scheme. In understanding the robustness of a TRACE/PARCS ATWS-ED analysis result, it is essential to examine the sensitivity of the results to the choice of numerical scheme and time-step sizes. An illustrative example is the prediction of natural circulation in the core after the 2RPT and emergency depressurization. Dependent on the particular numerical scheme (SETS or SI) or time-step size (in the case of SETS) natural circulation is either predicted to be broken or preserved. In the current work, the ATWS-ED consequences are not sensitive to either outcome in terms of natural circulation. Additional details on this aspect of the analysis will be reported in a the report describing ATWS-ED sensitivity studies.

Low Pressure/Low Flow

In simulating the ATWS-ED transients, in many instances code failures occur when the core is depressurized and the power is at decay-heat level. Simulating natural circulation flow at low pressures is challenging because of the relatively high specific volume of steam and a small change in flow can result in a large change in steam void in the flow channel. Another difficulty is in the periodic changes in the direction of flow when the flow is oscillating and the boiling boundary is constantly shifting. The experience of conducting these ATWS-ED transient analyses with TRACE/PARCS could be extended to evaluating small light water reactors that also rely on natural circulation cooling and operate at lower pressures than current power reactors.

Low Flow Dryout

The ATWS-ED results indicate that the maximum PCT can occur under low-flow conditions when the channel is nearly fully voided. In a recent assessment of TRACE/PARCS for applications to BWRs [19], it is noted that for low mass flux conditions (<500 kg/m^2-s) the overprediction of critical power by TRACE, compared to test data, is between 20% and 35%

while for larger mass fluxes, the predictions are within the 10% error margin. This suggests that the range of uncertainty in low-flow conditions should be recognized in interpreting the prediction of dryout by TRACE. Also, rewetting of the fuel rod and axial conduction in the clad could be effective in limiting the temperature excursion during dryout. At present, there is limited experience in exercising the fine mesh nodalization model in TRACE when coupled to PARCS. The NRC staff currently are evaluating the sensitivity of the maximum PCT to the nodalization of the heat structure for the fuel rod. In the current analysis, the predicted instances of dryout at low flowrates did not result in significant cladding heat-up (the PCT remains well below 1478 K); therefore, the current analysis conclusions are not impacted by this.

Boron Reactivity Worth

During the phase of the transient following the injection of soluble boron, TRACE/PARCS is likely to overpredict nodal boron reactivity in highly voided cells. This non-conservative bias could be eliminated through extrapolation, but would require extrapolation to negative effective densities. The ATWS-ED transient is susceptible to this non-conservatism, owing to the formation of void in the inter-assembly bypass during ED with dissolved boron present. In the current analysis, consideration was given to the potential to overestimate boron reactivity worth for ATWS-ED transients. Therefore, the safety conclusions of the current study account for this issue.

6 REFERENCES

1. J. Harrison, GE Hitachi, letter to U.S. Nuclear Regulatory Commission, "Accepted Version of GE Licensing Topical Report NEDC-33006P-A, Revision 3 (TAC No. MD0277)," MFN 09-362, June 19, 2009, ADAMS Accession No. ML091800512.

2. L-Y. Cheng et al., "BWR Anticipated Transients Without Scram in the MELLLA+ Expanded Operating Domain – Part 1: Model Development and Events Leading to Instability," NUREG/CR-7179, BNL-NUREG-105323-2014, Brookhaven National Laboratory, March 3, 2014.

3. L-Y. Cheng et al., "BWR Anticipated Transients Without Scram in the MELLLA+ Expanded Operating Domain – Part 2: Sensitivity Studies for Events Leading to Instability," NUREG/CR-7180, BNL-NUREG-105327-2014, Brookhaven National Laboratory, March 20, 2014.

4. U.S. Nuclear Regulatory Commission, "Summary of Trip Report for Site Visit to Brookhaven National Laboratory January 2012," February 12, 2015, ADAMS Accession No. ML15043A807.

5. U.S. Nuclear Regulatory Commission, "Summary of Trip Report for Site Visit to Brookhaven National Laboratory October 2010," February 12, 2015, ADAMS Accession No. ML15043A803.

6. TRACE/PARCSv5.0 User's Manual, Volume 1: Input Specification, U.S. Nuclear Regulatory Commission, Office of Nuclear Regulatory Research, August 10, 2012.

7. L-Y. Cheng et al., "TRACE/PARCS Core Modeling of a BWR/5 for Accident Analysis of ATWS Events," *Trans. Am. Nucl. Soc. 109*, pp 979-982, November 2013.

8. U.S. Nuclear Regulatory Commission, "Safety Evaluation by the Office of Nuclear Reactor Regulation Related to Amendment No. 140 to Facility Operating License No. NPF-69 Nine Mile Point Nuclear Station, LLC, Nine Mile Point, Unit No. 2, Docket No. 50-410," December 22, 2011, ADAMS Accession No. ML113560333.

9. "Nine Mile Point Unit 2 Updated Final Safety Analysis Report," Rev 19, October 2010.

10. L-Y. Cheng et al., "TRACE/PARCS Core Modeling of a BWR/5 for Accident Analysis of ATWS Events," *Trans. Am. Nucl. Soc. 109*, pp 979-982, November 2013.

11. Y. Xu and T. Downar, "GenPMAXS-V6 Code for Generating the PARCS Cross Section Interface File PMAXS", University of Michigan, Draft March 2012.

12. Y. Xu and T. Downar, "Modified CMFD Method for PARCS", Letter Report, University of Michigan, August 1, 2011.

13. J. Harrison, GE Hitachi, letter to U.S. Nuclear Regulatory Commission, "Response to NRC's Data Request to Support Confirmatory ATWS Calculations Regarding MELLLA Plus," MFN 09-681, November 4, 2009, ADAMS Accession No. ML093170371.

14. GE Hitachi Nuclear Energy, “Safety Analysis Report for Nine Mile Point Nuclear Station Unit 2 Constant Pressure Power Uprate (PUSAR)”, NEDO-33351P, Rev. 0, May 31, 2009, ADAMS Accession No. ML091610104.

15. J. Harrison, GE Hitachi, letter to U.S. Nuclear Regulatory Commission, “Accepted Version of GE Licensing Topical Report NEDC-33173P, Applicability of GE Methods to Expanded Operating Domains, (TAC No. MD0277),” October 5, 2010, ADAMS Accession No. ML102920131.

16. B. Ade et al., “SCALE/TRITON-PARCS Code Validation with BWR Steady-State Plant Operating Data”, ORNL/TM-2011/256, Oak Ridge National Laboratory, November 2011.

17. J. Harrison, GE Hitachi, letter to U.S. Nuclear Regulatory Commission, “Supplemental Response to NRC Information Requests 10, 13, and 14 - Confirmatory ATWS Calculations Regarding MELLLA+,” MFN 10-213, Supplement 1, October 29, 2010.

18. U.S. Nuclear Regulatory Commission, “Standard Review Plan,” NUREG 0800, Section 15.8, March 2007.

19. V. H. Sanchez, et al., “Validation and Application of the Thermal Hydraulic System Code TRACE/PARCSfor Analysis of BWR Transients,” *Science and Technology of Nuclear Installations*, vol. 2012, Article ID 247482, 2012.

APPENDIX A

Supplemental TRACE Calculation Notebook
BWR/5 Model for ATWS Analysis

TABLE OF CONTENTS

LIST OF FIGURES

LIST OF TABLES

Nomenclature

Acronym	Definition
3D	Three dimensional
ADI	Alternating Direction Implicit
ADS	Automatic Depressurization System
ATWS	Anticipated Transient Without SCRAM
ATWS-ED	Anticipated Transient Without SCRAM with Emergency Depressurization
ATWS-I	Anticipated Transient Without SCRAM with Instability
BLP	Bottom of lower plenum
BNL	Brookhaven National Laboratory
BOC	Beginning-of-cycle
BWR	Boiling Water Reactor
CB	Control Block in TRACE/PARCSInput
CHAN	Channel Component in TRACE Input
CONTAN	Containment Component in TRACE Input
DC	Downcomer
DW	Drywell
ED	Emergency Depressurization
EOFPL	End-of-Full-Power-Life
EPU	Extended Power Uprate
FW	Feedwater
FWC	Feedwater Controller
GE	General Electric
GEH	GE Hitachi
HCTL	Heat Capacity Temperature Limit
HWL	High Water Level
ISL	Information Systems Laboratories, Inc.
LOCA	Loss of Coolant Accident
LP	Lower Plenum
LPV	Lower Plenum Valve
LTR	Licensing Topical Report
LWL	Low Water Level
MELLLA	Maximum Extended Load Line Limit Analysis
MELLLA+	Maximum Extended Load Line Limit Analysis Plus
MSFBT	Minimum Stable Film Boiling Temperature
MSIV	Main Steam Isolation Valve
NMP2	Nine Mile Point Unit 2
NRC	Nuclear Regulatory Commission
OOS	Out-of-Service
PARCS	Purdue Advanced Reactor Core Simulator
PHE	Peak-Hot-Excess-Reactivity

Acronym	Definition
RAI	Request for Additional Information
SC	Suppression Chamber
SEPD	Steam Separator/Dryer Component in TRACE Input
SETS	Stability Enhancing Two-Step method
SI	Semi-Implicit numerics
SLCS	Standby Liquid Control System
SP	Suppression Pool
SRV	Safety Relief Valve
SRVOOS	Safety Relief Valve Out of Service
SV	Signal Variable in TRACE Input
TAF	Top-of-Active Fuel
TRACE	TRAC-RELAP Advanced Computational Engine
TRACG	Transient Reactor Analysis Code (GE version)
UFSAR	Updated Final Safety Analysis Report
WW	Wetwell
Zr	Zirconium
γ	Mixing Coefficient
θ	Remixing Coefficient

1 INTRODUCTION

This supplemental notebook provides documentation of the non-proprietary updates to the TRACE/PARCS base BWR/5 model [1]. The specific changes to be made to modify the base model for the simulation of anticipated transient without scram with emergency depressurization (ATWS-ED) have been cited in the footnotes of the base model notebook and are summarized in Table A.1. These changes were discussed in a series of staff guidance documents [2, 3].

Table A.1 Summary of Required Changes to the Base BWR/5 Model

Item	Comment
1	The following models for the VESSEL component will be modified for the ATWS-ED analysis. • addition of new boron mixing model and removal of the flow control valve in the lower plenum • modification to 3D level tracking for the vessel
2	For the ATWS-ED analysis 3D level tracking will be turned off in ring 3 between axial levels 9 (TAF) and 12 (feedwater sparger).
3	For the ATWS-ED analysis a different dynamic gas-gap option will be used (NFCI=3 initially, however NFCI=-13 was the eventual guidance) to allow for the modeling of clad rupture. In addition, metal-water reaction and axial conduction (NMWRX=1 and IAXCND=1) will be activated for the TRACE/PARCScalculations.
4	A higher reverse loss coefficient of K=97.3E9 will be used in the ATWS-ED model to mitigate negative flow in the water rods.
5	For the ATWS-ED analysis a small amount of carryover (XCO=0.001) and carryunder (XCU=0.0025) will be specified to better emulate the performance of real steam separators.
6	A new signal variable for the mass flow in the steamline will be defined for the ATWS-ED analysis. The location of the flow sensor will be downstream of the MSIVs reflecting the instrumentation in the model BWR/5 plant.
7	The modeling of SRV/ADS valves will be modified for the ATWS-ED analysis. The valve loss coefficient, valve delay and valve rate of opening will be revised. In addition individual valves with modified control logic are to be used to represent the different banks of SRVs.
8	The HCTL limit will be changed to 344.26 K (160°F) for the ATWS-ED analysis.
9	For the ATWS-ED analysis the “Relief Mode Analytical Limit” will be used as the setpoints for the opening pressures.
10	Several settings of the FW controller will be modified for the ATWS-ED analysis and among them are the maximum FW flowrate, location of the steam flow sensor, and the proportional gain of the water level differential.
11	For the modeling of boron mixing in the lower plenum the lower plenum flow valve will be replaced in the ATWS-ED analysis by a control logic that releases the appropriate amount of boron into the core flow to emulate the effect of boron mixing/remixing.
12	Heat structures in the wetwell of the containment will be incorporated in the ATWS-ED analysis.
13	The ATWS-I analysis assumed one train of the RHR was operational. In the ATWS-ED analysis two trains of RHR will be assumed to be operational and thus two suppression pool coolers will be modeled.

The implementation of the changes required development of new models and updates to the TRACE input deck. Table A.2 summarizes the new models and updated TRACE input

parameters. As indicated in the table, details of each new model and the corresponding updates to the TRACE input deck are described in subsequent sections of this notebook.

Table A.2 Summary of Changes as Implemented in the Base BWR/5 Model

Input Model/ Parameter	Item in Table A.1	Modifications
Downcomer level tracking options. Remove lower plenum valve (LPV).	1, 2	See Section 2.1 Modified VESSEL 3-D level tracking in ring 3. Removed LPV (component #34). Set NAMELIST variable **IMFR**=3. Reset VESSEL axial flow area fraction at R2, L3 to its original value.
Water rod inlet reverse flow loss coefficient. Activate cladding rupture model. Activate metal water reaction model (Cathcart-Pawel). Activate axial conduction with implicit numeric. Initial oxide layer on fuel rods.	3, 4	See Section 2.2 For all CHANs: **wrrlossi**=9.73E10 **NFCI**=-13 **nmwrx**=1 **iaxcnd**=1 NAMELIST variables: **DOXLAYER**=3.0E-6 (for BOC) =6.0E-6 (for PHE) =10.0E-6 (for EOFPL) **FOXLAYER**=-1 **NRSLV**=1
Separator carryover. Separator carryunder.	5	See Section 2.3 For SEPD 45 & 46: **xco**=0.001 **xcu**=0.0025
Feedwater control (FWC) steam flowrate sensing location. FWC level mismatch gain. FWC maximum feed flowrate.	6, 10	See Section 2.4 Defined **SV**-161 to provide steam flow downstream of MSIVs and use this SV as input to **CB**-72 and **CB**-51. In **CB**-71 the proportional gain of level difference was increased to 10. In **CB**-76 the maximum feedwater flowrate was increased to 2954.95 kg/s (1.3xnominal).
SRV relief setpoints. SRV internal losses. SRV delay. SRV rate.	7, 9	See Section 2.5 **Kfac** = **Kfacr**=0.786 **intlossoff**=1, **KOPEN** data specified in a table **rvmx**=2.0
HCTL	8	See Section 2.6 Specified setting for **TRIP** 6 (ADS trip for ED cases) to be 344.26 K.

Input Model/ Parameter	Item in Table A.1	Modifications
Boron transport control system.	11	See Section 2.7 Relocated SLCS lower plenum pipe (**PIPE** 195) to inject to **VESSEL** L4, R3 (negative face). Modified **FILL** 196 to be a type 10, taking generalized states from the boron mixing control system.
Suppression pool (SP) heat structure.	12	See Section 2.8
SP heat exchanger.	13	See Section 2.9 Assumed two-loop operation. Doubled SP cooler flow to 236 kg/s in **CB**-34.

2 NEW MODELS AND INPUTS

The following sections of the notebook discuss modifications to the base BWR/5 model, the development of new models, and the listing of corresponding changes to the TRACE input model.

2.1 VESSEL Component

Two changes were made in the VESSEL component. One was the removal of the lower plenum flow valve and the other was the modification in the 3-D level tracking option for ring 3 (R3) of the vessel.

The base BWR/5 model [1] exploited a valve in the lower plenum (LPV) to emulate the effect of boron stratification and mixing/remixing in the bottom of the lower plenum (BLP). The LPV controlled flowrates through the BLP. The function of the LPV was to isolate the BLP from the core flow when the boron would be stratified. The opening and closing of the LPV was controlled to simulate mixing and remixing.

A new methodology based on an external control system has been developed to achieve a similar objective of tracking and isolating stratified boron from the TRACE calculation flows (see Section 2.7). This new approach negates the need of the LPV. In the updated model the component VALVE 34 was removed. Together with the removal of the valve in vessel axial level L3 the axial flow area in (L3, R3) was restored from zero to its original value. Also, NAMELIST variable IMFR=3 was added to the input to send the VESSEL component phasic mass flows to the TRACE/PARCS output plot file (xtv file).

According to the NRC staff [3], use of the level tracking feature in the transient appears to have a significant impact on the calculation of the condensation heat transfer in the downcomer. When the level tracking feature is enabled below the feedwater (FW) injection sparger location, the interfacial heat transfer area appears to be under-estimated and the inlet subcooling response to the level reduction is damped (over-estimated inlet subcooling). The staff recommended level tracking be disabled in the vessel ring 3 for all nodes starting at the FW injection sparger and below until reaching a node near the level tracking strategy area (e.g.

TAF). The staff guidance [3] led to disabling the 3D level tracking option in R3 between axial levels 9 and 12 inclusive. In addition the scheme suggested by the staff disabled level tracking in axial levels 1 through 4 (the base model assumed no level in that region of the vessel). The updated level tracking scheme is shown in Table A.3 with the new changes highlighted. In the table a '1' and '-1,' respectively, indicate the engagement and disabling of the 3D level tracking option.

Table A.3 3D Level Tracking Option for the VESSEL

Axial Level	Ring 1	Ring 2	Ring 3
17	-1	-1	-1
16	-1	-1	-1
15	1	1	1
14	1	1	1
13	1	1	1
12	1	1	-1
11	-1	-1	-1
10	-1	-1	-1
9	-1	-1	-1
8	-1	-1	1
7	-1	-1	1
6	-1	-1	1
5	-1	-1	1
4	-1	-1	-1
3	-1	-1	-1
2	-1	-1	-1
1	-1	-1	-1

2.2 CHAN Component and Initial Oxide Thickness

The staff provided the following guidance [3] in regard to updating the input for the CHAN component:

1. retard reverse flow in water rod by increasing the reverse flow loss coefficient.
2. activate the TRACE cladding rupture model.
3. activate the metal-water reaction option in TRACE.
4. specify some nominal initial oxide thickness.
5. enable axial conduction for the CHAN component and solve with implicit numerics.

Staff experience indicated that code execution seemed to be challenged by flow reversal in the water rods. Since flow reversal in the water rods is beneficial in terms of providing cooling to the active channel, this flow reversal was artificially retarded by increasing the reverse flow loss coefficient by a factor of 1.0E9 at the water rod inlet (bottom of the water rod). This was accomplished by setting **wrrlossi**=9.73E10.

2.2.1 Models for High Temperature

The rest of the changes in the CHAN component input were to activate several fuel models to capture the onset of certain phenomena at high temperatures. The first was to activate the

TRACE cladding-rupture model. The particular option for fuel-clad interaction (FCI) recommended by the staff was **NFCI**=-13, dynamic gas-gap model with elastic cladding deformation, plastic cladding deformation, clad rupture, and the FRAPCON relocation model turned on. The initial recommendation of **NFCI**=3 [3] later was found to not be working properly.

The staff also directed BNL to activate the option for metal-water reaction. At high temperatures (around 1000 K), the cladding oxidation reaction is exothermic and adds additional heat as the zirconium in the cladding reacts with the water coolant. TRACE has two options for treating the metal-water reaction; the Baker-Just model, and the Cathcart-Pawel model. The former model is consistent with 10 CFR 50 Appendix K, and is considered conservative. The Cathcart-Pawel model is a best-estimate and should be used for ATWS calculations. The Cathcart-Pawel metal-water reaction model was selected by setting **nmwrx**=1.

The staff requested that BNL activate the axial-conduction option for the fuel channels. Under ATWS conditions, the cladding surface might exceed the minimum stable film boiling temperature (MSFBT). At this point, TRACE will treat heat transfer from the cladding only as inverted annular film boiling. Therefore, heat removal is limited and the temperature continues to rise. TRACE will not predict the onset of transition boiling or rewet unless the cladding temperature is dropped below the MSFBT. Once above it, if axial conduction is disabled, the only heat- removal mechanism is film boiling. However, if it is enabled, heat transfer axially through the cladding also will be treated. Prediction of phenomena, such as reflood, must account for this heat-transfer mechanism in order to properly simulate the propagation of a quench front, and thus, the rewetting of the cladding surface. Therefore, the staff requested that BNL activate this model for the ATWSED calculations. The axial conduction option was activated by setting **iaxcnd**=1.

When axial conduction (**iaxcnd**=1) is enabled for the channel component, NAMELIST variable **NSRLV** controls the numerical-solution scheme for axial conduction. The default is to treat axial conduction with explicit numerics. However, **NRSLV**=1 allows the problem to be treated with ADI numerics (i.e., implicit). The implicit method is preferred and **NRSLV**=1 was one of the new NAMELIST variables specified in the updated input.

2.2.2 Determination of Oxide Layer Thickness

When using either metal-water reaction option, the TRACE user manual [4] recommends specifying some initial oxide layer thickness. If no initial oxide layer is specified, then TRACE will conservatively overpredict the rate of the metal-water reaction, even at temperatures below the threshold temperature (around 1000 K). Therefore, the staff directed BNL to specify some nominal thickness.

The thickness may be specified in one of two ways. In the first approach, an additional array can be input for the channel components once the oxide option is activated. Setting the **FOXLAYER** NAMELIST flag to 1 allows the user to specify an **OXLAYER** array for the channel component to set the initial thickness of the oxide layer. Implementing this approach would require substantial modification to the CHAN component input. Secondly, using this option would likely require some kind of calculation of the oxide layer based on the reults of the FRAPCON code calculation .

A second option is to use the **DOXLAYER** NAMELIST variable in TRACE. The **DOXLAYER** option will specify a constant, default, oxide layer to all surfaces. This option is preferred because it is implemented simply by making a single change to the input specifications. The following describes calculating an average oxide-thickness based on the results of the FRAPCON calculations at each cycle exposure statepoint. In TRACE, the rate of metal-water

reaction depends on several factors, among which are the clad temperature and the thickness of pre-existing oxide on the clad surface. This oxide layer has the effect of insulating the underlying clad from the coolant, and thus, slowing down the metal-water reaction. TRACE on the other hand, ignores the existence of this oxide layer in the heat-transfer calculations.

In TRACE, the Cathcart-Pawel metal-water reaction is only calculated when the cladding temperature rises above 1073 K. A significant spike in metal-water reaction energy source occurs if there is no initial oxide layer included in the TRACE cladding model, as the steam required for the oxidation of Zr does not have to diffuse through an initial ZrO_2 layer. A user input for the initial oxide layer thickness is converted internally in TRACE into the appropriate kinetic parameter of interest, and is used as the initial condition for integrating the parabolic rate equation. FRAPCON calculations can be used to estimate the initial thickness of the oxide layer for a given reactor operating history, typically of the order of a few microns for relatively fresh fuel.

NRC staff provided a set of FRAPCON outputs [5] for developing inputs for the dynamic gap-model. This set of FRAPCON outputs also gives the thickness of the oxide layer as a function of burnup. Based on these FRAPCON results, an average oxide thickness, the arithmetic mean of the oxide thickness over the length of a fuel rod (the FRAPCON model divided the full length fuel rod into 16 axial regions of equal length), is calculated as a function of burnup. Table A.4 lists the burnup at the end of each time-step and the corresponding average oxide layer thickness.

Table A.4 Average Oxide Thickness as a Function of Burnup

Burnup Step	Time (days)	Burnup (GWd/t)	Avg Oxide Thickness (microns)
0	0	0	0
1	0.1	0	0
2	0.2	0	0
3	0.3	0.001	0.000938
4	0.4	0.002	0.001313
5	0.5	0.004	0.002188
6	0.6	0.006	0.003313
7	0.7	0.009	0.0045
8	0.8	0.012	0.005875
9	0.9	0.016	0.007625
10	1	0.021	0.009313
11	1.1	0.025	0.01125
12	1.5	0.047	0.019625
13	2	0.074	0.030813
14	2.5	0.102	0.041688
15	6	0.296	0.118688
16	12	0.629	0.250938
17	20	1.073	0.427313
18	44	2.405	0.959375
19	66	3.626	1.449813
20	88	4.847	1.943063
21	100	5.513	2.213188
22	115	6.345	2.552125
23	130	7.178	2.892438
24	142	7.843	3.165625
25	158	8.731	3.531813
26	170	9.397	3.807188
27	181	10.008	4.06075
28	192	10.618	4.315
29	200	11.062	4.500375
30	207	11.45	4.662938
31	220	12.163	4.96275
32	250	13.782	5.6505
33	275	15.125	6.225938
34	300	16.445	6.797938
35	325	17.751	7.3695
36	350	19.028	7.93425
37	375	20.291	8.498563
38	400	21.539	9.062625

Burnup Step	Time (days)	Burnup (GWd/t)	Avg Oxide Thickness (microns)
39	425	22.773	9.626125
40	450	23.992	10.18913
41	480	25.428	10.86163
42	520	27.286	11.7465
43	560	29.12	12.63625
44	600	30.931	13.53163
45	640	32.696	14.417
46	680	34.414	15.29506
47	720	36.086	16.16531
48	760	37.711	17.02681
49	800	39.313	17.89438
50	840	40.892	18.76625

Results of Table A.4 are plotted in the following three figures showing the relationships between oxide thickness, burnup and time.

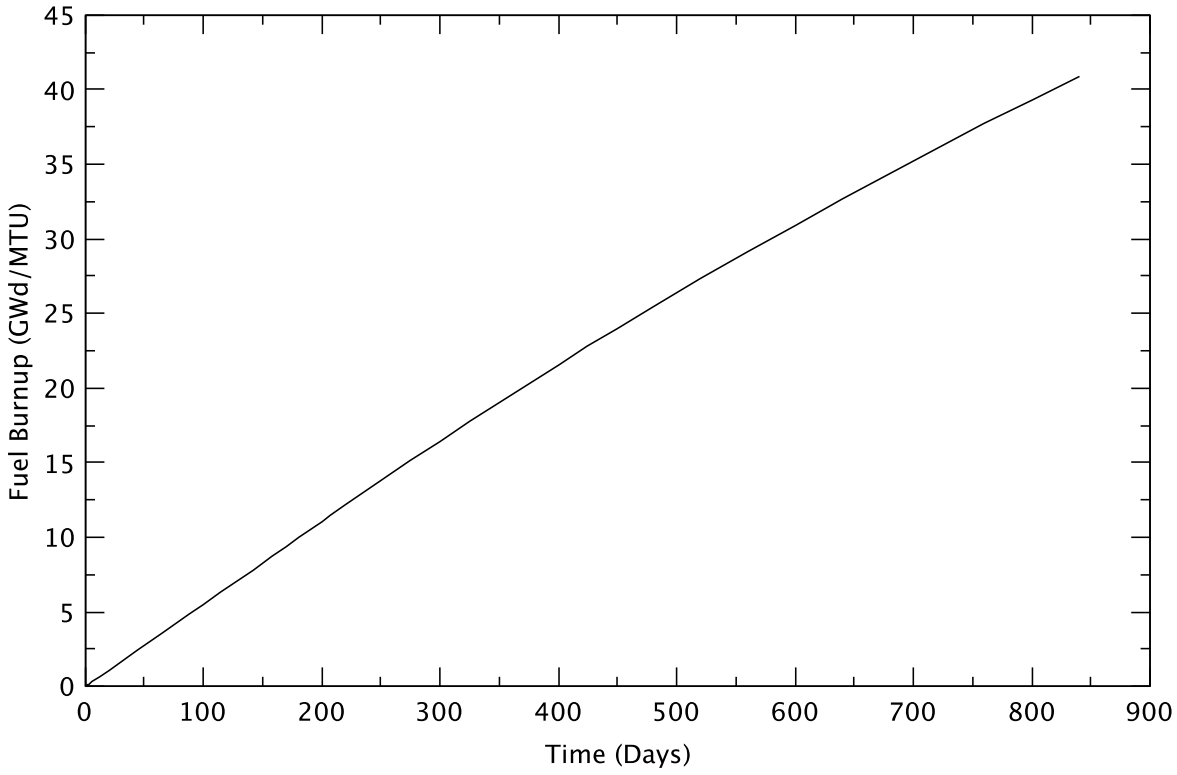

Figure A.1 Fuel Burnup as a Function of Time.

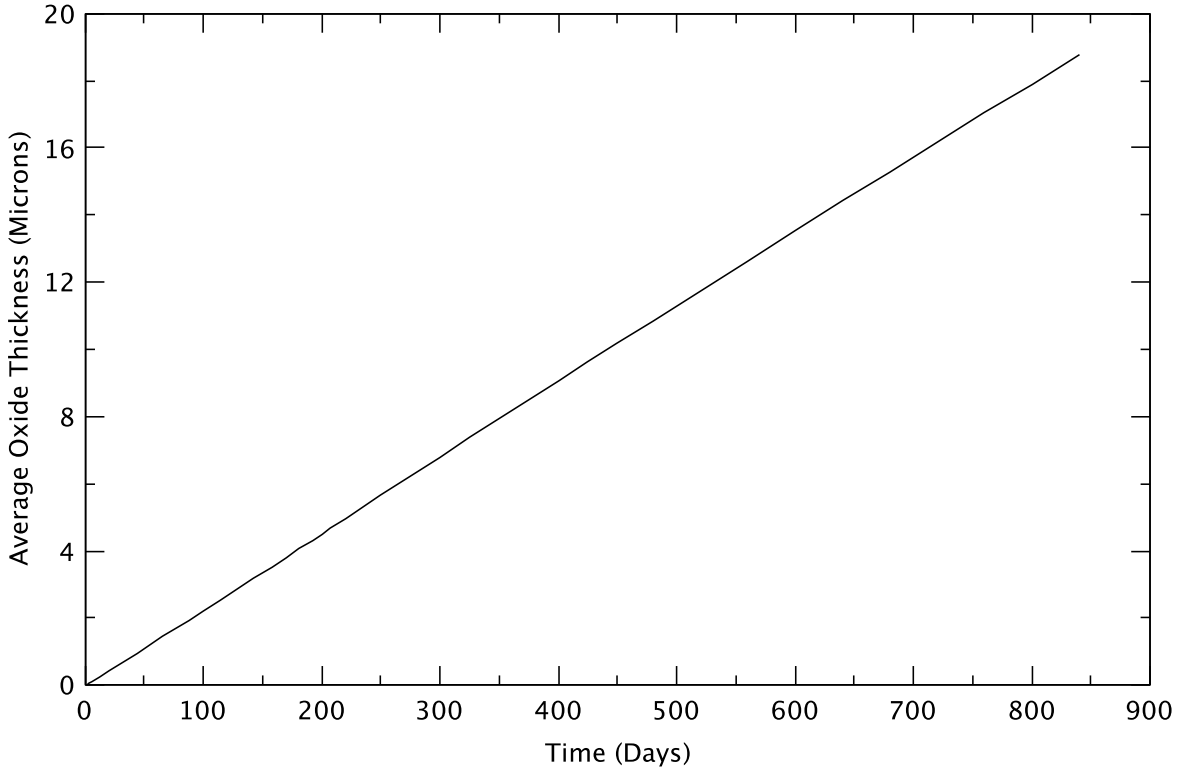

Figure A.2 Average Oxide Layer Thickness as a Function of Time.

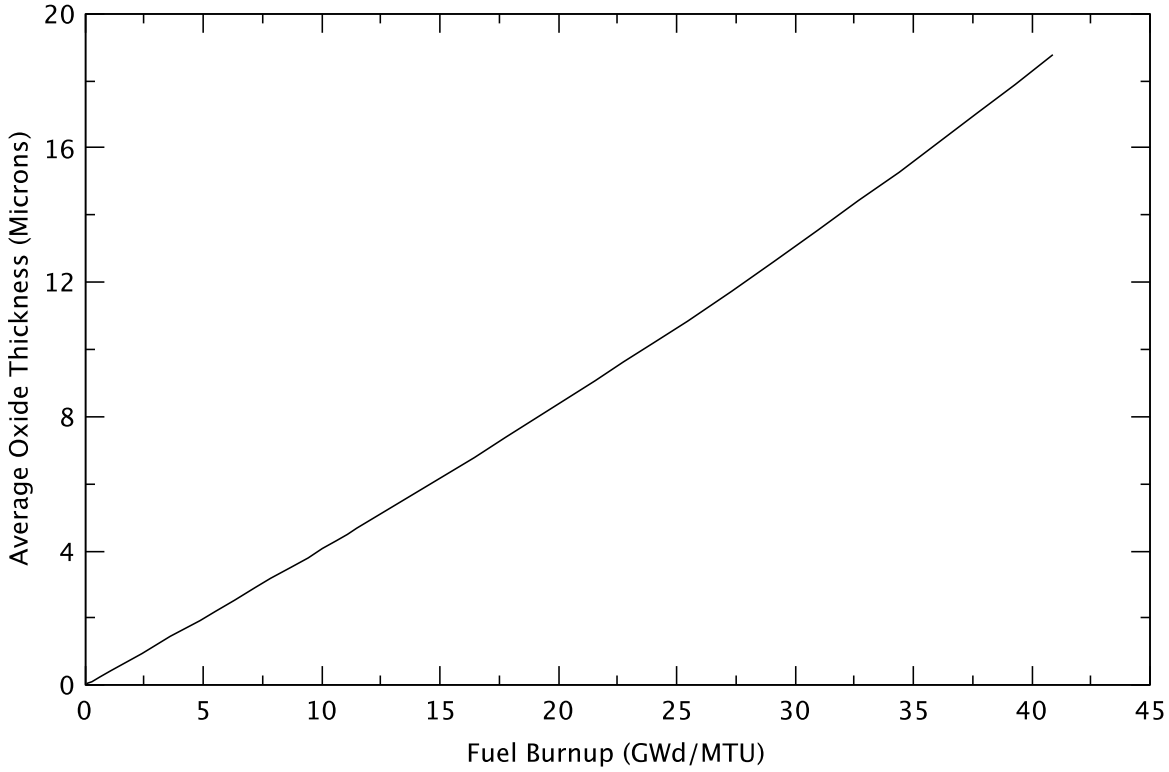

Figure A.3 Average Oxide Layer Thickness as a Function of Burnup.

As a demonstration of the derivation of the average oxide thickness listed in Table A.4 the detailed outputs from FRAPCON are reproduced in Table A.5 Sample FRAPCON Output of

Oxide Thickness for three burnup steps that are close to the three cycle conditions of interest, namely BOC, PHE and EOFPL.

Table A.5 Sample FRAPCON Output of Oxide Thickness

Axial Region	Axial Location (m)	Oxide Layer Thickness (microns)		
		Step 33 (15.125 GWd/t) (~BOC)	Step 40 (23.992 GWd/t) (~PHE)	Step 45 (32.696 GWd/t) (~EOFPL)
1	0.11906	2.695	4.33	6.048
2	0.35719	4.681	7.759	10.507
3	0.59531	5.899	9.859	13.314
4	0.83344	6.659	11.115	15.132
5	1.07156	7.235	11.981	16.579
6	1.30969	7.608	12.451	17.583
7	1.54781	7.763	12.57	18.053
8	1.78594	7.847	12.634	18.353
9	2.02406	7.75	12.448	18.169
10	2.26219	7.592	12.224	17.825
11	2.50031	7.41	12.014	17.412
12	2.73844	7.062	11.589	16.568
13	2.97656	6.566	10.898	15.363
14	3.21469	5.719	9.502	13.318
15	3.45281	4.466	7.367	10.325
16	3.69094	2.663	4.285	6.123
Averaged Thickness		6.2259375	10.18913	14.417

The initial oxide layer thickness for the three exposure conditions of BOC, PHE, and EOFPL can be inferred from Table A.4 or Figure A.3 based on the burnup corresponding to the respective cycle condition. Table A.6 Core Average Burnup gives the average core burnup at three exposure points. The data are derived from the PARCS steady-state .dep file for the model BWR/5 core with GE14 fuel assemblies, and MELLLA+ operating conditions.

Table A.6 Core Average Burnup

Average Burnup (GWd/mt)		
BOC	**PHE**	**EOFPL**
13.8	23.9	32.2

Based on the average burnup from Table A.6 and the corresponding average oxide layer thickness from Table A.5 (also from Figure A.3 and Table A.4) the following initial oxide layer thickness is suggested for each cycle condition of interest.

BOC – 3 microns
PHE – 6 microns
EOFPL – 10 microns

The above values were suggested while considering the existence of lower-than-average burnup in some fuel rods at any given cycle condition. In summary, the NAMELIST variables specified to define the initial oxide thickness are as follows:

DOXLAYER=3.0e-6 (for BOC)
=6.0e-6 (for PHE)
=10.0e-6 (for EOFPL)
FOXLAYER=-1
NRSLV=1

2.3 SEPD Component

The base BWR/5 separator model currently is an "ideal-ideal" separator without carryover or carryunder. Since the transient response is highly sensitive to the inlet enthalpy response, the staff recommended specifying a realistic carryunder [3]. Specifying a fixed carryover and carryunder in the NRC staff's ATWS-I sensitivity study [3] appears to improve the prediction of the dynamic vessel's level response. Therefore, the staff directed BNL to specify a carryover of 0.1% and a carryunder of 0.25% for the ATWS-ED calculations. A carryunder fraction of 0.25% is typical for GE separators and is appropriate for use in the ATWS analysis. A small carryover fraction should also be applied; 0.1% is recommended. While 0.1% is small for a typical separator, the vessel model does not include a dryer, and therefore, the carryover fraction should be representative of the combined carryover of the separator and dryer. A more characteristic carryover fraction would be about 1% if only the separator were considered. For SEPD components 45 and 46, the following two input parameters were specified:

xco=0.001
xcu=0.0025

2.4 Feedwater Control System

In a staff assessment, the feedwater controller in the base BWR/5 model, when compared to analyses performed for the reference plant with TRACG, indicates that early in the transient evaluation, the level is over-predicted [3]. This is due to a difference in the base BWR/5 model for the feedwater controller (FWC) and the three-element plant controller. The primary difference is the location of the sensor for the steam flow signal that is part of the three-element control scheme. The TRACG input deck specifies the sensor's location for the steam flow signal at the MSIV. In the TRACE calculation, this signal was taken at the main steam-line flow restrictor. The staff recommended that to better match the reference analysis, the BWR/5 model FWC sensed steam-flow signal should be derived from a point in the steam line downstream of the MSIV.

When compared to the TRACG analyses for the reference plant, the staff noted that the base BWR/5 FWC did not provide as rapid a dynamic response to reduce FW flow during the transient [3]. This is likely due to a relatively strong contribution to the FW controller response from 1) nominal FW flowrate, and, 2) the integrated level-difference signal.

The FWC for the base BWR/5 model specifies a maximum FW flowrate of 2500 kg/s; it is not consistent with maximum FW system performance for the reference BWR/5. An upper bound of 130% rated should be specified. This corresponds to the maximum achievable core flowrate as analyzed for the FWC failure-to-maximum-demand event.

The parametric effect of increasing the integral gain of the level-difference signal was demonstrated in a sensitivity calculation that the staff undertook [3]. The increase in the proportional gain increases the rapidity of the level response, and it is closer to the reference TRACG calculations in terms of response. As a means to improve the dynamic response of the controller, the staff recommended increasing the proportional gain of the level mismatch from 5 to 10 [3].

Based on the three staff recommendations the following changes were made to the BWR/5 model:

- Defined **SV**-161 to provide steam flow downstream of the MSIVs and use this SV as input to **CB**-72 and **CB**-51.
- In **CB**-71 the proportional gain of level difference was increased to 10.
- In **CB**-76 the maximum feedwater flowrate was increased to 2954.95 kg/s (1.3xnominal).

2.5 Safety Relief Valve Model

The reference BWR/5 plant includes 18 safety relief valves (SRVs) that are arranged in five banks with staggered relief-mode opening pressures. The SRV analytical limit opening and closing pressures were provided for the reference plant in response to staff RAIs [6]. Table A.7 provides the setpoint characteristics for SRV bank pressure.

Table A.7 SRV Relief Mode Pressure Setpoints by Bank

Bank	Number of Valves	Opening Pressure (MPa)	Closing Pressure (MPA)
1	2	7.830	7.327
2	4	7.899	7.396
3	4	7.968	7.465
4	4	8.037	7.534
5	4	8.106	7.602

The TRACG values correspond well with the average of the nominal relief mode and the safety-mode analytical limit. To garner better agreement with the range of the pressures, the staff directed BNL to use the relief mode analytical limit values which are higher than the nominal value of the relief mode. However, the basis for the TRACG values is unclear, while there is a clear basis for the relief mode analytical limit. Table A.7 lists the analytical limits for SRV opening and closing in relief mode operation. These setpoints are used in the TRACE model control system for the SRV/ADS.

Two SRVs are presumed to be out-of-service and are presumed to be the lowest pressure bank SRVs. Seven of the SRVs are part of ADS. The ADS is comprised of the highest pressure SRVs, in other words, four valves from Bank 5 and three valves from Bank 4.

The base BWR/5 model derived the SRV geometry based on the NMP2 LOCA TRACE model [7]. The staff recommended [3] replacing the loss coefficient of 4.5 for the SRV with 0.786 from the NMP2 UFSAR. The higher loss coefficient (4.5) in the base BWR/5 model was derived by lumping losses in the SRV discharge line into a local loss at the valve's throat. The resultant lumped loss coefficient is too large, and results in TRACE not properly predicting SRV choking.

When the SRV is partially open, local losses are increased. To account for this effect, there are two options: 1) TRACE will internally evaluate the local losses, or, 2) a table can be specified

that correlates local loss to the valve's open area fraction. For the greatest consistency with the reference plant, the staff recommended option 2 with the loss parameters taken from the reference TRACG input deck and specified in the KOPEN data for the SRV.

To properly account for the condition of a partially opened SRV, the nodalization of the SRV/ADS must be remodelled completely. The operable SRVs can no longer be lumped into a single valve but require modeling as separate banks with their own lumped valve. Table A.8 defines the operational characteristics of the SRVs by groups, A, B, C1, C2, and D. Figure A.4 shows the corresponding layout of the new valve groupings, each group with its own valve and its own branch off the main steamline.

Table A.8 SRV Grouping

Bank	Number of Valves	Opening Pressure (MPa)	Closing Pressure (MPa)	Valve Group	Number of Valves in Group	ADS
1	2	7.830	7.327	OOS	2	No
2	4	7.899	7.396	A	4	No
3	4	7.968	7.465	B	4	No
4	4	8.037	7.534	C1	1	No
				C2	3	Yes
5	4	8.106	7.603	D	4	Yes

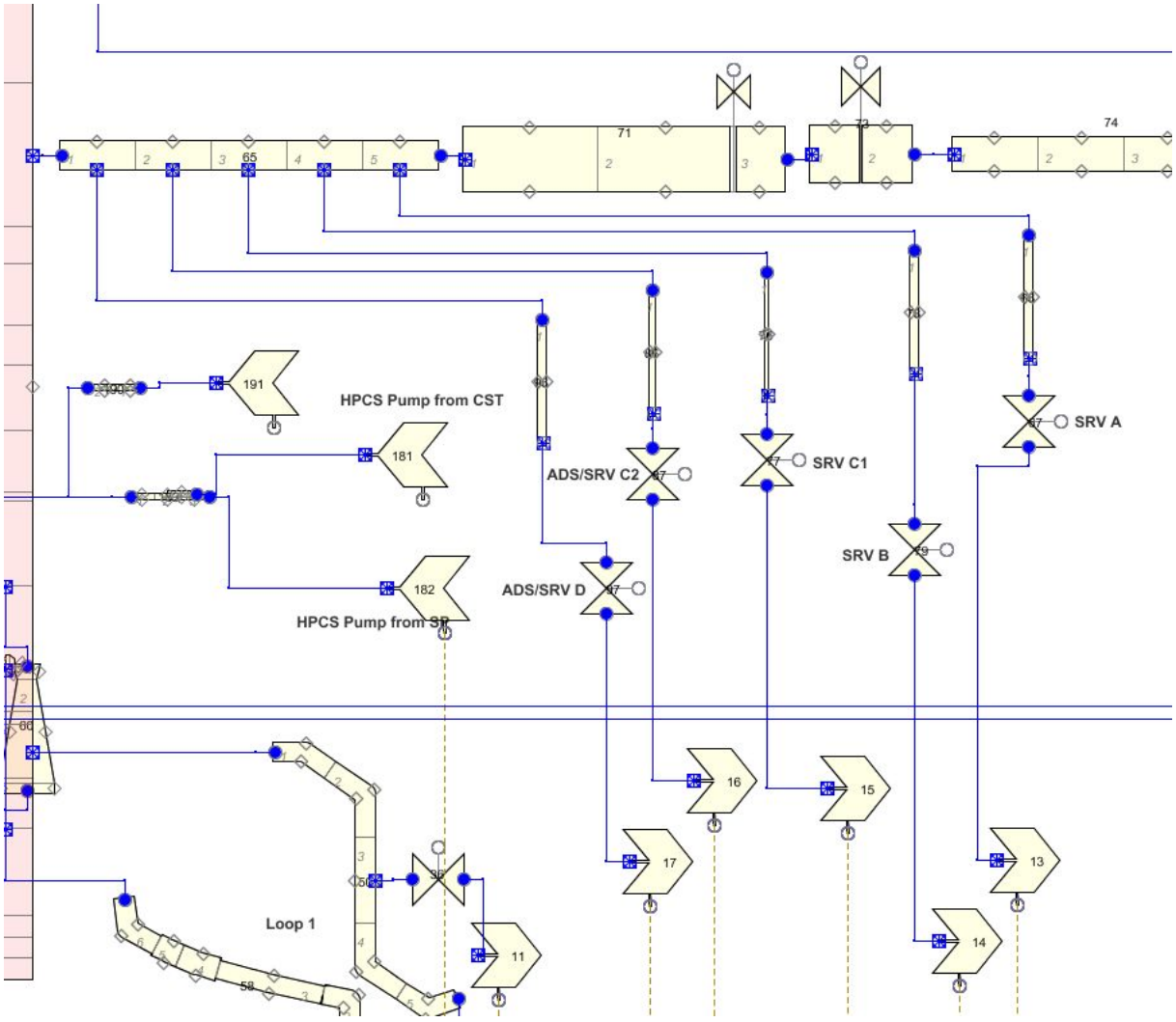

Figure A.4 Layout of SRV Banks

The main steam line PIPE 65 is renodalized from four to five nodes, enabling each valve group to branch off a separate node. Table A.9 identifies hydraulic components associated with each valve group.

Table A.9 Components Associated with Each SRV Bank/Group

SRV Bank	Valve Group	PIPE 65 Cross Flow Connection	Standpipe	Single Junction Valve	Break Connection	Valve Function
5	D	Cell 1	PIPE 96	VALVE 97	Break 17	SRV/ADS
4	C2	Cell 2	PIPE 86	VALVE 87	Break 16	SRV/ADS
	C1	Cell 3	PIPE 76	VALVE 77	Break 15	SRV
3	B	Cell 4	PIPE 78	VALVE 79	Break 14	SRV
2	A	Cell 5	PIPE 66	VALVE 67	Break 13	SRV
1	OOS	Not modeled				

It is noted that the standpipe volume is based on the half-volume of an SRV. The junction area (A_J) in cell face #1 is derived from the area of the stub tube for the main steam tee in the original ISL model. The flow area in cell face #2 is the full flow area (100%) of the SRV.

The SRVs are modeled by single-junction valves. The valves' properties are summarized in Table A.10. The valves' operation is controlled by two control signals, CB-31 and CB-32, the former for valves that belong to the ADS group and the latter for those that only perform the relief function. The valve-loss coefficient when fully open is 0.786, corresponding to the loss (K_F) in face #2 of the standpipe. The valve's local loss coefficients with partial opening is based on the reference TRACG input deck and is specified in the KOPEN data for the valve.

Table A.10 SRV/ADS Valve Properties

Valve Group	Single Junction Valve	Number of SRV Valves	Valve Function	Control Signal
D	VALVE 97	4	SRV/ADS	CB-31
C2	VALVE 87	3	SRV/ADS	CB-31
C1	VALVE 77	1	SRV	CB-32
B	VALVE 79	4	SRV	CB-32
A	VALVE 67	4	SRV	CB-32

The control logic for the SRV/ADS is shown in Figure A.5. The various trips, signal variables and control blocks are summarized in Table A.11. An adjustment table is defined for each valve group to control its opening and closing according to the output of one of the two control blocks, CB-31 and CB-32. The valve groups controlled by these two control blocks are identified in Table A.12 and Table A.13. The two valve groups that perform the ADS function, C2 and D, receive their control input from CB-31 while the other valve groups receive their control signal from CB-32.

For the single-junction valves (**VALVE** 97, 87, 77, 79 and 67) the following additional changes were made to the TRACE input to reflect the new SRV model:

Kfac = **Kfacr** = 0.786 [3]
Intlossoff = 1 (TRACE internal additive valve flow loss model is not included and the flow loss is based on the KOPEN table)
NKOPEN = 11 (number of pairs of data in the KOPEN table)
KOPEN table.
rvmx = 2.0 (maximum rate of VALVE flow-area fraction or relative valve stem position adjustment (1/s)) [3]

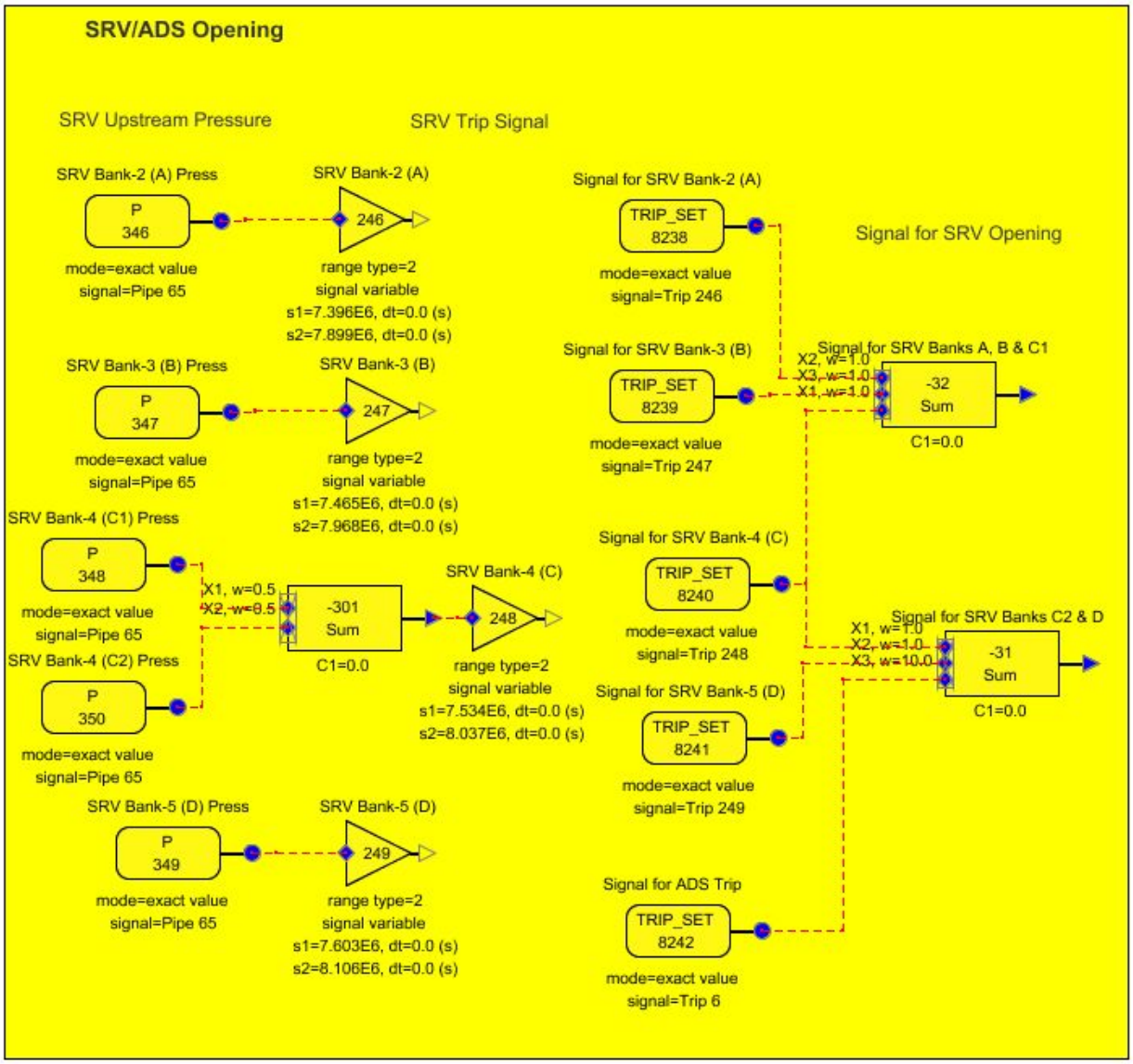

Figure A.5 Control Logic for the SRV/ADS

Table A.11 Control Variables for the SRV/ADS

Trips					
Trip # (IDTD)	**Signal range type # (ISRT)**	**Variable (IDSG)**	**Setpoint 1 (setp-1)**	**Setpoint 2 (setp-2)**	**Function**
6	2	SP liquid temperature (SV-111)	0.0	344.26 K	Initiate opening of ADS valves (HCTL)
246	2	SRV upstream pressure (SV-346)	7.396E+06	7.899E+06	Control SRV Bank 2
247	2	SRV upstream pressure (SV-347)	7.465E+06	7.968E+06	Control SRV Bank 3
248	2	SRV upstream pressure (CB-301)	7.534E+06	8.037E+06	Control SRV Bank 4
249	2	SRV upstream pressure (SV-349)	7.603E+06	8.106E+06	Control SRV Bank 5

Signal variables		
SV #	**Signal Source**	**Parameter type**
111	FILL-182	Liquid temperature: SP temperature
346	PIPE 65, cell 5	Pressure: SRV Bank 2 upstream pressure
347	PIPE 65, cell 4	Pressure: SRV Bank 3 upstream pressure
348	PIPE 65, cell 3	Pressure: SRV Groups C1 & C2 upstream pressure
350	PIPE 65, cell 2	Pressure: SRV Groups C1 & C2 upstream pressure
349	PIPE 65, cell 1	Pressure: SRV Bank 5 upstream pressure
8238	TRIP-246	Trip set status value for SRV Bank 2
8239	TRIP-247	Trip set status value for SRV Bank 3
8240	TRIP-248	Trip set status value for SRV Bank 4
8241	TRIP-249	Trip set status value for SRV Bank 5
8242	TRIP-6	Trip set status value for HCTL

Control blocks				
CB #	**Type**	**Gain**	**Inputs**	**Remark**
-301	sum	1.0	SV-348 (wt=0.5) SV-350 (wt=0.5)	Calculate the mean of two pressures
-31	Sum	10.0	SV-8242 (wt=10.) SV-8241 (wt=1.) SV-8242 (wt=1.)	See Table A.15.
-32	Sum	1.0	SV-8238 (wt=1.) SV-8239 (wt=1.) SV-8240 (wt=1.)	See Table A.13.

Table A.12 Number of Valves Open According to Output of CB-31

CB-31 Output	SRVs Open	Number of Valves Open
0.0	0	0
1.0	Group C2	3
2.0	Group C2 & D	3+4 = 7
10.0	Group C2 & D	3+4 = 7
11.0	Group C2 & D	3+4 = 7
12.0	Group C2 & D	3+4 = 7

Table A.13 Number of Valves Open According to Output of CB-32

CB-32 Output	SRVs Open	Number of Valves Open
0.0	0	0
1.0	Group A	4
2.0	Groups A, B	4+4 = 8
3.0	Groups A, B, C1	4+4+1 = 9

2.6 Heat Capacity Temperature Limit

The staff directed BNL to revise the HCTL from 175°F to 160°F. The HCTL had been increased to 175°F to assure a timing for the emergency depressurization (ED) that was in better agreement with the reference TRACG calculations. However, the early timing of the ED in the previous TRACE calculations was linked to higher thermal power in the reactor, caused by numerous differences in the plant model, including the feedwater control system and differences in the predicted rate of condensation heat transfer in the downcomer. If the HCTL is too high, then the suppression pool may exceed temperature limits purely as a function of exhausting steam into the pool once the true capacity is exhausted. According to the staff's Safety Evaluation for the MELLLA+ Licensing Technical Report (Reference [1] in the main body), an HCTL of 160°F is appropriate.

TRIP 6 which actuates the ADS for the ED cases on suppression-pool temperature was revised to have a setpoint of 344.26 K (160°F).

2.7 Boron Transport Model

During executable testing, it was found that the transient reactor power response was also sensitive to the size of the selected time-step. While not fully diagnosed, the staff found that transport of boron in the bottom of the lower plenum also was sensitive to it. This issue was identified when calculations were performed using SETS and semi-implicit (SI) numerics. The use of SI limits numerical diffusion and is attributed to significant differences in the predicted axial distribution of boron in the bottom of the lower plenum. Since the calculation is sensitive to the time-step size, and TRACE internally controls the time-step size, it is possible for TRACE to predict different transient progressions based on factors such as the computing platform. This was not considered robust, and therefore, the staff sought to develop revised guidance for treating boron injection into the lower plenum to achieve a more robust calculation scheme. The new methodology is described in the boron transport methodology document, which was provided to BNL [2].
The new approach is based on an external control system that evaluates flow conditions in the lower plenum to decide if entraining conditions exist. If they do, then the controller will allow the

injection of boron into the TRACE vessel. TRACE then will internally track the entrained boron. For boron that becomes stratified, the controller will externally track the amount of stratified boron by solving the stratified boron continuity equation. It is useful to think of stratified and entrained boron as two different masses in this approach. Remixing is the phenomenon by which stratified boron may be removed and converted to entrained boron. In the stratified boron continuity equation, the source term of stratified boron mass is injected boron that is not entrained at the time of injection.

The following describes a scheme developed to model boron transport in the lower plenum by using TRACE control components. It is needed for a more realistic simulation of the effect of boron injection in the lower plenum because TRACE does not have a mechanistic model explicitly able to simulate the mixing, stratification, and remixing of boron. The NRC staff provided modeling guidelines and an approach to enable the TRACE simulation to approximate the expected behavior of the borated solution once injected into the vessel [2].

The key phenomena of interest are the following: stratification, entrainment, remixing, and circulation. Herein, the term circulation refers to an "alternative" flow path of boron into the core, whereby previously entrained boron travels with the reactor coolant first into the core, through the separators, down the downcomer and returns to the core. The circulation of boron is handled by TRACE implicitly when the solute-tracking option is turned on in a TRACE calculation (ISOLUT=1). Therefore, the proposed method [2] focuses on adequately treating the mixing and remixing phenomena.

The boron transport model captures the following:

- inhibited boron transport into the core when low-flow conditions exist, and the injected solution stratifies in the lower vessel
- the onset of entraining conditions, and the remixing of the stratified boron

The model simulates the SLCS injection using a combination of a FILL component and a PIPE component that will inject at a specified time-dependent flowrate and an effective boron concentration that accounts for boron mixing and remixing. The mechanisms for mixing and remixing in BWRs are discussed in more detail in [2].

Depending on core flow conditions, boron injected through the SLCS may either mix or become stratified. When fully mixed, the boron injected into the vessel is completely entrained in the core flow and becomes available to circulate to the core. Under reduced core flow conditions the mixing is not 100% efficient and the boron solution will stratify or settle to the bottom of the reactor vessel, removing some of the injected boron from circulation to the core. Such removal of the boron can be simulated by reducing the concentration of the source boron. Conceptually, the source boron once it has entered the vessel is split into two streams, entrained and stratified. The fractional split between the two is denoted by an empirical factor γ the mixing coefficient. Thus,

$$\text{Boron in entrained stream} = \gamma * C_{SLCS} * W_{SLCS} \quad (1)$$

$$\text{Boron in stratified stream} = (1.0-\gamma) * C_{SLCS} * W_{SLCS} \quad (2)$$

where,

C_{SLCS} = Nominal value of boron concentration in the SLCS,
W_{SLCS} = Mass flowrate of boron solution in the SLCS,
γ = Mixing coefficient.

Qualitatively, when entraining conditions exist, the mixing coefficient is unity, and when the core flowrate is low and the solution is presumed to stratify, the mixing coefficient is zero.

A second phenomenon that affects boron transport in the reactor vessel is remixing that occurs when the core flowrate is sufficiently high to entrain borated solution that has stratified in the bottom of the lower plenum (BLP). This is characterized by a flow-dependent remixing coefficient θ. The boron delivered by this remixing stream is given by,

$$\text{Boron in remixing stream} = \theta * C_{BLP} * W_{BLP} \quad (3)$$

where,

C_{BLP} = Boron concentration in the bottom of lower plenum,
W_{BLP} = Liquid mass flowrate of core flow that egresses the lower plenum,
θ = Remixing coefficient.

The boron transport model is designed to keep track of the delivery of entrained boron into the core due to mixing and remixing. An effective injection concentration can then be calculated according to the following equation, which sums all sources of newly entrained boron and the two sources represented by equations (1) and (3).

$$C_{FILL} * W_{SLCS} = \gamma * C_{SLCS} * W_{SLCS} + \theta * C_{BLP} * W_{BLP} \quad (4)$$

where C_{FILL} is the effective injection concentration.

In a TRACE calculation, C_{FILL} is evaluated as a function of time by using control components and the output becomes the boron concentration for the FILL component representing the SLCS boron tank. It is noted that the actual concentration of boron injected into the reactor vessel is C_{SLCS} and when the mixing coefficient γ is less than unity, some of the boron injected into the vessel will settle in the BLP. It is necessary to know the amount of boron (and its concentration) that has stratified there because this is the source of boron for the remixing (second term on the right-hand side of equation (4)). This necessitates setting up and iteratively solving the stratified boron continuity equation for the BLP. Since TRACE cannot directly simulate stratification, a control system external to the thermal-hydraulic components must calculate and artificially track the concentration of stratified boron solution in the lower plenum. The following equation is the continuity equation for the lower plenum's mass of stratified boron. Only the stratified mass is considered because TRACE will internally track entrained boron. This continuity equation is fully generalized and may be used to account for conditions such as prompt stratification (i.e., stratification of the flow as it is injected into the vessel) and remixing occurring simultaneously.

$$M_B(t) = C_{BLP} \int_{BLP} \rho dV = \int_{t'=0}^{t} [(1-\gamma) C_{SLCS} W_{SLCS} - \theta C_{BLP} W_{BLP}] dt' \quad (5)$$

where,

M_B is the mass of stratified, soluble boron in the lower plenum,
ρ is the liquid density in the BLP,
V is the liquid volume in the BLP,
t is time.

This equation tracks the addition of boron to the lower plenum through stratification (first term inside the time integrand), and the removal of boron from the lower plenum due to remixing (second term inside the integrand). This equation can be solved in TRACE iteratively using

control blocks to determine the time-dependent, average concentration of stratified boron in the lower plenum, i.e., C_{BLP}.

In equations (4) and (5), W_{BLP} represents the "sweeping" flow through the bottom of the lower plenum and it is based on the mass flow calculated by TRACE. It then becomes important to understand the meaning of the bottom of the lower plenum in this context. Since the stratified boron is being tracked in an external controller, the methodology relies on the specification of the control volume that defines the BLP. NRC staff recommended a control volume that encompasses all cells in the vessel below the downcomer exit point. This lower portion of the lower plenum is the region of interest because this volume is isolated from the total jetpump flow. Physically, the lower plenum's control volume represents the portion of it that may stagnate when the core flowrate is low. TRACE will internally calculate any portion of the total core flow that sweeps through this lower plenum control volume; however, since it is isolated, any flow entering the region also must exit. This approach for defining the BLP control volume allows for ease in subsequently defining the "sweeping" flow through the bottom of the lower plenum (represented as W_{BLP} in the equations above).

The control volume for the BLP then is defined to be the six cells occupying axial levels L1, L2, and L3 in rings R1 and R2 of the BWR/5 TRACE VESSEL component. The lower plenum sweeping flowrate, $W_{BLP,}$ is then defined as the positive liquid mass flow exiting this control volume at the interface between axial levels three and four in rings 1 and 2. W_{BLP} has two components, a ring 1 (R1) and a ring 2 (R2) contribution; they are summed to give the net contribution. The respective contribution is set to zero if the axial liquid flow between L3 and L4 in a ring is negative, i.e., flow enters the control volume from axial level 4.

To simulate the total delivery of entrained boron into the core due to both mixing and remixing, the SLCS injection is simulated as occurring upstream of both the SLCS injection sparger and the lower plenum. The proposed location of injection location is directly beneath the jet pump's outlet nozzle. Further, TRACE is known to not conserve momentum for vessel cells with a zero velocity boundary condition along the flow direction, as is the case at the bottom of the downcomer. To partially offset the loss of momentum at this location, the NRC staff recommended directing the SLCS injection radially inward at the outer face of ring three. While the momentum addition and momentum loss will not fully cancel out each other, this approach aims to minimize the numerical impact of the SLCS injection on total momentum. Furthermore, the injection temperature and mass flowrate are set to be equal to the nominal values for the SLCS to preserve mass and energy.

The final component of this methodology is the specification of the flow-dependent values of the mixing and remixing coefficient. The NRC staff provided specific modeling guidelines to address the important physical phenomena associated with boron transport, and documented their basis [2]. For lower-plenum injection, the staff recommends using GEH's mixing and remixing coefficients [8].

The boron transport model implemented in the TRACE input model for the BWR/5 is a set of control components that solves for C_{FILL} and C_{BLP} using the continuity equations expressed in Equations (4) and (5). Specifically, the control system calculates the following two parameters:

$$C_{FILL} = (\theta * C_{BLP} * W_{BLP}) / W_{SLCS} + \gamma * C_{SLCS} \quad (6)$$

$$C_{BLP} = M_B / M_{BLP} \quad (7)$$

In equation (7) M_B is obtained from the time integration indicated in equation (5) while M_{BLP} is the mass of liquid in the BLP. M_{BLP} is evaluated by summing the liquid inventory in the six cells of the BLP control volume. The liquid inventory in a cell is calculated by,

$$(1-\alpha)*\rho_l*V_f$$

where,

α = gas void fraction in the cell,
ρ_l = density of liquid in the cell,
V_f = cell free volume.

A control system, shown in Figure A.6, was established in the TRACE BWR/5 model to implement the boron transport methodology described above. Table A.14 lists and defines trips, signal variables (SV) and control blocks (CB) that are part of the boron transport control system. It is noted that in evaluating $C_{FILL,}$ a special logic is implemented to handle the particular case of no SLCS flow ($W_{SLCS} = 0$) thus avoiding division by zero in equation (6). FILL 196, the component that acts as the SLCS tank for injection into the lower plenum was modified to be a type-10 FILL; it inherits all the required generalized-state parameters from the boron transport control system. The boron injection point also was relocated to inject radially inward from the outside surface of ring 3 in axial level 4.

Table A.14 Control Components for the Boron Transport Control System

Control Component	Function
TRIP 196	Initiate lower plenum boron injection; trip is based on time
TRIP 401	Trip (type 10) is ON when SLCS flow (CB 474) is less than or equal to 0.0 ON when $W_{SLCS} \leq 0.0$ OFF when $W_{SLCS} > 0.0$
SV 136	Total core flow evaluated at the outlet of (JetPump 60)
SV 196	Trip set status of TRIP 196
SV 401	Liquid mass flow in ring 1, level 3 = W_l(R1, L3) [1]
SV 402	Liquid mass flow in ring 2, level 3 = W_l(R2, L3) [2]
SV 403	Trip set status of TRIP 401 = 1.0 when TRIP 401 is ON = 0.0 when TRIP 401 is OFF
SV 431	Void fraction in ring 1, level 1 = α(R1, L1)
SV 432	Void fraction in ring 1, level 2 = α(R1, L2)
SV 433	Void fraction in ring 1, level 3 = α(R1, L3)
SV 437	Liquid density in ring 1, level 1 = ρ_l(R1, L1)
SV 438	Liquid density in ring 1, level 2 = ρ_l(R1, L2)
SV 439	Liquid density in ring 1, level 3 = ρ_l(R1, L3)
SV 441	Void fraction in ring 2, level 1 = α(R2, L1)
SV 442	Void fraction in ring 2, level 2 = α(R2, L2)
SV 443	Void fraction in ring 2, level 3 = α(R2, L3)
SV 447	Liquid density in ring 2, level 1 = ρ_l(R2, L1)
SV 448	Liquid density in ring 2, level 2 = ρ_l(R2, L2)
SV 449	Liquid density in ring 2, level 3 = ρ_l(R2, L3)
SV 468	Normalized core flowrate = output of (CB 89)
CB 89	Normalized core flow = (SV 136)*7.3149E-5 100% core flow = 13670 kg/s

Control Component	Function
CB 196	Calculate time after TRIP 196 by integrating (SV 196)
CB 400	Constant = 0.0
CB 403	Equals 1.0 if (SV 401) > 0.0; otherwise equals 0.0
CB 404	Equals 1.0 if (SV 402) > 0.0; otherwise equals 0.0
CB 405	(SV 401) * (CB 403) = positive flow contribution from (R1, L3)
CB 406	(SV 402) * (CB 404) = positive flow contribution from (R2, L3)
CB 434	(1.0 – (SV 431)) = 1.0 - α(R1, L1)
CB 435	(1.0 – (SV 432)) = 1.0 - α(R1, L2)
CB 436	(1.0 – (SV 433)) = 1.0 - α(R1, L3)
CB 437	(CB 434) * (SV 437) * V(1,1) = mass of liquid in (R1, L1), where V(1,1) = free volume of VESSEL (R1, L1)
CB 438	(CB 435) * (SV 438) * V(1,2) = mass of liquid in (R1, L2), where V(1,2) = free volume of VESSEL (R1, L2)
CB 439	(CB 436) * (SV 439) * V(1,3) = mass of liquid in (R1, L3), where V(1,3) = free volume of VESSEL (R1, L3)
CB 444	(1.0 – (SV 441)) = 1.0 - α(R2, L1)
CB 445	(1.0 – (SV 442)) = 1.0 - α(R2, L2)
CB 446	(1.0 – (SV 443)) = 1.0 - α(R2, L3)
CB 447	(CB 444) * (SV 447) * V(2,1) = mass of liquid in (R2, L1), where V(2,1) = free volume of VESSEL (R2, L1)
CB 448	(CB 445) * (SV 448) * V(2,2) = mass of liquid in (R2, L2), where V(2,2) = free volume of VESSEL (R2, L2)
CB 449	(CB 446) * (SV 449) * V(2,3) = mass of liquid in (R2, L3), where V(2,3) = free volume of VESSEL (R2, L3)
CB 450	(CB 437)+(CB 438)+(CB 439)+(CB 447)+(CB 448)+(CB 449) = total mass of liquid in R1 & R2 in the lower plenum (L1 to L3)
CB 462	SLC vapor mass flow = 0.0
CB 463	SLC liquid temperature = 316.48 K
CB 464	SLC vapor temperature = 574.249 K
CB 465	SLC vapor volume fraction = 0.0
CB 466	SLC fluid pressure = 8.7217E6 Pa
CB 467	SLC partial pressure of non-condensable gas = 0.0
CB 470	Mixing coefficient, γ. This variable is a function of normalized core flow.
CB 471	Remixing coefficient, θ. This variable is a function of normalized core flow.
CB 472	C_{SLCS} = Boron concentration in SLCS tank = 0.02369 kg-boron/kg-water
CB 473	1.0 - (CB 470) = 1.0-γ
CB 474	W_{SLCS} = SLCS mass flowrate after trip to initiate boron injection.
CB 475	(CB 473)*(CB 472) = (1.0-γ)* C_{SLCS}
CB 476	(CB 472)*(CB 470) = γ* C_{SLCS}
CB 477	Reset (CB 474) with a minimum value of 1.0E-10. This is to avoid division by zero in (CB 481).
CB 478	(CB 474)*(CB 475) = (1.0-γ)* C_{SLCS}* W_{SLCS}
CB 479	W_{BLP} = (CB 405)+(CB 406) = total recirculation flow through the lower plenum
CB 480	(CB 479)*(CB 485)*(CB 471) = W_{BLP}* C_{BLP}*θ
CB 481	(CB 480)/(CB 477) = W_{BLP}* C_{BLP}*θ/ W_{SLCS}

CB 482	Logic switch based on value of (SV 403), i.e.
	If (SV 403) = 1.0, Output = (CB 475) = (1.0-γ)* C_{SLCS}
	If (SV 403) = 0.0, Output = (CB 481) = W_{BLP}* C_{BLP}*θ/ W_{SLCS}

CB 483	(CB 478) – (CB 480) = (1.0-γ)* C_{SLCS}* W_{SLCS} - W_{BLP}* C_{BLP}*θ

Control Component	Function
CB 484	Integrate (CB 483) over time. This is the mass of stratified boron in the lower plenum, $M_B(t)$
CB 485	(CB 484) / (CB 450) This gives the stratified boron concentration in the lower plenum, C_{BLP}
CB 486	(CB 476) + (CB 482) This is the effective injection boron concentration C_{FILL} $C_{FILL} = \gamma^* C_{SLCS} + W_{BLP}^* C_{BLP}^* \theta W_{SLCS}$ when $W_{SLCS} > 0.0$ $C_{FILL} = C_{SLCS}$ when $W_{SLCS} \leq 0.0$
[1] The request for liquid mass flow in the axial direction necessitates setting NAMELIST variable IMFR = 1. [2] The axial flow area fraction at R2, L3 is reset to its original value. A value of 0.0 was specified when a single junction valve was placed at R2, L3 to control boron mixing and remixing in the lower plenum.	

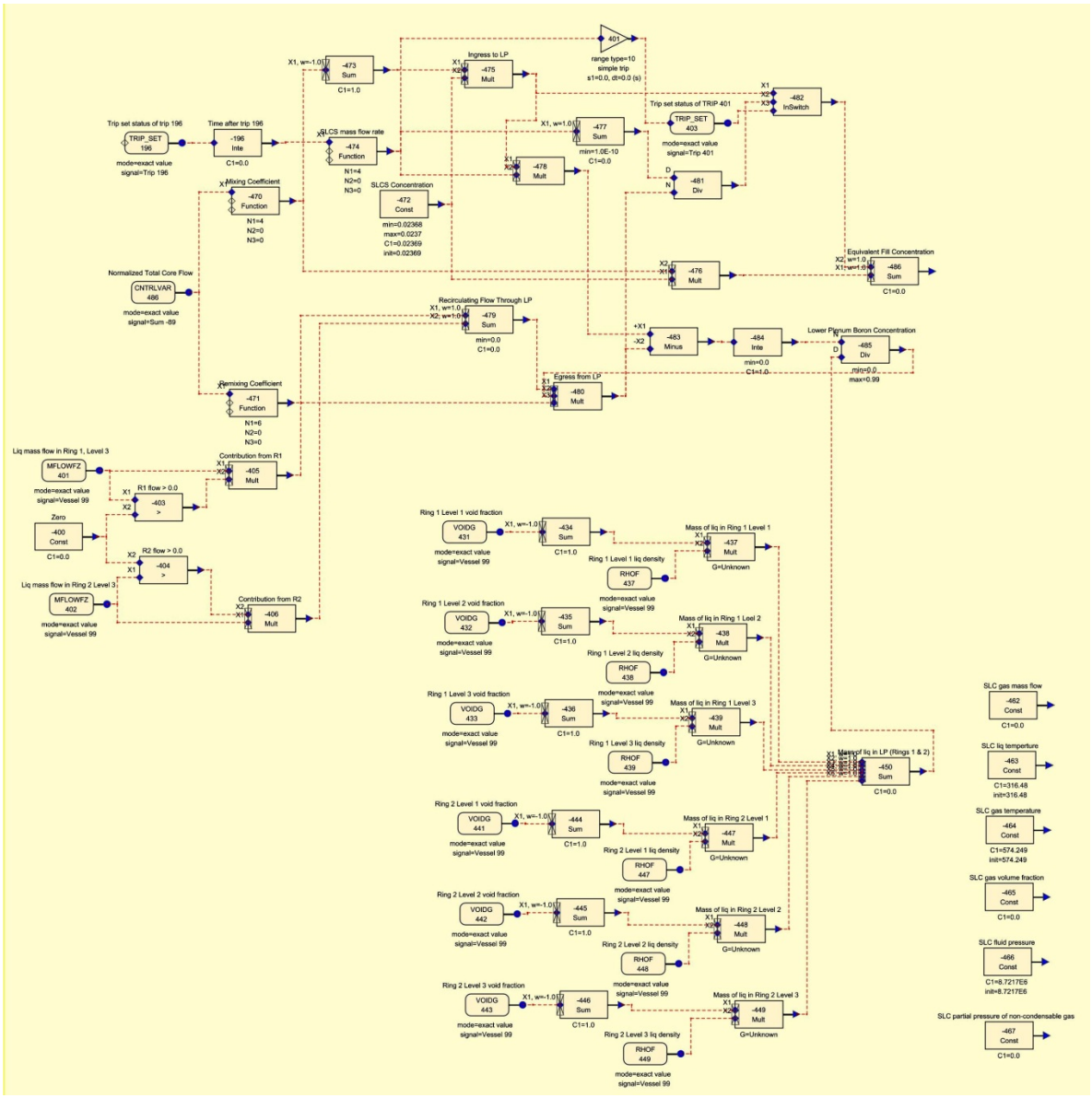

Figure A.6 Boron Transport Control System

The staff proposed a test problem whereby the controller is driven by artificial signals supplied to the control system. The primary signal is a core flowrate boundary condition. This problem was used to test the staff's prototype controller. In particular, the staff proposed a test problem wherein the controller is driven by an externally supplied core flowrate table that varies core flow as a function of time. The core flowrate varies between 0% and 120% of rated flow. This allows full exercise of the different mixing and remixing regimes. The flowrate initially drops to allow for predicting the accumulation of stratified boron. Then, flowrate is set to a flow above the entrainment threshold but below the remixing threshold to confirm that the stratified boron inventory is held static. Finally, the core flowrate is increased to verify the depletion of the stratified boron.

The boron transport control system, as implemented in the BWR/5 model, was verified against the results of the staff's test calculation based on the prototype controller. The results indicate that this implementation generates control block outputs that match the results of the prototype controller for the agreed-upon problem [3].

2.8 Suppression Pool Heat Structure

A recent code fix in V5.509 corrects an error in previous calculations of heat transfer between the containment fluid and the heat structures. For calculations where the heat capacity of the containment is important, as in the case of ATWS-ED [3], the staff recommended modeling the containment's heat structures. The addition of these structures provides heat sinks and increases the suppression pool's heat capacity.

Following is a description of changes made to the CONTAN component of the base BWR/5 model for the added containment heat structures. The modified CONTAN component retains the basic two-compartment setup of the original CONTAN model [7], a drywell and a wetwell. There is no change to the junction connections between the two compartments. Notable changes to the original model are the following:

- updated geometrical inputs to align with the containment design parameters used in the power uprate analyses of the reference BWR/5 plant [9]
- added containment-specific heat structures

The revised CONTAN component data in the TRACE input are based on the following tables in [9]. These tables are referenced as {S1} through {S4} in deriving the CONTAN data.

S1: Table 6.2-1 Thermophysical Properties of Passive Heat Sinks
S2: Table 6.2-2 Modeling of Passive Heat Sinks
S3: Table 6.2-3 Containment Design Parameters
S4: Table 6.2-9 Initial Conditions for Containment Response Analysis

The derivation of the geometrical inputs for the CONTAN model is discussed first followed by the development of the inputs for the containment heat structures. It is noted that in the following discussion, the TRACE inputs and their corresponding input variable names are indicated in bold type.

Compartment Data

Compartment Identification (**ICTBL**):
992 = wetwell (WW) = suppression pool (SP) + suppression chamber (air space)
991 = drywell (DW)

All geometric data are derived assuming that the suppression pool is at the minimum LWL (low water level) of 23.47 ft {S3} (7.154 m).

The DW free volume (**VOL for 991**) is calculated as follows:

DW net free volume including downcomer (DC) vent volume = 306200 ft^3 {S3, footnote 1}

DC vent volume = DC length in air space * DC flow area
DC length in air space = DW floor thickness + height of suppression chamber (SC)
SC wall area = 10363 ft^2 {S2, Heat Sink No. 14}
SP diameter, internal diameter (ID) = 91 ft [10]
Height of SC = 10363/(π *91) = 36.25 ft = 11.05 m
DC floor thickness = 0.4008+0.01562+4. {S2, Heat Sink No. 8} = 4.4164 ft
DC length in air space = 36.25+4.4164 = 40.67 ft
Number of DCs = 121 {S3}
DC diameter, ID = 23.25 in {S3} = 0.59055 m

DC flow area = 121* π (23.25/12)^2/4 = 356.7 ft^2 = 33.14275 m^2
DC vent volume = 356.7*40.67 = 14510 ft^3
DW net free volume = 306200-14510 = 291690 ft^3 = 8260 m^3

(**VOL for 991**) = **8260 m^3**

The DW spill volume (**VMAX for 991**) is calculated as follows:

Assume DW floor area (excluding space occupied by DCs) = SP surface area
= 5800 ft^2 {S3, footnote 4} = 539.0 m^2
Assume DC has a 6" (0.1524 m) extension above the DW floor

DW spill volume = 5800*6/12 = 2900 ft^3 = 82.1 m^3

(**VMAX for 991**) = **82.1 m^3**

Area of interface between pool and vapor in DW (**APOOL for 991**) = SP surface area

(**APOOL for 991**)[5] = **539.0 m^2**

Initial liquid mass in DW (**RML for 991**) arbitrarily is set to 0.1 kg

(**RML for 991**) = **0.1 kg**

Liquid volume table versus pool depth for the DW (**DEPTH for 991**)

(**DEPTH for 991**) = [vol, depth] in pairs = [**0.0 0.0 82.1 0.1524**]

The WW free volume (**VOL for 992**) is calculated as follows:

WW free volume = SP volume + SC (air space) volume
SP volume = 145200 ft^3 {S3, footnote 3} = 4112 m^3
SC (air space) volume = 199800 ft^3 {S3, footnote 2} =5658 m^3
WW free volume = 4112+5658 = 9770 m^3

(**VOL for 992**) = **9770 m^3**

The WW spill volume (**VMAX for 992**) is set to equal the free volume.

(**VMAX for 992**) = **9770 m^3**

Area of interface between pool and vapor in WW (**APOOL for 992**) = SP surface area

(**APOOL for 991**)[e] = **539.0 m^2**

Initial liquid mass in WW (**RML for 992**) = (density of water)*(SP volume)

Density of water at 90°F °F (305.4 K) and a pressure of ~ 1 atm = 995 kg/m^3
Initial liquid mass in WW (**RML for 992**) = 995*4112 = 4.091*10^6 kg

[5] This parameter is not used because the compartment pool level tracking flag is on (**ITRKL=1**), and the interface area is based on the depth table input (**DEPTH**).

(**RML for 992**) = **4.091*10^6 kg**

Height of WW = Height of SC + LWL in SP
Height of WW = 36.25+23.47 =59.27 ft = 18.2 m

Liquid volume table versus pool depth for the WW (**DEPTH for 992**)

(**DEPTH for 992**) = [vol, depth] in pairs = [**0.0 0.0 9770.0 18.2**]

Initial conditions for DW (Compartment **991**) {S4}:

Pressure (P) = 0.75 psig = 15.446 psia = 1.065*10^5 Pa
Temperature (**TL & TV**) = 135°F = **330.4 K**
Relative humidity = 40%

Initial partial pressure of air (PA) = P-PV
PV = partial pressure of water vapor

Using the definition of relative humidity,

Relative humidity = PV/PG
Where PG = saturation pressure at the same temperature as the water vapor in air

At 135 °F, PG = 2.5375 psia.

PV = (relative humidity)*PG = 0.4*2.5375 = 1.0150 psia

Initial partial pressure of air (PA) = 15.446-1.015 = 14.431 psia = 9.950*10^4 Pa

(**P for 991**) = **1.065*10^5 Pa**
(**PA for 991**) = **9.950*10^4 Pa**

Initial conditions for WW (Compartment **992**) {S4}:

Pressure (P) = 0.75 psig = 15.446 psia = 1.065*10^5 Pa
Temperature (**TL & TV**) = 90°F = **305.4 K**
Relative humidity = 100%

At 90 °F, PG = 0.69813 psia.

PV = (relative humidity)*PG = 1.0*0.69813 = 0.69813 psia

Initial partial pressure of air (PA) = 15.446-0.69813 = 14.7479 psia = 1.017*10^5 Pa

(**P for 992**) = **1.065*10^5 Pa**
(**PA for 992**) = **1.017*10^5 Pa**

The following two passive junction data for the downcomer pipe have been updated.

Equivalent pipe length for dowmcomer flow junction with the SP (**RLEN for DC**)
= DC length in air space + DC submergence + DC extension above DW floor
= 40.67 ft + 9.5 ft {S3} + 0.5 ft = 50.67 ft = 15.45 m

(**RLEN for DC**) = **15.45 m**

Minimum pressure difference for flow to occur in DC (**DPCR for DC**)
= elevation of the exit of the DC above the SP floor
= SP LWL – DC submergence
= 23.47-9.5 = 13.97 ft = 4.2581 m

(**DPCR for DC**) = **- 4.2581 m**

The negative sign for **DPCR** indicates that the input is an elevation and not pressure. This also requires specifying **ITRKL=1** for the receiver compartment, i.e., compartment **992**.

Heat Structure Data

Four containment-specific heat structures are defined for the CONTAN component (**NHS**).

(**NHS**) = **4**

Level tracking on heat structures (**ITRKH**) is turned on for all four heat structures.

(**ITRKH**) = [**1 1 1 1**]

All COTAN heat structures are located within the WW, i.e., compartment **992**.

User identification of compartment (**ICTBL**) where inner heat structure surface is located
(**ICTCI**) = **992**
User identification of compartment (**ICTBL**) where outer heat structure surface is located
(**ICTCO**) = **992**

(**ICTCI**) = [**992 992 992 992**]
(**ICTCO**) = [**992 992 992 992**]

Number of vertical nodes in heat structure (**NODAX**) = 1

(**NODAX**) = [**1 1 1 1**]

Number of radial nodes in heat structure (**NODRA**) = 3

(**NODRA**) = [**3 3 3 3**]

User identification of heat structure (**IHSTB**) = 1, 2, 3, 4

The four heat structures are the following:

IHSTB 1 = Suppression pool wall
IHSTB 2 = Suppression chamber wall
IHSTB 3 = Reactor pedestal (RP) in SP
IHSTB 4 = Reactor pedestal in SC

(**IHSTB**) = [**1 2 3 4**]

The correspondence of the four heat structures with the heat sinks identified for the reference BWR/5 plant is shown in Table A.15.

Table A.15 CONTAN Heat Structures for a BWR/5

IHSTB	Heat Sink No. {S2}	Description	Exposed Surface Area {S2} (ft^2)	Inner Radius [9] (ft)	Thickness[1] {S2} (ft)	Material {S2}
1	15	SP Wall	6706 (623.0 m^2)	45.5 (13.87 m)	5.22 (1.59 m)	Concrete
2	14	SC Wall	10363 (962.8 m^2)	45.5 (13.87 m)	5.22 (1.59 m)	Concrete
3	10	RP in SP	1430 (132.9 m^2)	10.125 (3.086 m)	4. (1.219 m)	Concrete
4	9	RP in SC	2134 (198.3 m^2)	10.125 (3.086 m)	4. (1.219 m)	Concrete

[1]Wall thickness does not include stainless-steel liner.

For all heat structures in the SP (**IHSTB** = 1 and 3) both the inner and outer surfaces are located in the liquid region (**IREGI** = **IREGO** =1). For all heat structures in the SC (**IHSTB** = 2 and 4) both the inner and outer surfaces are located in the vapor region (**IREGI** = **IREGO** = 0). The outer surfaces are assumed insulated and so the medium in contact with the surface is unimportant. The corresponding TRACE inputs are

(**IREGI**) = [**1 0 1 0**]
(**IREGO**) = [**1 0 1 0**]

The radius of curvature of inner surface of heat structures (**RADI**) are based on data shown in Table A.15. The radius of curvature of outer surface of heat structures (RADO) are calculated as **RADI** + Thickness (from Table A.15). The corresponding TRACE inputs are

(**RADI**) = [**13.87 13.87 3.086 3.086**]
(**RADO**) = [**15.46 15.46 4.305 4.305**]

For each heat structure, the inner and outer surfaces (IC and OC, respectively) are assumed to have the same axial elevations.
The elevation of the lower extremity (HL) of IHSTB 1 and 3 is zero (bottom of SP).
The elevation of the lower extremity (HL) of IHSTB 2 and 4 is 7.154 m (SP LWL).
The elevation of the upper extremity (HU) of IHSTB 1 and 3 is 7.154 (SP LWL).
The elevation of the upper extremity (HU) of IHSTB 2 and 4 is (SP LWL) + (height of SC) = 7.154 + 11.05 = 18.20 m

The corresponding TRACE/PARCSinputs for the elevations of the heat structures are as follows:

(**HLIC**) = (**HLOC**) = [**0.0 7.154 0.0 7.154**]
(**HUIC**) = (**HUOC**) = [**7.154 18.2 7.154 18.2**]

The characteristic length for computation of Grashof number for each heat structure (**HDAVG**) is set to be the height of the heat structure, i.e.,

(**HDAVG**) = [**7.154 11.05 7.154 11.05**]

The total heat structure area of inner surface (**AREAI**) is based on the data in Table A.15.

(**AREAI**) = [**623.0 962.8 132.9 198.3**]

The corresponding outer surface area (**AREAO**) for the SP wall and the SC wall is set to zero to simulate an insulated boundary condition.

The reactor pedestal (RP) outer surface area is estimated as follows.

Ψ = Tabulated inner surface area / Calculated inner surface area

Outer surface area of RP heat structure = ψ * (Calculated outer surface area)

The tabulated inner surface area is from Table A.15.
The calculated inner/outer surface area is $\pi * (2*R_{i/o})*H$
R_i, R_o and H are the inner and outer radius and height of the heat structure respectively.

For **IHSTB**=3 and 4,
R_i = (**RADI**) =3.086 m
R_o = (**RADO**) = 4.305 m
H = (**HDAVG**) = 7.154 m for IHSTB=3 and 11.05 m for IHSTB=4

$\Psi_3 = 132.9/(\pi * (2*3.086)*7.154) = 0.9581$
$\Psi_4 = 198.3/(\pi * (2*3.086)*11.05) = 0.9255$

For **IHSTB**=3,
(**AREAO**) = $0.9581 * \pi * (2*4.305)*7.154 = 185.4$ m^2

For **IHSTB**=4,
(**AREAO**) = $0.9255 * \pi * (2*4.305)*11.05 = 276.6$ m^2

The corresponding TRACE/PARCSinput for (**AREAO**) is,

(**AREAO**) = [**0.0 0.0 185.4 276.6**]
This completes the geometric input for the CONTAN heat structures.

The initial temperatures of the ith heat structure (**TEMPHT**)$_i$ are set to equal to the temperature of the adjoining compartment. The corresponding TRACE inputs are,

(**TEMPHT**)$_1$ = [**305.4 305.4 305.4**]
(**TEMPHT**)$_2$ = [**305.4 305.4 305.4**]
(**TEMPHT**)$_3$ = [**305.4 305.4 305.4**]
(**TEMPHT**)$_4$ = [**305.4 305.4 305.4**]

The thermophysical properties of the heat structures are based on the data for concrete in {S1}.

Density of heat structure (**ROW**) = 144 lbm/ft^3 = 2307 kg/m^3
Heat capacity of heat structure (**CPW**) = 0.20 Btu/lbm-°F = 837 J/kg-K
Thermal conductivity of heat structure (**CW**) = 0.54 BTU/hr-ft-°F = 0.934 W/m-K

The corresponding TRACE inputs are,

(**ROW**) = [**2307.0 2307.0 2307.0 2307.0**]
(**CPW**) = [**837.0 837.0 837.0 837.0**]

(**CW**) = [**0.934 0.934 0.934 0.934**]

The complete listing of the CONTAN component input is reproduced below.

```
*******   type     num        userid        component name
contan             999             1           Containment
* ncompt           nhs         ncool          njct         njctf
       2             4             0             2             0
*  njcts        ncomtb        ncomtv         nnlev         cstep
       0            10             0             0           1.0
* compartments
* itrkl *           1           1e
* itrks *         992           0e
* ictbl *         991         992e
*   vol *      8260.0      9770.0 e
*  vmax *        82.1      9770.0 e
*     p *     1.065E5     1.065E5 e
*    tl *      -330.4      -305.4 e
*    tv *       330.4       305.4 e
*  frsb *         0.0         0.0 e
*  frab *         1.0         1.0 e
*  cuch *         1.0        -1.0 e
*  dpdt *         0.0         0.0 e
* apool *       539.0       539.0 e
*    pa *      9.95E4     1.017E5 e
*   rml *         0.1     4.091E6 e
* nword *           2           2 e
* depth1*         0.0         0.0        82.1      0.1524e
* depth2*         0.0         0.0      9770.0        18.2e
* heat structures
* itrkh *           1           1           1           1e
* ictci *         992         992         992         992e
* ictco *         992         992         992         992e
* nodax *           1           1           1           1e
* nodra *           3           3           3           3e
* ihstb *           1           2           3           4e
* iregi *           1           0           1           0e
* irego *           1           0           1           0e
*  radi *       13.87       13.87       3.086       3.086 e
*  rado *       15.46       15.46       4.305       4.305 e
*   row *      2307.0      2307.0      2307.0      2307.0 e
*   cpw *       837.0       837.0       837.0       837.0 e
*    cw *       0.934       0.934       0.934       0.934 e
*   hli *         0.0       7.154         0.0       7.154 e
*   hui *       7.154        18.2       7.154        18.2 e
*   hlo *         0.0       7.154         0.0       7.154 e
*   huo *       7.154        18.2       7.154        18.2 e
* hdavg *       7.154       11.05       7.154       11.05 e
* areai *       623.0       962.8       132.9       198.3 e
* areao *         0.0         0.0       185.4       276.6 e
* tempht*       305.4       305.4       305.4e
* tempht*       305.4       305.4       305.4e
* tempht*       305.4       305.4       305.4e
```

```
* tempht*       305.4       305.4       305.4e
* passive junctions
*  ict1 *         992         991e
*  ict2 *         991         992e
* ijctb *         994         993e
* itypp *           2           3e
*    hd *     0.59055     0.59055e
*  area *     1.64344    33.14275e
*  rlen *         5.0       15.45e
*    fr *        12.0       1.37e
*  dpcr *    1732.689     -4.2581e
*
*
```

2.9 Suppression Pool Heat Exchanger

The base BWR/5 model assumed one train of the RHR was operational. In the ATWS-ED analysis, two trains of RHR are assumed to be operational and thus two suppression-pool coolers are modeled. This modification is achieved by doubling the suppression-pool cooler's flow to 236 kg/s in **CB**-34.

3 REFERENCES

1. L-Y. Cheng et al., “BWR Anticipated Transients Without Scram in the MELLLA+ Expanded Operating Domain – Part 1: Model Development and Events Leading to Instability,” Appendix A: TRACE Calculation Notebook, NUREG/CR-7179, BNL-NUREG-105323-2014, Brookhaven National Laboratory, March 3, 2014.

2. U.S. Nuclear Regulatory Commission, “Summary of Trip Report for Site Visit to Brookhaven National Laboratory October 2010,” February 12, 2015, ADAMS Accession No. ML15043A803.

3. U.S. Nuclear Regulatory Commission, “Summary of Trip Report for Site Visit to Brookhaven National Laboratory January 2012,” February 12, 2015, ADAMS Accession No. ML15043A807.

4. “TRACE/PARCSV5.435 User’s Manual, Volume 2: Modeling Guidelines,” U.S. Nuclear Regulatory Commission, January 20, 2011.

5. L-Y. Cheng et al., “TRACE/PARCS Core Modeling of a BWR/5 for Accident Analysis of ATWS Events,” Trans. Am. Nucl. Soc. 109, pp 979-982, November 2013.

6. U.S. Nuclear Regulatory Commission, “Summary of Trip Report for Site Visit to Brookhaven National Laboratory October 2010,” February 12, 2015, ADAMS Accession No. ML15043A803.

7. U.S. Nuclear Regulatory Commission, “Safety Evaluation by the Office of Nuclear Reactor Regulation Related to Amendment No. 140 to Facility Operating License No. NPF-69 Nine Mile Point Nuclear Station, LLC, Nine Mile Point, Unit No. 2, Docket No. 50-410,” December 22, 2011, ADAMS Accession No. ML113560333.

8. J. Harrison, GE Hitachi, letter to U.S. Nuclear Regulatory Commission, “Response to NRC's Data Request to Support Confirmatory ATWS Calculations Regarding MELLLA Plus,” MFN 09-681, November 4, 2009, ADAMS Accession No. ML093170371.

9. Nine Mile Point Unit 2 Updated Final Safety Analysis Report Rev 19, October 2010.

10. Figure 2.1-2 Mark II Containment of Nine Mile Point 2 in Reference [9]

NRC FORM 335
(12-2010)
NRCMD 3.7

U.S. NUCLEAR REGULATORY COMMISSION

BIBLIOGRAPHIC DATA SHEET

(See instructions on the reverse)

1. REPORT NUMBER
(Assigned by NRC, Add Vol., Supp., Rev., and Addendum Numbers, If any.)

NUREG/CR-7181
BNL-NUREG-105328-2014

2. TITLE AND SUBTITLE

BWR Anticipated Transients Without Scram in the MELLLA+ Expanded Operating Domain
Part 3: Events Leading to Emergency Depressurization

3. DATE REPORT PUBLISHED

MONTH	YEAR
June	2015

4. FIN OR GRANT NUMBER

V6150 / F6018

5. AUTHOR(S)

Lap-Yan Cheng, Joo Seok Baek, Arantxa Cuadra, Arnold Aronson,
David Diamond, Peter Yarsky

6. TYPE OF REPORT

Technical

7. PERIOD COVERED (Inclusive Dates)

6/1/10 - 6/30/15

8. PERFORMING ORGANIZATION - NAME AND ADDRESS (If NRC, provide Division, Office or Region, U. S. Nuclear Regulatory Commission, and mailing address; if contractor, provide name and mailing address.)

Nuclear Science & Technology Department
Brookhaven National Laboratory
Upton, NY 11973-5000

9. SPONSORING ORGANIZATION - NAME AND ADDRESS (If NRC, type "Same as above", if contractor, provide NRC Division, Office or Region, U. S. Nuclear Regulatory Commission, and mailing address.)

Division of Systems Analysis
Office of Nuclear Regulatory Research
U.S. Nuclear Regulatory Commission
Washington DC 20555-0001

10. SUPPLEMENTARY NOTES

Tarek Zaki, NRC Project Manager

11. ABSTRACT (200 words or less)

This is the third in a series of reports on the response of a BWR/5 boiling water reactor to anticipated transients without reactor scram (ATWS) when operating in the expanded operating domain MELLLA+. In this report ATWS events initiated by the closure of main steam isolation valves are analyzed. The objectives were to improve the ability to model such events with the TRACE/PARCS code package, and to simulate them for a sufficiently long time (2500 s) to understand the response of key components and also the potential for fuel damage or damage to the wetwell (suppression pool). These events automatically trip the recirculation pumps. The operator's responses are to activate the emergency depressurization system when the wetwell has reached the heat capacity temperature limit, and to control power through controlling water level and injecting soluble boron.

Models were developed for three different statepoints in the fuel cycle: beginning-of-cycle, peak-hot-excess-reactivity, and end-of-full-power-life. Eleven cases were assessed to determine the effect of three different strategies for controlling water level, two initial flowrates, two different locations for injecting boron, and two different numerical schemes. In all cases, the event is mitigated successfully in terms of minimizing the degree of damage to the fuel, and assuring the ability of the containment to fulfill its function.

12. KEY WORDS/DESCRIPTORS (List words or phrases that will assist researchers in locating the report.)

TRACE/PARCS; Anticipated Transients Without Scram (ATWS); Boiling Water Reactor (BWR); emergency depressurization; operator actions; reactor analysis; containment function; Maximum Extended Load Line Limit Analysis Plus (MELLLA+)

13 AVAILABILITY STATEMENT

unlimited

14 SECURITY CLASSIFICATION

(This Page)
unclassified

(This Report)
unclassified

15. NUMBER OF PAGES

16. PRICE

Federal Recycling Program

UNITED STATES
NUCLEAR REGULATORY COMMISSION
WASHINGTON, DC 20555-0001

OFFICIAL BUSINESS

NUREG/CR-7181 BWR Anticipated Transients Without Scram in the MELLLA+ Expanded Operating Domain, Part 3 June 2015